THESIS
2
2000

This is to certify that the

thesis entitled

An Experimental Study on the Effect of Static and Dynamic Impulsive Blade on Turbulent Slit Jet

presented by

Tahir Z. Hakim

has been accepted towards fulfillment
of the requirements for

MS degree in Mechanical Engineering

Major professor

Date 8 May 97

O-7639

MSU is an Affirmative Action/Equal Opportunity Institution

LIBRARY
Michigan State
University

PLACE IN RETURN BOX to remove this checkout from your record.
TO AVOID FINES return on or before date due.
MAY BE RECALLED with earlier due date if requested.

DATE DUE	DATE DUE	DATE DUE

11/00 c:/CIRC/DateDue.p65-p.14

AN EXPERIMENTAL STUDY ON THE EFFECT OF STATIC AND DYNAMIC IMPULSIVE BLADE ON TURBULENT SLIT JET

By

Tahir Z. Hakim

A THESIS

Submitted to

Michigan State University

in partial fulfillment of the requirements

for the degree of

MASTER OF SCIENCE

Department of Mechanical Engineering

1997

ABSTRACT

An experimental study was performed to determine the effect of a static and impulsive blade on a free jet. The study showed that for both the cases the free jet defected, but there was a lag in the defection of the flow when under the influence of the Dynamic impulsive jet. Although the ratio of the speed of the impulsive blade to free jet was 0.03, the free jet angle of deflection did not coincide with the Static mode of operation of the impulsive jet and lagged by 10 to 20 degrees at various down stream locations.

TABL

LIST
NON

1

2

3

4

TABLE OF CONTENTS

LIST OF FIGURES v
NOMENCLATURE viii
English viii
Greek viii
Symbols viii
Definitions viii
1. INTRODUCTION 1
1.1 Motivation 1
1.2 Objective 5
2. EXPERIMENTAL APPARTUS 6
2.1 Flow System 6
2.2 Slit Jet 8
2.3 Deflector Blade 8
2.3.1 Operation of DB Assembly 9
2.3.1.1 Positioning of the Deflector Blade 9
2.3.1.2 Running of the Deflector Blade 10
2.4 Deflector blade Detection Device 11
2.5 Pressure Transducer 13
2.6 Hot Wire Anemometers 13
2.7 Visualization 14
2.8 Data Acquisition and Processing 15
2.9 Traverse Control 15
3. DATA PROCESSING 27
3.1 Introduction 27
3.2 Digital Camera Processing 27
3.3 X-Array Calibration and Processing 28
3.4 Transient Velocity Calculations 32
3.5 Normalization of Data 33
4. RESULTS AND DISCUSSION 34
4.1 Introduction 34
4.2 Steady State Measurements 34
4.2.1 Velocity Profile with out DB 34
4.2.2 Velocity Profile for Yb/Wj = -0.5 35
4.3 Velocity Profiles For Deflected Flow 36
4.3.1 Velocity Profile for Yb/Wj = -0.1 36
4.3.2 Velocity Profile for Yb/Wj = 0.125 37
4.3.3 Velocity Profile for Yb/Wj = 0.175 37
4.4 Transient Motion (DB) Study 38
4.4.1 Introduction 38
4.4.2 Velocity of Deflector Blade (DB) 39
4.5 Comparison of Steady State Results with Transient 40
4.5.1 Flow Angles 40

5. U
S
S
S
S
S
S
6. S
7. R
8. R
APPEND

4.5.2 Velocity Profiles 41
5. UNCERTAINTY CONSIDERATIONS 129
5.1 Pressure Transducers 129
5.2 Uncertainty in positioning of DB 129
5.3 Traverse control - Uncertainty 130
5.4 DB Assembly 130
5.5 Optical Encoders 130
5.6 Hot Wire Anemometers 131
6. SUMMARY AND CONCLUSION 132
7. RECOMMENDATIONS 133
8. REFERENCES 135
APPENDIX A: DEFLECTOR BLADE ASSEMBLY 136

LIST

Figu
Figu

Figu
Fig
Fig

Fig
Fig
Fig
Fig
Fig
Fig
Fig
Fig

Fig
Fig
Fig
Fig
Fig
Fig
Fig
Fig

Fig

Fig

Fig

Fig

Fig

Fig

Fig

Fig

Fig

LIST OF FIGURES

Figure 1. Schematic representation of an Induction System-MAFS 3
Figure 2. Schematic representation of an Induction System fitted with an auxiliary supply source 4
Figure 3. Air flow apparatus. (Wind tunnel) 16
Figure 4. Schematic of reversible blower used in wind tunnel 17
Figure 5. Calibration Curve to estimate speed(m/sec) in the wind tunnel for a given Voltage (volts) of reversible blower 18
Figure 6. Slit jet assembly 19
Figure 7. Experimental facility 20
Figure 8. Set up for transient detection of DB 21
Figure 9. Optical encoder voltage response 22
Figure 10. Optical encoder voltage response to moving blade 23
Figure 11. Schematic of X-array hot wire probe 24
Figure 12. Tuft probe used for measuring the steady state angles 25
Figure 13. Nominal Angle of deflection measured by DYCAM for Yb/Wj=$\propto$ 26
Figure 14. Velocity distribution <U>/Uo at X/Wj=1.5 and Yb/Wj=$\propto$ 42
Figure 15. Velocity distribution <V>/Uo at X/Wj=1.5 and Yb/Wj=$\propto$ 43
Figure 16. U-rms.at X/Wj=1.5 and Yb/Wj=$\propto$ 44
Figure 17. V-rms.at X/Wj=1.5 and Yb/Wj=$\propto$ 45
Figure 18. Velocity distribution <U>/Uo at X/Wj=1.5 and Yb/Wj=-0.5 . . . 46
Figure 19. V-rms. for X/Wj=1.5 and Yb/Wj=-0.5 47
Figure 20. U-rms. for X/Wj=1.5 and Yb/Wj=-0.5 48
Figure 21. Velocity distribution <U>/Uo at X/Wj=1.5 and Yb/Wj=-0.1 (Nominal deflection angle of jet=30°) 49
Figure 22. Velocity distribution <V>/Uo at X/Wj=1.5 and Yb/Wj=-0.1 (Nominal deflection angle of jet=30°) 50
Figure 23. U-rms. at X/Wj=1.5 and Yb/Wj=-0.1 (Nominal deflection angle of jet=30°) 51
Figure 24. V-rms.at X/Wj=1.5 and Yb/Wj=-0.1 (Nominal deflection angle of jet=30°) 52
Figure 25. Velocity distribution <U>/Uo at X/Wj=1.5 and Yb/Wj=0.125 (Nominal deflection angle of jet=45°) 53
Figure 26. Velocity distribution <V>/Uo at X/Wj=1.5 and Yb/Wj=0.125 (Nominal deflection angle of jet=45°) 54
Figure 27. Velocity distribution <U>/Uo at X/Wj=1.5 and Yb/Wj=0.175 (Nominal deflection angle of jet=48°) 55
Figure 28. Velocity distribution <V>/Uo at X/Wj=1.5 and Yb/Wj=0.175 (Nominal deflection angle of jet=48°) 56
Figure 29. Schematic representation of locations, of the hot wire probes used during the transient motion of the DB. 57
Figure 30. For given Yp/Wj and Yb/Wj, Independence of <U>/Uo measured

with respect to dYb/dt 58
Figure 31. For given Yp/Wj and Yb/Wj, Independence of <V>/Uo measured with respect to dYb/dt 59
Figure 32. For given Yp/Wj, difference in measured angle between the steady state and transient (for transient Vb/Uo=0.03) 60
Figure 33. Histogram of flow angles at Yb/Wj=-0.525 and Yp/Wj=-0.5 61
Figure 34. Histogram of flow angles at Yb/Wj=-0.4 and Yp/Wj=-0.5 62
Figure 35. Histogram of flow angles at Yb/Wj=-0.275 and Yp/Wj=-0.5 63
Figure 36. Histogram of flow angles at Yb/Wj=-0.15 and Yp/Wj=-0.5 64
Figure 37. Histogram of flow angles at Yb/Wj=-0.025 and Yp/Wj=-0.5 65
Figure 38. Histogram of flow angles at Yb/Wj=+0.1 and Yp/Wj=-0.5 66
Figure 39. Histogram of flow angles at Yb/Wj=+0.175 and Yp/Wj=-0.5 . . . 67
Figure 40. Histogram of flow angles at Yb/Wj=-0.525 and Yp/Wj=-0.2 68
Figure 41. Histogram of flow angles at Yb/Wj=-0.4 and Yp/Wj=-0.2 69
Figure 42. Histogram of flow angles at Yb/Wj=-0.275 and Yp/Wj=-0.2 70
Figure 43. Histogram of flow angles at Yb/Wj=-0.15 and Yp/Wj=-0.2 71
Figure 44. Histogram of flow angles at Yb/Wj=-0.025 and Yp/Wj=-0.2 72
Figure 45. Histogram of flow angles at Yb/Wj=+0.1 and Yp/Wj=-0.2 73
Figure 46. Histogram of flow angles at Yb/Wj=+0.175 and Yp/Wj=-0.2 . . . 74
Figure 47. Histogram of flow angles at Yb/Wj=-0.525 and Yp/Wj=0.2 75
Figure 48. Histogram of flow angles at Yb/Wj=-0.4 and Yp/Wj=0.2 76
Figure 49. Histogram of flow angles at Yb/Wj=-0.275 and Yp/Wj=0.2 77
Figure 50. Histogram of flow angles at Yb/Wj=-0.15 and Yp/Wj=0.2 78
Figure 51. Histogram of flow angles at Yb/Wj=-0.025 and Yp/Wj=0.2 79
Figure 52. Histogram of flow angles at Yb/Wj=+0.1 and Yp/Wj=0.2 80
Figure 53. Histogram of flow angles at Yb/Wj=+0.175 and Yp/Wj=0.2 81
Figure 54. Histogram of flow angles at Yb/Wj=-0.525 and Yp/Wj=0.4 82
Figure 55. Histogram of flow angles at Yb/Wj=-0.4 and Yp/Wj=0.4 83
Figure 56. Histogram of flow angles at Yb/Wj=-0.275 and Yp/Wj=0.4 84
Figure 57. Histogram of flow angles at Yb/Wj=-0.15 and Yp/Wj=0.4 85
Figure 58. Histogram of flow angles at Yb/Wj=-0.025 and Yp/Wj=0.4 86
Figure 59. Histogram of flow angles at Yb/Wj=+0.1 and Yp/Wj=0.4 87
Figure 60. Histogram of flow angles at Yb/Wj=+0.175 and Yp/Wj=0.4 88
Figure 61. Histogram of flow angles at Yb/Wj=-0.525 and Yp/Wj=0.6 89
Figure 62. Histogram of flow angles at Yb/Wj=-0.4 and Yp/Wj=0.6 90
Figure 63. Histogram of flow angles at Yb/Wj=-0.275 and Yp/Wj=0.6 91
Figure 64. Histogram of flow angles at Yb/Wj=-0.15 and Yp/Wj=0.6 92
Figure 65. Histogram of flow angles at Yb/Wj=-0.025 and Yp/Wj=0.6 93
Figure 66. Histogram of flow angles at Yb/Wj=+0.1 and Yp/Wj=0.6 94
Figure 67. Histogram of flow angles at Yb/Wj=+0.175 and Yp/Wj=0.6 95
Figure 68. Histogram of flow angles at Yb/Wj=-0.525 and Yp/Wj=0.8 96
Figure 69. Histogram of flow angles at Yb/Wj=-0.4 and Yp/Wj=0.8 97
Figure 70. Histogram of flow angles at Yb/Wj=-0.275 and Yp/Wj=0.8 98

Fig
Fig
Fig

Figure 71. Histogram of flow angles at Yb/Wj=-0.15 and Yp/Wj=0.8 99
Figure 72. Histogram of flow angles at Yb/Wj=-0.025 and Yp/Wj=0.8 100
Figure 73. Histogram of flow angles at Yb/Wj= +0.1 and Yp/Wj=0.8 101
Figure 74. Histogram of flow angles at Yb/Wj= +0.175 and Yp/Wj=0.8 . . . 102
Figure 75. Velocity distribution <U>/Uo at X/Wj=1.875 Yb/Wj=∝ 103
Figure 76. Velocity distribution <U>/Uo at X/Wj=1.875 Yb/Wj=-1.025 . . 104
Figure 77. Velocity distribution <U>/Uo at X/Wj=1.875 Yb/Wj=-0.9 . . . 105
Figure 78. Velocity distribution <U>/Uo at X/Wj=1.875 Yb/Wj=-0.775 . . 106
Figure 79. Velocity distribution <U>/Uo at X/Wj=1.875 Yb/Wj=-0.65 . . 107
Figure 80. Velocity distribution <U>/Uo at X/Wj=1.875 Yb/Wj=-0.525 . . 108
Figure 81. Velocity distribution <U>/Uo at X/Wj=1.875 Yb/Wj=-0.4 . . . 109
Figure 82. Velocity distribution <U>/Uo at X/Wj=1.875 Yb/Wj=-0.275 . . 110
Figure 83. Velocity distribution <U>/Uo at X/Wj=1.875 Yb/Wj=-0.15 . . 111
Figure 84. Velocity distribution <U>/Uo at X/Wj=1.875 Yb/Wj=-0.025 . . 112
Figure 85. Velocity distribution <U>/Uo at X/Wj=1.875 Yb/Wj=0.1 113
Figure 86. Velocity distribution <U>/Uo at X/Wj=1.875 Yb/Wj=0.175 . . 114
Figure 87. Velocity distribution <V>/Uo at X/Wj=1.875 Yb/Wj=∝ 115
Figure 88. Velocity distribution <V>/Uo at X/Wj=1.875 Yb/Wj=-1.025 . . 116
Figure 89. Velocity distribution <V>/Uo at X/Wj=1.875 Yb/Wj=-0.9 . . . 117
Figure 90. Velocity distribution <V>/Uo at X/Wj=1.875 Yb/Wj=-0.775 . . 118
Figure 91. Velocity distribution <V>/Uo at X/Wj=1.875 Yb/Wj=-0.65 . . 119
Figure 92. Velocity distribution <V>/Uo at X/Wj=1.875 Yb/Wj=-0.525 . . 120
Figure 93. Velocity distribution <V>/Uo at X/Wj=1.875 Yb/Wj=-0.4 . . . 121
Figure 94. Velocity distribution <V>/Uo at X/Wj=1.875 Yb/Wj=-0.275 . . 122
Figure 95. Velocity distribution <V>/Uo at X/Wj=1.875 Yb/Wj=-0.15 . . 123
Figure 96. Velocity distribution <V>/Uo at X/Wj=1.875 Yb/Wj=-0.025 . . 124
Figure 97. Velocity distribution <V>/Uo at X/Wj=1.875 Yb/Wj=0.1 125
Figure 98. Velocity distribution <V>/Uo at X/Wj=1.875 Yb/Wj=0.175 . . 126
Figure 99. Velocity profiles (<U>/Uo) as a function of position of DB (-0.525≤Yb/Wj≤-0.15) 127
Figure 100. Velocity profiles (<U>/Uo) as a function of position of DB (-0.15≤Yb/Wj≤0.175) 128
Figure A-1. Deflector Blade design 147
Figure A-2. Deflector Blade carriage 148
Figure A-3. Center rod used for carrying the DB-carriage 149
Figure A-4. Center rod with locking nut 150
Figure A-5. Center rod holder 151
Figure A-6. Spring loaded pullers (Primary drivers) 152
Figure A-7. Deflector blade-knife edge under pulling force 153
Figure A-8. I-beam used to connect the DB with the DB carriage 154
Figure A-9. Stops for the main spring. 155
Figure A-10 End plates for holding the DB assembly 156
Figure A-11 Remote mechanism used for the release of the DB 157

NOME

ENGLI

A:
B:
CR:
DB:
g:
M:
K:
L_{DB}:
L_j:
n:
P_{atm}:
P_{Tr}:
Q:
Sj:
Std.dev
T_{DB}:
U:
Uo:
V:
Vb:
Wj:
Yb:
Yp:
S.S:
Z:

GREEK

β:
γ:
η:
at γ

SYMBO

<>:
~:

NOMENCLATURE

ENGLISH

A : Coefficient in Collis and Williams
B : Coefficient in Collis and Williams
CR : Center Rod
DB : Deflector blade
g : Force of gravity
IM : Interrupter module
K : Spring stiffness
L_{DB} : Deflector blade length
L_J : Length of the Slit jet
n : Coefficient in Collis and Williams
P_{atm} : Atmospheric pressure
P_{Tx} : Pressure Transducer
Q : Magnitude of the velocity measured by the hot wire
Sj : Slit jet
Std.dev : Standard deviation
T_{DB} : Thickness of DB
U : Mean Velocity in X-direction
Uo : Velocity in wind tunnel
V : Mean Velocity in Y- direction
Vb : Velocity of DB
Wj : Width of the slit Jet
Yb : Position of DB
Yp : Position of the probe
S.S : Steady State
Z : Vertical height in the Bernoulli's equation

GREEK

β : Angle between a slant wire and the probe axis, generic velocity measure.
γ : In plane flow angle
η : Ratio of voltage of a hot wire at an angle divided by the voltage of the same wire at $\gamma = 0$.

SYMBOLS

$< >$: Average value of the velocities
$\sim$: RMS value of the velocity

DE

DEFINITIONS

Deflector blade : The knife edge that deflects the flow field coming from the slit jet.

Impulsive blade : Same as above.

1.1 M

The

system

the reso

intake n

monitor

sensors,

is inferr

The

.Unstea

measure

sensor a

known

connect

auxiliary

known r

If the

engine r

1. INTRODUCTION

1.1 Motivation:

The basic motivation behind the experiment is related to an automobile induction system . In the automobile induction system, see Figure 1 , the intake air passes through the resonator, air cleaner, mass flow air sensor, and throttle body before it enters into the intake manifold of the engine. The amount of air that is coming into the engine is monitored by the MAFS (mass air flow sensor). This sensor utilizes small hot wire sensors, which measures the speed of the incoming air .The mass flow going to the engine is inferred on the basis of data taken from the MAFS.

The current problem is to exactly measure the mass flow rate in the induction system .Unsteady flow effects , with the corresponding differences in the ratio between the measured velocity and the desired spatial average value , makes the reading of the MAFS sensor an unreliable indicator of the mass flow rate. Conversely , if the true mass flow is known , then the sensor can be calibrated . For this, if we have an auxiliary supply source connected to the induction system, see Figure 2 and monitor the mass flow (in) air in the auxiliary supply system, then the sensor output $E_s(t)$ can be calibrated as a function of the known mass flow $E_s(\dot{m}^o(t))$.

If the auxiliary supply source is maintained at a constant pressure, irrespective of the engine rpm, then the inflow from the auxiliary system will be correctly modulated and we

will h

comin

Th

systen

deflec

comin

Th

the bl

the bl

flow p

experi

the jet

visuali

auxilia

will have known mass into the engine at all times. This can be done by controlling the air coming into the inlet of the auxiliary supply system.

This experiment is the first step to the knowledge that one needs to build up such a system as stated above. In this experiment we see how the fluid field behaves when it is deflected by an impulsive blade. It is analogous to what we would do to control the fluid coming into the auxiliary supply plenum with the help of fine blades.

The experiment is , firstly a study of the steady analysis of the problem, that is, when the blade is in a fixed position, and secondly, it is a study of the transient condition , when the blade is in motion .The latter depicts what would occur when the blades move into the flow path of the jet which would otherwise enter into the auxiliary supply manifold. In the experiment, we have assumed the width of the inlet duct to be analogous to the width of the jet. Hence we do our experiment by keeping the above apparatus in mind and by visualizing the effect of high speed blades as they partially open or close the inlet to the auxiliary air supply.

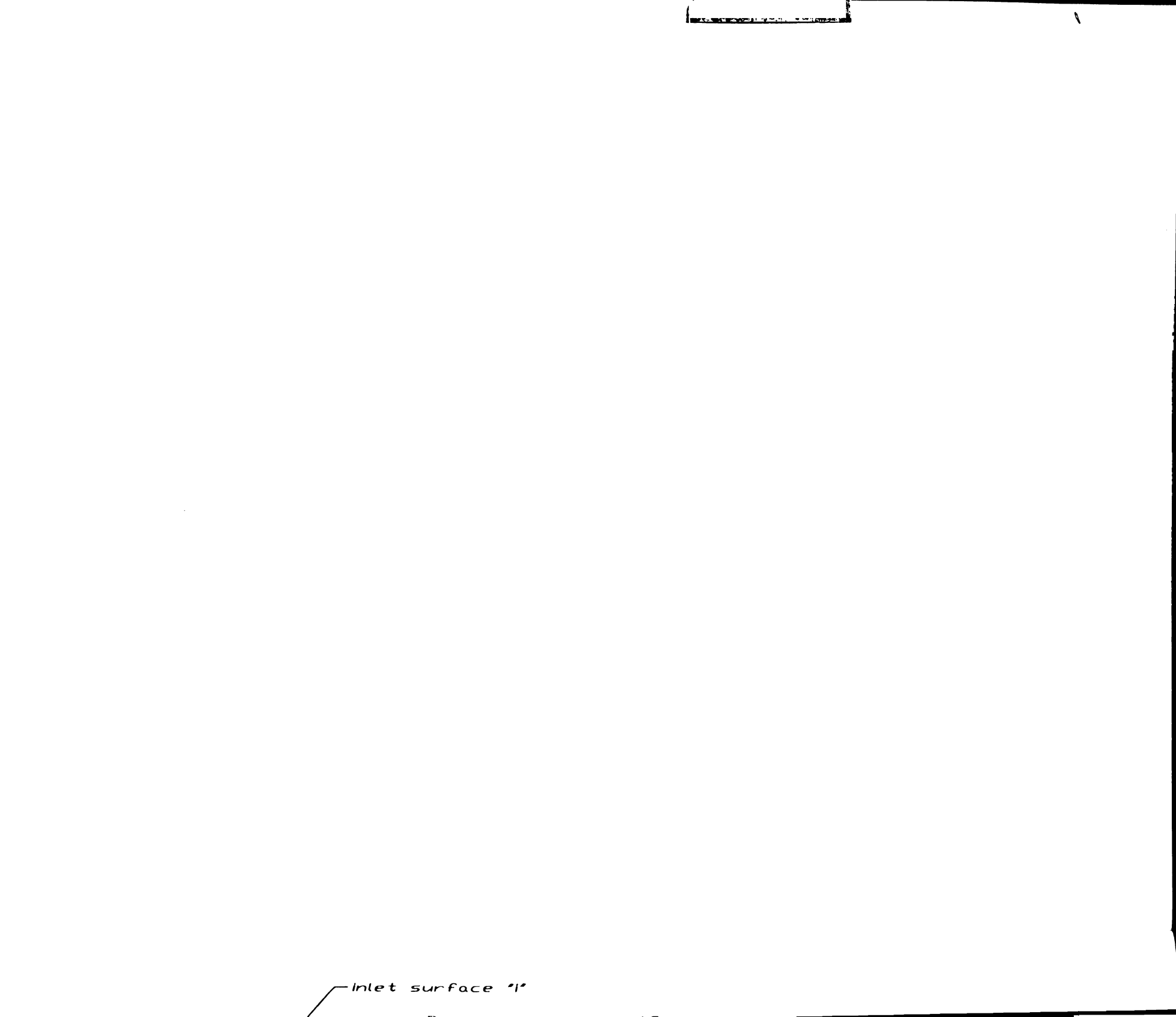
Inlet surface "1"

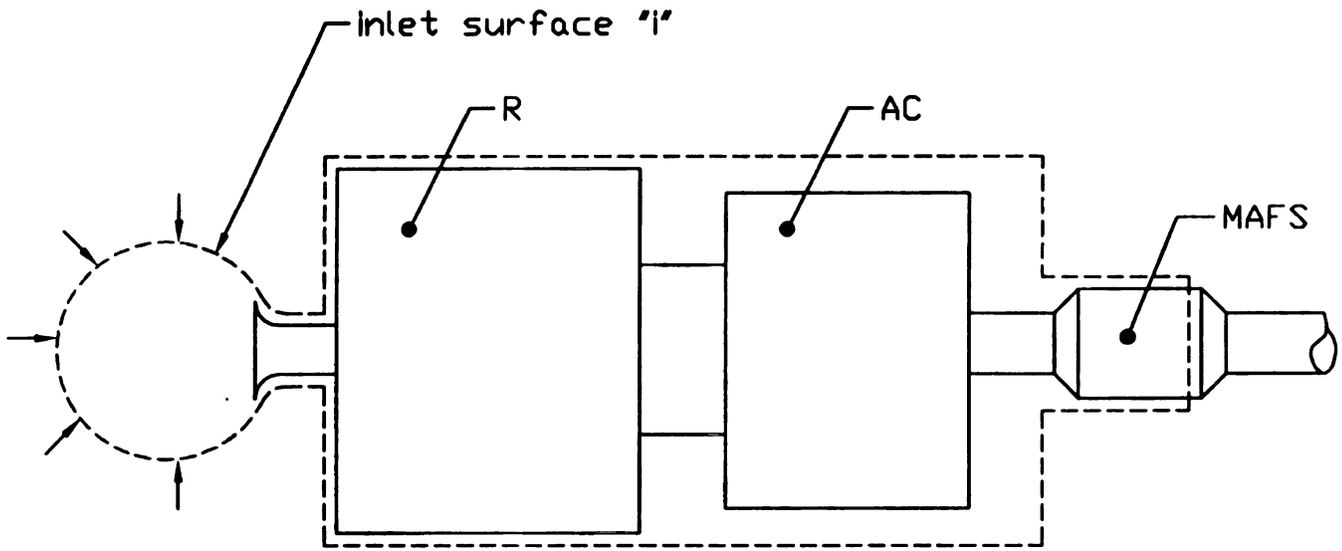

R - Resonator
AC - Air Cleaner
MAFS - Mass Air Flow Sensor

Fig. 1: Schematic Representation of an Induction System, atm→MAFS

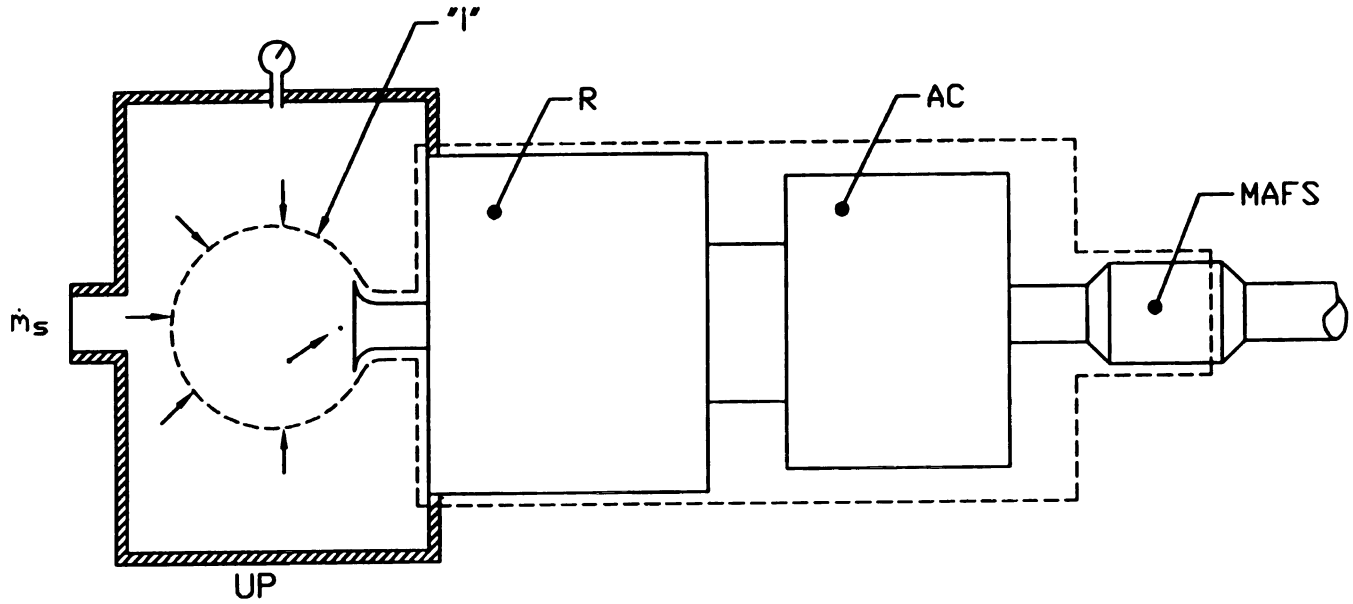

UP - Upwind Plenum
"I" - Inlet to Control Volume
R - Resonator
AC - Air Cleaner
MAFS - Mass Air Flow Sensor

Fig. 2: Schematic Representation of an Induction System fitted with an auxiliary supply source.

Notes: $\dot{m}_s$ = programmed mass flux
* shows the location of the $\vec{V}(t)$ measurements

1.2 C

Th

the int

ways:

positio

1.2 Objective.

The objective of this thesis work is to determine how the turbulent jet behaves under the influence of an impulsive blade. This character of the flow field can be studied in two ways:

i). To observe the deflection of the jet when the deflector/impulsive blade is pre-positioned in the flow field .

ii). To record the main flow field with deflector blade in transient state.

2.

A

Th

bio

mo

clos

the

exp

limit

T

that

press

A rel

in Fig

So

contra

Le

transd

equatic

2. EXPERIMENTAL APPARATUS

2.1 Flow System

As shown in Figure 3 ,for the experimental work, a high-flow device/apparatus was used,. This device had dimensions of 2090 x 95 x 95 mm. The fan was powered by a reversible blower of Cincinnati Fan Model No. PB-141A, run by a 3 hp, 3450 rpm motor (Balidor model no. M3610T). The flow rates through the blower was adjustable manually by closing and opening of the suction duct of the blower, Figure 4. Therefore, the control of the inflow speed through the Sj (Slit jet) can be monitored to the requirement of the experiment .The velocity , at the vena contracta was selected to be 35 m/sec .This limitation was imposed by the calibrating unit present in the lab.

The speed of the inflow was determined by the pressure drop between the ambient and that inside of the wind tunnel; Using the Bernoulli equation and knowing the mean pressure value with in the tunnel the inflow velocity could be calculated (as shown later). A relation between the voltage and the velocity in the wind tunnel, thus obtained is shown in Figure 5. which is used to maintained the required speed in the wind tunnel .

So through the experiment, the pressure transducer monitored the velocity at vena contracta used to normalize the measured velocities in the flow field.

Let P_{atm} be the atmospheric pressure and P_{Tx} be the measured pressure by the pressure transducer (having a certain mp value in inches of water/volts).From the Bernoulli equation; we have:

Usir

now

as P

has i

Ther

Whe

N

(m/se

drop

There

Px.Tx

$$P_{ATM} - P_{TX} = \rho V^2/2$$

Using the above equation ;

$$V = [(P_{ATM} - P_{TX}) \times 2] / \rho \qquad \rho = \text{density of air.}$$

now let $(P_{ATM} - P_{TX}) = P^*$

as P* is the pressure measured by the pressure transducer , and each pressure transducer has it own mp. Value inch H_2O/ volts. Also this $P^* = \rho_w g z$ and ρ_w = density of water

Therefore combining all the equations we have;

$$V = (2 g(\rho_w / \rho) z)^{0.5}$$

Where Z= in of water/ volts * volts

= Mp value of Tx * volts.

Now by interpolating the density of air and bringing the values in the same units (m/sec)we have the resulting equation to calculate the velocity of air as a result of pressure drop between ambient and the pressure inside the wind tunnel measured by the Px.Tx

$$V = (2 * 9.81 * 1.94/.00232 * .0254 * \text{Mp value of Tx.} * \text{volts})^{0.5} = \text{m/ sec}$$

Therefore with the help of the above equation, knowing the voltage generated by the Px.Tx (pressure transducer), we can find the resultant velocity at the vena contracta .

2.2 S

Th

40mm

the a

time

2.3

=1.

flo

fab

pr

st

d

p

2.2 Slit Jet

The slit jet assembly shown in Figure. 6 .It is characterized by a slit width of (Wj) of 40mm and a length of 300mm for the present experiment. The plenum, which is open to the atmosphere upstream of the jet , is characterized by the dimensions 775mm (or 12.916 times the width) x 475mm (or 1.583 times the length)x 460mm as the upstream dimension.

2.3 Deflector blade .

A traveling deflector blade, guided by runners such that its leading edge was at X/Wj =1.5 and driven by tensioned springs as shown in Figure. 7, is used to interrupt the jet flow. The apparatus, to achieve this dynamic interruption of the jet, was designed and fabricated as part of the present thesis effort. A detailed description of this unit is presented in Appendix A; a brief description is given below.

The deflector blade was positioned at various insertion depths to record the steady state response of the jet. In its dynamic mode, the tensioned springs propelled the deflector blade from its initial position: $Y_b(0)$=-101 mm=-2.525*Wj, to a designated final position. The final positions, $y(\infty)$, of

$y(\infty)$ = -4 mm = -0.1*Wj

= +5 mm = 0.125*Wj

= +7 mm = 0.175*Wj

wer

y(x

usec

A

imp

T

Figu

The

mea

2.3.

As s

appa

2.3.

i

je

fl

pa

were selected for further study. It was determined that a final position of 7 mm or $y(\infty)/Wj=0.175$ was compatible with the objectives of this investigation and this value was used for the dynamic measurements.

An arresting technique, which stopped the blade at the desired location was an important aspect of this design. See Appendix A.

Three IR (Infra red) photo cells or optical encoders (OP) ,were used, as shown in Figure 8. and as described in section 2.4, to determine the velocity of the blade: dy_B/dt. The second and third photo cell provided the relevant blade velocity information for the measurements reported in this thesis.

2.3.1 Operation of DB assembly

As stated earlier, that the DB assembly is an additional device fitted over the slit jet apparatus. The mode of operation is as follows:

2.3.1.1 Positioning of the DB

First of all, the DB has to be positioned at the vena-contracta, the width of the Sj is 40 mm (Wj). As the fluid from the plenum enters the wind tunnel in the form of a jet, a vena-contracta is formed downstream the exit plane of Sj. In case of an ideal fluid, the jet width continues to decrease and streamlines become as asymptotically parallel [Valentine (1967)]. In case of a real fluid, however, the vena-contracta

(minimum jet width) forms within slit jet width, downstream the exit plane. In addition, depending upon the Reynolds number of the jet, symmetric vortex motion is developed; these motions make significant contributions to the spread of the jet [BW, Clark and Kit (1980), Foss and Korschelt (1983)]. For this particular experiment Wj = 40 mm, means that vena-contracta would occur at 60 mm,(= 1.5*Wj) downstream the exit plane. So, the DB had to be positioned at 60 mm from the knife edges of the Sj. For this, the four screws (in the end plates) were used to position the DB. As turning these screws through the same pitch led to the vertical movement of the upper two halves, which then moved the whole DB assembly up or down. Thus, the vertical positioning of the DB assembly can be done easily in this manner. The lateral placing of the DB over Lj (length of the jet) is done by placing the bottom half of the end plates over the support plate (wooden) of the Sj. Once the adjustment has been made, with the help of the vernier and the adjusting screws, next comes the running of the DB over the rails.

2.3.1.2 Running of the DB

Once the whole set-up is done, the DB is ready to run over its length. For this, the two pullers are popped on to the DB , and then the DB is pulled back against the spring force to a predetermined position and then released. As soon as the DB is released it accelerates towards its termination point, which is the end of the center rod. The alignment of the DB tip and that of the tip of the knife edge of the Sj is done by a

thin thread pendulum. The pendulum is placed on the Sj knife edge and the thread with a weight attached hangs down under the influence of gravity. The center rod is placed in such a way, by loosening the nuts in the center rod holder, that when the DB is locked in position, the tip of the knife edge of the DB just touches the thread pendulum. In this way, both the tips of the knife edges of the Sj and the DB are aligned and this determines the start position of the DB knife edge with respect to Wj ($-20 < Wj < 20$). As soon as the blade hits the end of the center rod, the 10 mm spring-loaded balls in the DB carriage pop in position on the indents on the center rod, thus locking the DB carriage in position. The pullers, which are still under the influence of the spring, continue their motion by popping off the DB. So, the DB is held in the desired position and the primary drivers disengage. For the next run, again the pullers are attached to the DB and the whole routine is repeated, except now the end position of the blade is known, so unless no incremental change in the DB position is desired, the adjustment of the center rod is not undertaken.

2.4 DB- Detection Device

As mentioned earlier, in the operation of the DB, that the DB accelerates toward the end position, or its destination. This means that the velocity of DB is a function of X ($V = F(X)$). Therefore, the position of the DB can be determined empirically or by analytical considerations. In this experiment the position of DB at a certain instant in time is done

by e

enc

the

less

bloc

outp

I

was

Spe

+/-

gave

soor

volt

I

such

in be

rail a

time

In th

dista

the s

by empirical methods , the set up is shown in Figure 8. For this, three IR's , optical encoders (OP) or interrupter modules (IM) were used.

The Optical encoder has two parts to it, one is called the emitter and the other is called the detector. When a certain power supply is given to the IM, the output from the IM is less than the supply voltage, as soon as the gap between the emitter and the detector is blocked, the same amount of magnitude of that of the supplied voltage appears as an output.

In this experiment, a five-volt supply was used and given to the IM. The power supply was cannibalized from an old computer,(since power supply to a floppy disks is five volts). Special emphasis was given to a five-volt supply as the A/D board responses to an input of +/- 10 volts. So, as soon as the five volt supply was switched on, the IM responded and gave an output of 0.81 - 0.82 volts with fluctuations of +/- 5 milli-volts, Figure 9. But as soon as something is placed in between the gap of IM, there is a rise in voltage to 5+/- 0.7 volts figure10.

Therefore, a thin strip of metal of 2 mm thickness was placed over the DB carriage in such a way that when DB hits the end position of its run, the tip of the metal strip passes in between the gap of the IM. For this, three optical encoders were mounted on the side rail along the travel path of the DB refer figure 8. So whenever there was a variation in the time series of the output voltage of the IM it is known that the DB is at that particular IM. In the experiment, the last IM is switched on when the DB had completed its travel. The distance between the first and the second IM (or OP) is 60 mm and the distance between the second and the third is 48 mm. Figure 10. shows the response of the IM when the DB

has

par

N

bet

+/-

in t

2.5

I

the

2.6

F

velo

temp

55M

- Mi

Tung

either

diam

all se

has passed through it. In this manner, the position of the DB can be detected at a particular instant in time during its travel from its initial to its final state.

NB: It is also worth mentioning here that as soon as some obstruction is placed in between the gap of the emitter and the detector, the voltage at once does not jump to 5 +/- 0.7 volts, but a slight time lag is in between. So for analyzing purposes, any variation in the output of the IM/OP is an indication of obstruction of the emitter detector gap.

2.5 Pressure Transducers

For the measurement of the pressure inside the wind tunnel and for the calibration of the hot wire sensors, A one TORR MKS Baraton pressure transducers was used.

2.6 Hot Wire Anemometers

Hot wire probes, fashioned as X-arrays were used for the measurement of the (U,V) velocity components in the flow field. Hot wire data were taken using constant temperature anemometers , the X-array sensor survey was accomplished using DISA 55M10 anemometers. All the X-array probes were built in turbulent shear flow laboratory - Michigan state University. Each hot wire sensor was constructed from 5 micro-meter Tungsten wire, the wire length was 3 mm with active region of 1mm in the center . On either side of the active region copper sulphate platting was added to the tungsten; its diameter was approximately 50 micron. The length to diameter ratio of 200 was kept for all sensors . Figure 11 indicates the general appearance of an X-array probe used during

the ex

and th

Th

compo

compo

betwe

condu

chang

the re

2.7 F

A

angle

threac

placed

Since

was n

a digit

mount

positic

interio

the experiment . All hot wire sensors probes were operated with an over heat ratio of 1.7 and the cold resistance of the wires were found in the range from 3.5- 5.0 Ohms.

The X-array probes were used to provide time series values for the U and the V components of the velocity at each measurement location. All the hot wire data was compensated for temperature to reduce the errors by the change in the fluid temperature between the calibration and the measurement . Temperature measurements were conducted using a thermistor with sensitivity of 2.03°K Ohms at 293°K. All temperature changes were assumed to be "long term (of the order of 10's of minutes)" and therefore the response time of the thermistor was considered to be sufficient.

2.7 Flow Visualization

A digital camera was used along with the tuft probe in order to estimate the mean flow angle of the turbulent flow downstream from the slit jet. The tuft is made of strands of thread mounted on a needle and held in a holder; see Figure 12 . The tuft probe was placed in the flow and the angle of deflection was indicated by the orientation of the tuft. Since the jet flow existed within an opaque wind tunnel, direct visualization of the tuft was not possible. For this reason, and because the information can be digitally processed, a digital camera (DYCAM DC-10) was used to record the flow angles. The camera was mounted inside the wind tunnel and photographs of the tuft were taken for different positions of the blade. Since the camera was operated in auto-mode, the lighting of the interior of the wind tunnel was produced by the flash of the camera. The photographs

obtained

The mear

Many phe

$-10 \leq Yb \leq$

2.8 Data

The da

Fast-16 A

bits with a

8-channel

sample all

Fast-16 bo

2.9 Traver

A linear

flow field.

personal co

obtained from the digital camera were processed on computer using PhotoShop software. The mean flow angle was detected as a function of the position of the blade, Figure 13 . Many photographs (1500) were taken to confirm for the mean flow angle for a range of -- -10≤ Yb≤ 10 (-0.25≤ Yb/Wj ≤ 0.25).

2.8 Data Acquisition and Processing

The data acquisition for the hot-wire X-array probe was accomplished with an Analog Fast-16 A/D Card with an IBM 486-66 PC clone. The A/D board had a resolution of 16 bits with a range of +/- 10 volts; the maximum sample rate of the system was 1 MHz. An 8-channel sample and hold card was used in conjunction with the A/D card in order to sample all the different channels at an instant in time and to hold the value until the Analog Fast-16 board can read each channel.

2.9 Traverse Control

A linear traverse was used for the positioning of the tuft and the hot wire probes in the flow field. The motion of the traverse was controlled by a stepper motor connected to a personal computer.

Fi

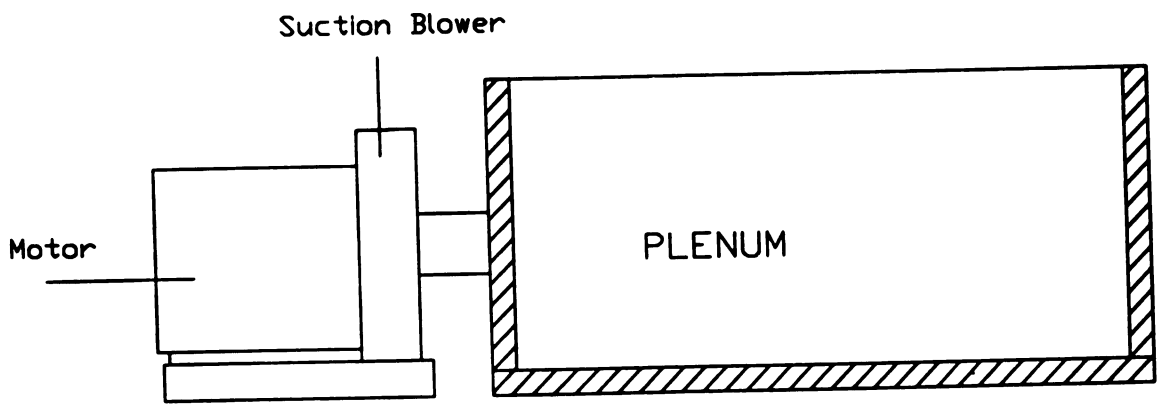

Fig 3. Air Flow appratus (Wind tunnel) , used for the generation of the jet.

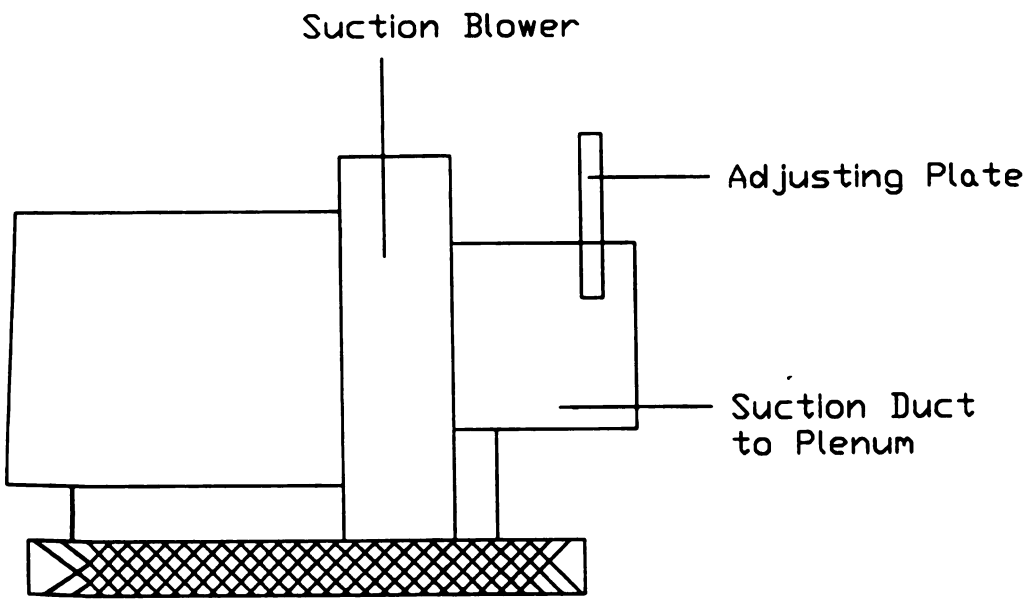

Fig 4. Reversible blower used in the wind tunnel , with adjustable Suction duct.

Calibration Curve for Wind Tunnel

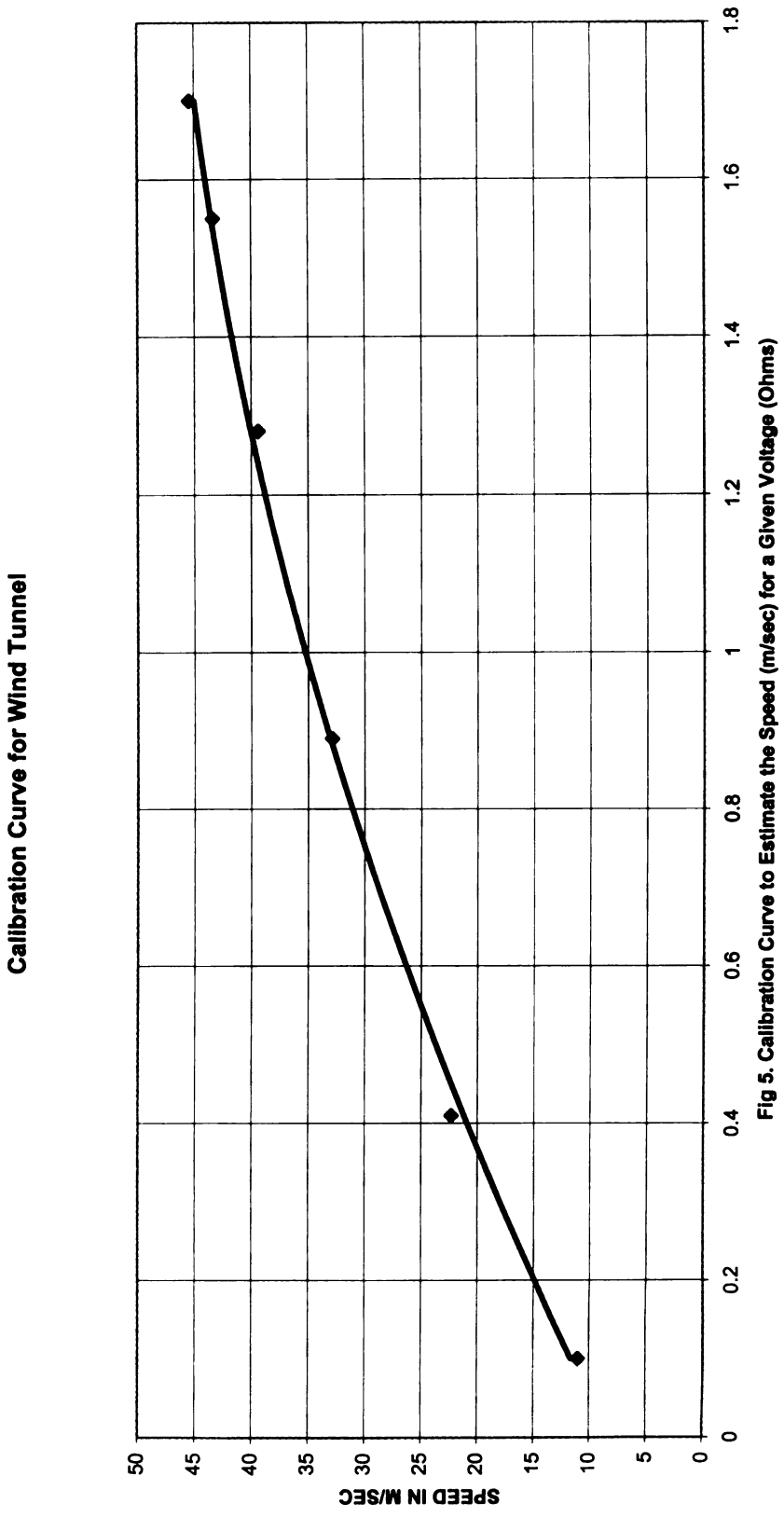

Fig 5. Calibration Curve to Estimate the Speed (m/sec) for a Given Voltage (Ohms)

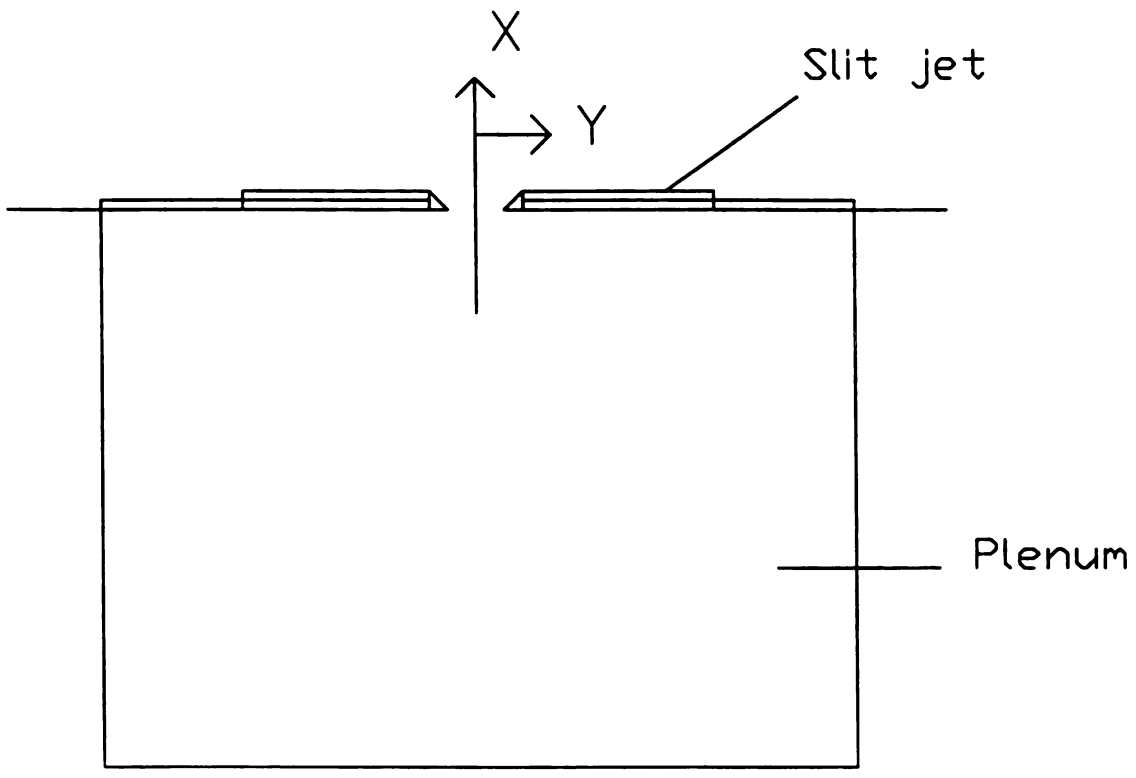

Fig 6. Slit Jet Assembly .

Air Plenum

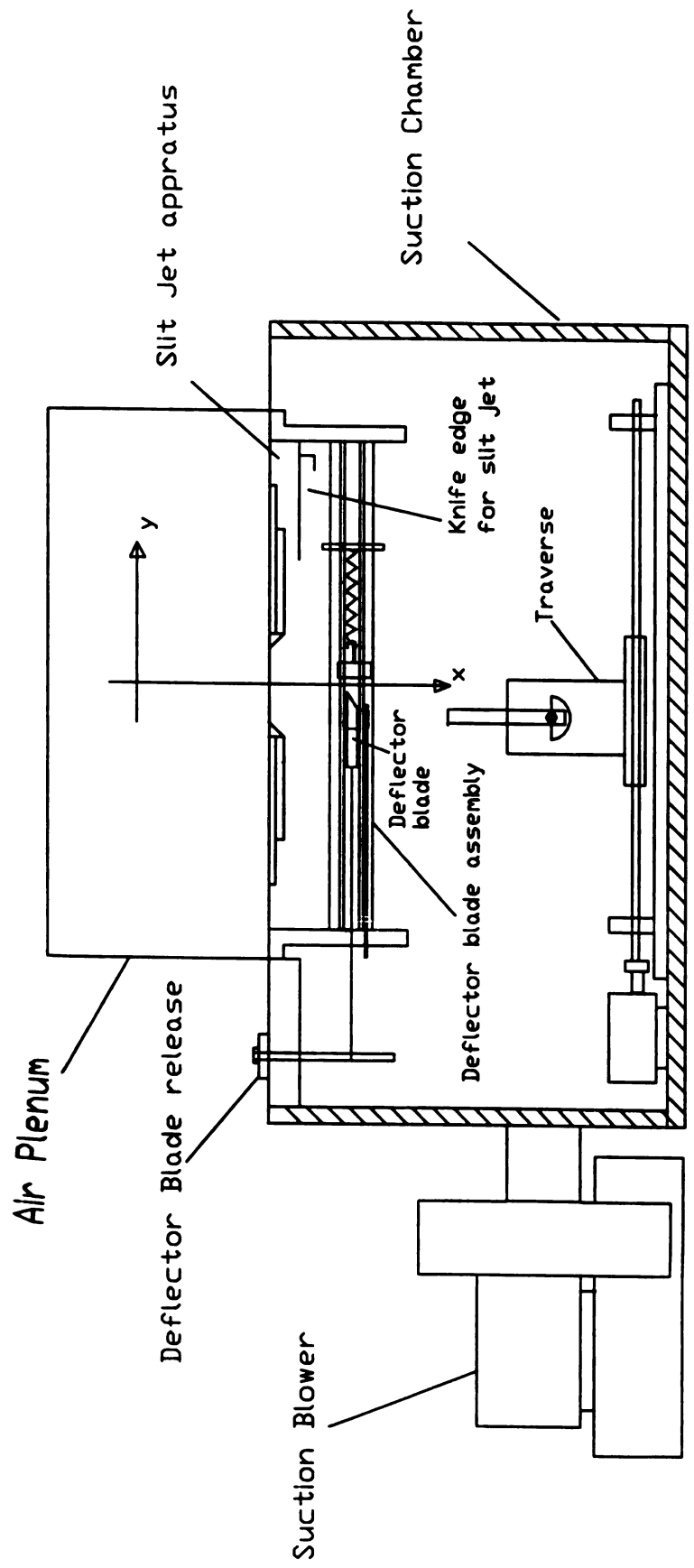

Figure 7. Experiment Facility Used in the Experiment.

DB
Center
DB

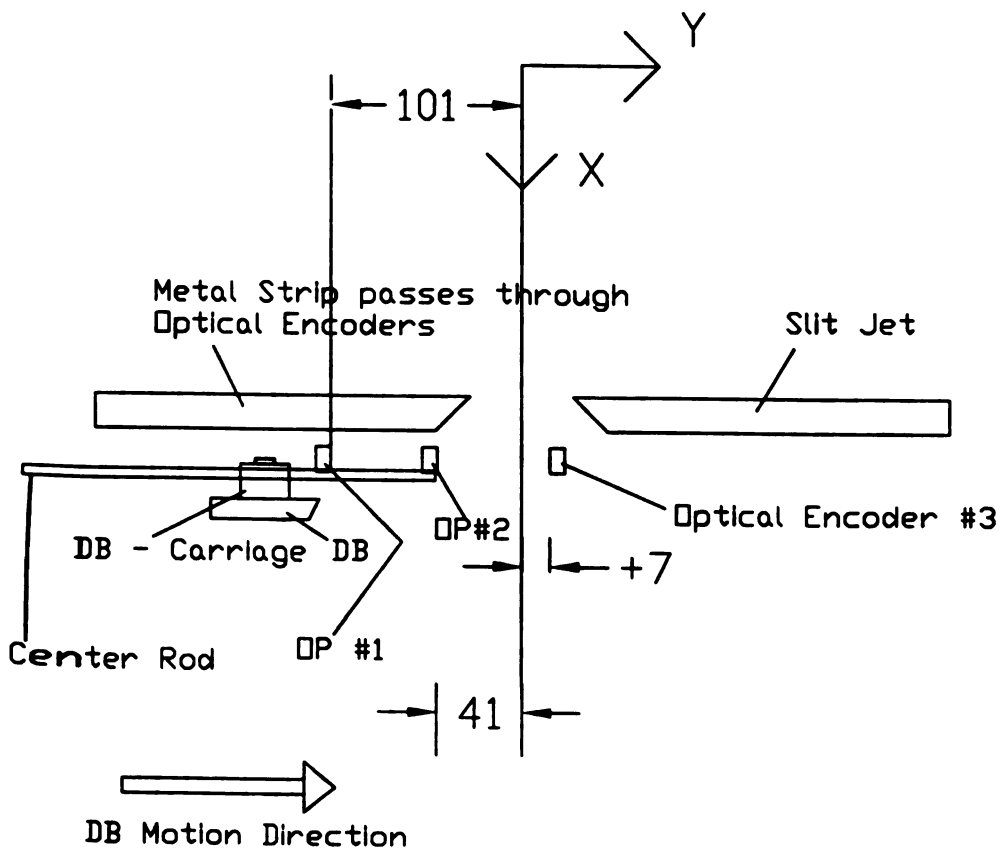

Figure 8. Set up for transient detection of DB

Optical Encoder Voltage Response

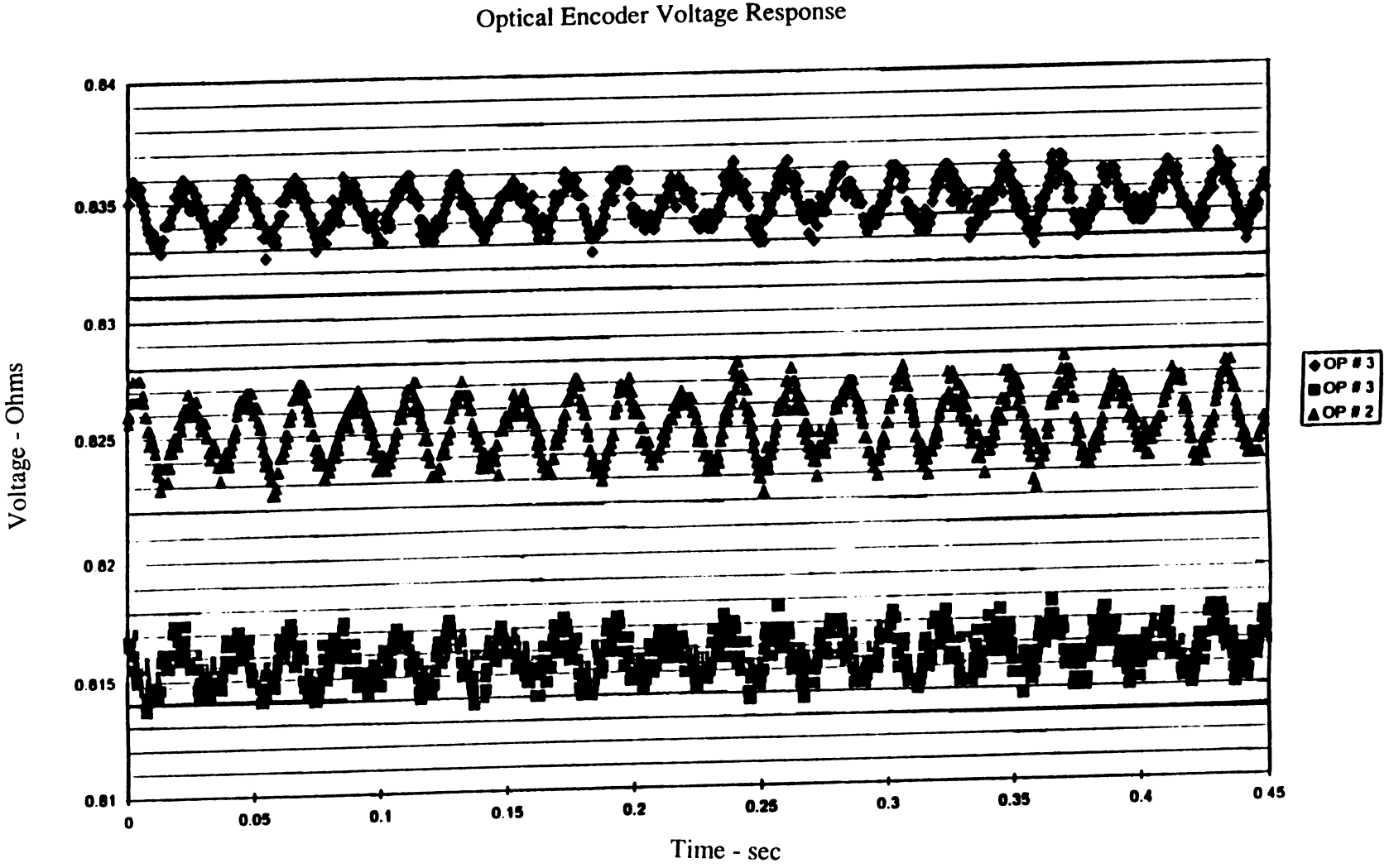

Fig 9. Optical Encoder Voltage response.

Optical encoder response to moving deflector blade

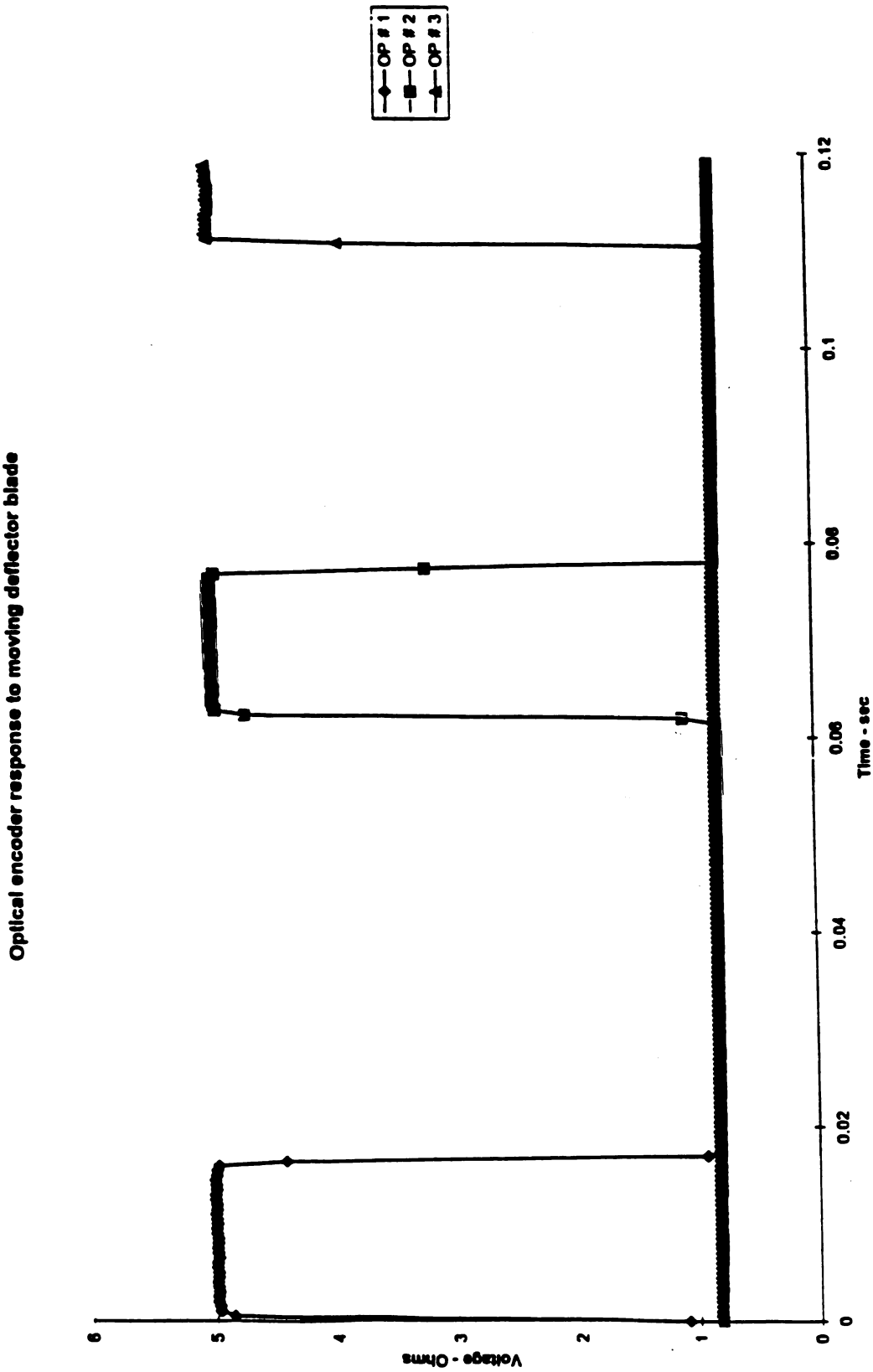

Fig 10. Optical Encoder response to moving blade.

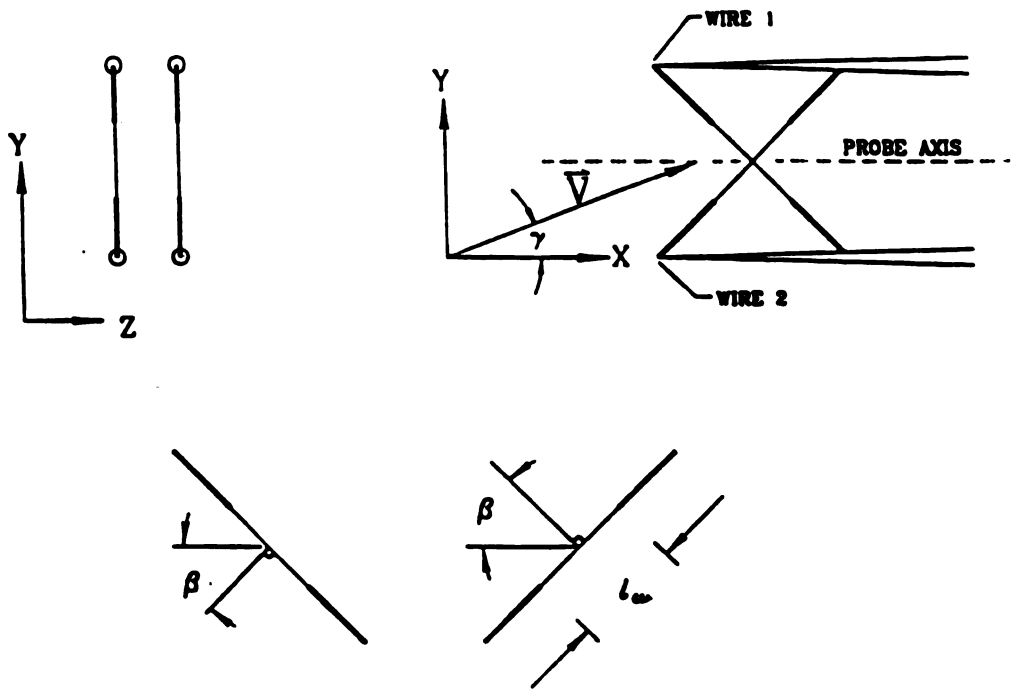

Fig 11. Schematic of X-array hot-wire probe.

Tuft p

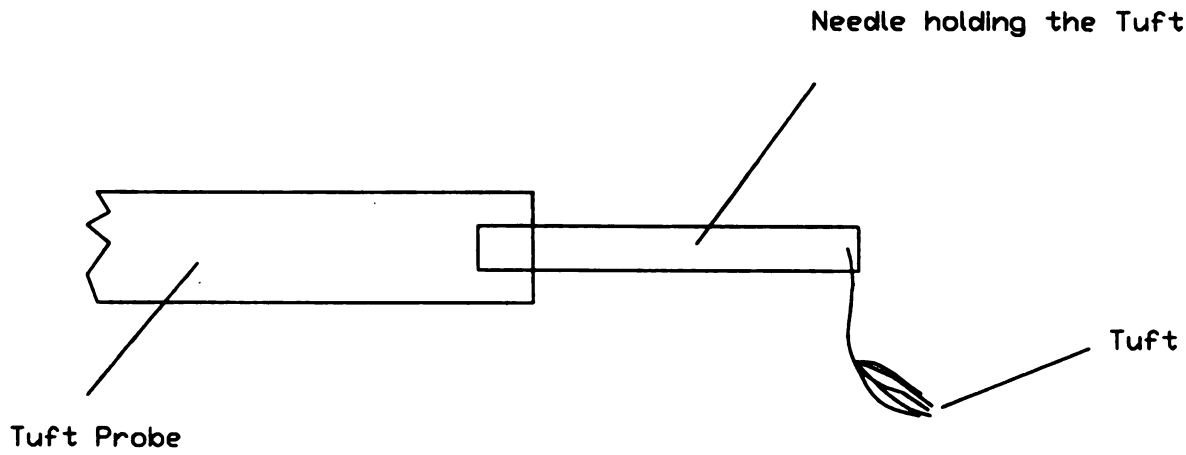

Figure 12. Tuft probe used for measuring the steady state angles

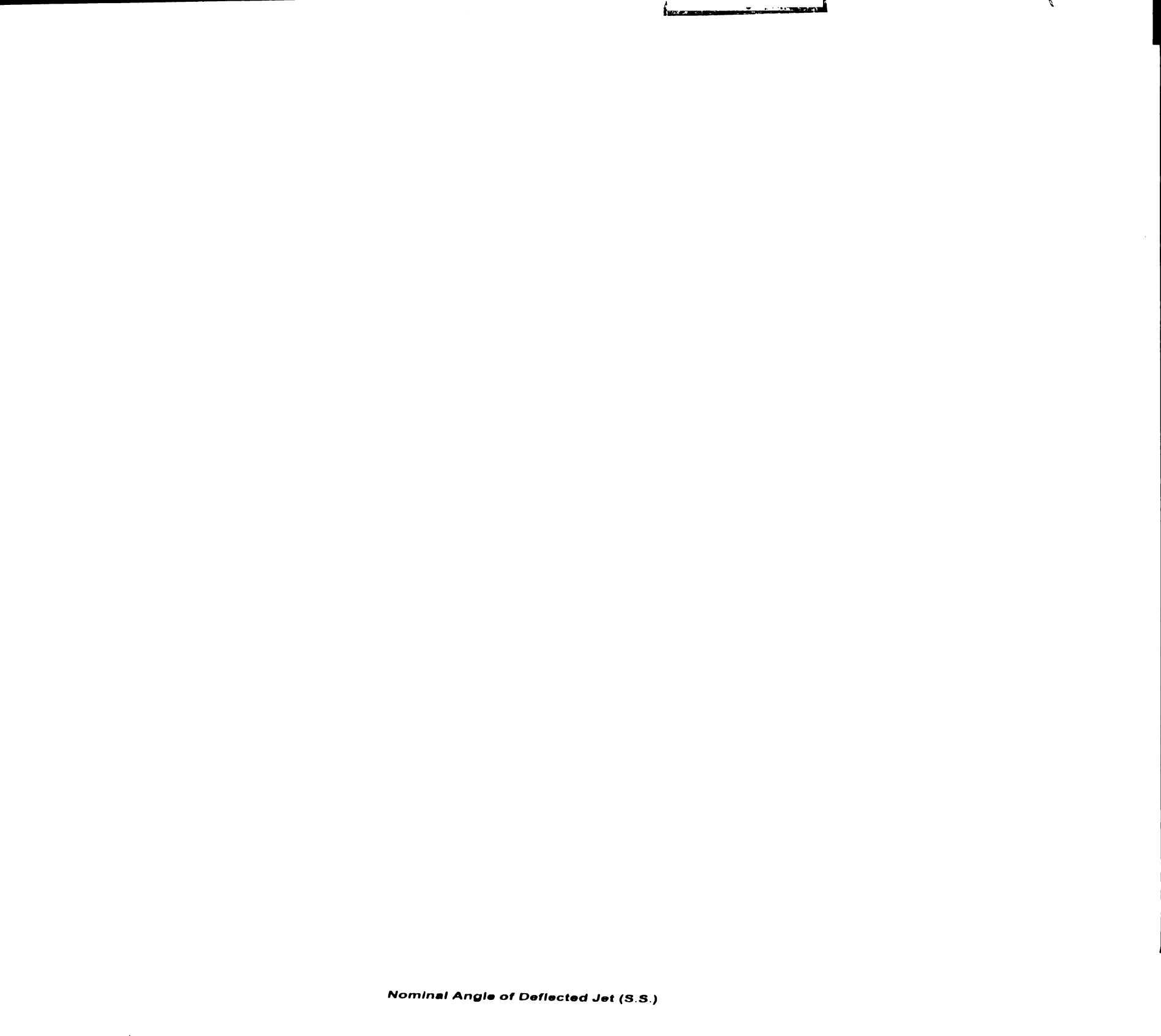
Nominal Angle of Deflected Jet (S.S.)

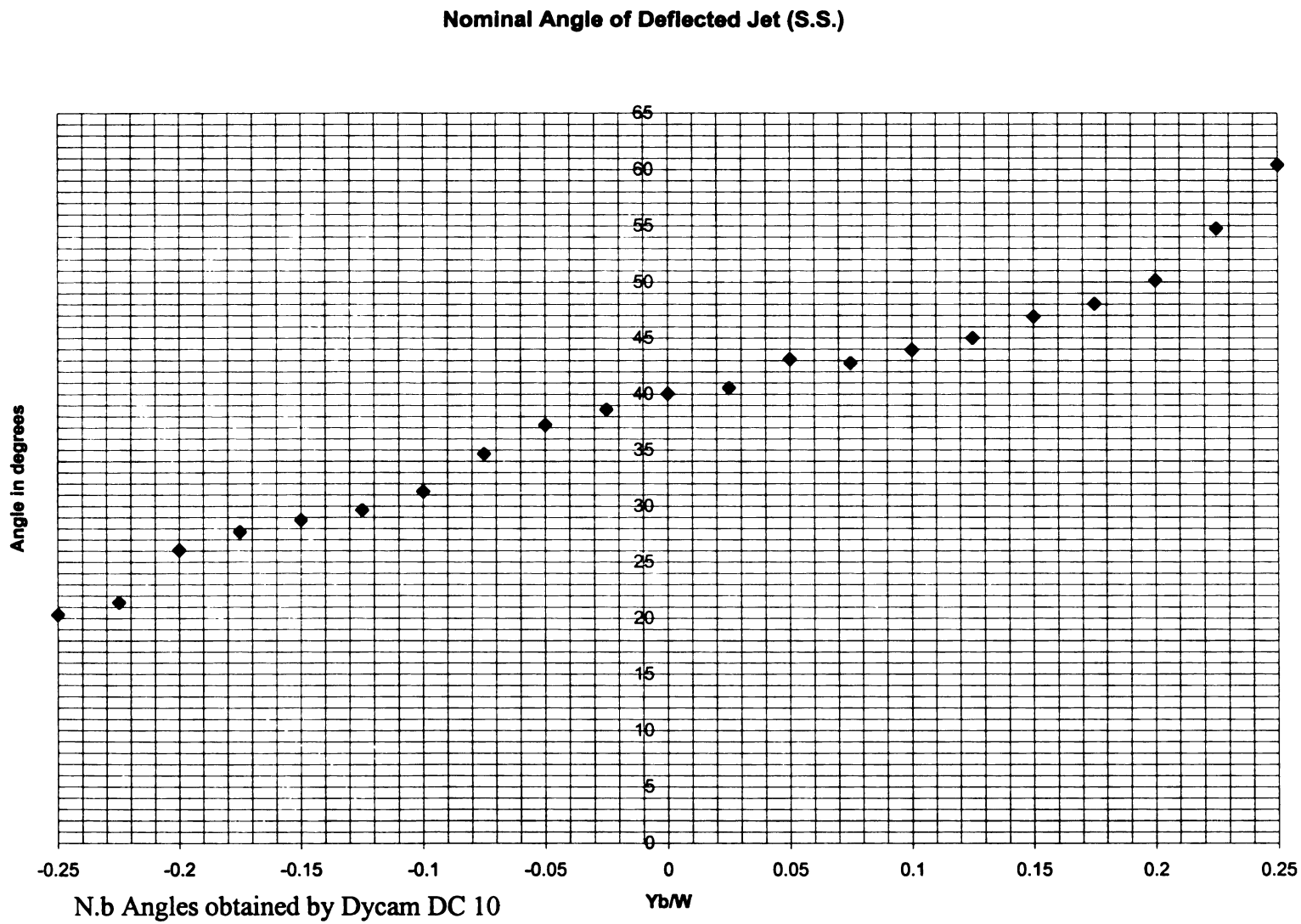

Figure 13. Nominal Angle of Deflection Measured by DYCAM for Yb/Wj = ∞

3.1 In

Th
proce
state
posit
Sect
3.5 (

3.2

ger
po
us
fo
je

d

3. DATA PROCESSING

3.1 Introduction

The information provided in the following section describes the data acquisition and processing. Section 3.2 describes how the mean flow angles were achieved for the steady state measurements. By "steady state" we mean that the blade was placed at a certain position in the flow field. Section 3.3 describes the processing algorithm for the probes. Section 3.4 describes how the position of the moving deflector (DB) was determined and 3.5 deals with further details for the reduction of the data.

3.2 Digital Camera Processing

An initial set of observations with the digital camera were recorded to establish the generic attributes of the deflected jet. Following these observations, the DB was positioned at the locations: $-10 \text{ mm} \leq y_B \leq 10 \text{ mm}$ (or $-0.25 \leq Yb/Wj \leq 0.25$) and the tuft was used to identify the flow angles within the deflected jet. (A series of y positions was used for this assessment, the individual tuft angles were averaged to record "the" angle of the jet.)

These data are presented in figure 13. As shown, there is a systematic increase of the deflection angle with respect to the DB position (y_B).

3.3 X-

An X
deflecti
of the p
voltage
were th
The
the con
the hot
to the w
this con

In the ab
between
between
equation

3.3 X-Array Calibration and Processing

An X-wire was used to provide two components of the velocity in the plane of deflection of the main flow. The plane of the probe is the plane parallel to the two wires of the probe, Figure 11 . The processing of the X-array hot-wire probe required two voltages from the wires in the probe to be known at the same instant. These voltages were then processed together to provide flow speed, Q (t) and also γ (t) the probe angle.

The simplest X-array processing algorithm is based on the "cosine law" and deals with the concept of effective cooling velocity (Bradshaw (1975)). This concept suggests that the hot wires in the X-array are only cooled due to the velocity component perpendicular to the wire, the flow coming at an angle nearly parallel to the inclined wire is ignored; in this concept. The effective cooling velocity "Qeff" is given by the relation.

$$Q_{eff} = Q \text{ Cos. } (\beta - \gamma) \tag{1}$$

In the above equation γ-angle was termed as the flow angle, and is defined as the angle between the axis of the probe and the in plane velocity vector, the angle β is the angle between the axis of the probe and the line perpendicular to the hot wire . The above equation can then be rewritten as ,

$$Q_{eff} = Q \text{ [Cos. } (\beta) \text{ Cos. } (\gamma) + \text{ Sin } (\beta) \text{ Sin } (\gamma) \text{]} \tag{2}$$

Substitu

We get

The two

U and V

The valu

be trans

Substituting the values,

$$U = Q \cos(\gamma) \tag{3}$$

$$V = Q \sin(\gamma) \tag{4}$$

We get the following equation,

$$Q_{eff} = U \cos(\beta) + V \sin(\beta) \tag{5}$$

The two sensors in the X-array are the used to solve the above equation for the unknown U and V by,

$$Q_{eff} = U \cos(\beta) + V \sin(\beta+) \tag{6}$$

$$Q_{eff} = U \cos(\beta-) + V \sin(\beta-) \tag{7}$$

The value of the "β" is determined from the calibration data , the above two equation can be transformed as ;

Wher

in cas

The

large

mod

i.e.

wh

th

A

m

co

pe

$$Q_{eff} = [(E^2 + A(\gamma = 0)) /(B (\gamma = 0)/ \text{Cos. } (\beta)^n]^{1/n(\gamma=0)} \quad (8)$$

$$Q_{eff} = [(E^2 .- A.(\gamma=0)) /(B (\gamma=0) / \text{Cos. } (\beta.)^{n-})]^{1/n-(\gamma=0)} \quad (9)$$

Where the - and + indicate the voltages and coeff. associated with -β and +β sensors , but in case of an X-array we have $Q=(U^2 + V^2)^{1/2}$ and $\tan^{-1} (v/u) = \gamma$, also .

The above "law" is valid for flow angles up to +/– 12 degrees (Foss et.al (1986)) but for larger angles of deflection or variation in the flow angles , the cosine law has to be modified ; because then the influence of the flow coming to the hot wire at a larger angle , i.e. parallel to wire would also added . Thus the Cosine law can be modified to

$$Q_{eff} = Q (\text{Cos}^2 (\beta–\gamma) + k^2 \text{Sin}^2 (\beta–\gamma)) \quad (10)$$

where the additional term $k^2\text{Sin}^2(\beta–\gamma)$ takes in account the cooling of the hot wire due to the "tangential: velocity, and the term k^2 is determined by the calibration data.

Alternatively, the algorithm described in Foss et.al (1995) provides a method by which the magnitude (Q) and direction (γ) of the local velocity can be determined. In this, the concept of speed-wire and an angle-wire is used. That is, the wire which is more perpendicular to flow direction is more responsive to the velocity magnitude and this was

designated

designated

The pr

angle of th

was repeat

γ). These

where n=n

At a giv

measured v

$\eta =$

In combina

is possible

convergent

0.5 degrees

In this a

relationship

of the wires

designated as a "speed-wire". The second wire, which is more tangential to the velocity, is designated as the "angle-wire".

The processing algorithm required an extended calibration data set; specifically the angle of the probe with respect to the flow was varied at a given speed and this process was repeated for six flow speeds. This provides the speed and the angle wire data as E(Q, γ). These data were fit to a modified the Collins and William relationship as:

$$E^2(Q, \gamma) = A(\gamma) + B(\gamma)\ Q^{n(\gamma)} \tag{11}$$

where $n=n_e$ also.

At a given speed Q, there is a unique value of the angle wire voltage: E(Q,0) and a measured voltage: E(Q,γ). These values are combined to define η as

$$\eta = \left[\frac{E_a(Q\gamma)}{E_a(Q,0)} - 1 \right] \tag{12}$$

In combination, (11) and (12) provide a pair of relations that can be iteratively solved. It is possible to show that the nature of the smoothed calibration data cause this to be a convergent calculation. The iterations are continued until convergence to a change in γ of 0.5 degrees is obtained.

In this algorithm, the initial γ value is determined by using the cosine effective cooling relationship and the technique of Bradshaw (1975) to infer (Q, γ) from E_1 and E_2 (voltages of the wires), as stated earlier as:

$$E_1^2 = A_1 + B_1 [Q \text{ Cos. } (\beta - \gamma)]^{n1}$$

$$E_2^2 = A_2 + B_2 [Q \text{ Cos. } (\beta_2 \gamma)]^{n2}$$

Convergence is achieved for the range $-36 \leq \gamma \leq 36$ degrees.

Thus knowing "γ"and the velocity vector is speed wire. The value of Q_{eff} from previous calculations, is the first estimate of the flow speed. The γ is computed as $\gamma = \gamma(n)$ and n is given by the Equ. 12.were $E(\gamma, Q)$ is the measured voltage of the angle wire and $E(O, Q)$ is computed, for the angle wire. The flow speed can be computed from equation 8, and 9. Using speed wire voltage and distinct "γ" values closer to that interpolated results between the two equations.

The speed wire/angle wire processing algorithm has been shown to immerse the sensitivity of the probe to $\pm$ 36 degrees. Throughout this experiment the X-array has been used to take measurements: given the two-component velocity fields.

3.4 Transient Velocity Calculations

When the DB is in the motion from OP1 to OP3 , it is desired to know the U and V velocity component of the jet, which is being deflected by moving DB with the help of a static probe(X- array). The speed of the DB under the spring force is not uniform. But with the help of the OP,s we are able to determine the position at a certain instant in time , by analyzing the time series of voltages.

Then

using

const

corre

As t

each

3.5

A

locat

norm

Berr

tunn

Then by correlating the position of the DB or Yb/Wj , with the time series of the hot wire using quadratic polynomials of "t" in the form of , At^2+Bt+C (where A,B,C are constants of the equation), We were able to find the two velocity components corresponding to a specific position of the DB in space.

As there were variation in speed of the DB over each run ,so individual co-relations for each data set where required to estimate the U and V components.

3.5 Normalization of Data

All the data in this study is presented in non-dimensional form. The measurement locations are normalized by the total width of Sj and the velocity components are normalized by the incoming velocity, measured by the pressure transducer and utilizing the Bernoulli equation (a pressure differential is taken between the atmosphere and the wind tunnel and is used in the Bernoulli equation).

4. RESULTS AND DISCUSSION

4.1 Introduction

The experiment was conducted in two parts. Results of the first part deals with the steady state measurement of the Sj under the influence of the pre-positioned DB. The results of this is then used as the basis of the second part of the experiment when the DB is in transient motion. Sections 4.2 - 4.3 deals with steady state measurements and section 4.4 through the end of the chapter, deal with the transient study.

4.2 Steady State Measurements

4.2.1 Velocity profile with out DB

To conduct the steady state measurements, it was first to be decided what speed of the jet is to be used in the wind tunnel. As the pre-existing calibration unit in the turbulent shear flow laboratory has a limitation of 37 meters/second on it, so the speed selected for the measurement had to be less than this in order to have a proper calibration done for the hot wire. The speed was then selected to 35 meters/second, and the same was maintained in the wind tunnel, with the help of the calibration curve chosen for it. The hot-wire sensor was calibrated for six speeds ranging from 1 to 37 m/s and then inserted into the wind tunnel.

The velocity survey was carried out from $-1 \leq Yp/Wj \leq 1$ at $X/Wj = 1.5$ in the wind tunnel using the hot wire probe; the symbol Y_P represents theY location of the probe. The $\langle U \rangle/U_0$ distribution is shown in Figure 14. From this it can be observed that the slit-jet flow is not symmetrical about the central axis, and the most likely reason for this is the pressure of the suction blower on the $y<0$ side of the tunnel. The shift in the profile of the jet is found to be 2 mm from the center line inferred from the figures 14 to 17.

4.2.2 Velocity profile for Yb/Wj = -0.5

The DB was positioned at Yb/W = -0.5, and the velocity profile was obtained with 1 mm incremental traverse of the x-array probe; see Figure 18. The non-symmetrical behavior of the jet is again evident in these data. (Note that the probe was limited to Yp/Wj = -0.5 because of the DB's position). By placing the DB at -0.5 we observe that the fluctuation of U and V components has dropped by 36% and 35% respectively; see Figures 20 and 21. It is inferred that the DB has interrupted the regular formation of the small scale motions that are known to exist at the edges of the shear layer. It is these motions that are assumed to be responsible for the large fluctuation levels of the slit jet; see Figure 19 and 20.

4.3 V

Fo

, since

45^0 d

degre

4.3.1

W

obtai

has d

Furth

veloc

figur

fluct

featu

value

Note

4.3 Velocity Profile for Deflected Flow

For a deflection angle of 30^0 of flow, the probe was positioned parallel with the jet axis , since the X-array had a cone of $\pm$ 36 degrees in which it can capture the velocity. For the 45^0 deflection the probe was oriented at 25^0 giving a cone of observation: 9 to 81 degrees.

4.3.1 Velocity Profile for Yb/Wj = -0.1

When the DB is placed at Yb/Wj = -0.1 the angle of deflection was 30 $\pm$ 4 degrees as obtained from the DYCAM. The resulting velocity profile figure 21, shows that <U>/Uo has deflected to 6 mm from the center axis of the slit-jet in the direction of the insertion. Furthermore, Figure 21 and Figure 22 reveal a reduction in the U-component of the velocity with an increase in the V-component . However, looking at the <V~> / Uo ,see figure 24 , we observe that the jet profile is maintained , as there is minimum value of fluctuation in the V component when the <U> value at its maximum . Another distinct feature of the deflected jet is that the y-component velocity: <V> only exhibits positive values, the magnitude of which (as compared to the previous plot) has also increased. Note that the peak magnitude of <V> is half of <U>.

4.3.2 Velocity Profile for Yb/Wj = 0.125

A deflection of $45^0 \pm 1.5$ degrees results when the DB is place at Yb/Wj = 0.125. For this condition, the probe is oriented at 25^0 so that the deflected jet can be captured by the hot wire sensor. The velocity profiles obtained are restricted to $0.125 < Yp/Wj < 0.1$, because of the width of the DB. A remarkable increase in the <V> component of the velocity is indicated by these data. Note that $<V> \approx <U>$; see Figures 25 and Figure 26. In both of these figures we observe that the jet has become broader, as the stream lines of the jet are now under a strong influence of the V-component of the velocity which causes the widening of the jet. The jet edge has shifted to $y/Wj \approx 0.4$, i.e., 16 mm from the central line of the slit-jet.

4.3.3 Velocity Profile for Yb/Wj = 0.175

For the DB at Yb/Wj = 0.175, the angle of deflection is 48^0. The increase of the deflection angle is associated with a further reduction of the <U> component and <V> component. However, the <V> component is comparable to that of <U>. For Yb /Wj = 0.175, <U> is reduced by about 30% and <V> is increased to about 25% of Uo. The magnitude of the deflection for this case was large enough to satisfy the initial objective of a complete lateral displacement of the jet column. Hence, this case was selected for the study of the transient effects, see figures 27 to 28 .

In the intended practice there will be a set of moving blades that would be used for guiding the air flow in or out of the auxiliary plenum, thus maintaining the plenum at a constant pressure.(Refer to fig 1). Therefore, in the following section, a study (Transient) is carried out to determine the jet flow characteristics of the dynamic insertion of the DB.

4.4 Transient-Motion (DB) Study

4.4.1 Introduction

For the transient study of the experiment, the DB was run in the rails under the influence of the springs; and at the end of the travel it was stopped at a pre-determined position in the flow field to cause a deflection of the jet. With the knowledge from the steady state analysis, we know that when the DB is at 0.175, the jet would be totally deflected out of the slit-jet projected area to the y>0 side.

As the DB was run from one extreme to the other, see Figure 08 , the distance between the three IM was fixed and that of the first IM and the start position was also fixed. The distance between Op1 and OP2 was 60 mm and OP2 to OP3 was 48 mm, so once, the DB triggered OP1 it traveled 108 mm before stopping at +0.175 Wj.

4.4.2 Velocity of DB

There are six arbitrarily chosen positions for the X-array probes, i.e., Yp/Wj = -0.5, -0.2, 0.2, 0.4, 0.6, 0.8. as shown in the figure 29. All the measurements were executed using these locations. A single experiment was executed by releasing the DB at Yb=-200 mm=-5*Wj. The timing for the experiment was started as is passed the OP1 detector and continued until it came to rest at the termination: Yb=0.175*Wj. Twelve such experiments were executed for each position of the probe. Hence, 72 experiments were used to create the transient data reported herein.

For each run of the blade corresponding to the specific YP/Wj position, OP and hot-wire data were taken simultaneously.

In the study of the time series of the OP outputs, we observe that the velocity in between any specific two OP's is not constant. Of the total number of runs (72), the mean velocity of the DB calculated between OP1 and OP2 was 1.03 m/s with a standard deviation of 0.1487 m/sec and the mean velocity between OP2 and OP3 was 1.06m/sec with a std.dev of .0139 m/sec, giving nominal Vb/Uo of 0.03.

From the numerical values, it is obvious that the DB does not have a uniform velocity but it is in accelerated motion. Hence, a simple correlation between the blade speed and that of the hot wire time series was not possible. The correspondence between the blade speed between OP2 and OP3 and the position (Yb) was established as

4.5 Com

4.5.1 Flo

The flo

location, p

given Yb v

component

independer

revealed th

.Thus with

Yb/Wj , ca

state.. Thi

the transier

figure 32.

angles , see

these plots

is indicative

runs that is

$$y_B = y_B(OP2) + \frac{dy_B}{dt}(t - t(OP2))$$

4.5 Comparison of Steady State Results with Transient Results

4.5.1 Flow Angles.

The flow angles, recorded from the hot-wire readings for the 12 runs at each Yp location, permit the averaged angle from the transient condition to be evaluated for a given Yb value. The transient angle was calculated from the respective U and V velocity components . For each Yp the flow angle is dependent upon the position of the DB and is independent of the speed of it as shown in figure 30 and 31 respectively. In which it is revealed that for any chosen Yp and Yb <U>/Uo and <V>/Uo is independent of dYb/dt .Thus with the help of these two velocity components the angle obtained as function of the Yb/Wj , can be compared with the deflection angle obtained from the tuft in the steady state.. This direct comparison reveals a systematic trend wherein the flow angle $<\theta_{jet}>$ for the transient condition lags behind the value of $<\theta_{jet}>$ for the steady state condition see figure 32. The average value of the $<\theta$ jet > transient , is obtained from the histogram of angles , see figure 33 to 74. All these histograms are constructed from 12 runs . Seeing these plots it would be forth mentioning that , when the angles for each run is different , it is indicative of the vortices sheded by the jet . And when the angle is same for maximum runs that is the mean flow angle of the flow .

It is in

the pres

4.5.2 V

Vel

Yp val

profile

as the

the de

It is instructive to realize that this lag occurs for the low velocity ratio: $V_B/U_o \approx 0.03$, of the present experiment.

4.5.2 Velocity Profiles

Velocity profiles in the transient case can be reconstructed from the twelve runs at each Yp value. These profiles can be compared with the steady state profiles . The velocity profiles of <U> and <V> are shown in figure 75 to 98, and an overall behavior of the jet as the DB moves across the Wj is shown in figure 99 and 100, in which one can observe the deflecting trend of the Sj.

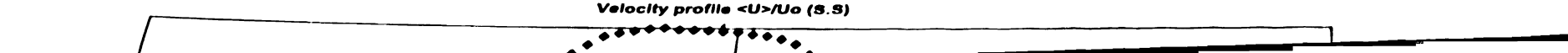
Velocity profile <U>/Uo (S.S)

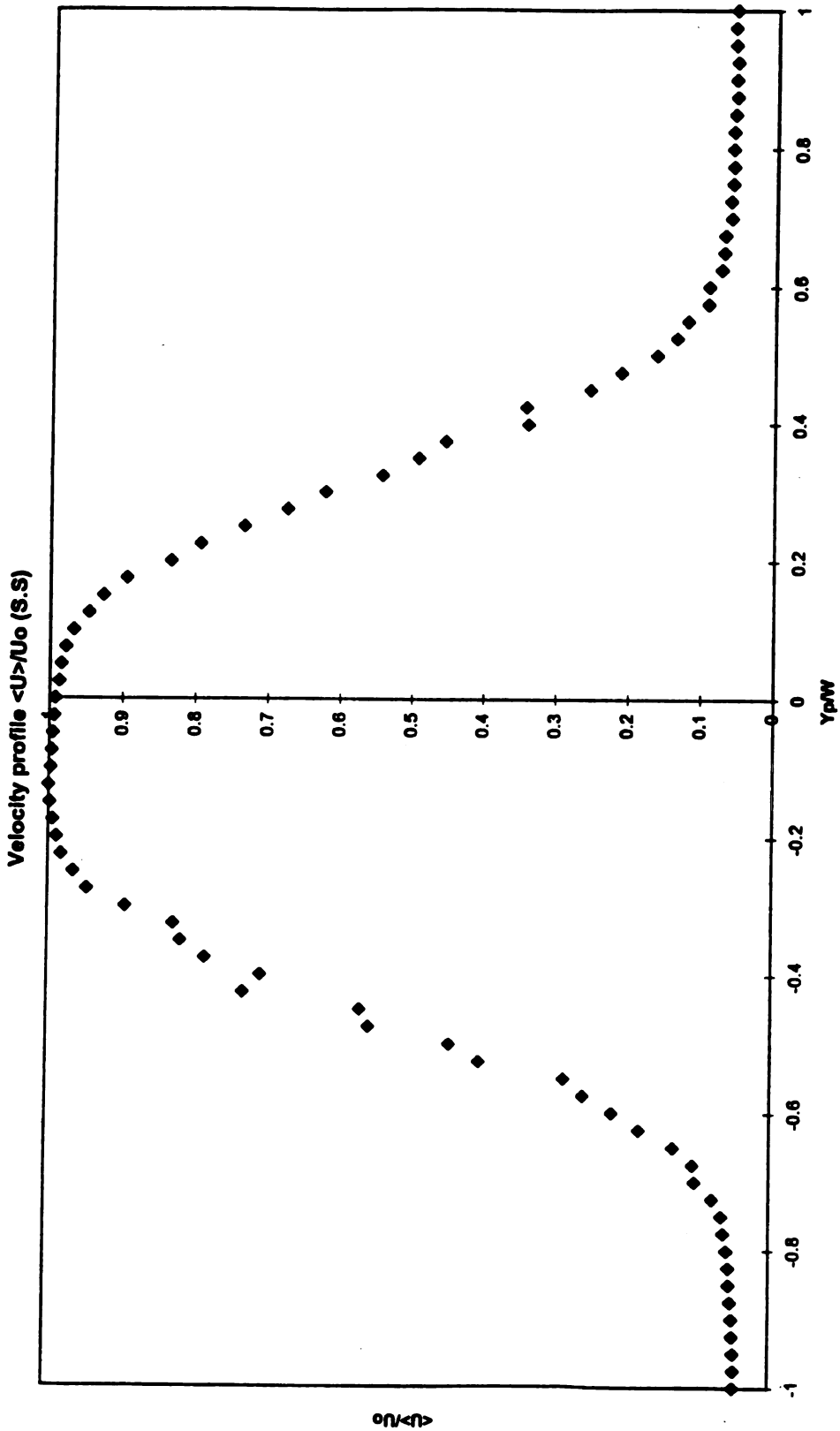

N.B Velocity profile at 60mm downstream of Sj with DB at infinty

Figure 14. Velocity distribution <U>/Uo at X/Wj=1.5 and Yb/Wj= ∞

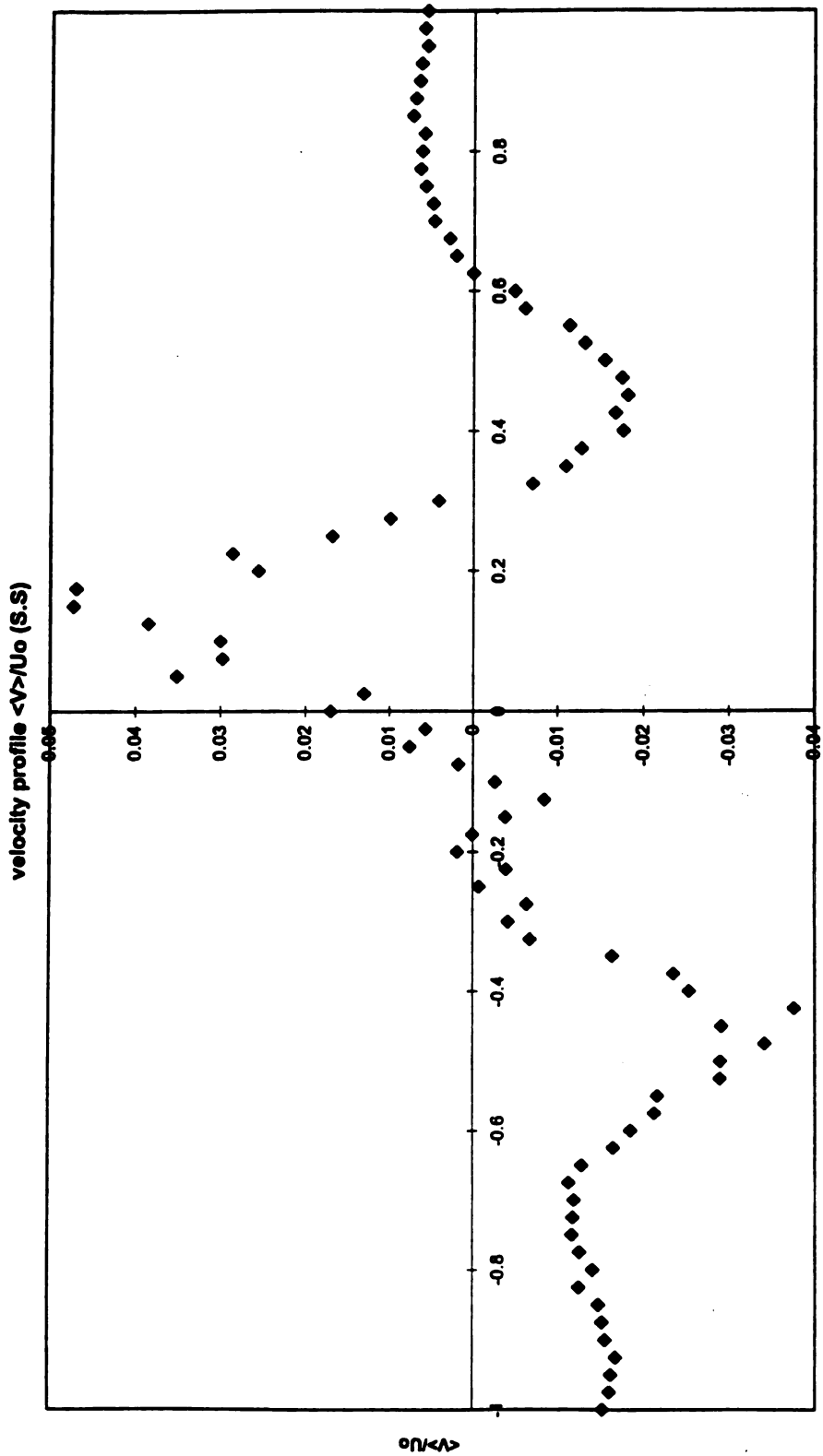

N.B Velocity profile at 60mm downstream of Sj with DB at infinty

Figure 15. Velocity distribution <V>/Uo at X/Wj=1.5 and Yb/Wj= ∞

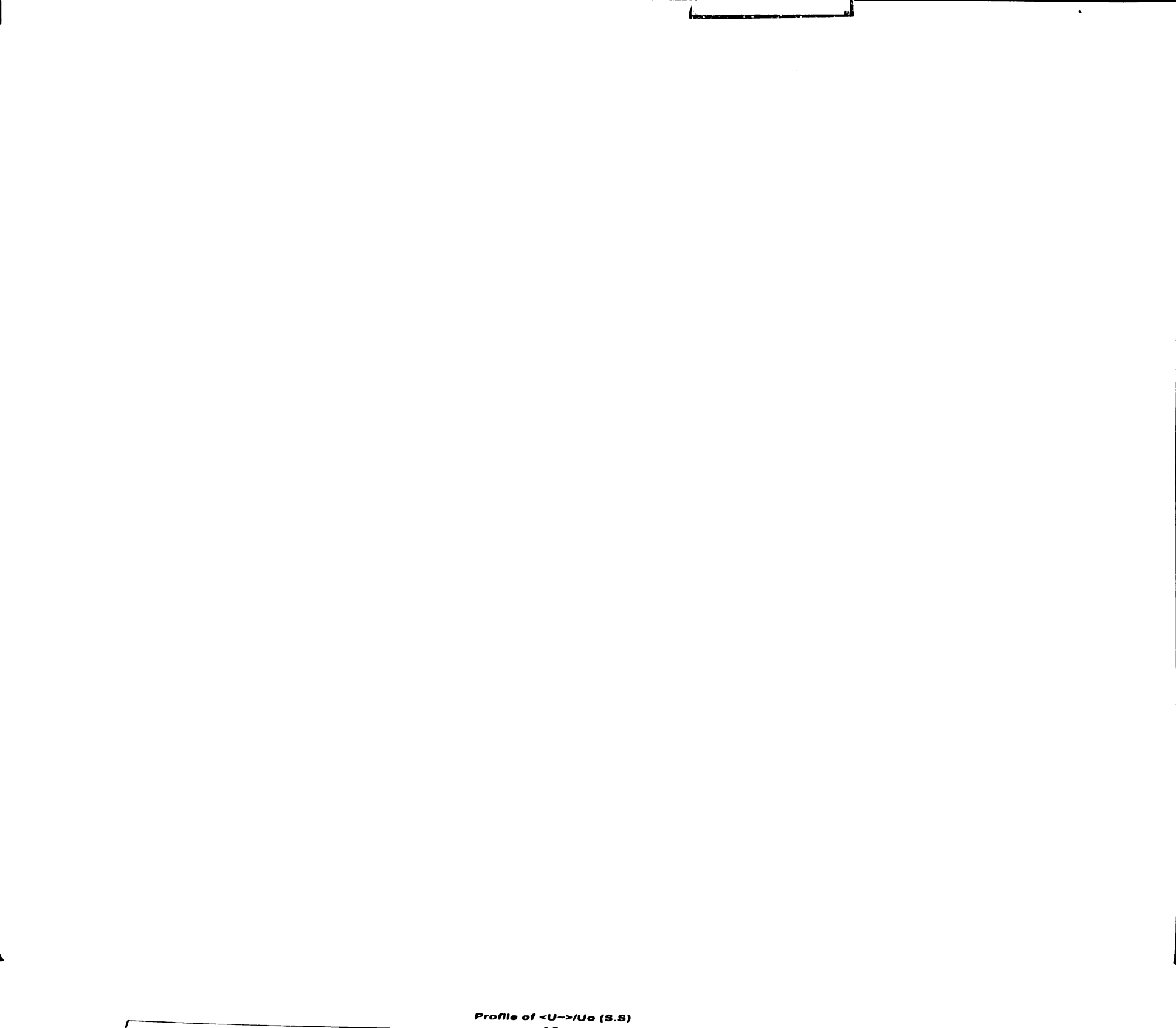
Profile of <U~>/Uo (S.S)

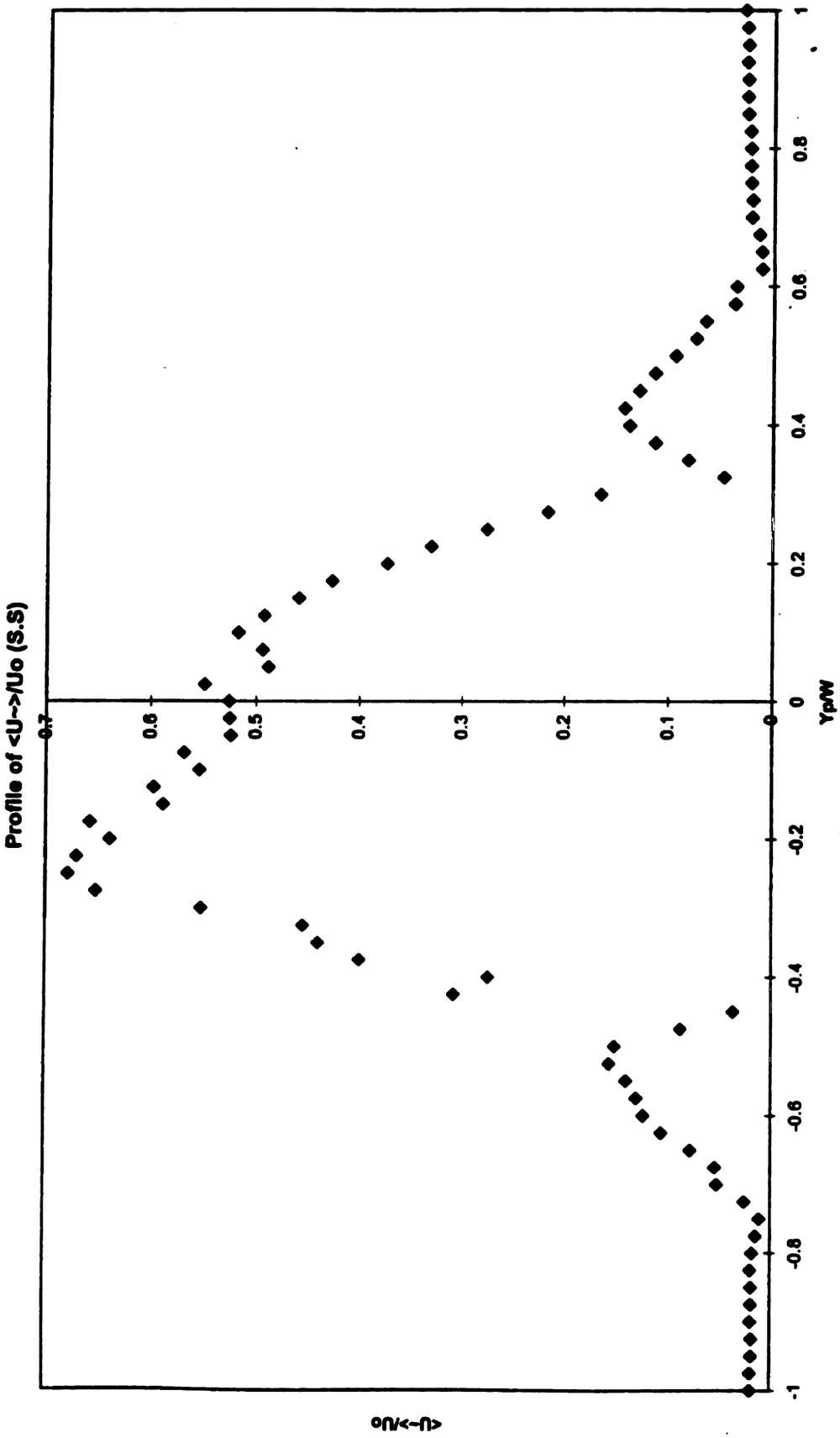

N.B Velocity profile at 60mm downstream of Sj with DB at infinty

Figure 16.U-rms at X/Wj=1.5 and Yb/Wj= ∞

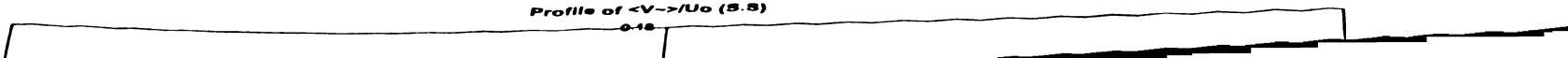

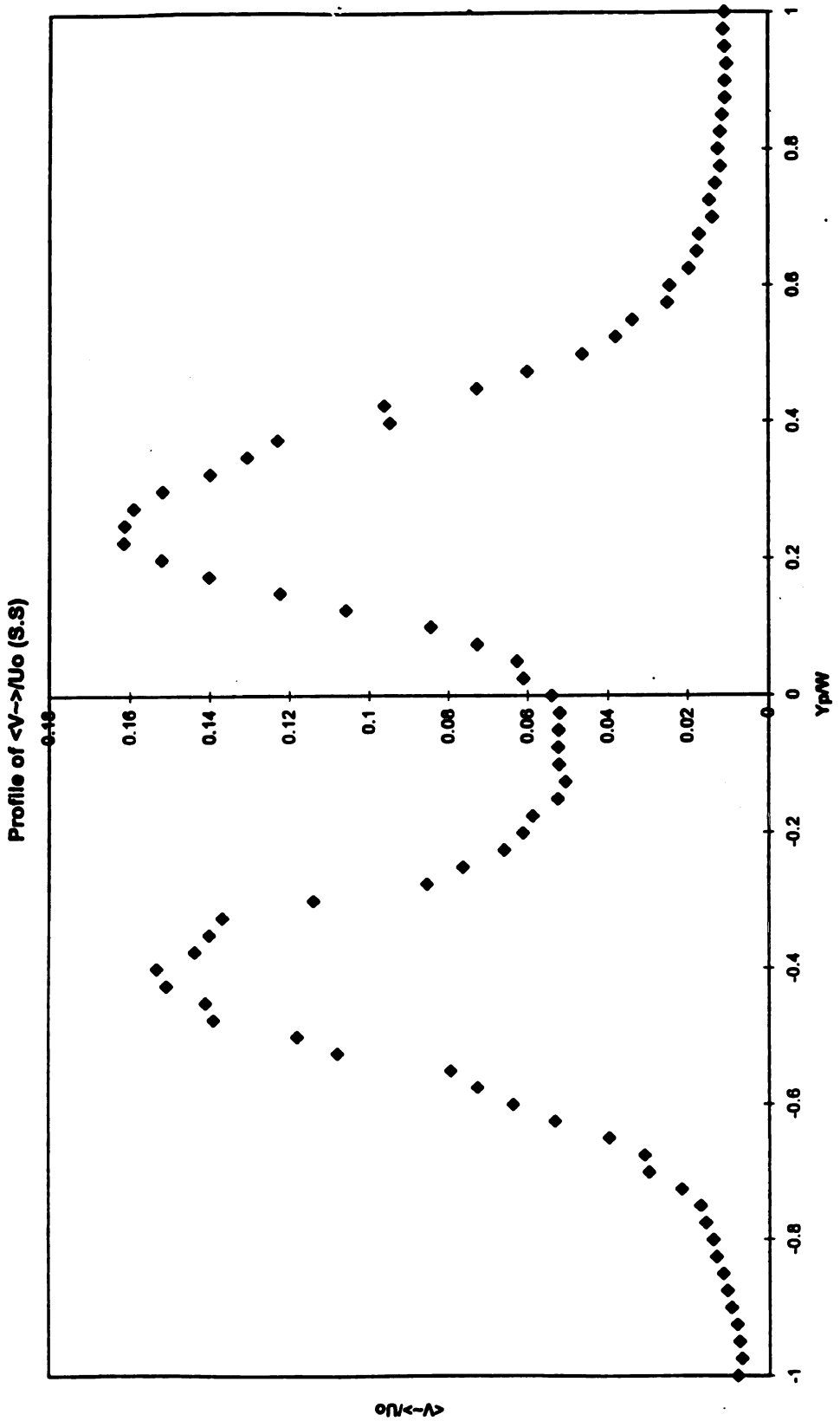

N.B Velocity profile at 60mm downstream of Sj with DB at infinty

Figure 17. V-rms. at X/Wj=1.5 and Yb/Wj = ∞

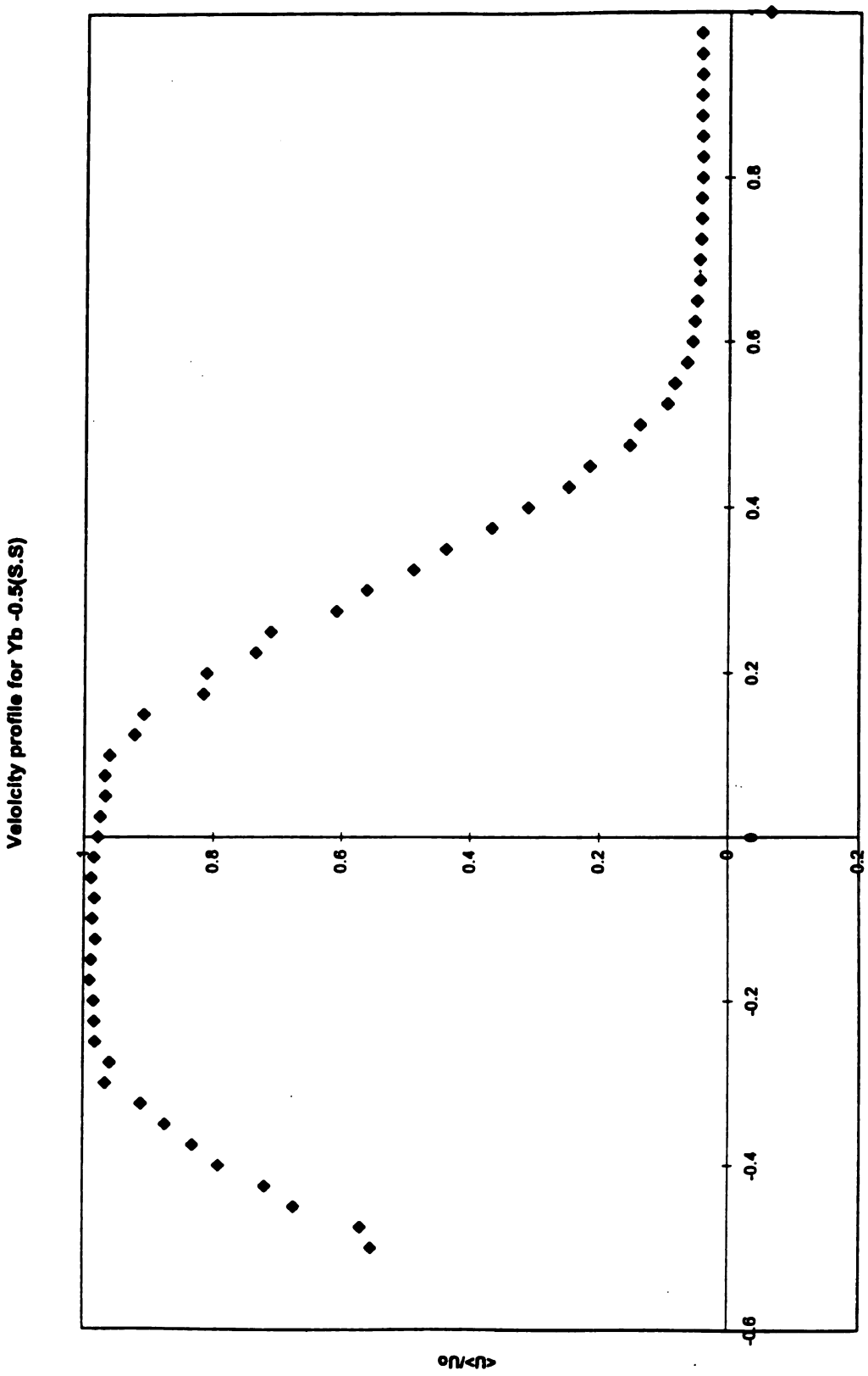

Figure 18. Velocity distribution <U>/Uo at X/Wj=1.5 and Yb/Wj= -0.5

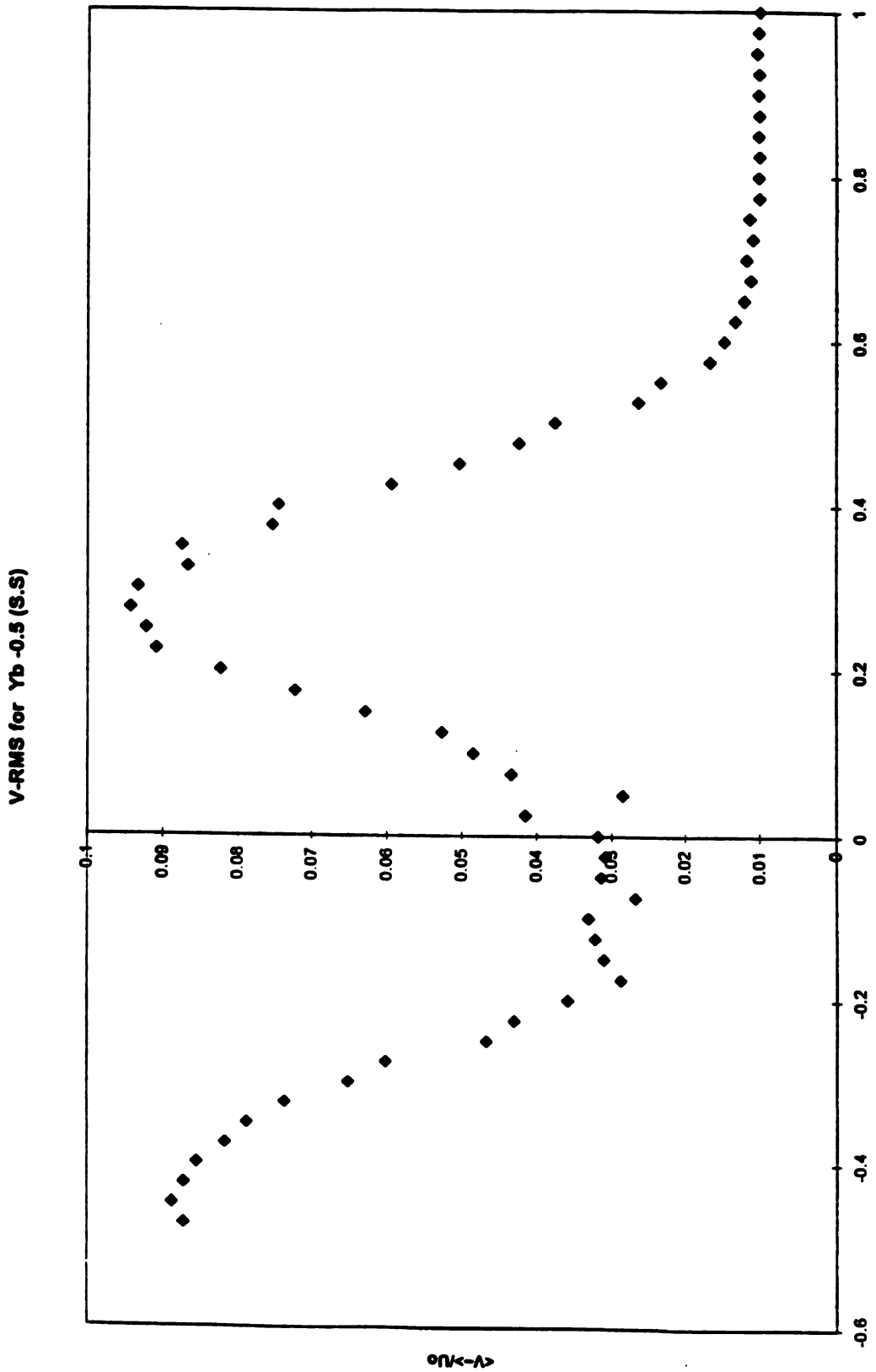

Figure 19. V-rms. for X/Wj = 1.5 and Yb/Wj= -0.5

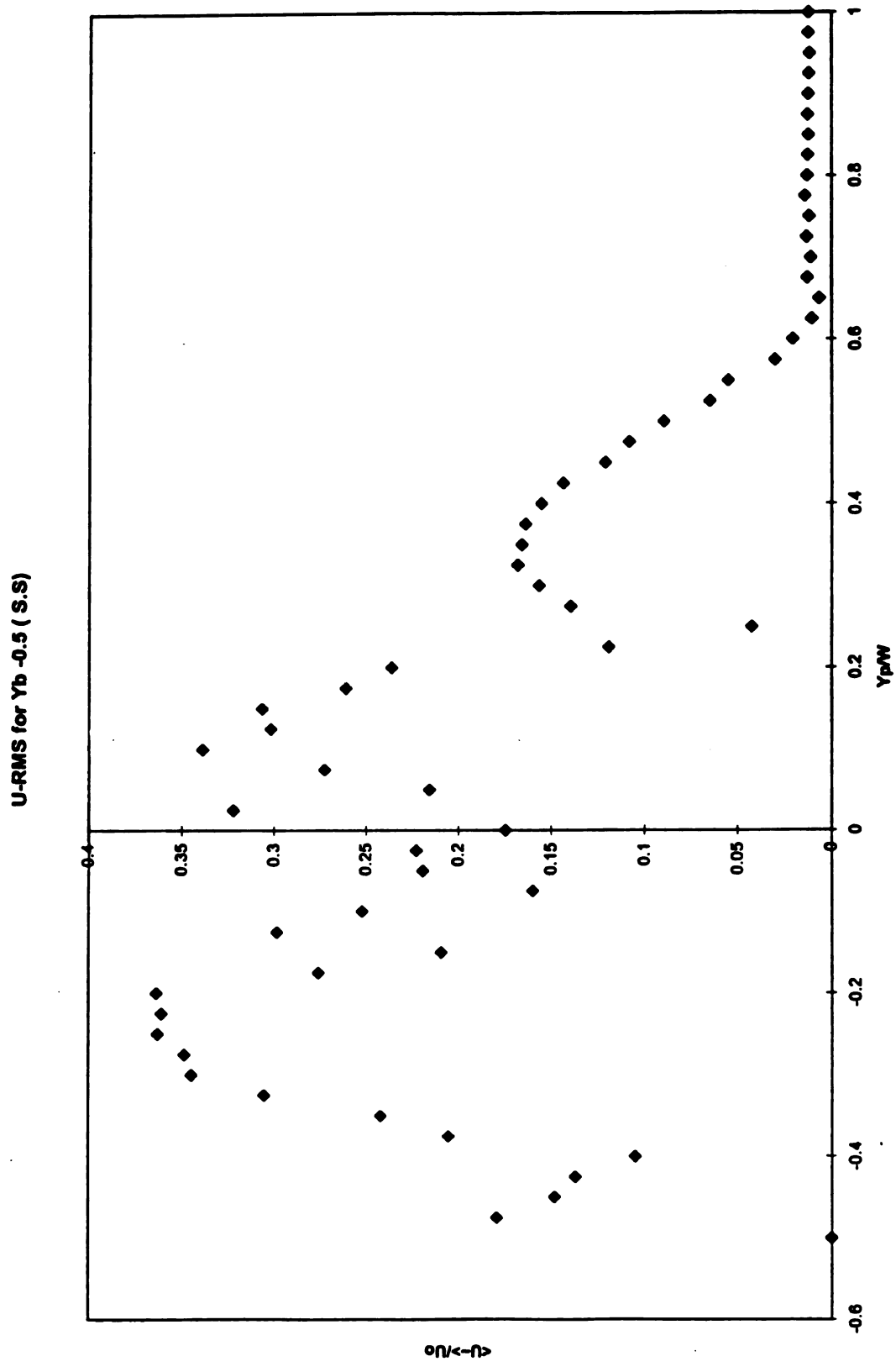

Figure 20. U-rms. for X/Wj = 1.5 and Yb/Wj = -0.5

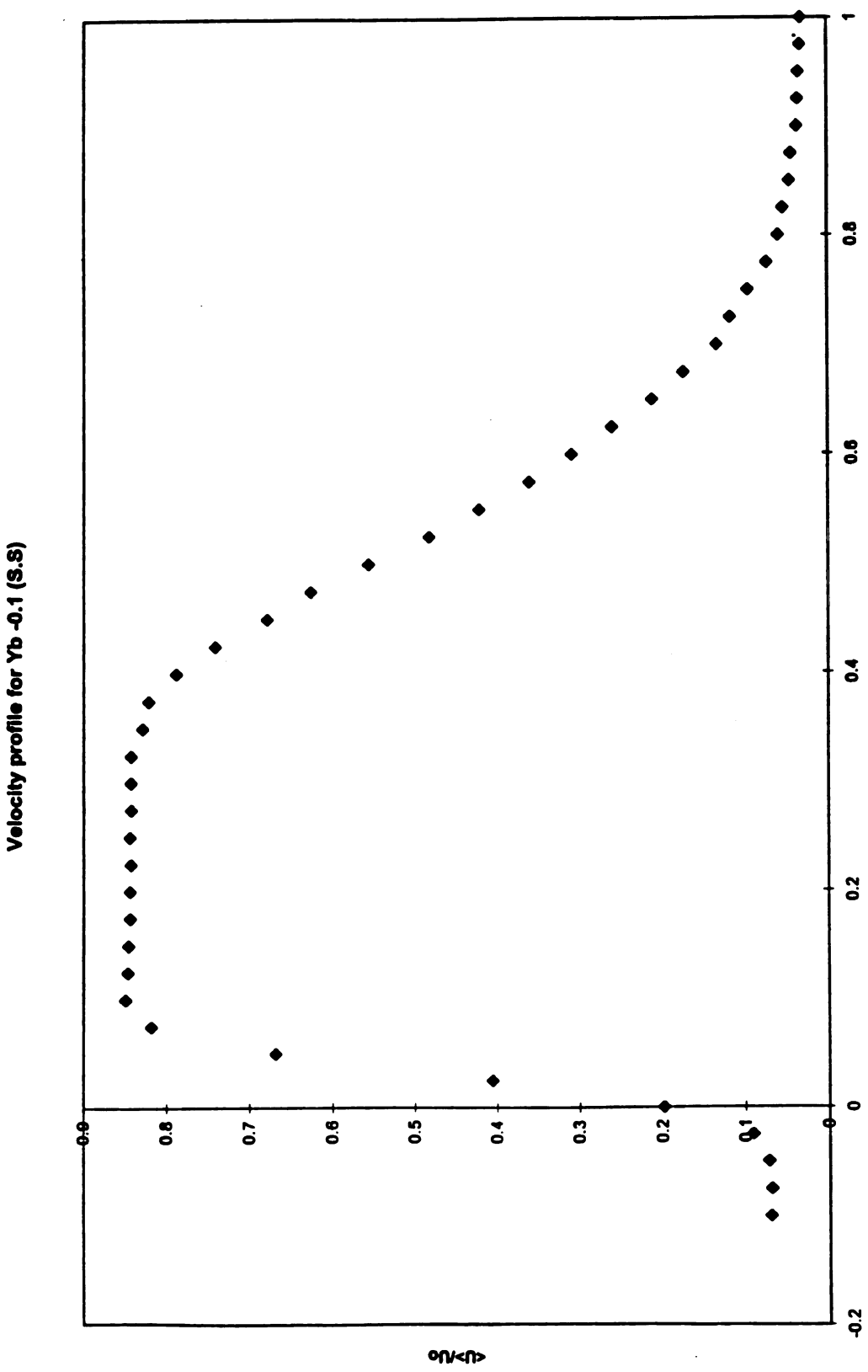

Figure 21. Velocity distribution <U>/Uo at X/Wj=1.5 and Yb/Wj= -0.1

(Nominal deflection angle of jet = 30 °)

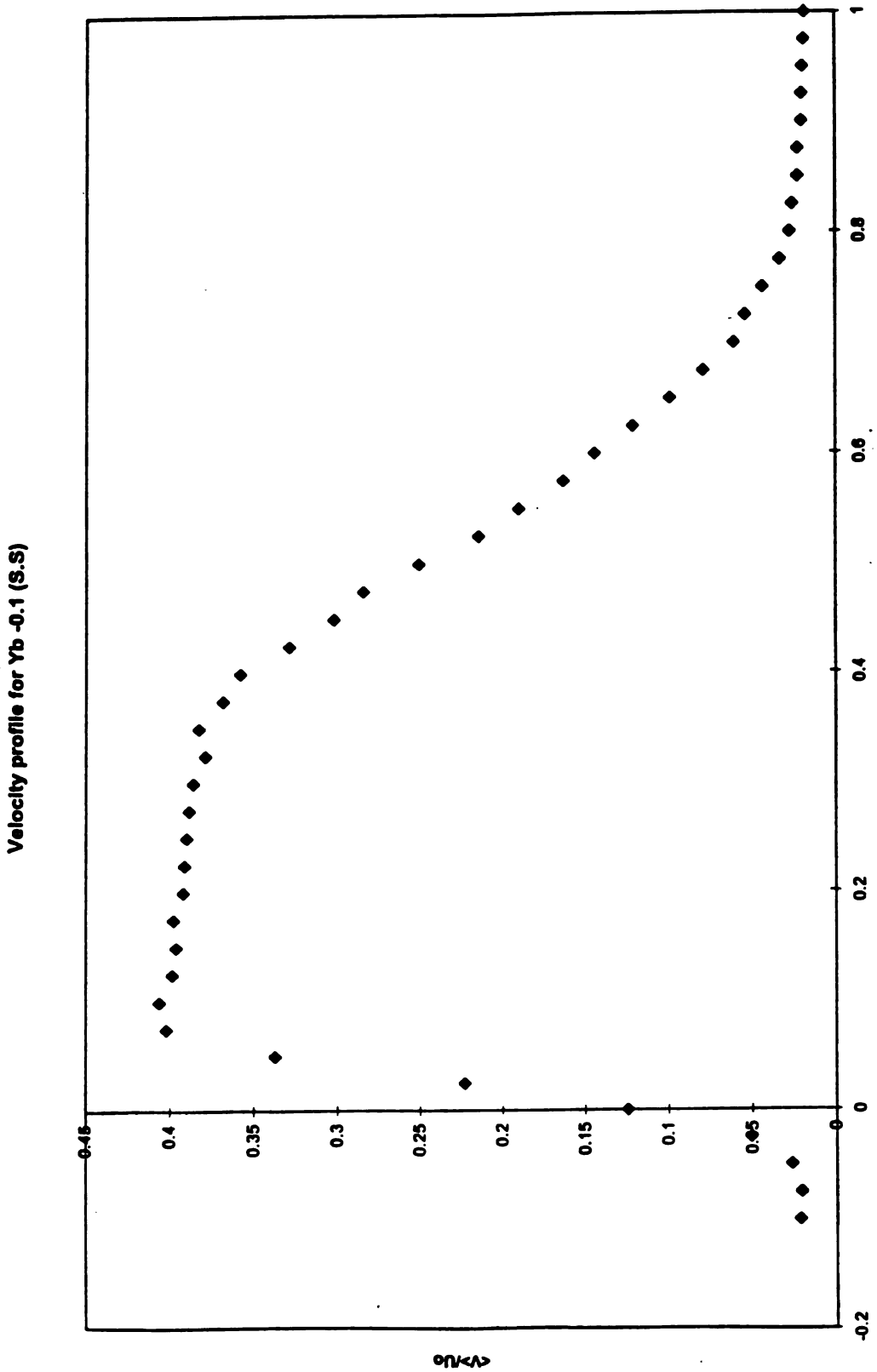

Figure 22. Velocity distribution <V>/Uo at X/Wj= 1.5 and Yb/Wj= -0.1

(Nominal deflection angle of jet = 30 °)

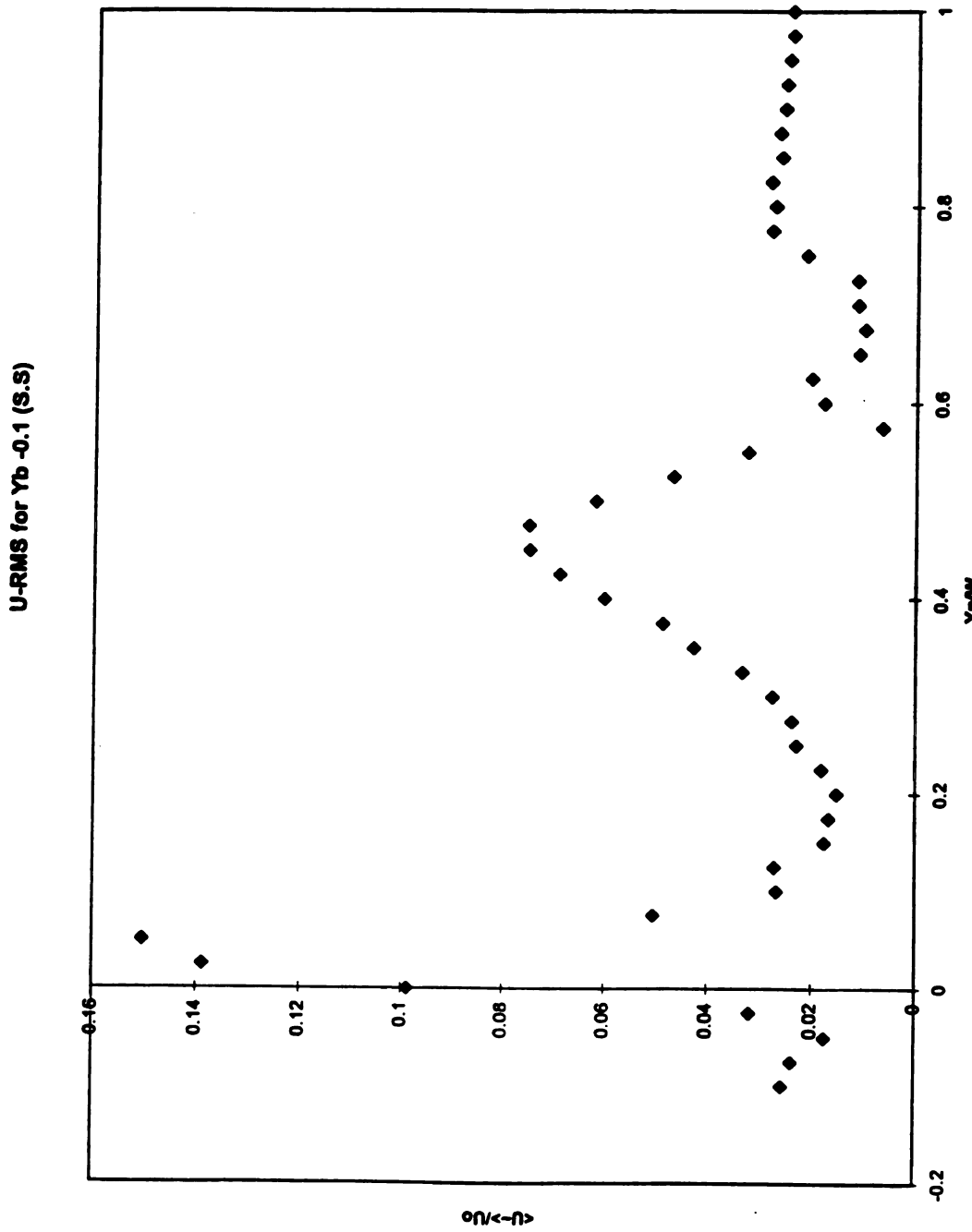

Figure 23. U-rms at X/Wj = 1.5 and Yb/Wj= -0.1

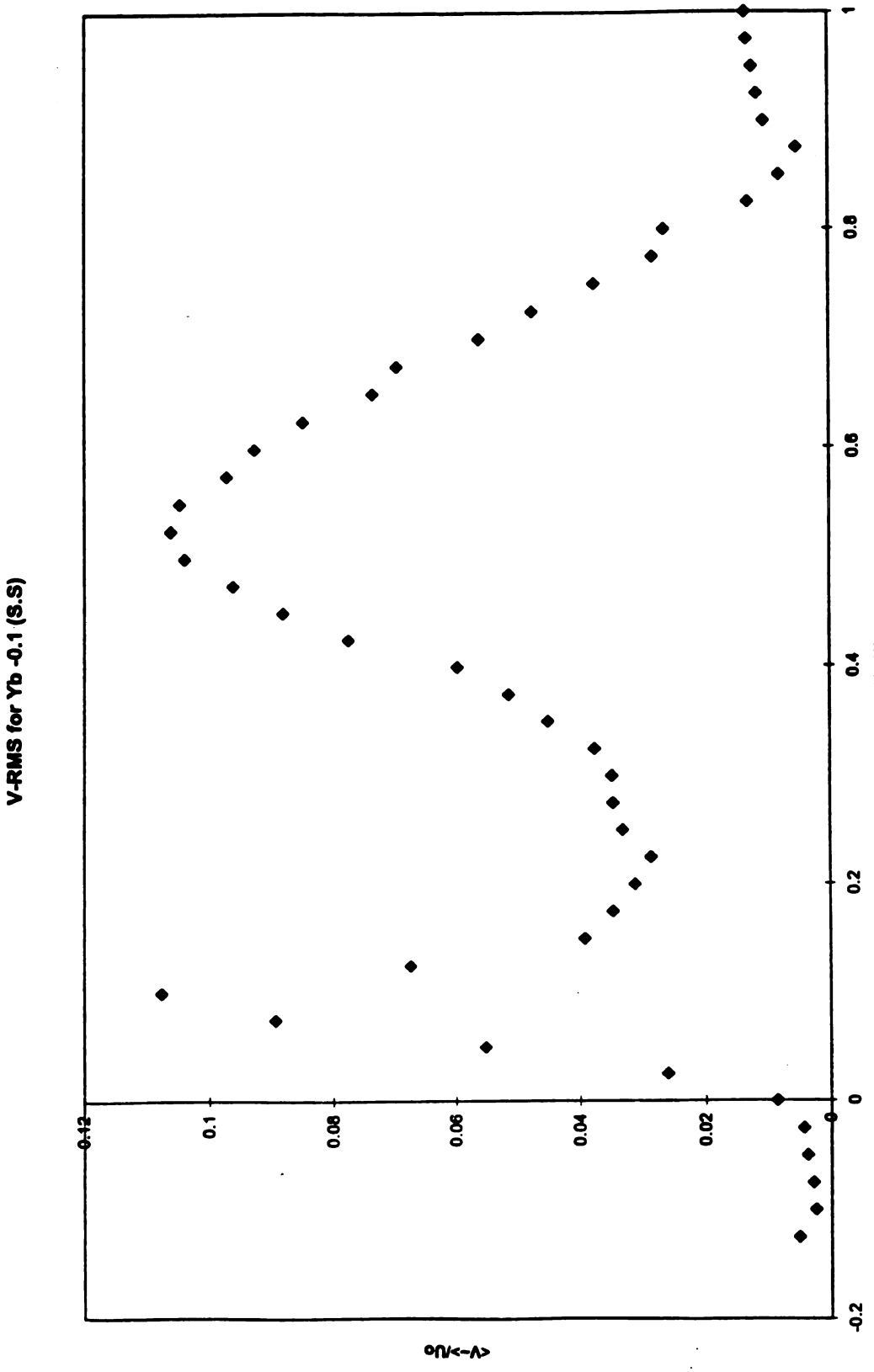

Figure 24. V-rms. at X/Wj = 1.5 and Yb/Wj= -0.1

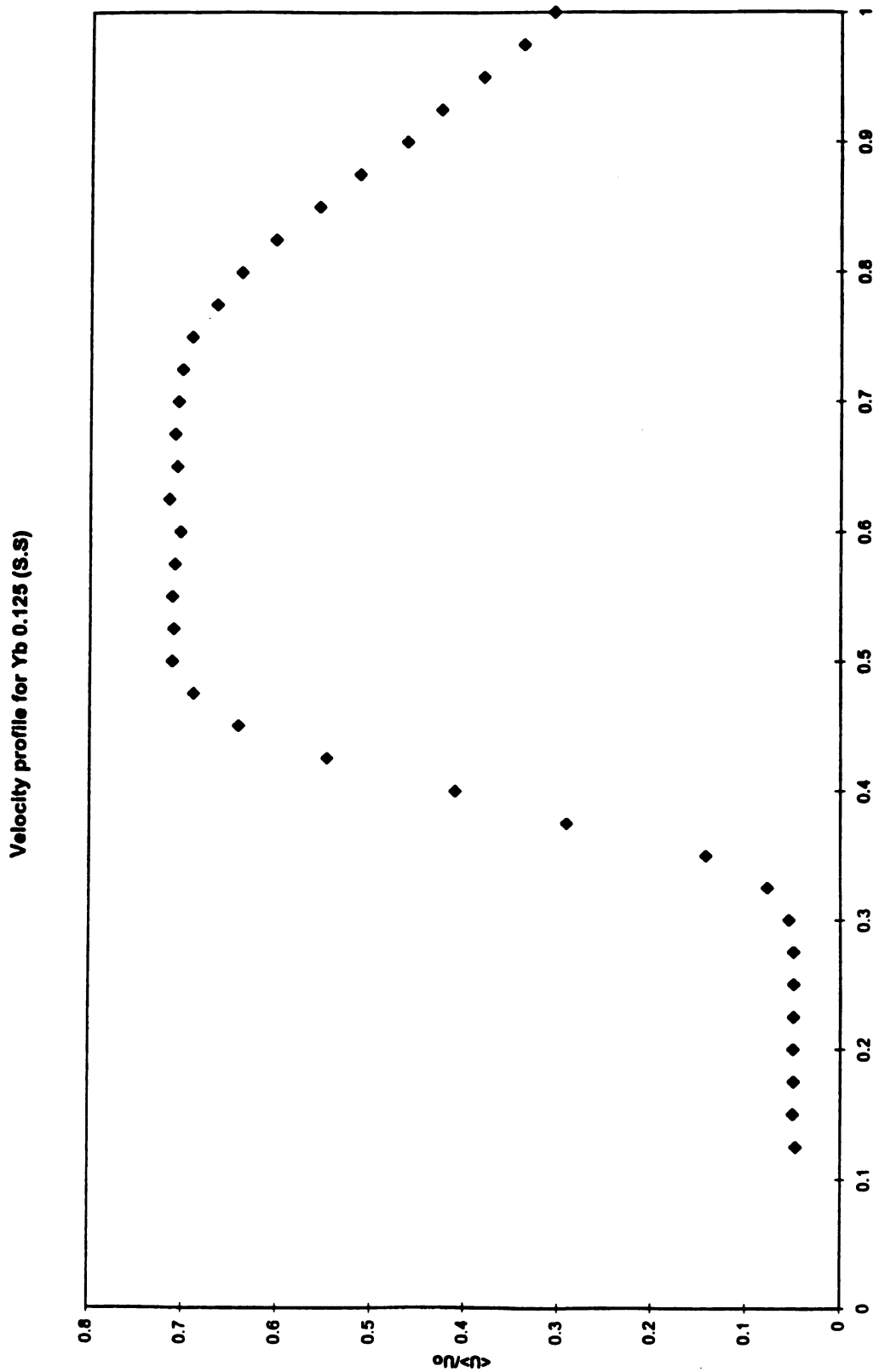

Figure 25. Velocity distribution <U>/Uo at X/Wj = 1.5 and Yb/Wj= 0.125
(Nominal deflection angle of jet = 45 °)

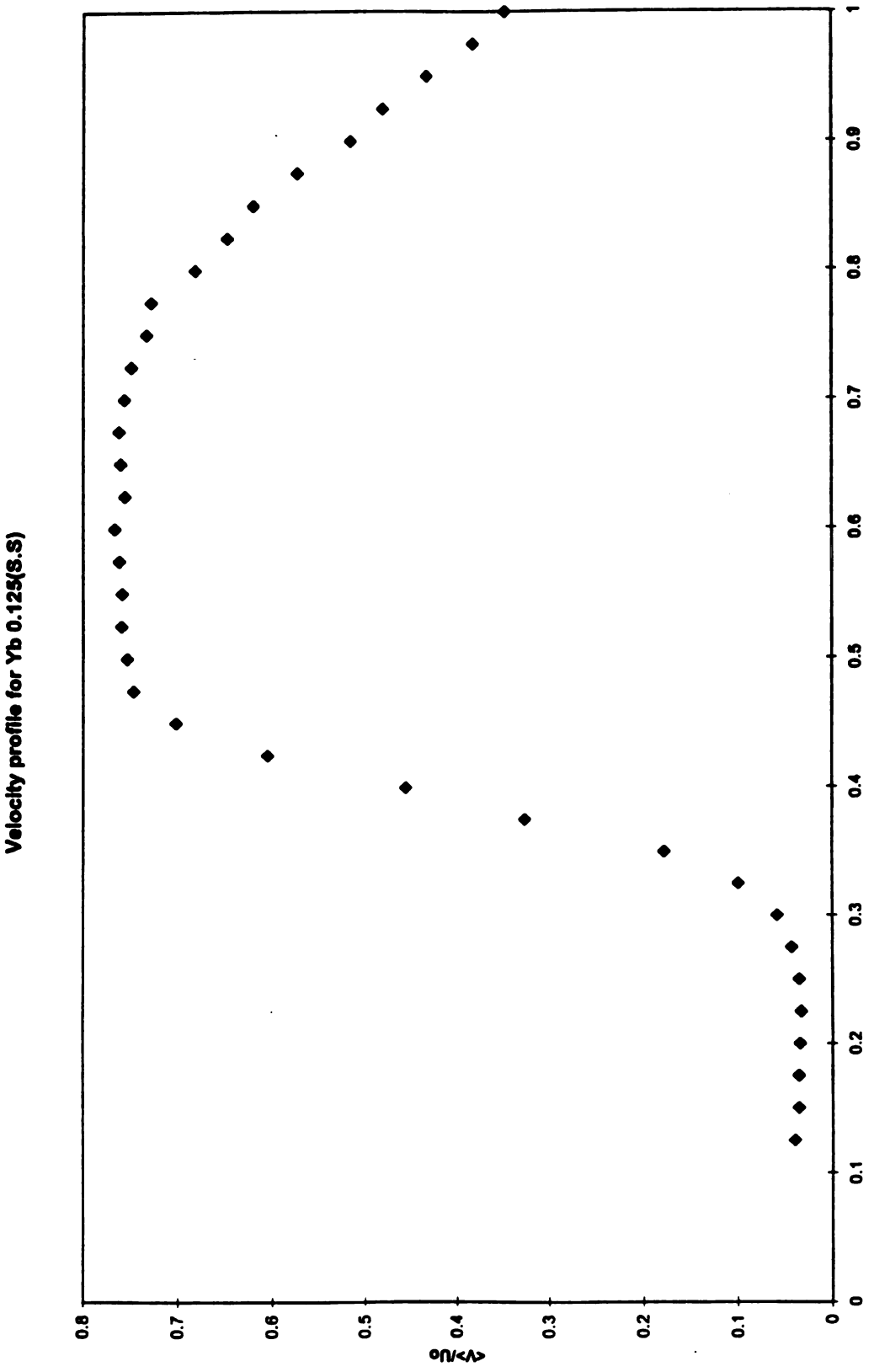

Figure 26. Velocity distribution <V>/Uo at X/Wj = 1.5 and Yb/Wj= 0.125
(Nominal deflection angle of jet = 45 °)

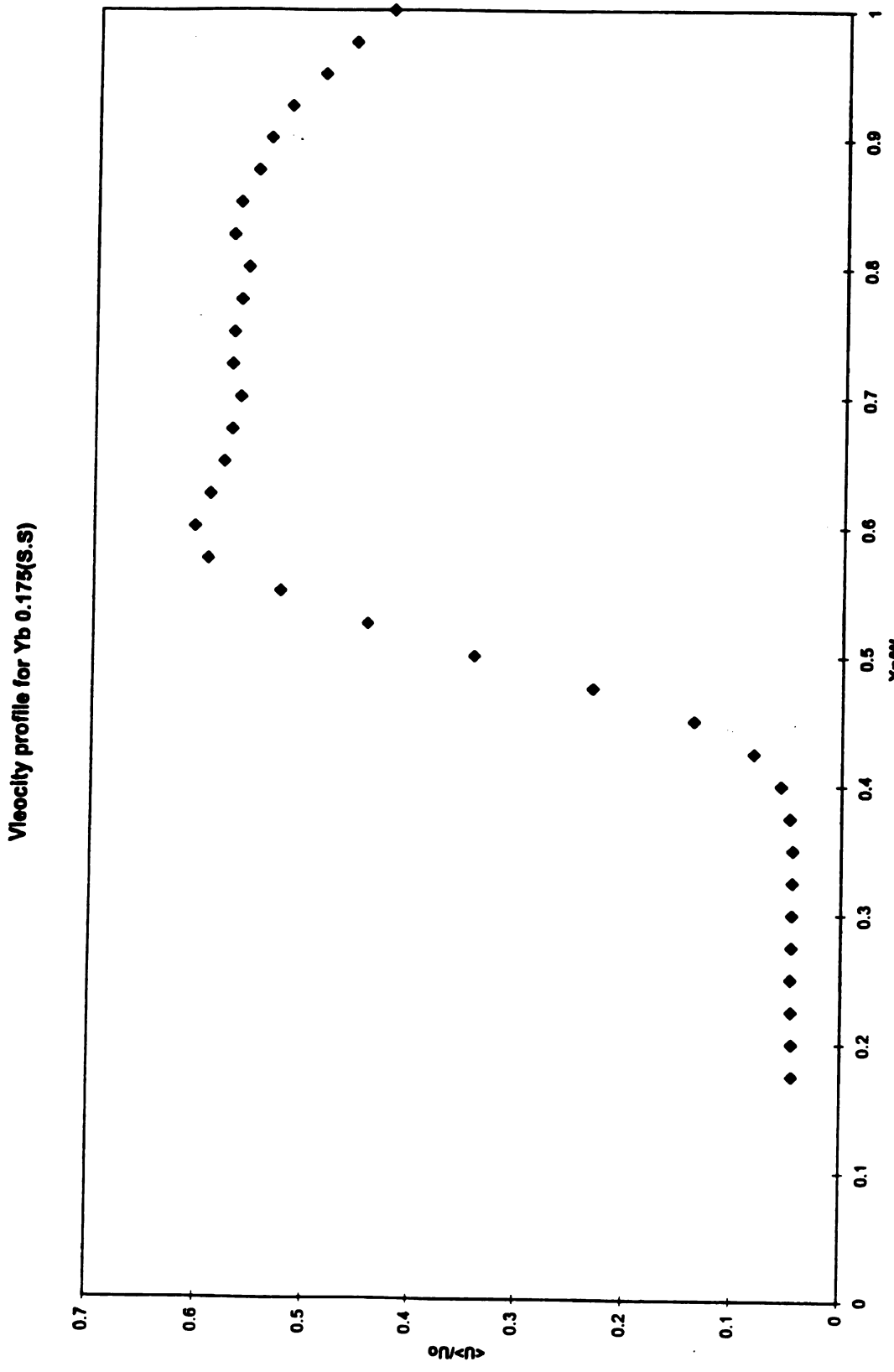

Figure 27. Velocity distribution <U>/Uo at X/Wj = 1.5 and Yb/Wj= 0.175
(Nominal deflection angle of jet = 48 °)

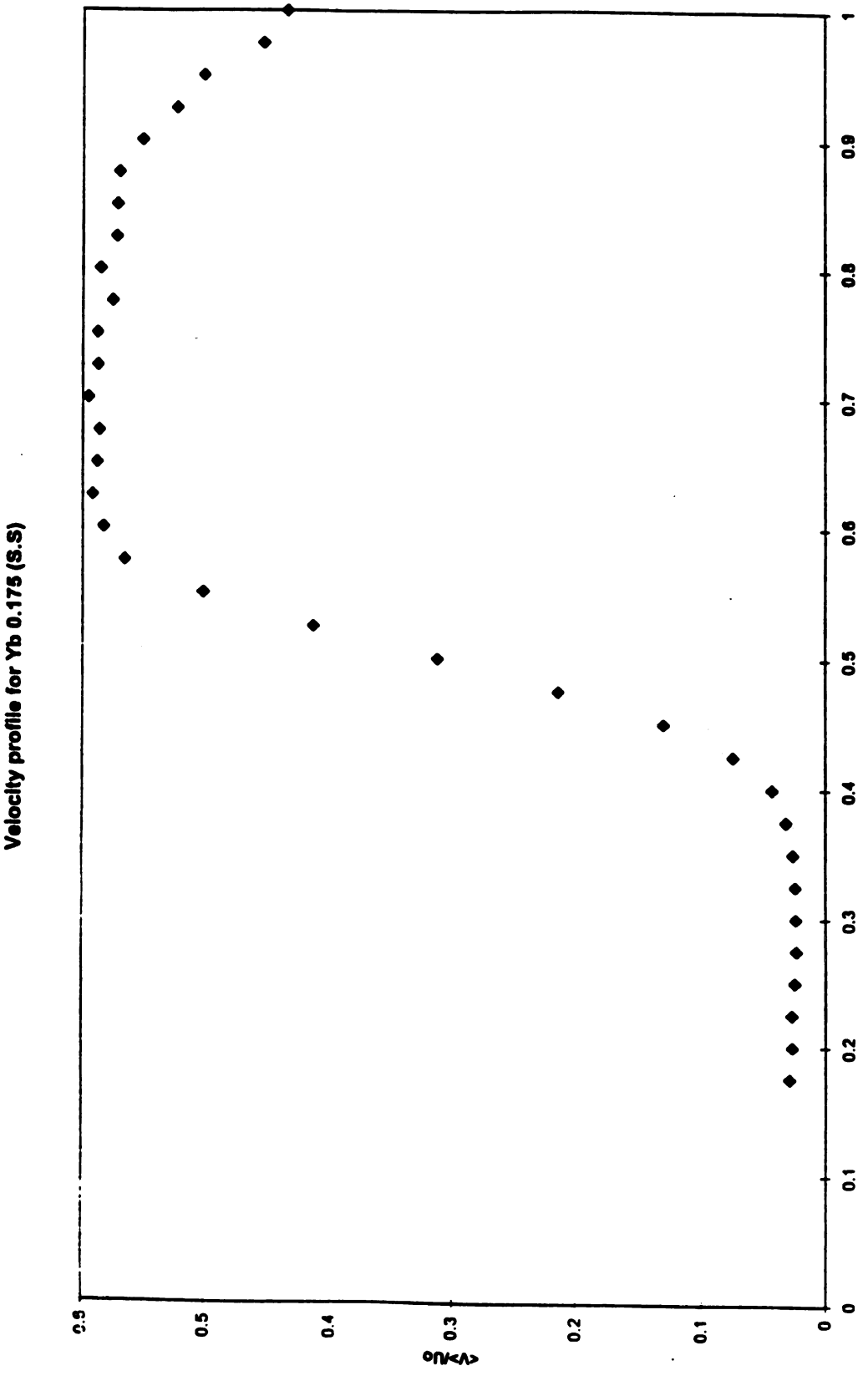

Figure 28. Velocity distribution <V>/Uo at X/Wj = 1.5 and Yb/Wj= 0.175
(Nominal deflection angle of jet = 48 °)

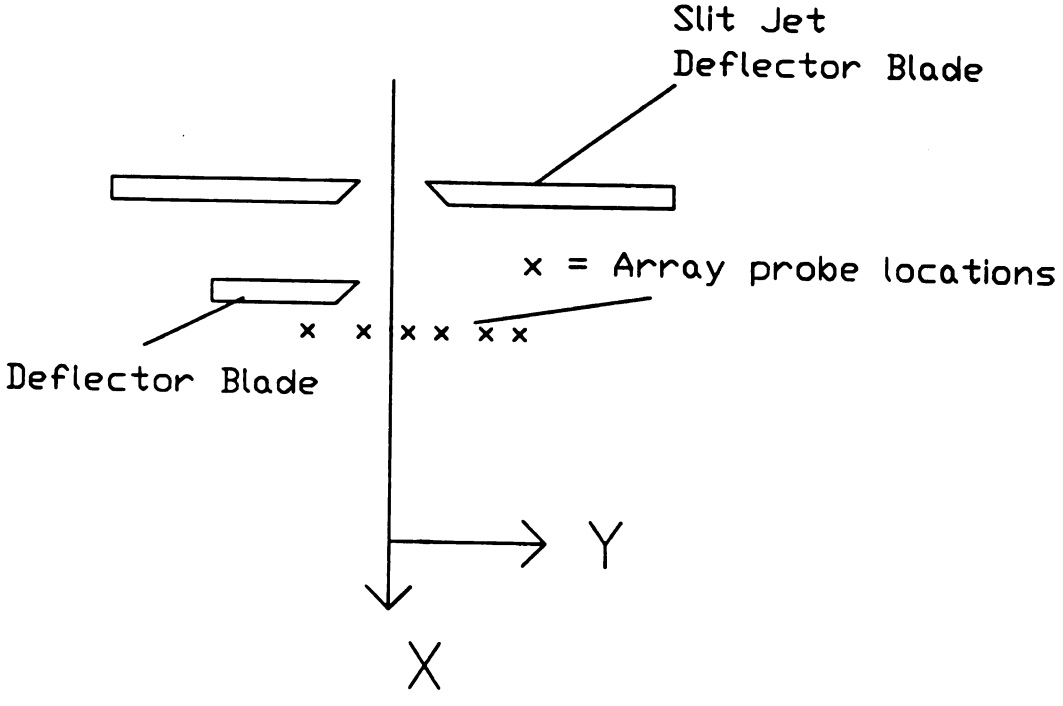

Figure 29. Schematic representation of locations, of the hot wire probes used during the transient motion of the DB.

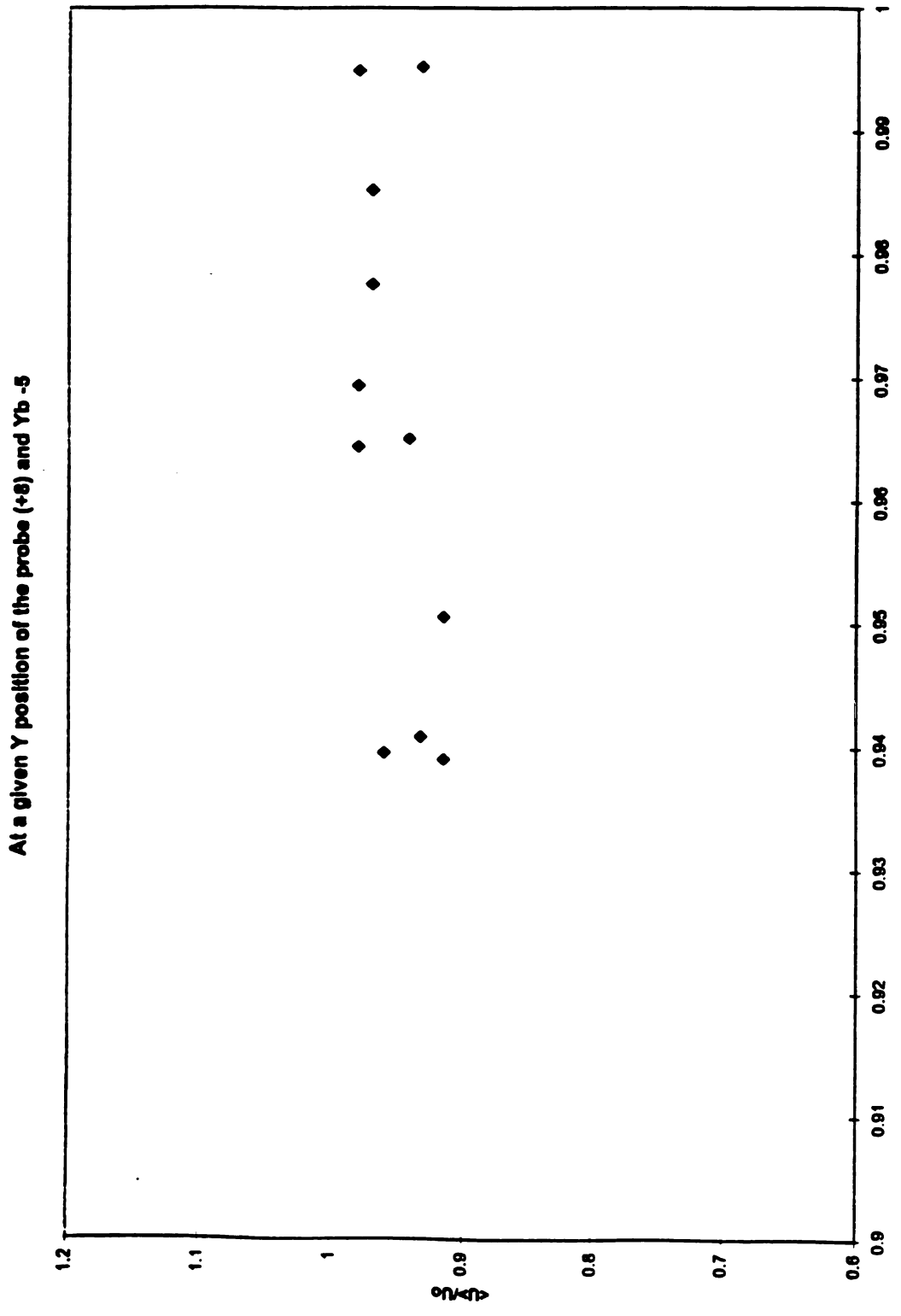

Figure 30. For given Yp/Wj and Yb/Wj , Independence of <U>/Uo measured with respect to dYb/dt

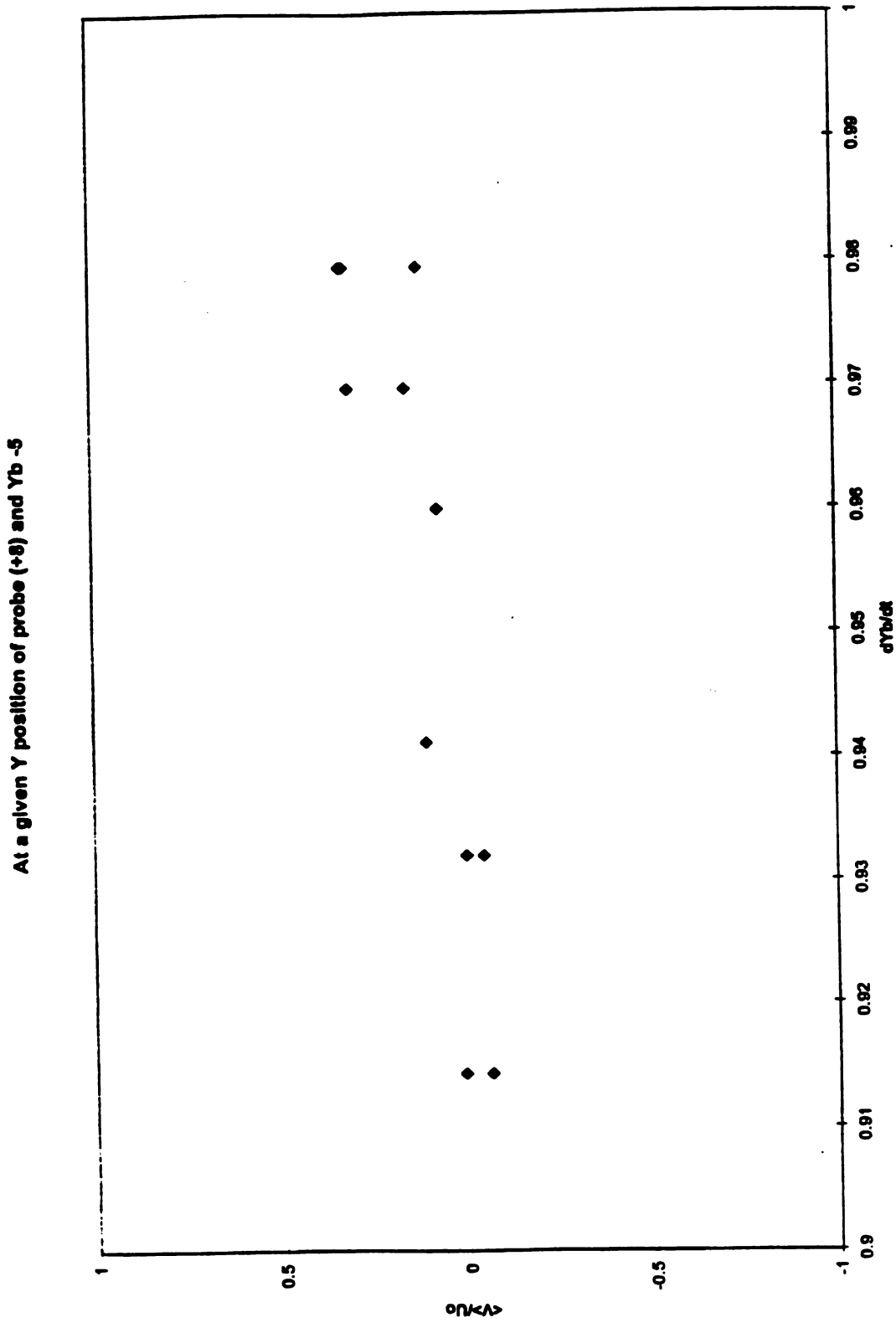

Figure 31. For given Yp/Wj and Yb/Wj, Independence of <V>/Uo measured with respect to dYb/dt.

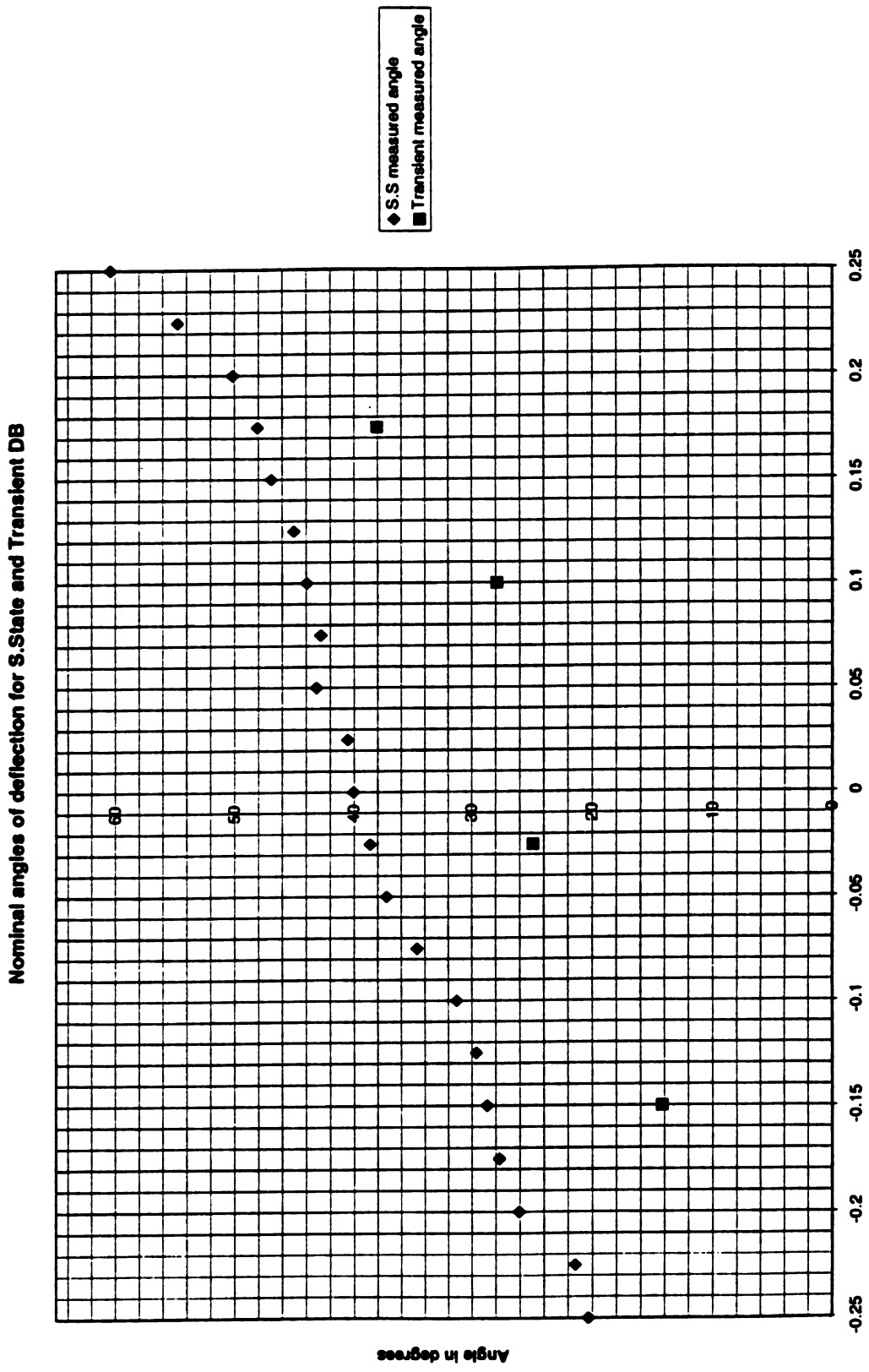

Figure 32. For a given Yb/Wj , difference in measured angle between the steady state and transient (for transient Vb/Uo = 0.03)

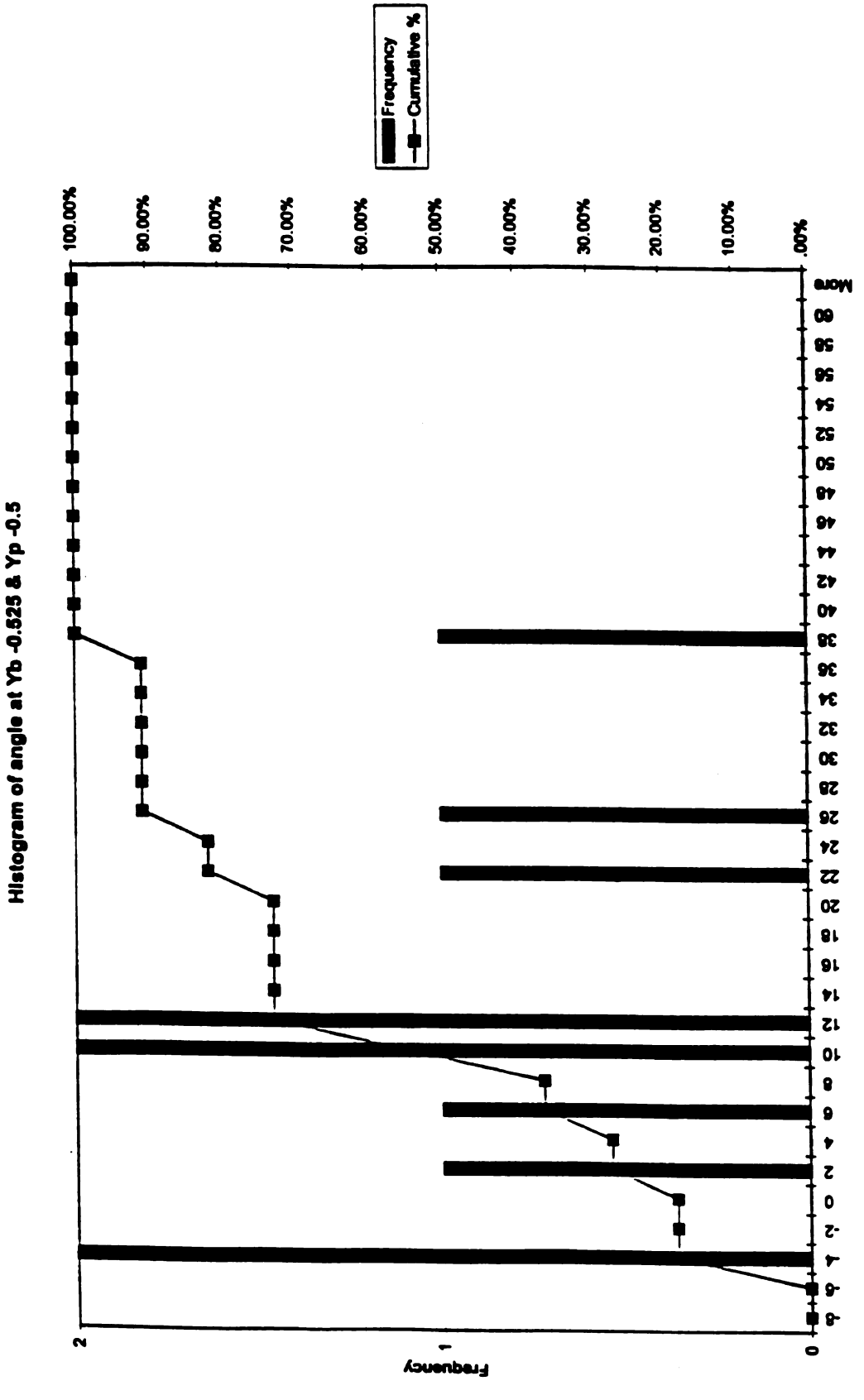

Figure 33. Histogram of flow angles at Yb/Wj=-0.525 and Yp/Wj= -0.5

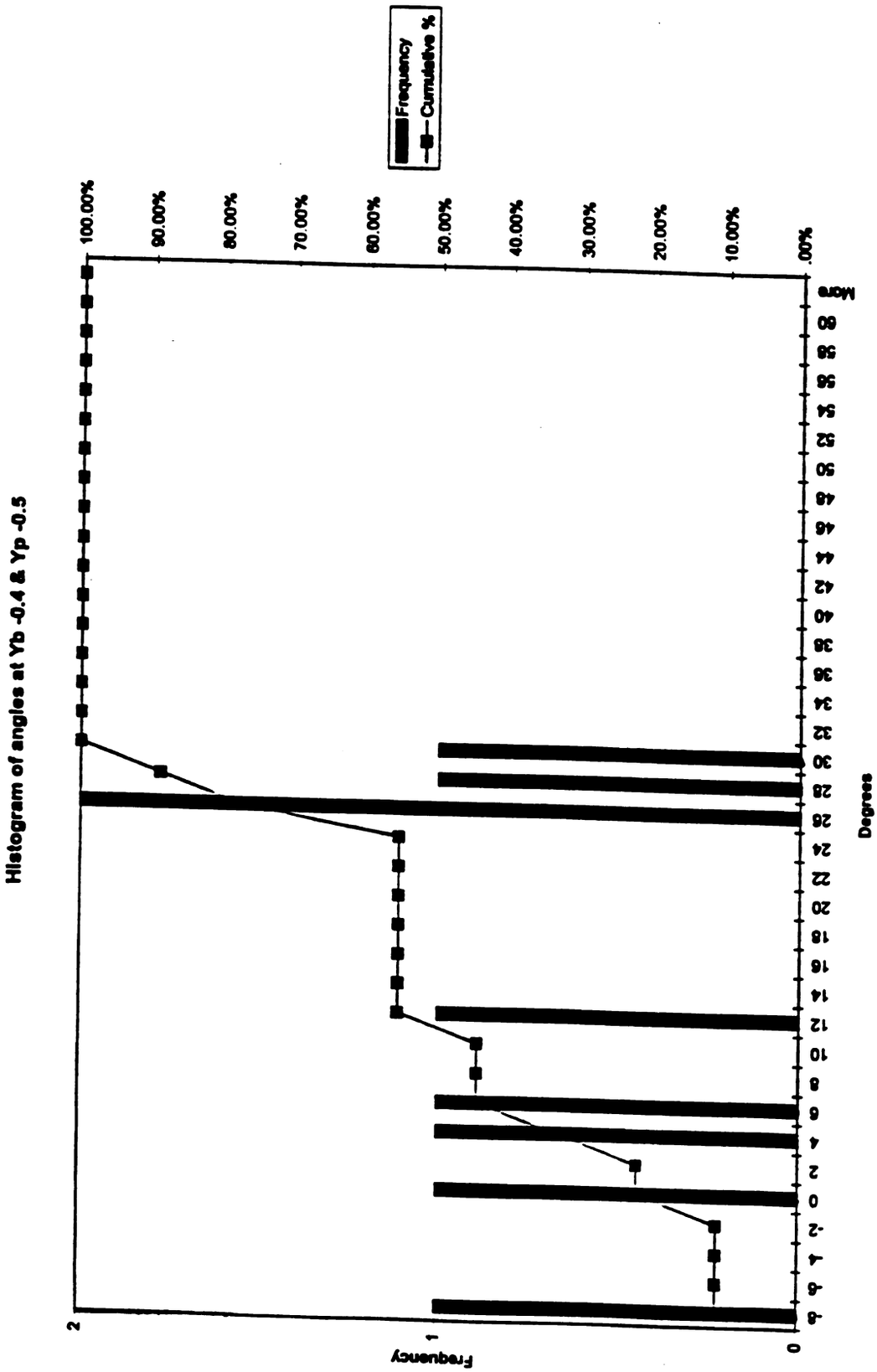

Figure 34. Histogram of flow angles at Yb/Wj=-0.4 and Yp/Wj= -0.5

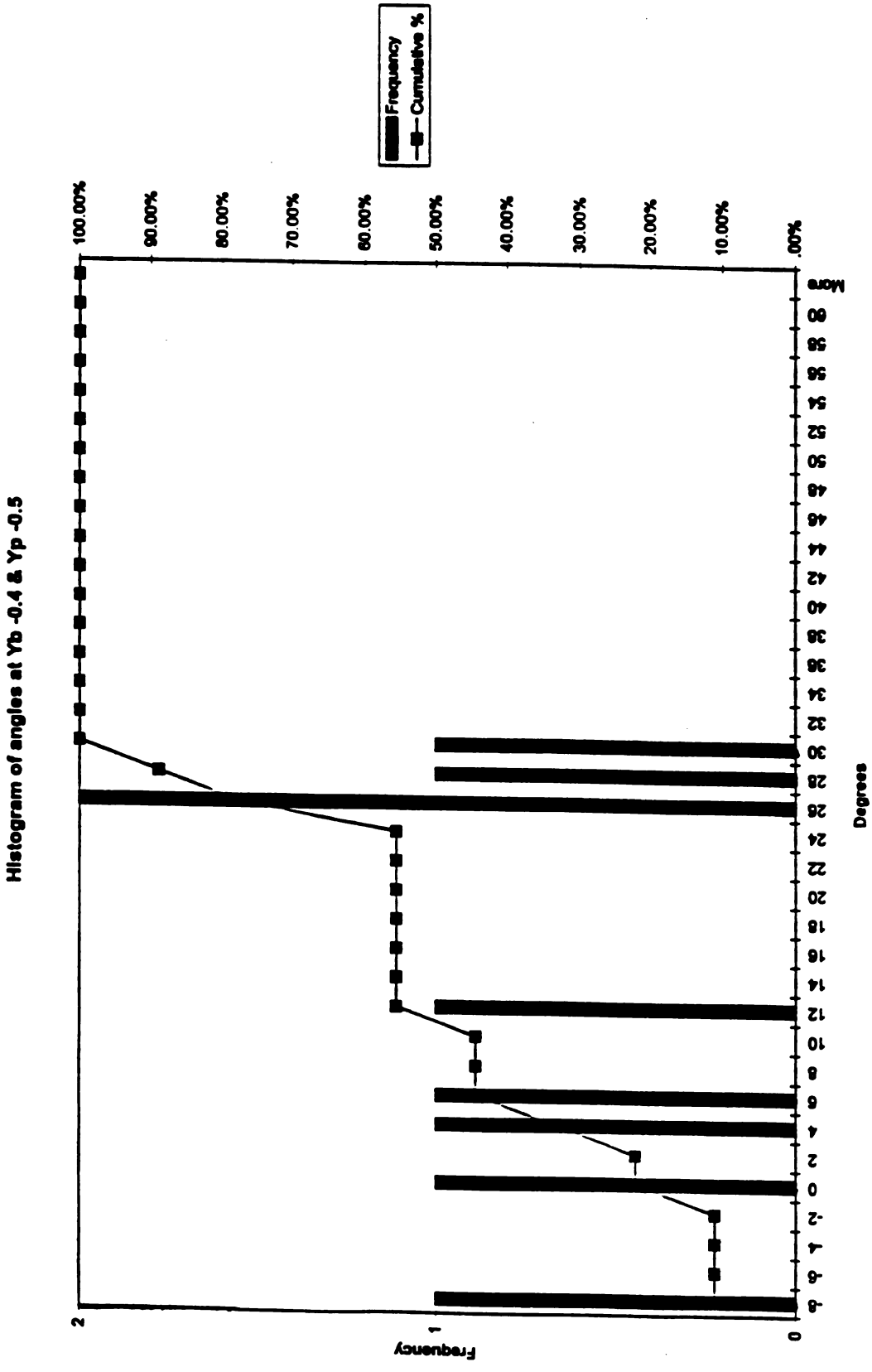

Figure 34. Histogram of flow angles at Yb/Wj=-0.4 and Yp/Wj= -0.5

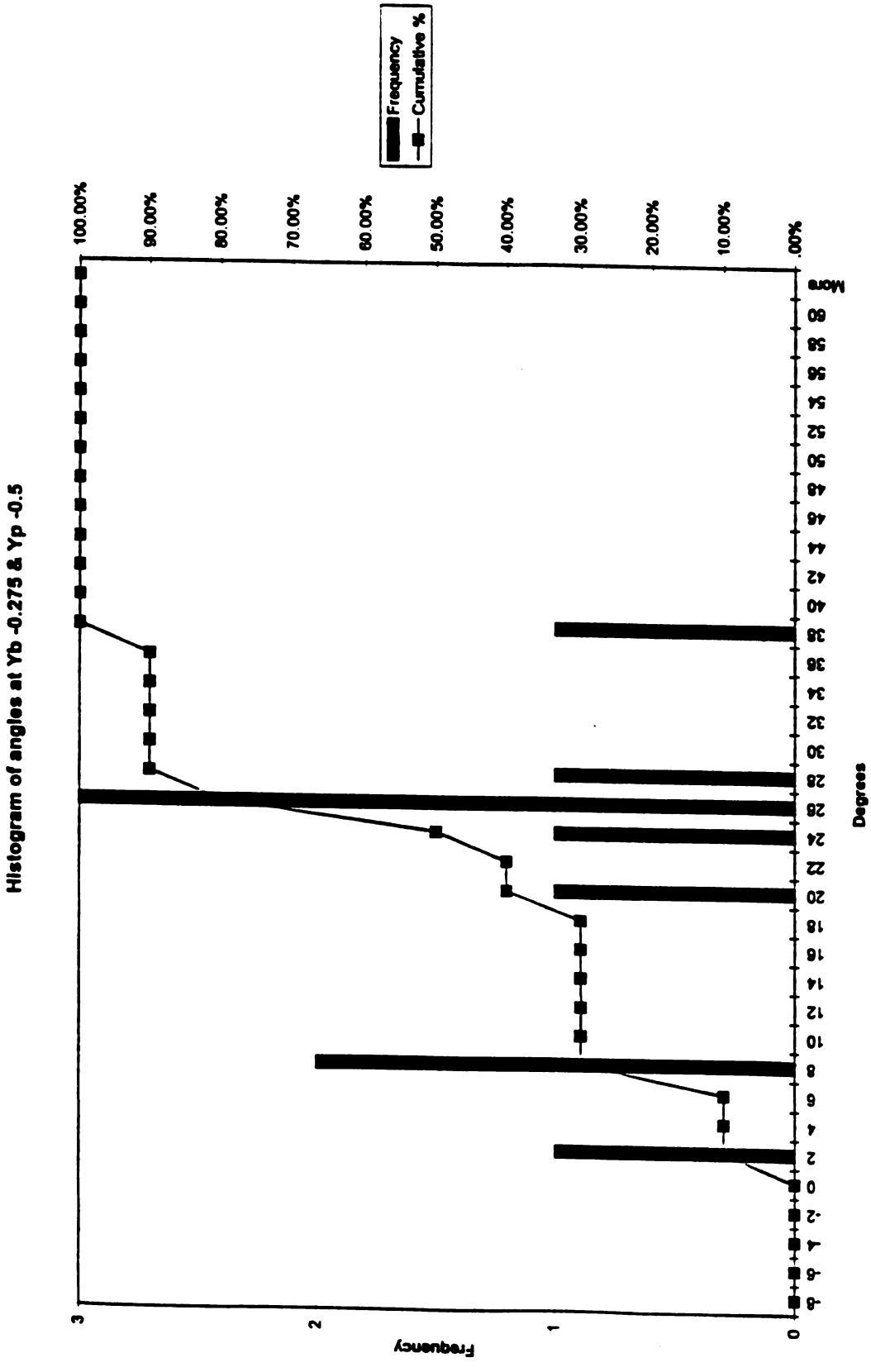

Figure 35. Histogram of flow angles at Yb/Wj=-0.275 and Yp/Wj= -0.5

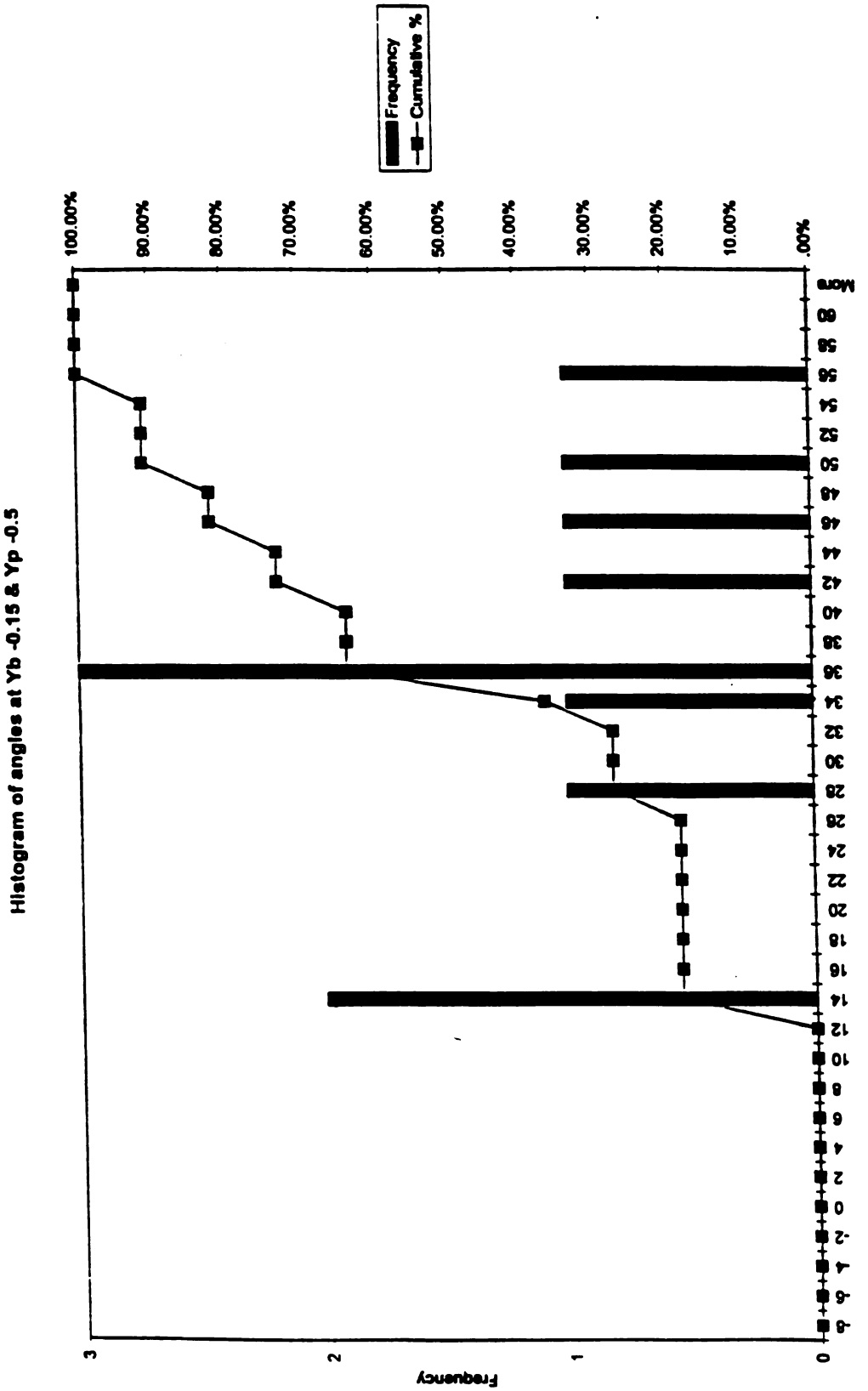

Figure 36. Histogram of flow angles at Yb/Wj=-0.15 and Yp/Wj= -0.5

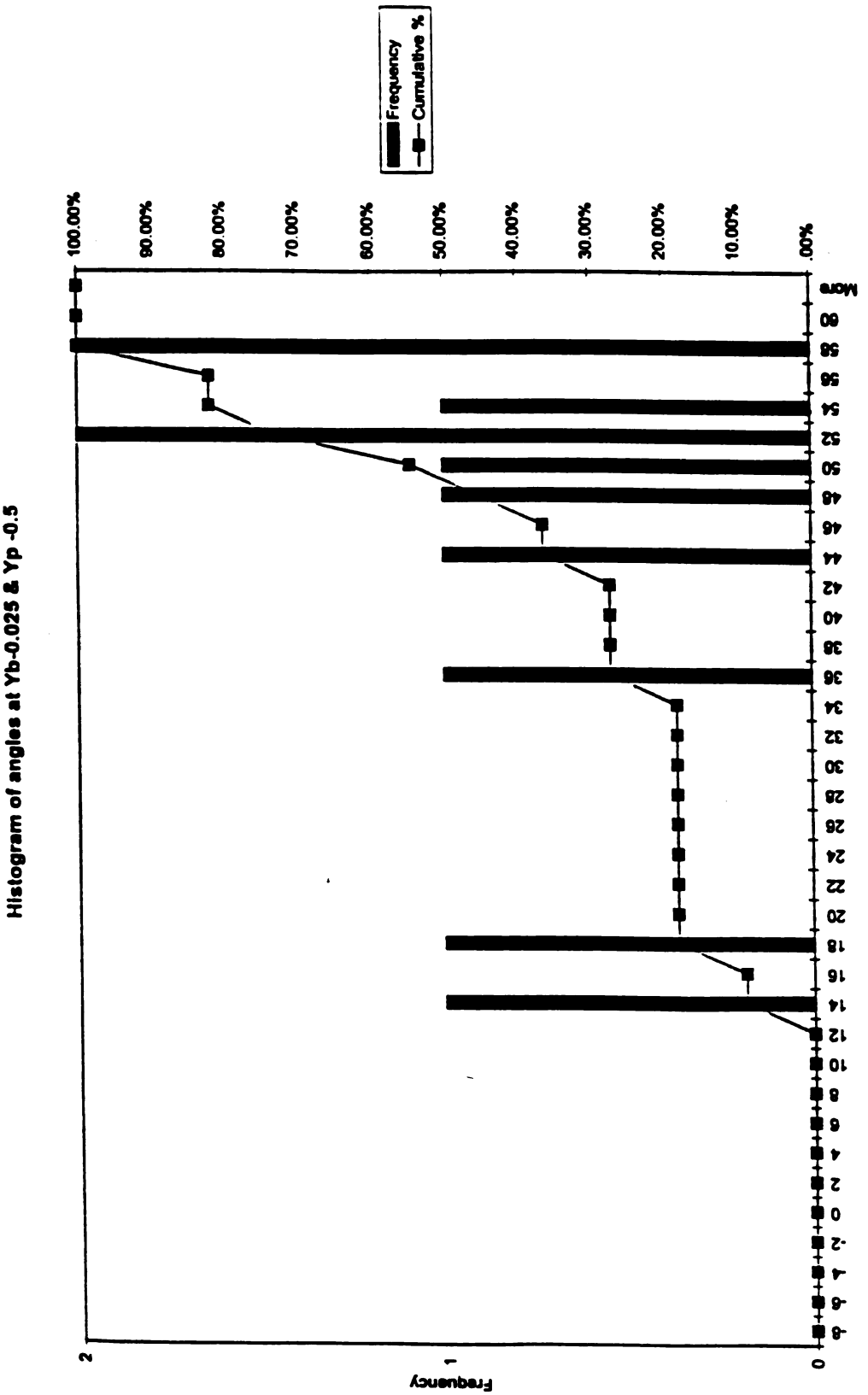

Figure 37. Histogram of flow angles at Yb/Wj=-0.025 and Yp/Wj= -0.5

Histogram of angles at Yb 0.1 & Yp -0.5

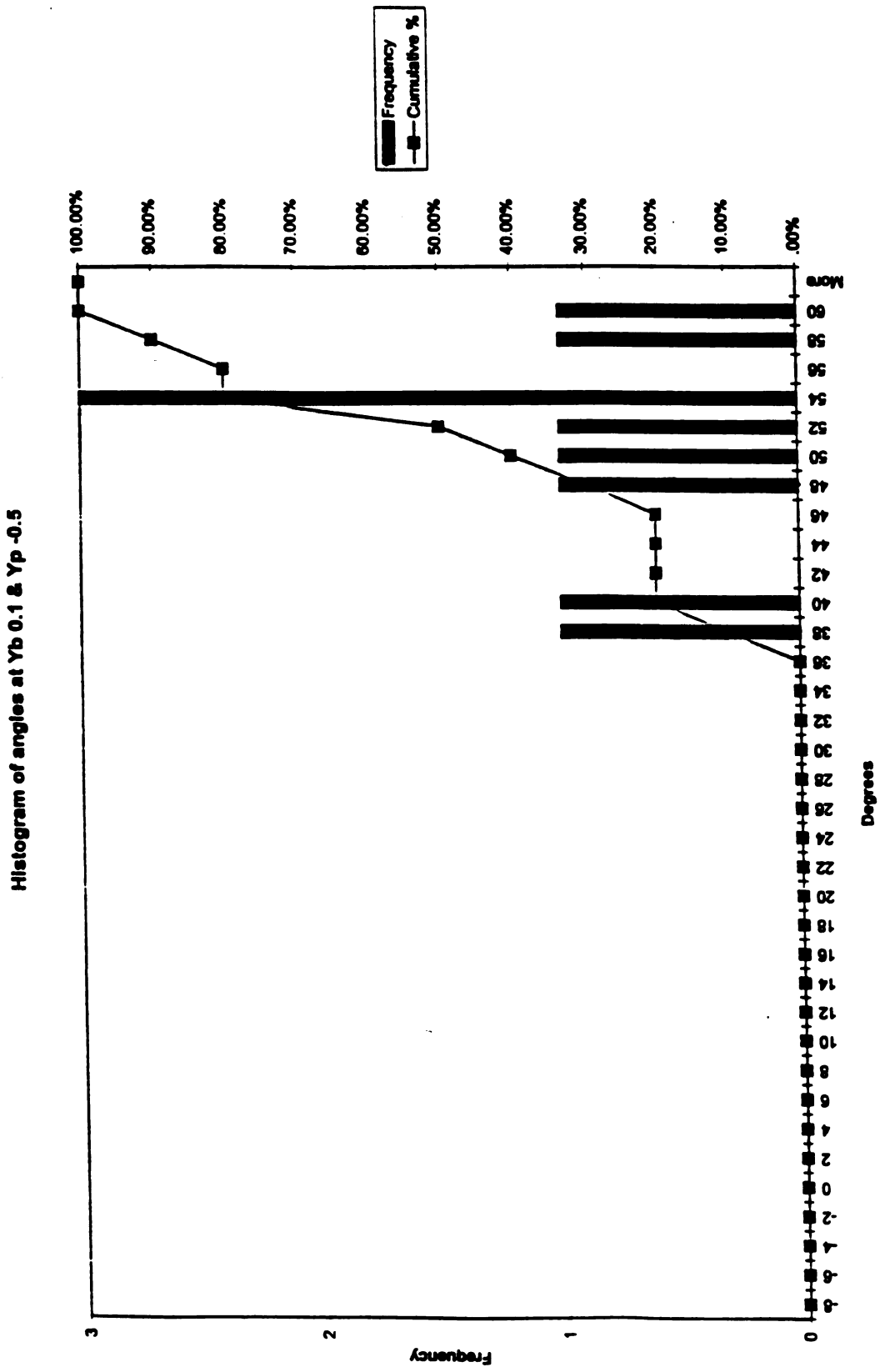

Figure 38. Histogram of flow angles at Yb/Wj=+0.1 and Yp/Wj= -0.5

100.00%
Histogram of angles at Yb 0.175 & Yp -0.5
2

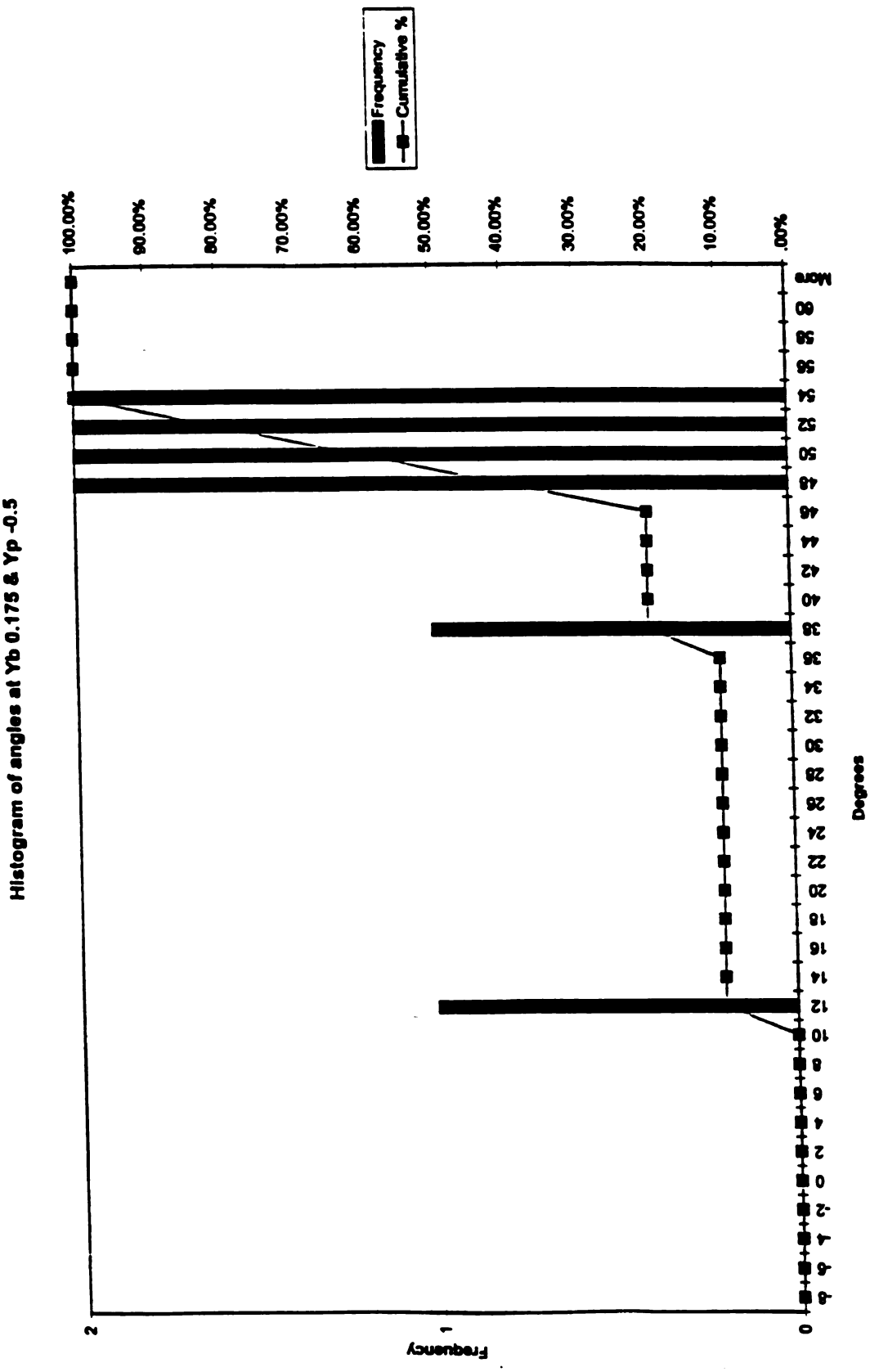

Figure 39. Histogram of flow angles at YbWj=+0.175 and YpWj= -0.5

Histogram for Yb -0.525 at Yp -0.2

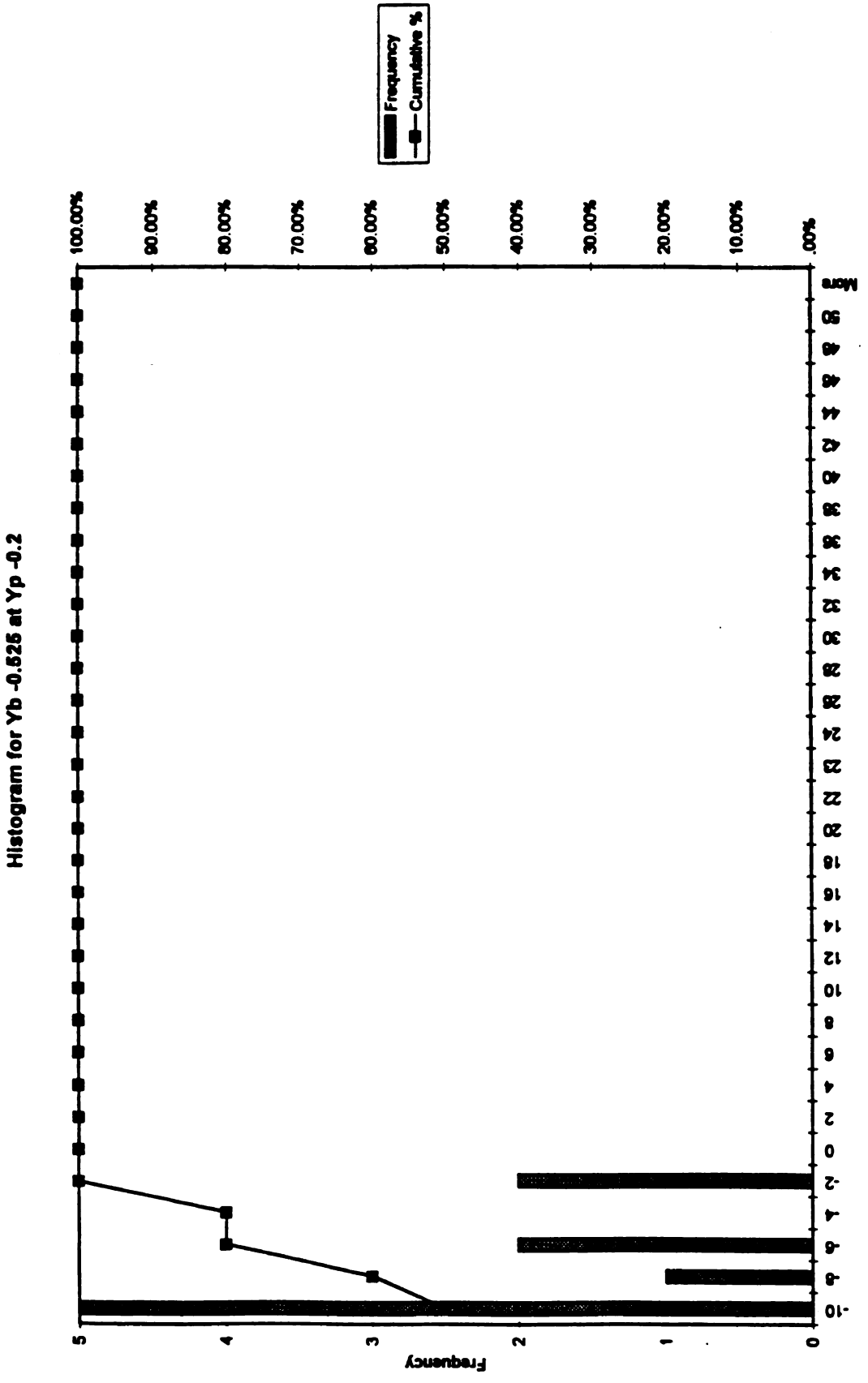

Figure 40. Histogram of flow angles at Yb/Wj=-0.525 and Yp/Wj= -0.2

Histogram for Yb -0.4 at Yp -0.2

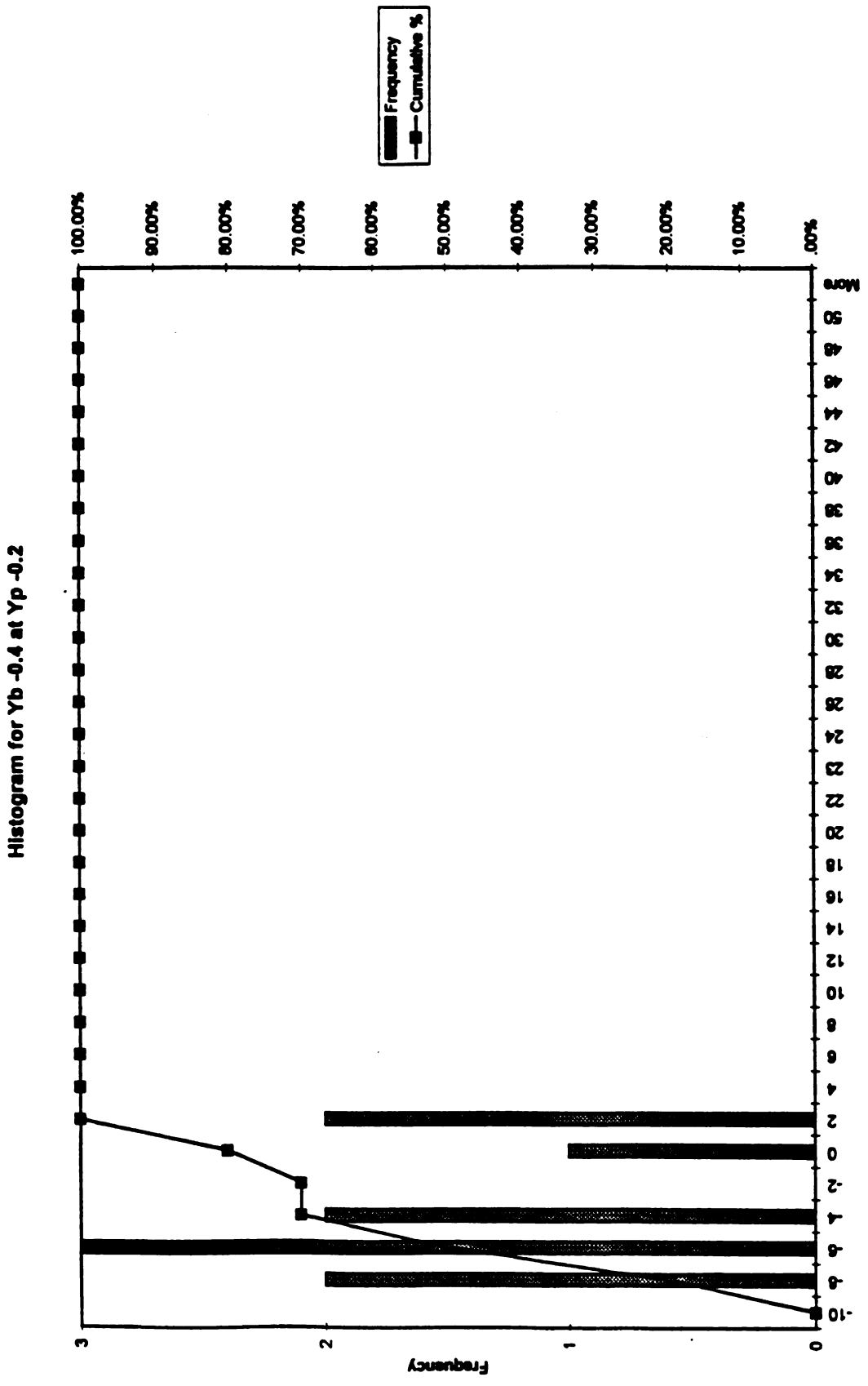

Figure 41. Histogram of flow angles at Yb/Wj=-0.4 and Yp/Wj= -0.2

Histogram for Yb -0.275 at Yp -0.2

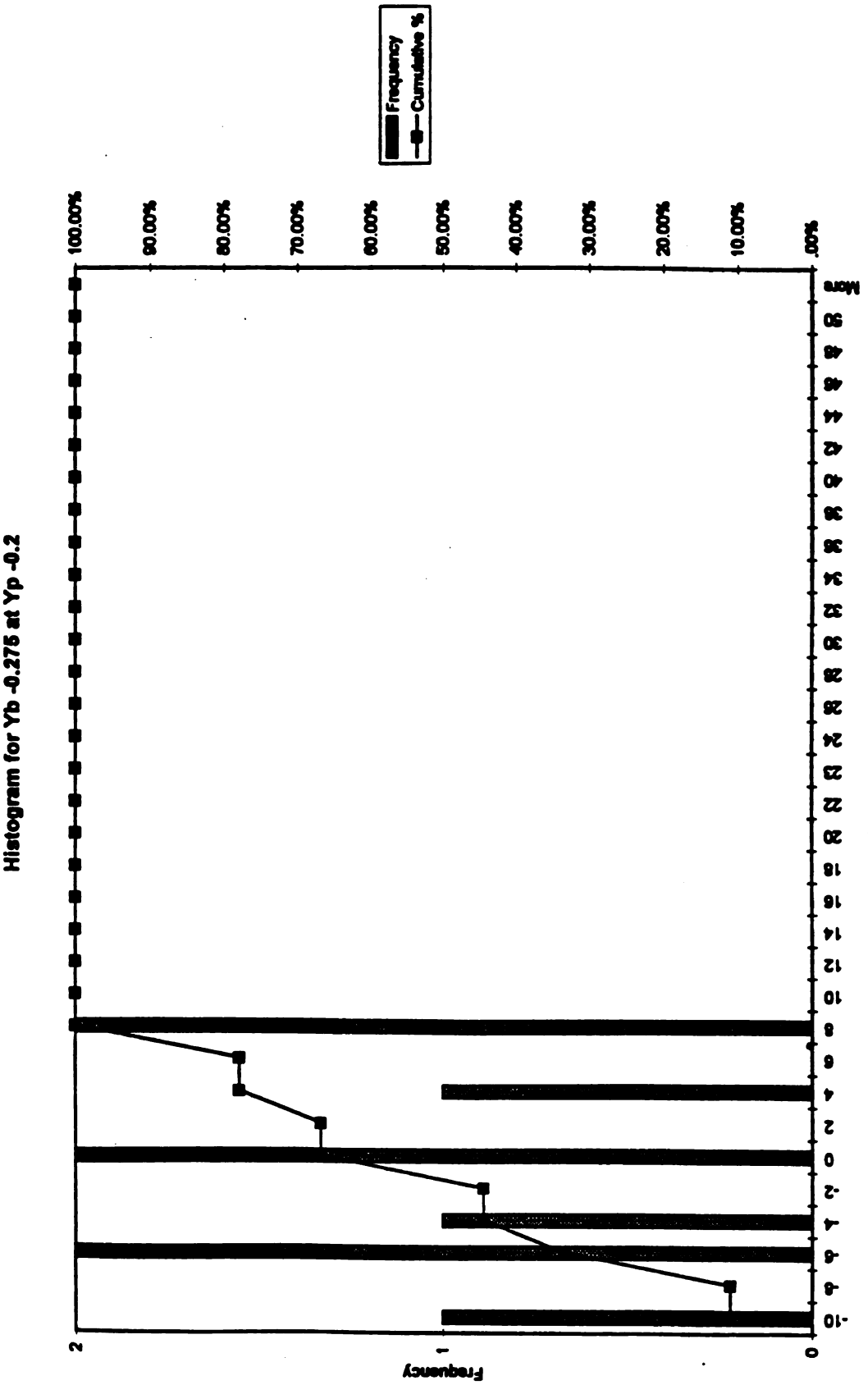

Figure 42. Histogram of flow angles at Yb/Wj=-0.275 and Yp/Wj= -0.2

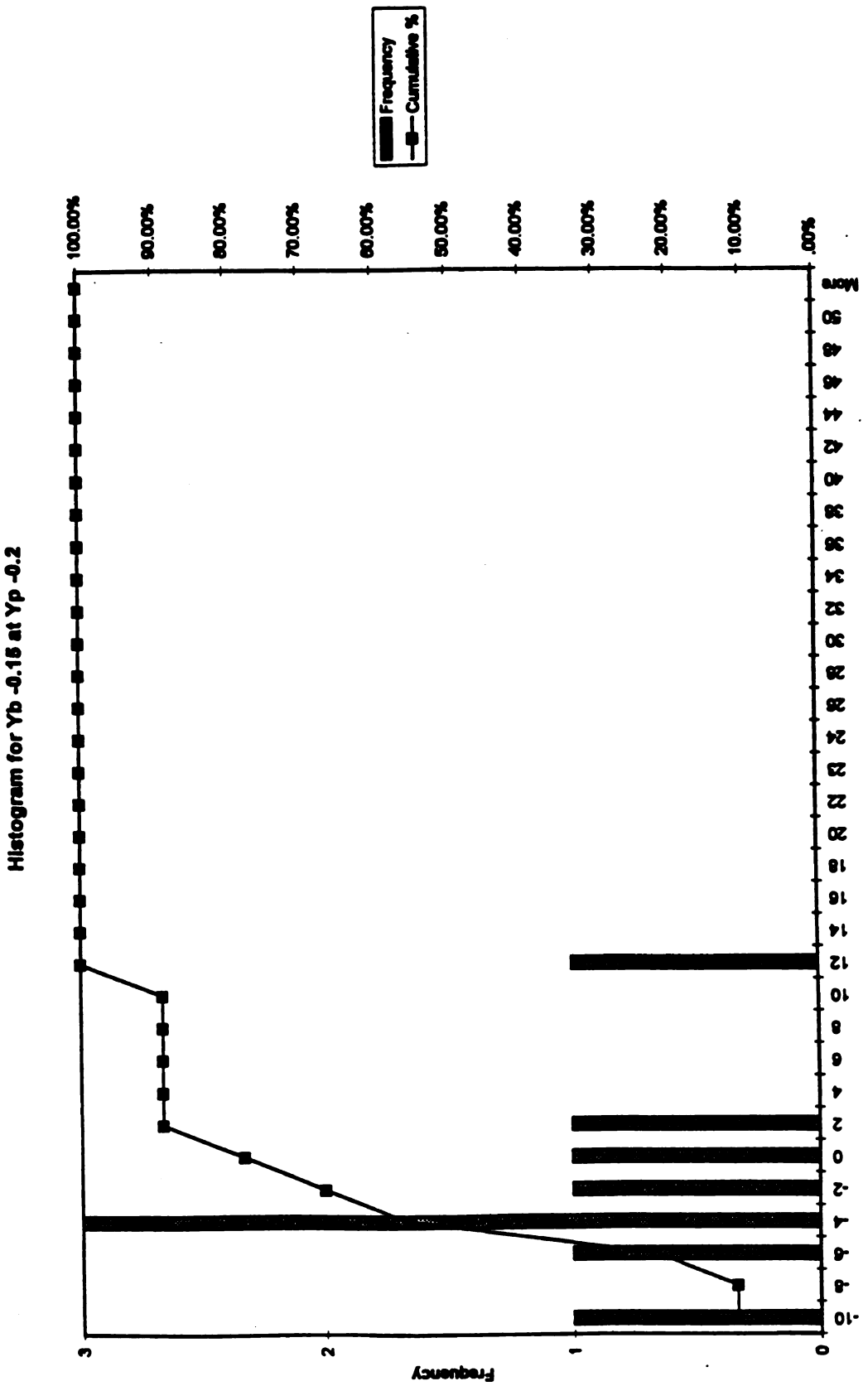

Figure 43. Histogram of flow angles at Yb/Wj=-0.15 and Yp/Wj= -0.2

Histogram for Yb -0.025 at Yp -0.2

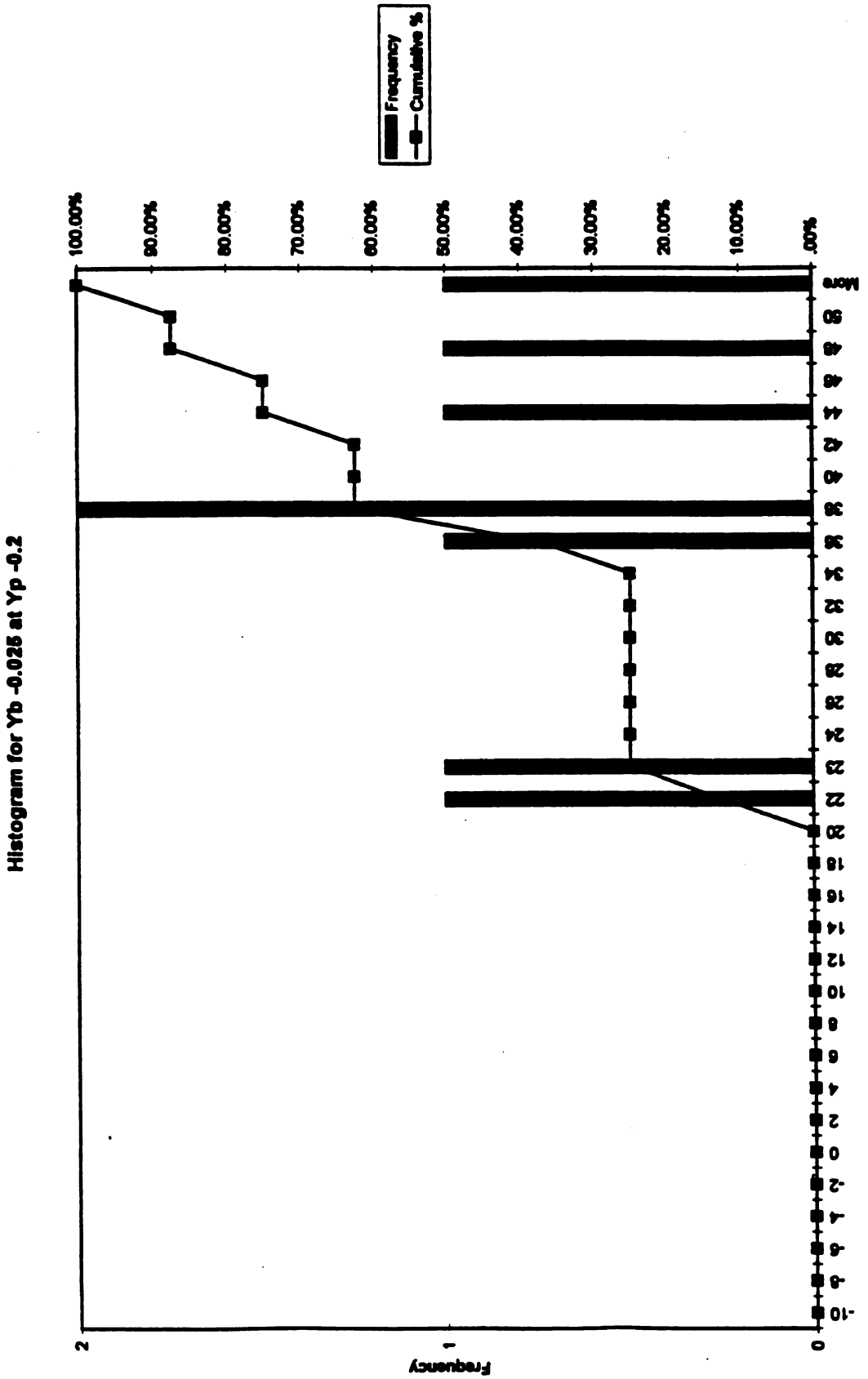

Figure 44. Histogram of flow angles at Yb/Wj=-0.025 and Yp/Wj= -0.2

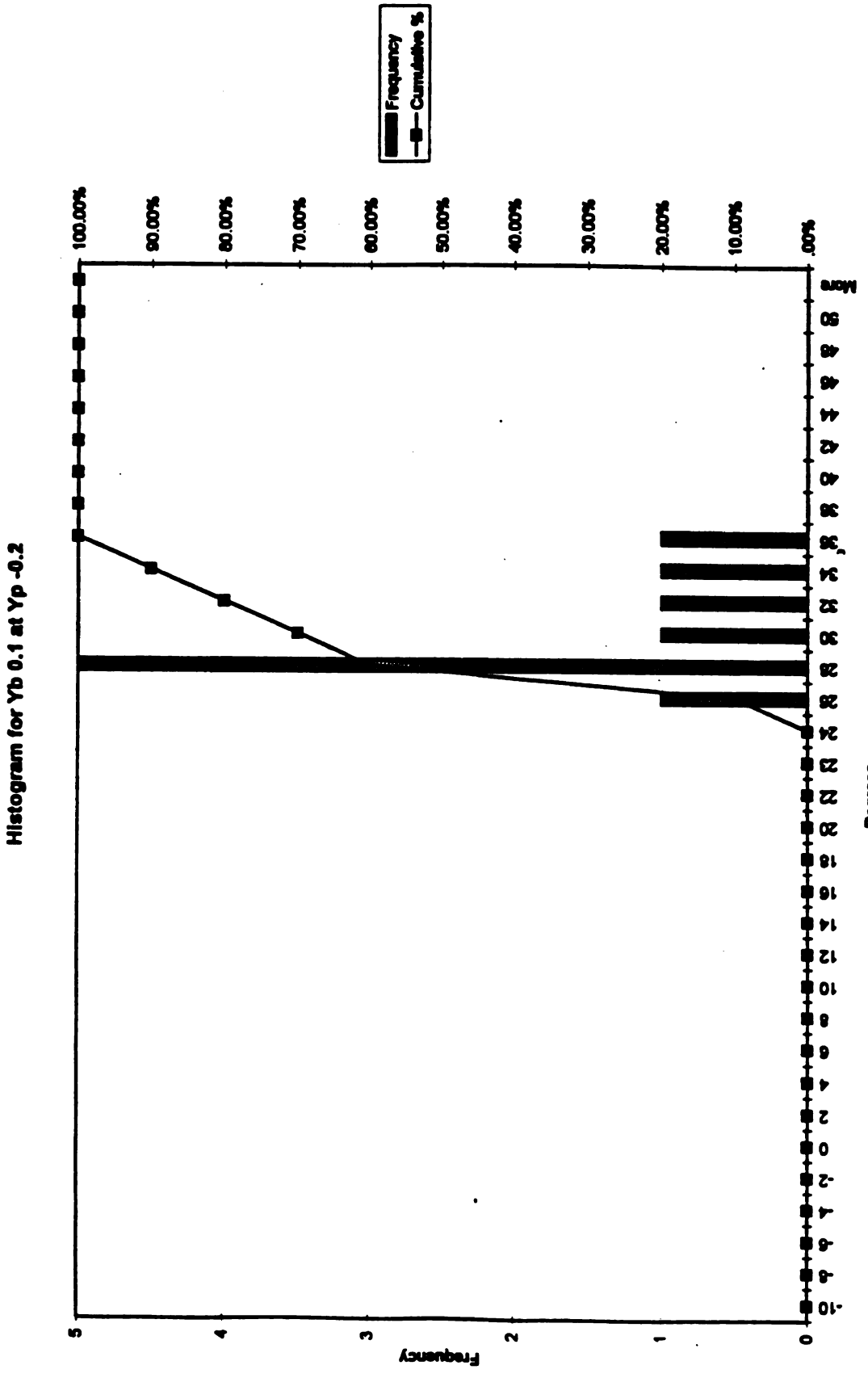

Figure 45. Histogram of flow angles at Yb/Wj=+0.1 and Yp/Wj= -0.2

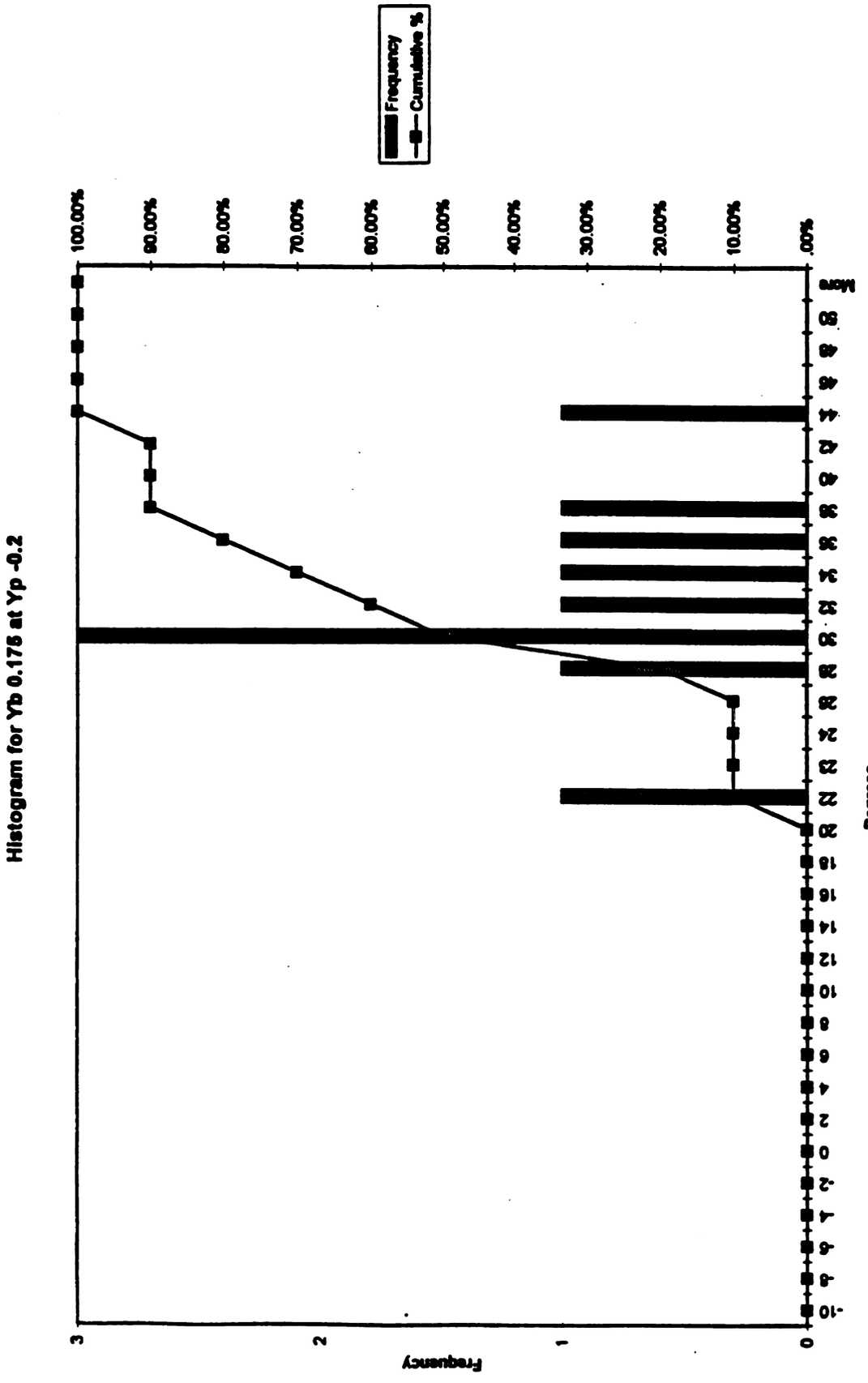

Figure 46. Histogram of flow angles at Yb/Wj=+0.175 and Yp/Wj= -0.2

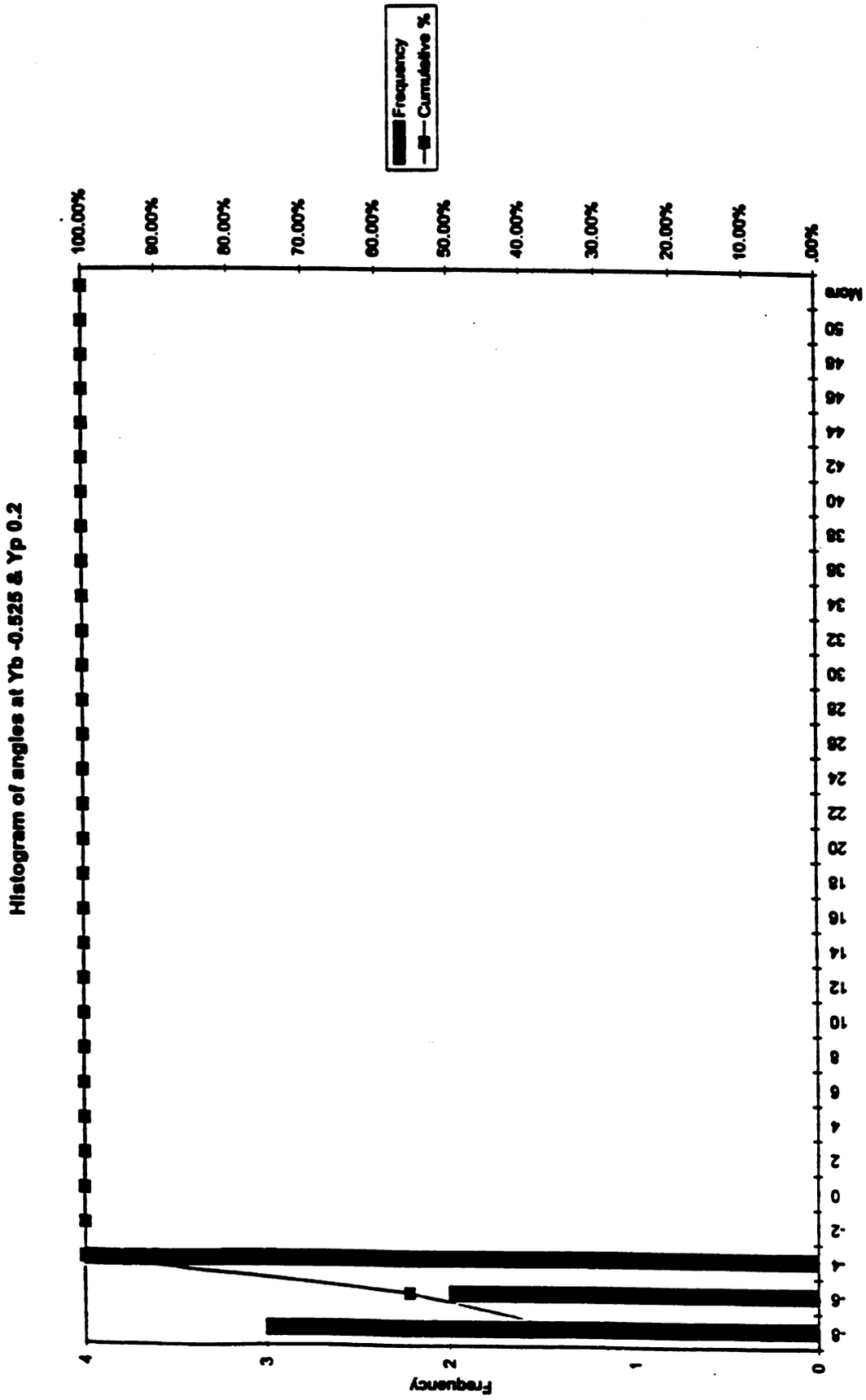

Figure 47. Histogram of flow angles at Yb/Wj=-0.525 and Yp/Wj= 0.2

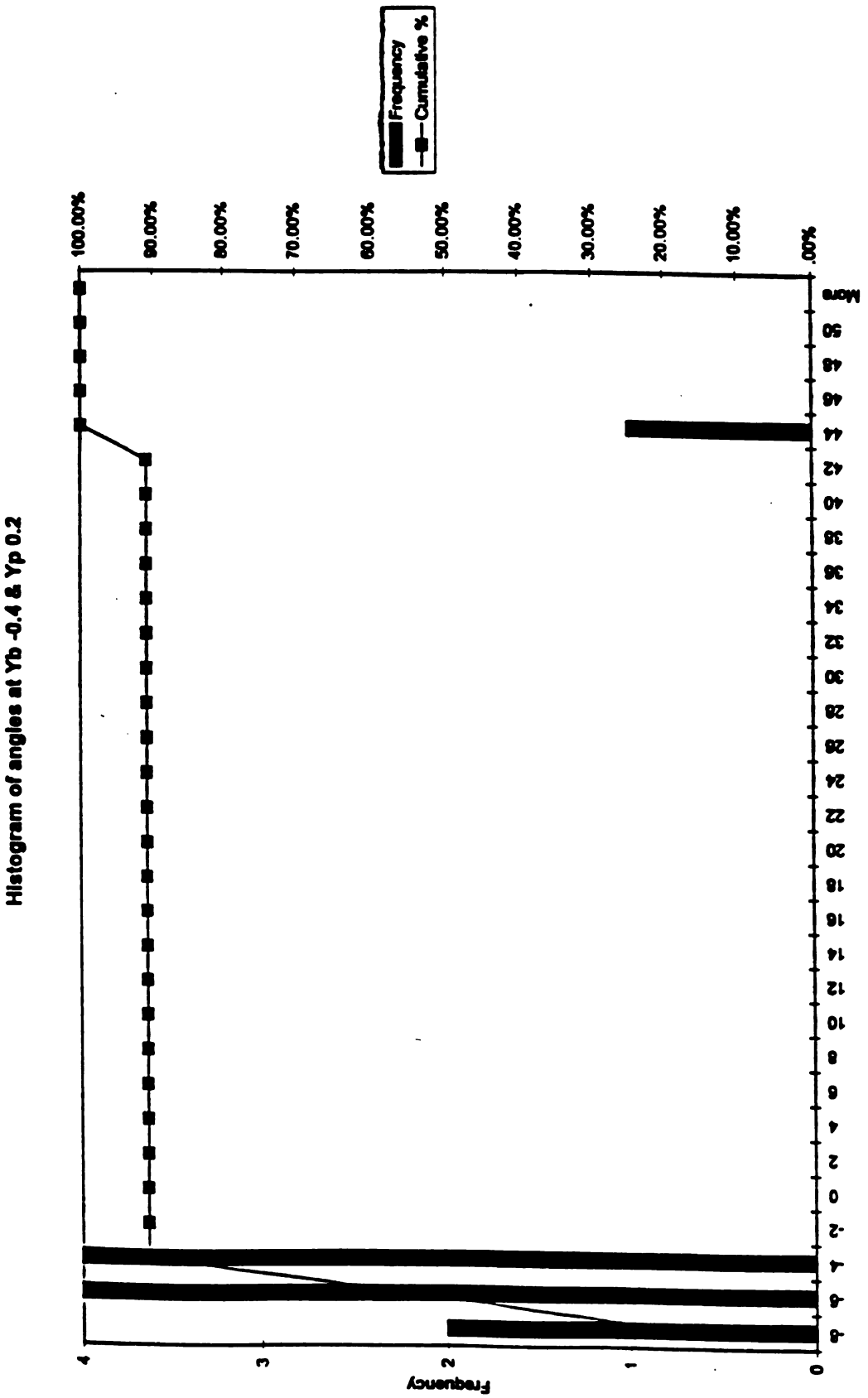

Figure 48. Histogram of flow angles at Yb/Wj=-0.4 and Yp/Wj=0.2

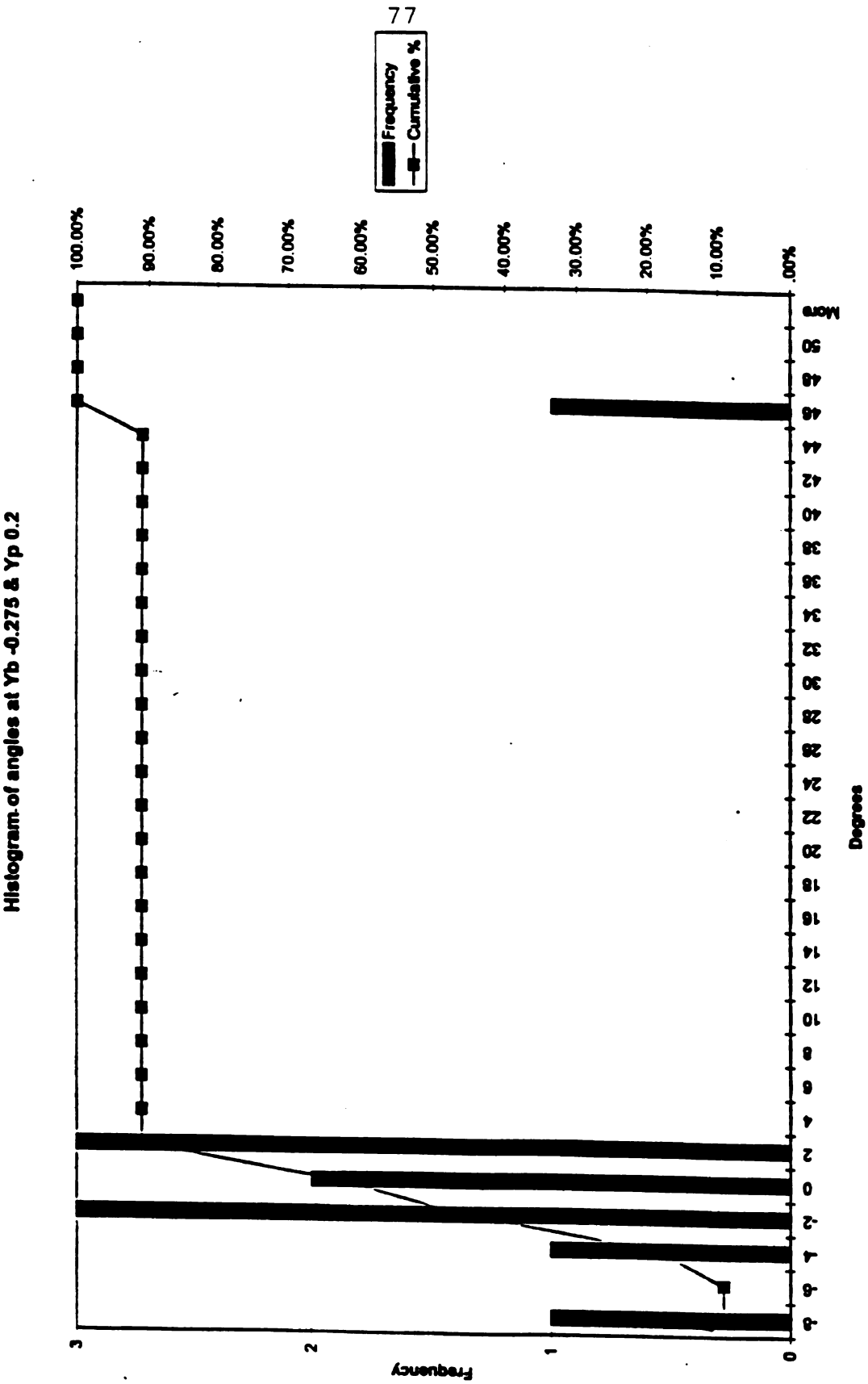

Figure 49. Histogram of flow angles at Yb/Wj=-0.275 and Yp/Wj= 0.2

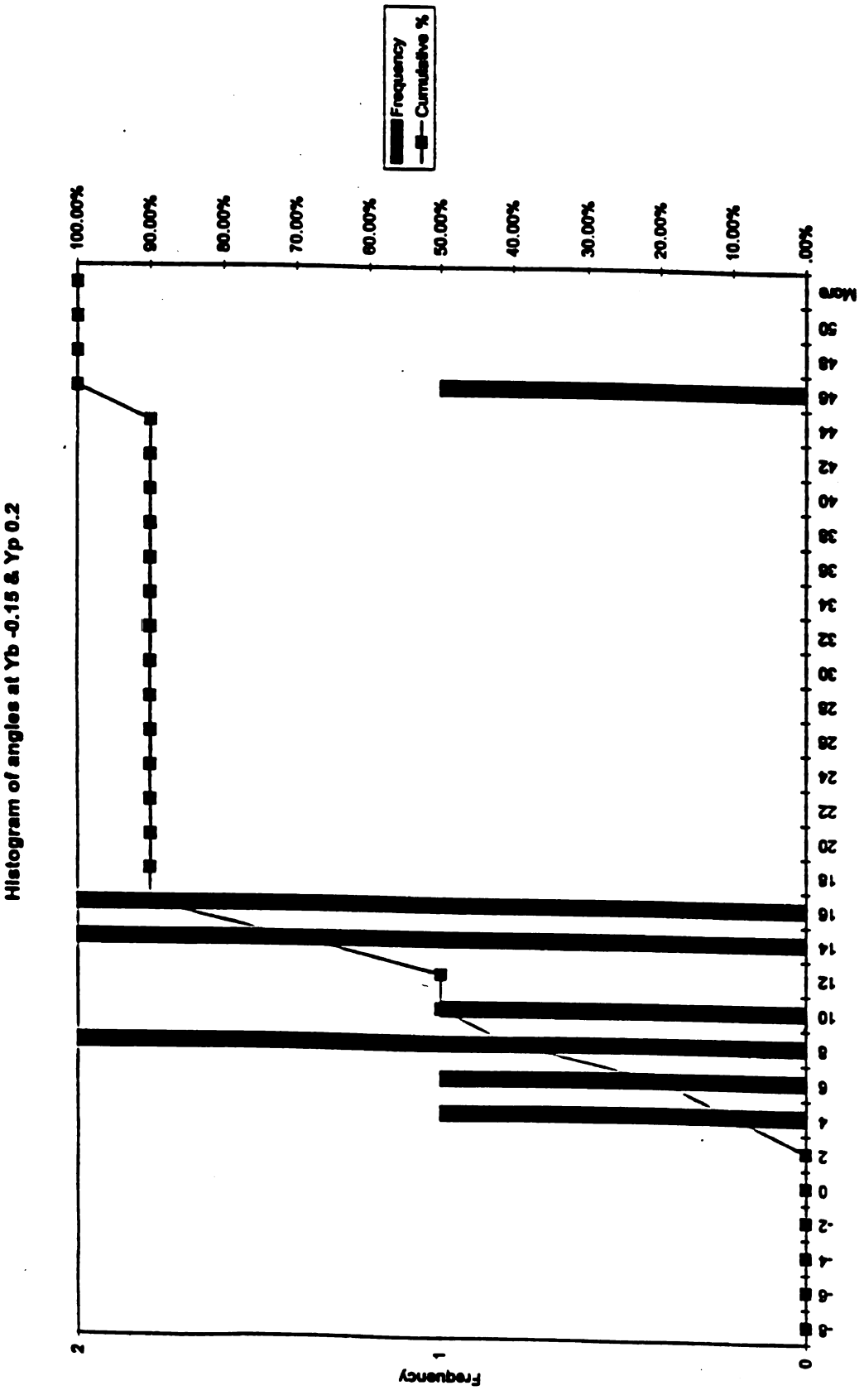

Figure 50. Histogram of flow angles at Yb/Wj=-0.15 and Yp/Wj= 0.2

Histogramof angles at Yb -0.025 & Yp 0.2

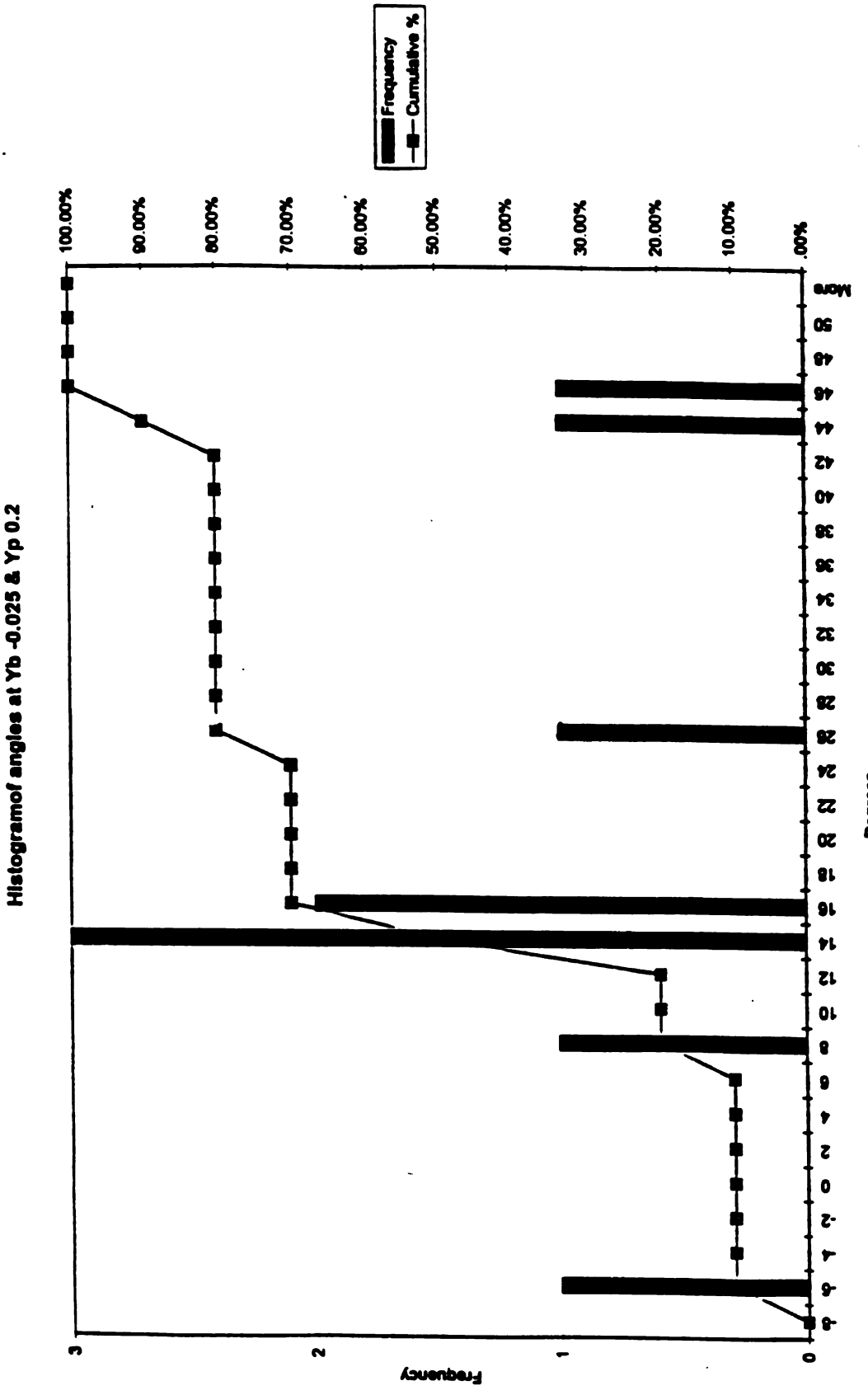

Figure 51. Histogram of flow angles at Yb/Wj=-0.025 and Yp/Wj= 0.2

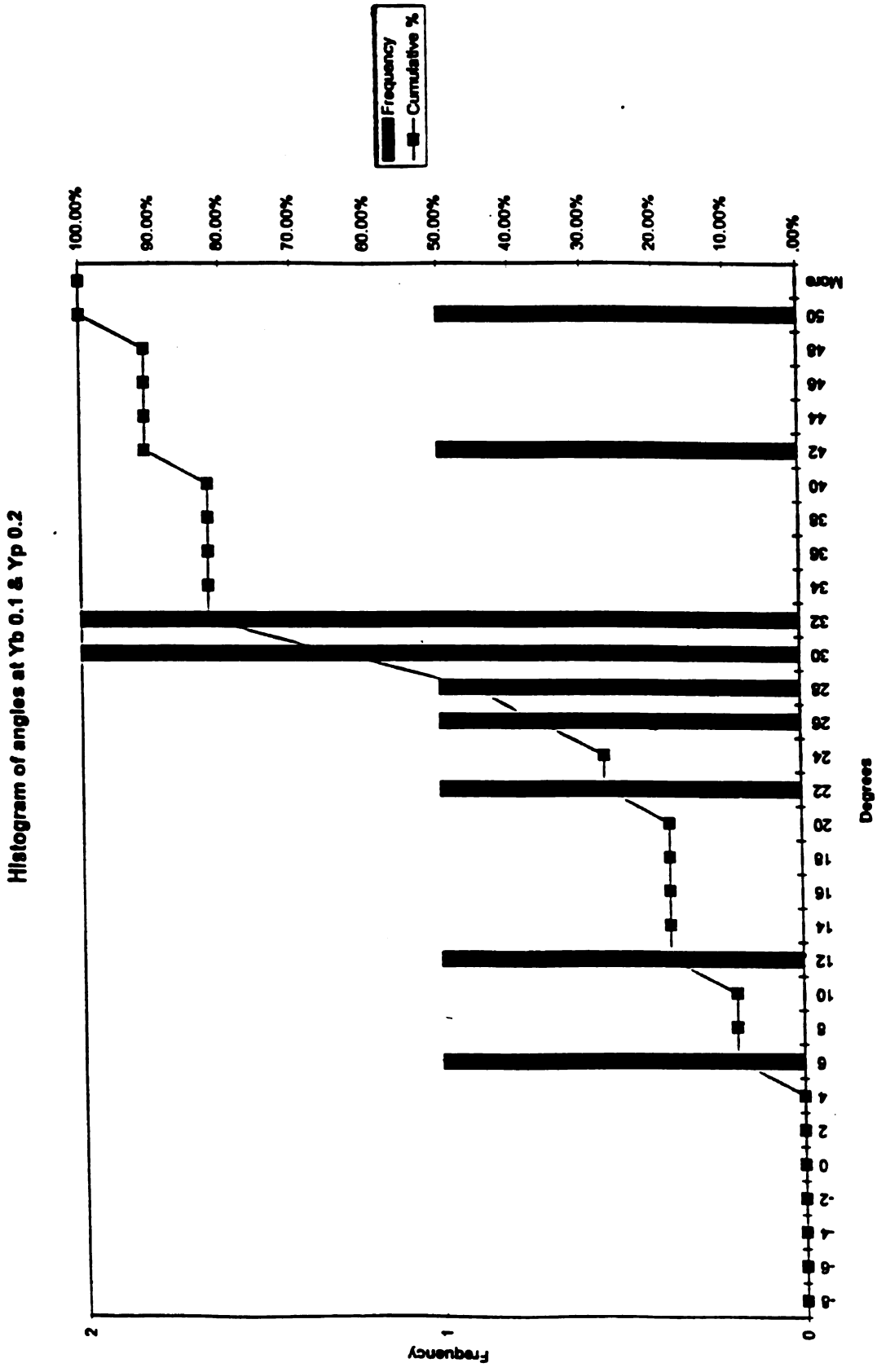

Figure 52. Histogram of flow angles at Yb/Wj=+0.1 and Yp/Wj= 0.2

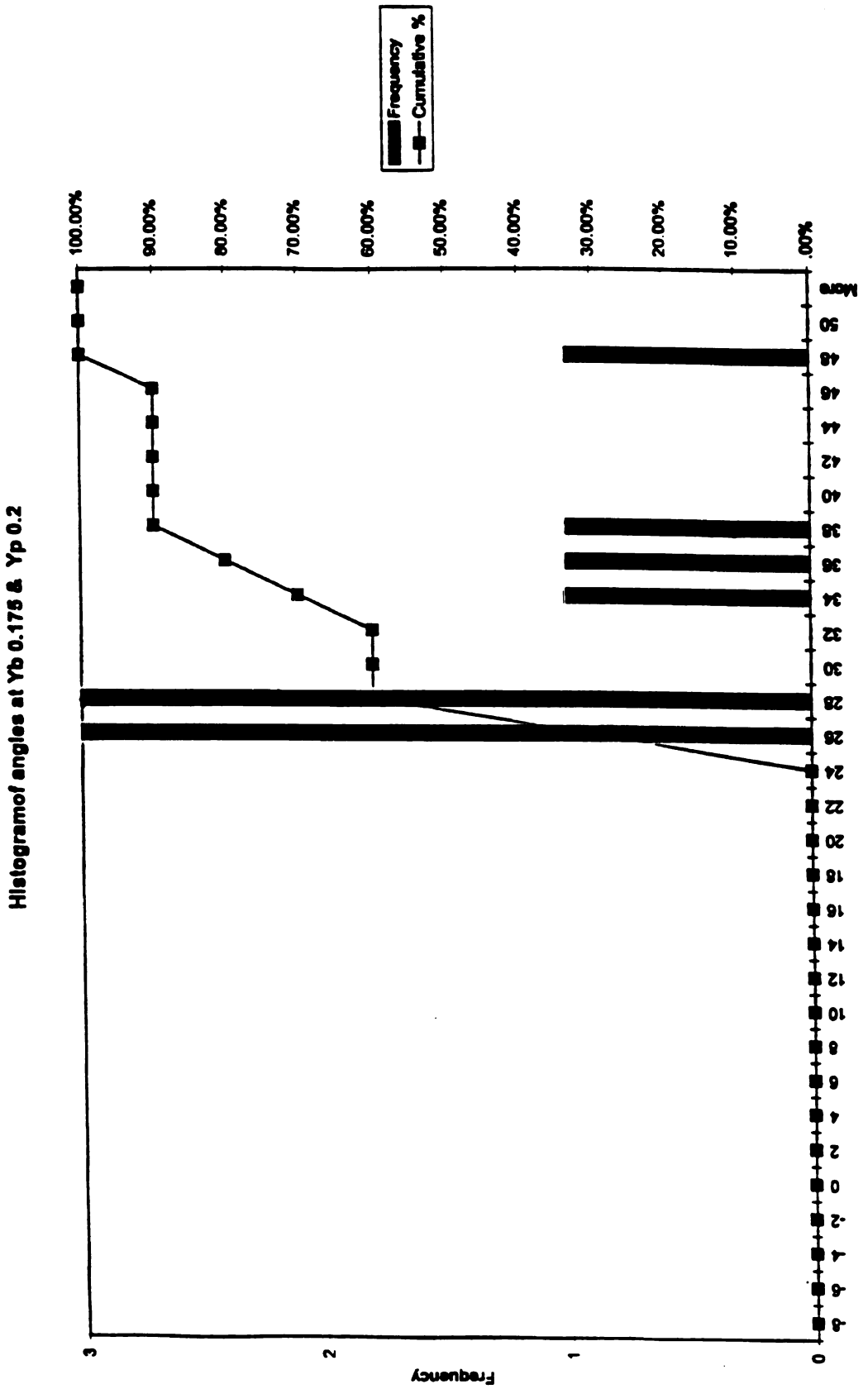

Figure 53. Histogram of flow angles at Yb/Wj=+0.175 and Yp/Wj= 0.2

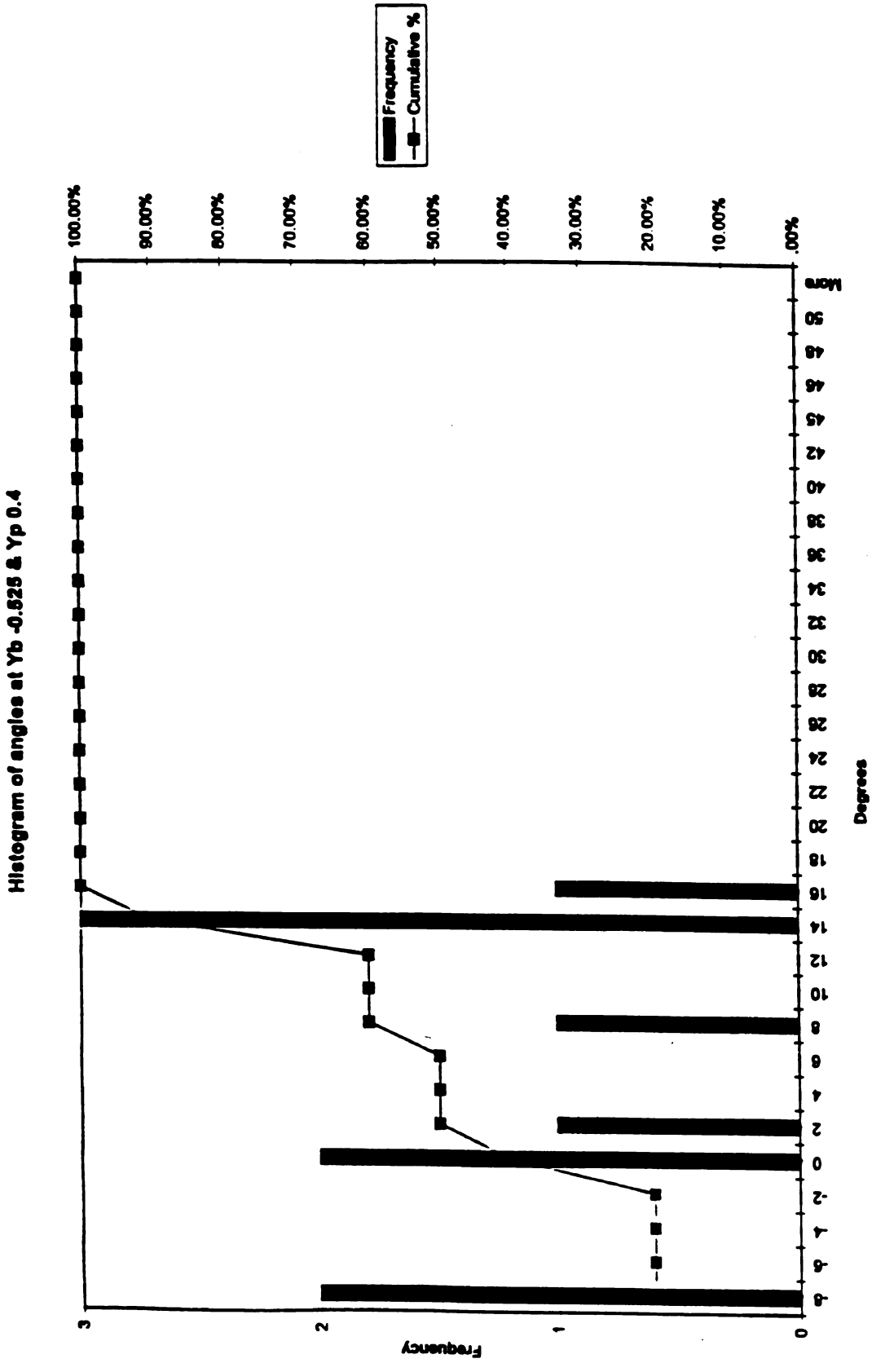

Figure 54. Histogram of flow angles at Yb/Wj=-0.525 and Yp/Wj= 0.4

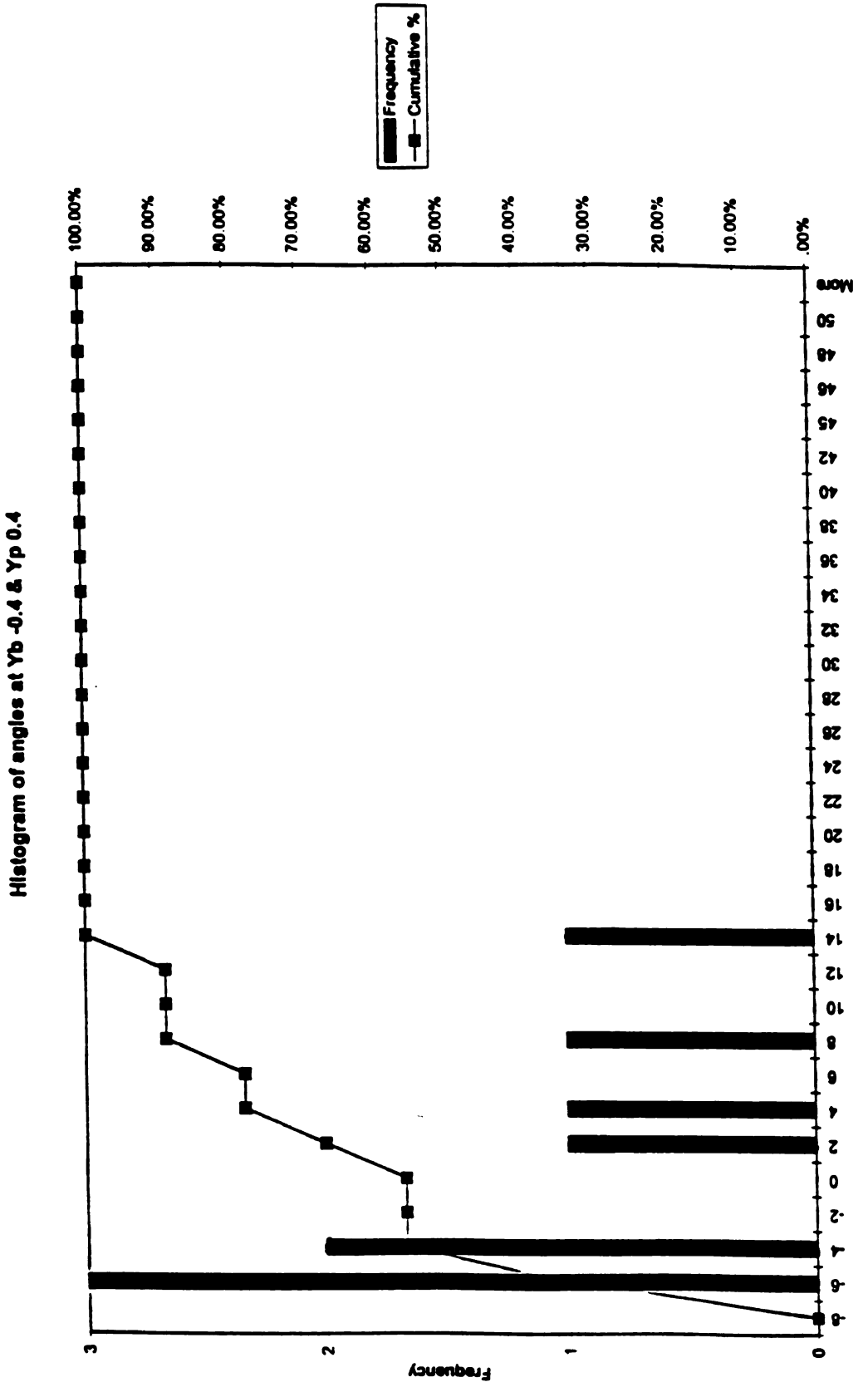

Figure 55. Histogram of flow angles at Yb/Wj=-0.4 and Yp/Wj=0.4

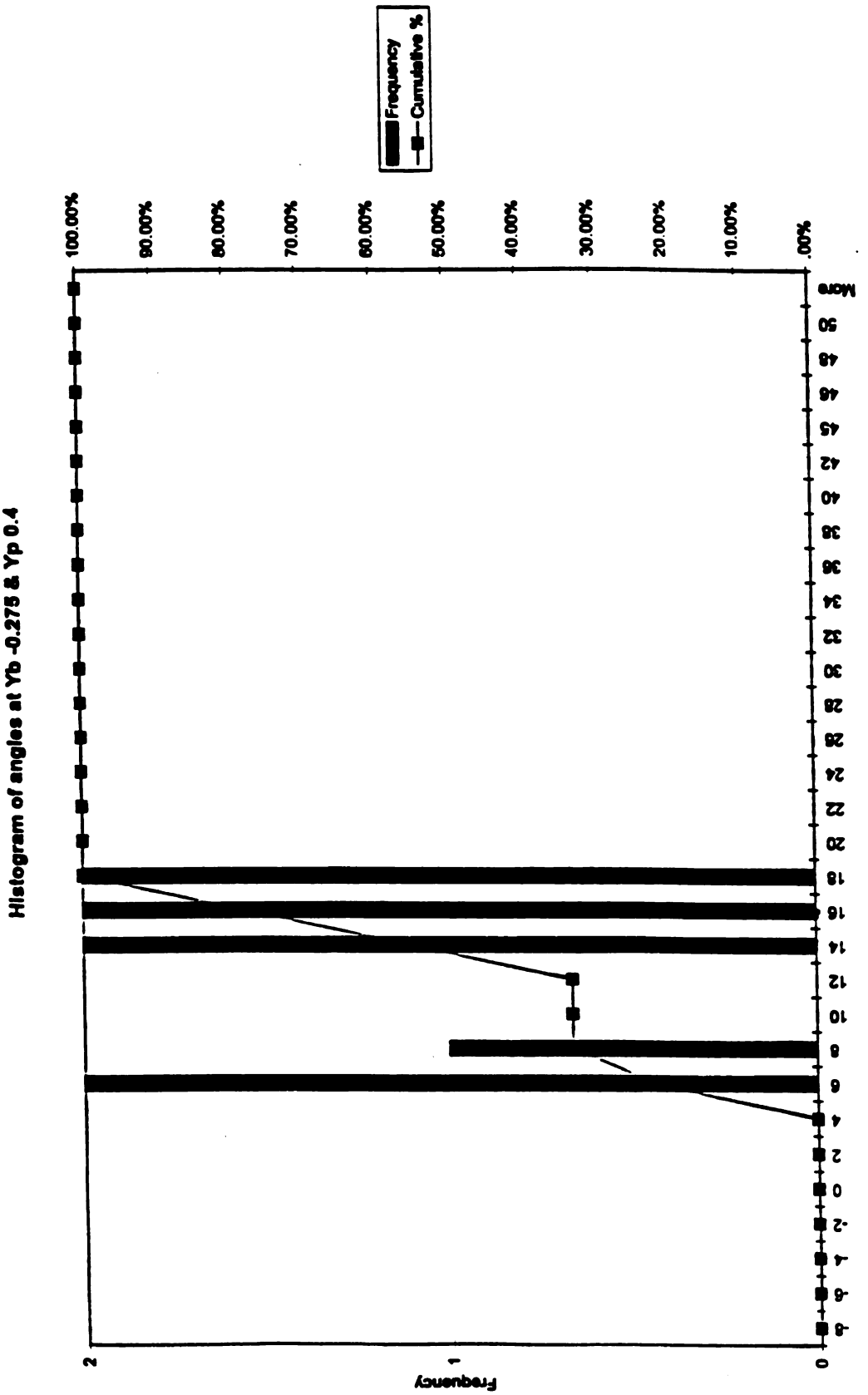

Figure 56. Histogram of flow angles at Yb/Wj=-0.275 and Yp/Wj= 0.4

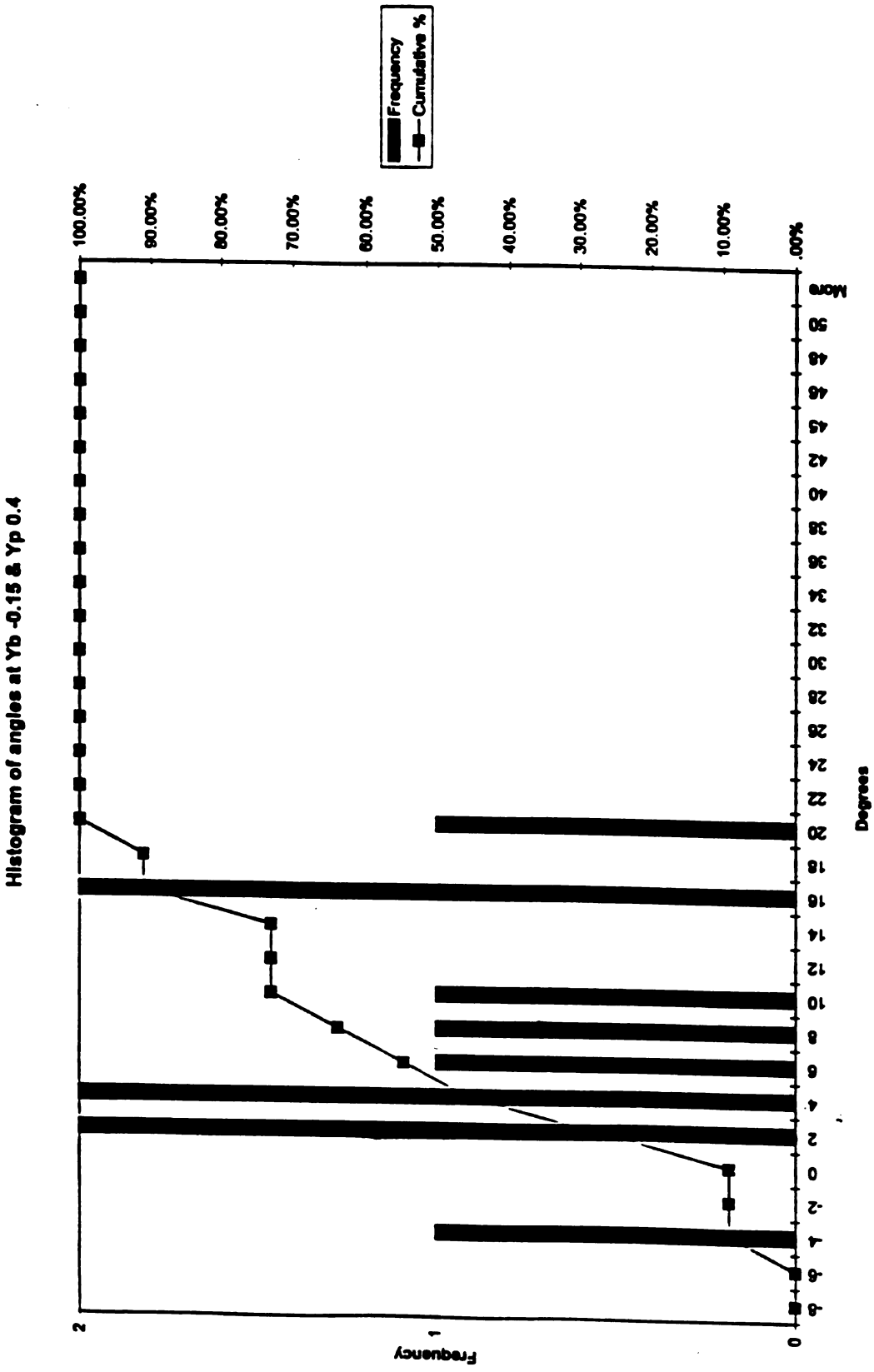

Figure 57. Histogram of flow angles at Yb/Wj=-0.15 and Yp/Wj= 0.4

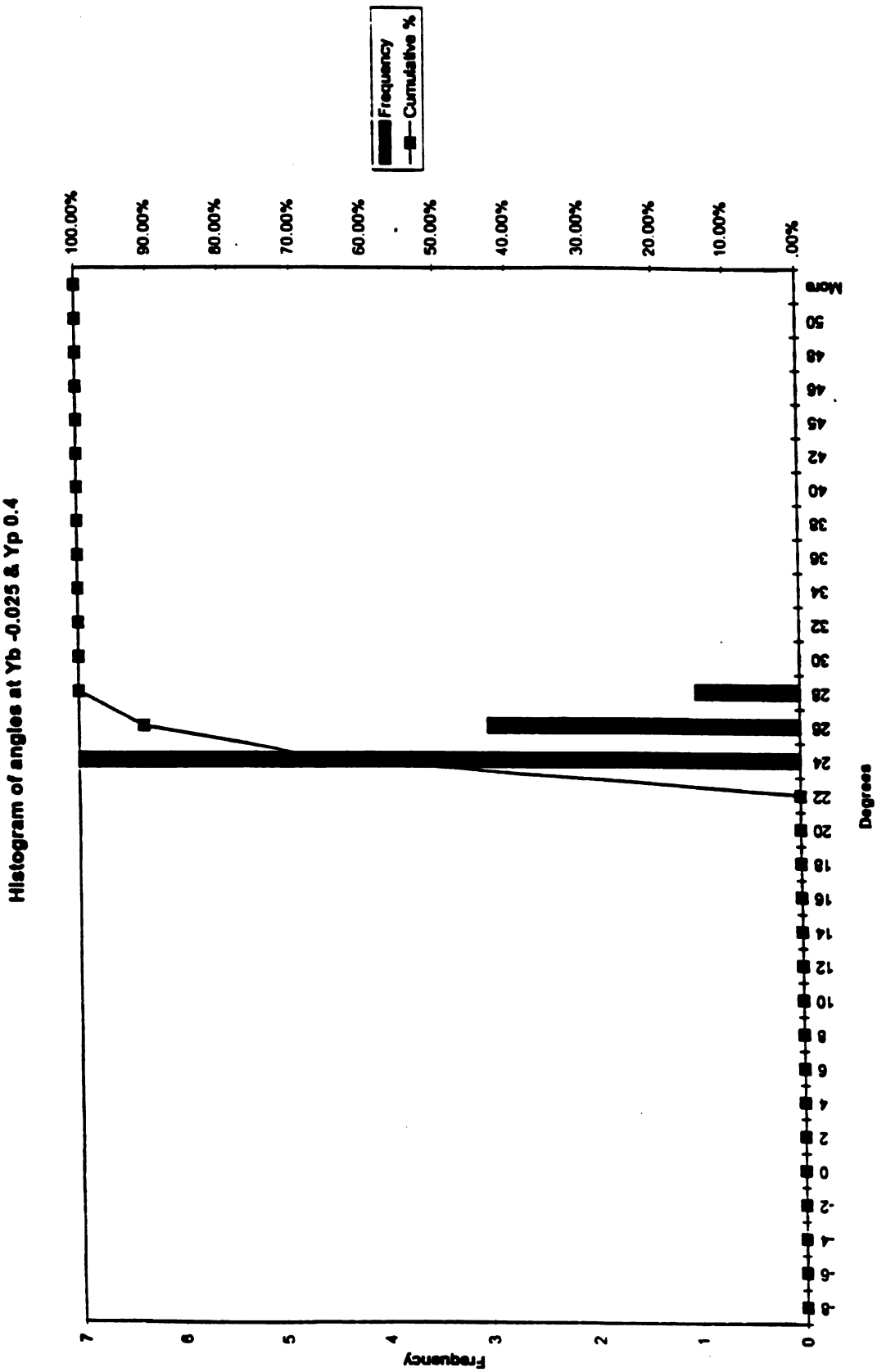

Figure 58. Histogram of flow angles at Yb/Wj=-0.025 and Yp/Wj= 0.4

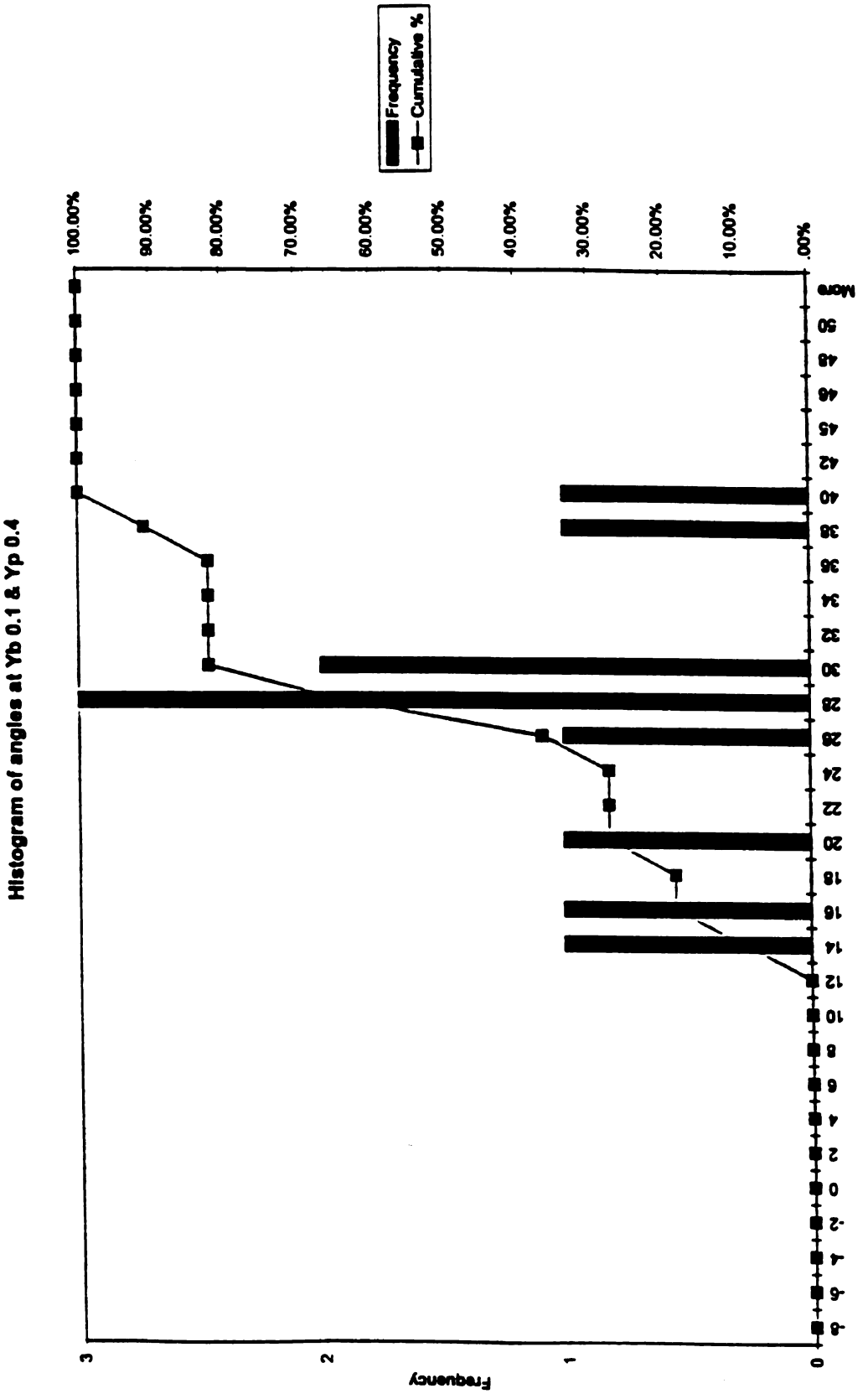

Figure 59. Histogram of flow angles at Yb/Wj=+0.1 and Yp/Wj= 0.4

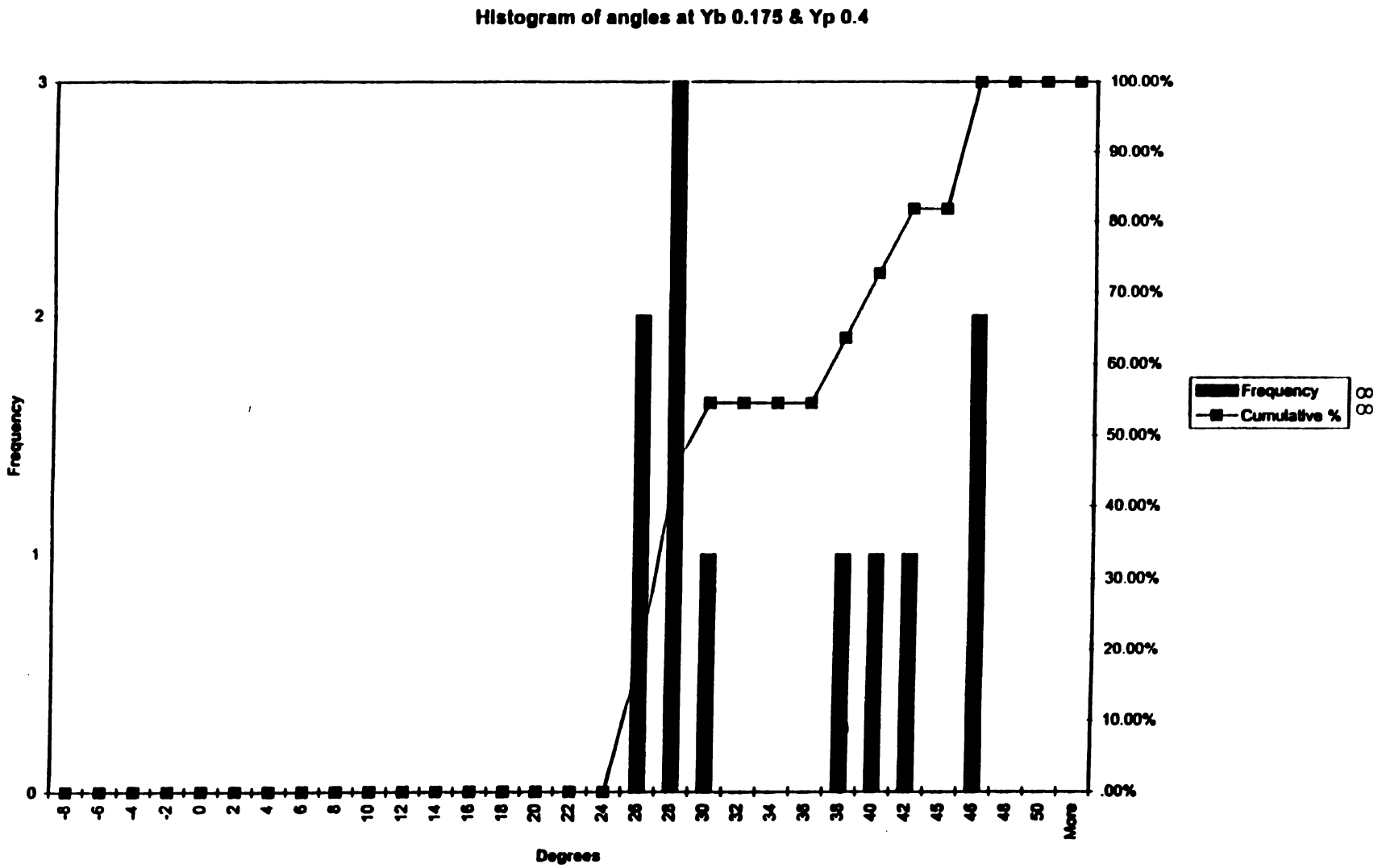

Figure 60. Histogram of flow angles at Yb/Wj=+0.175 and Yp/Wj= 0.4

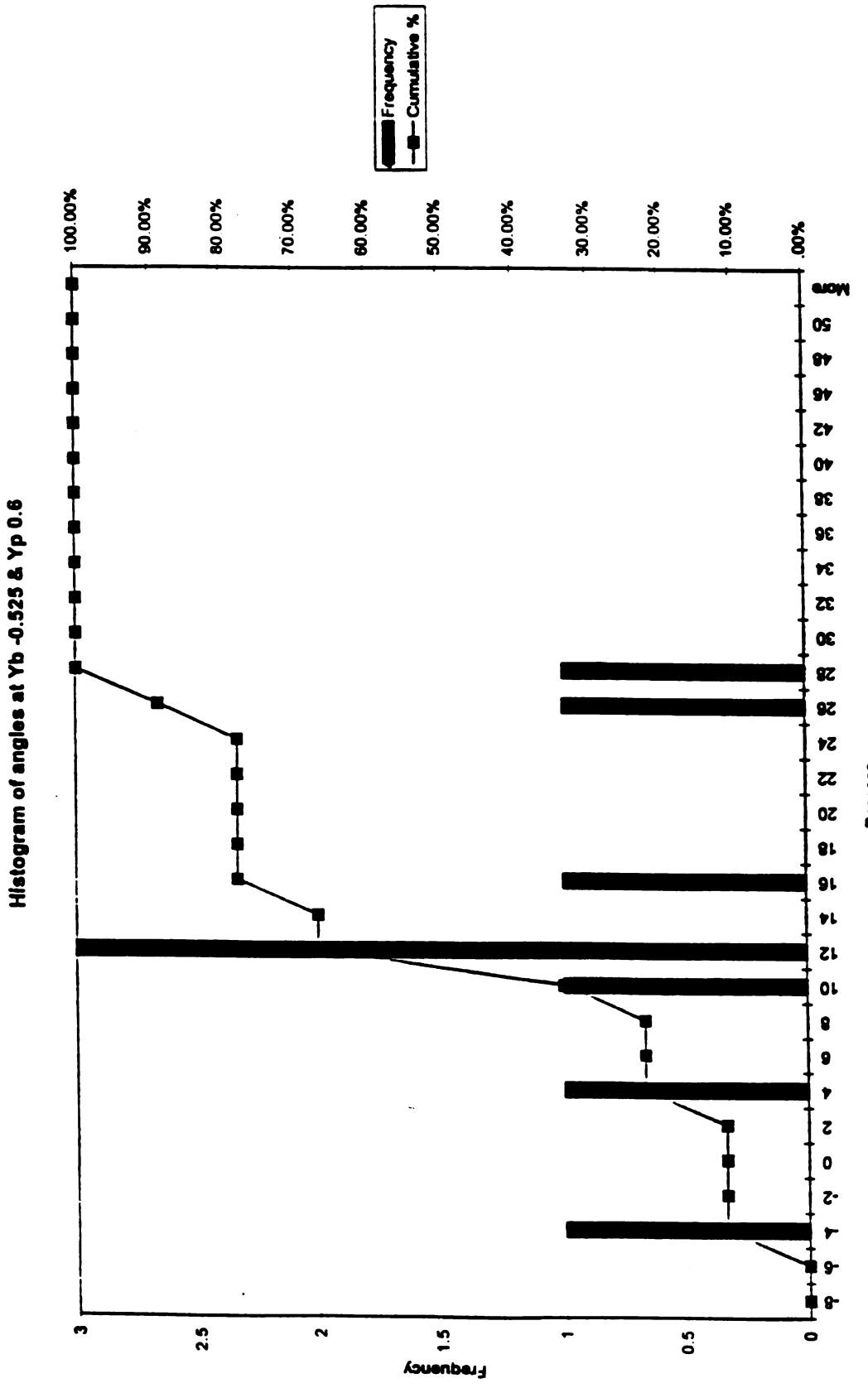

Figure 61. Histogram of flow angles at Yb/Wj=-0.525 and Yp/Wj= 0.6

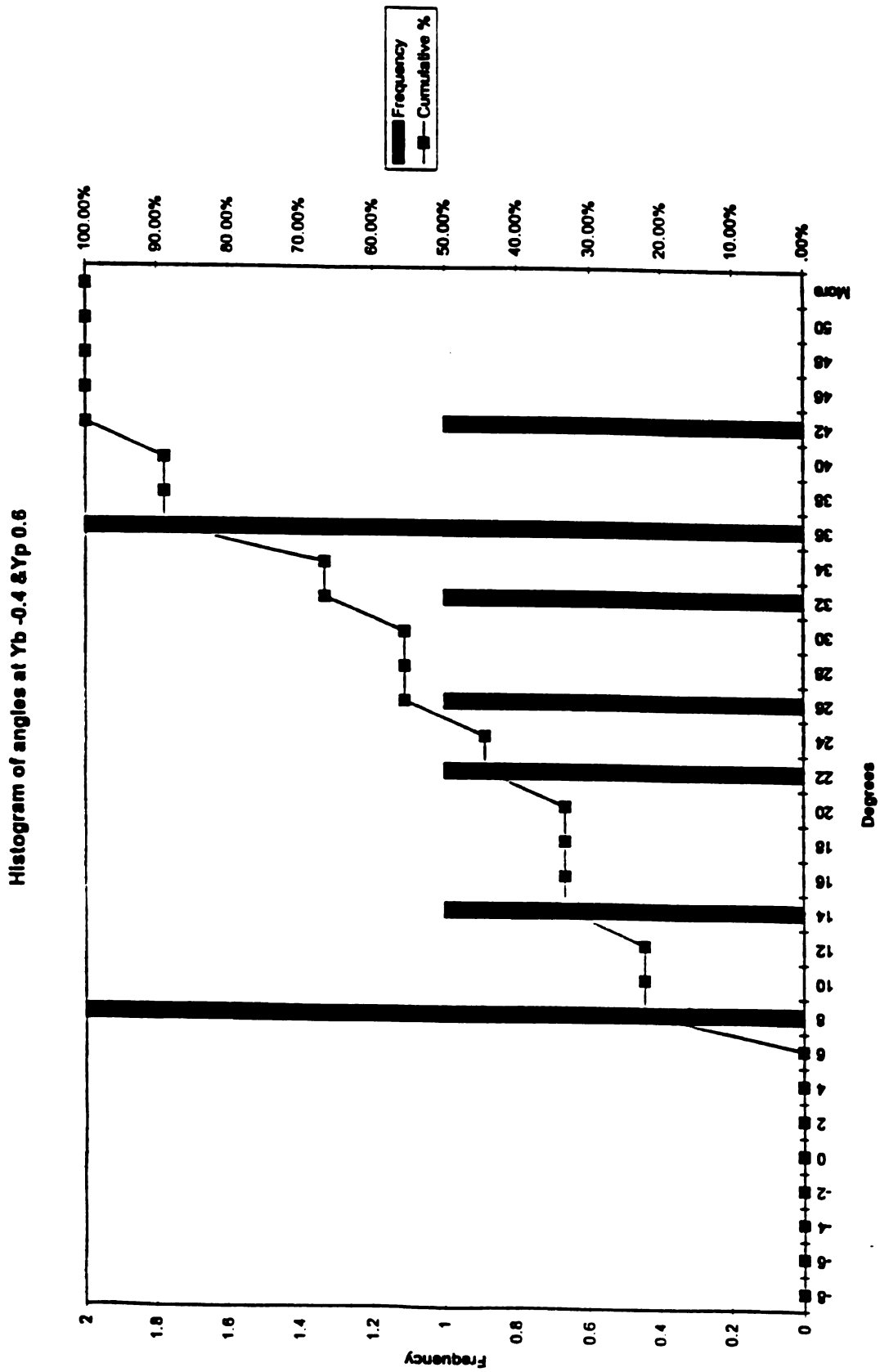

Figure 62. Histogram of flow angles at Yb/Wj=-0.4 and Yp/Wj=0.6

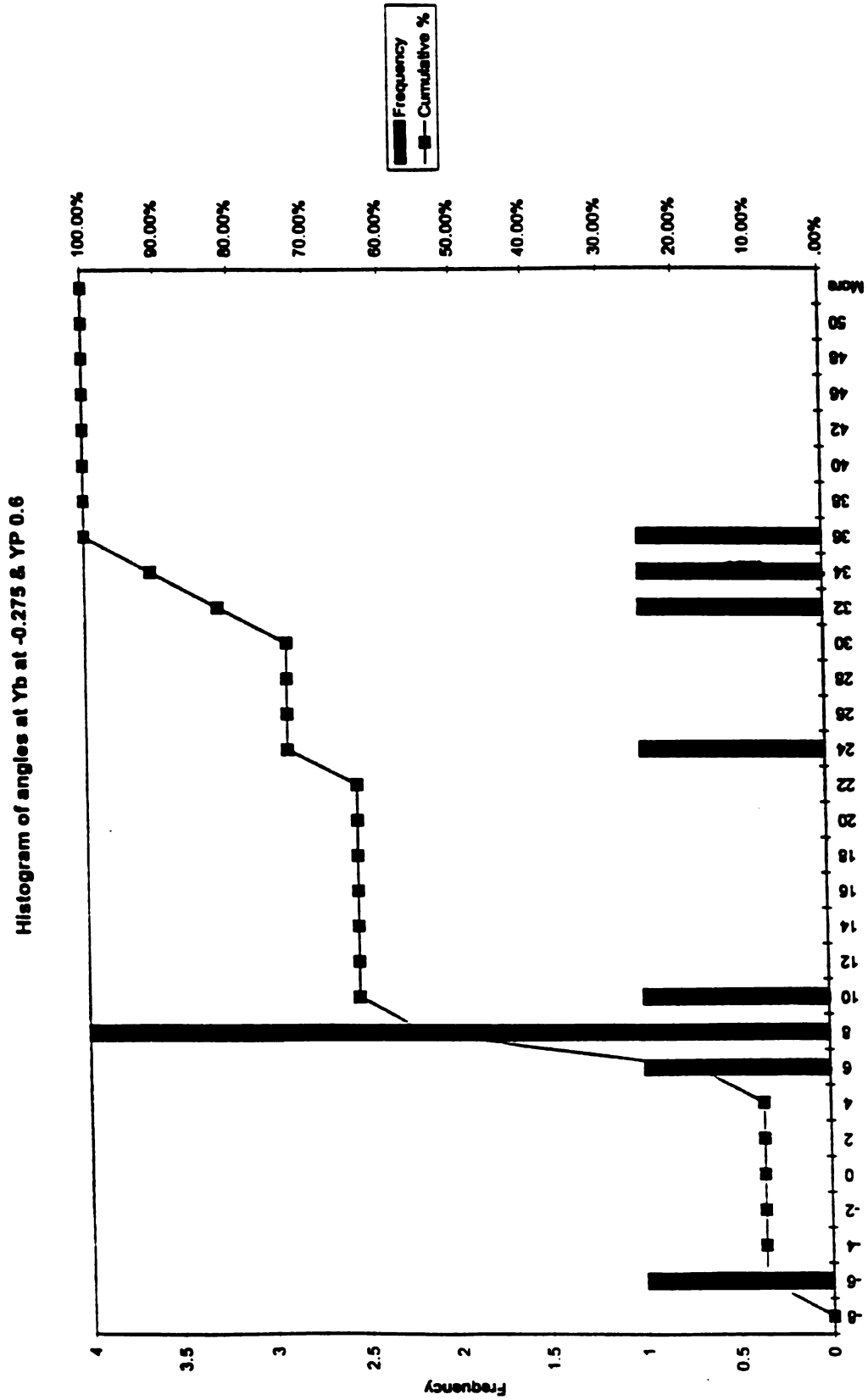

Figure 63. Histogram of flow angles at Yb/Wj=-0.275 and Yp/Wj= 0.6

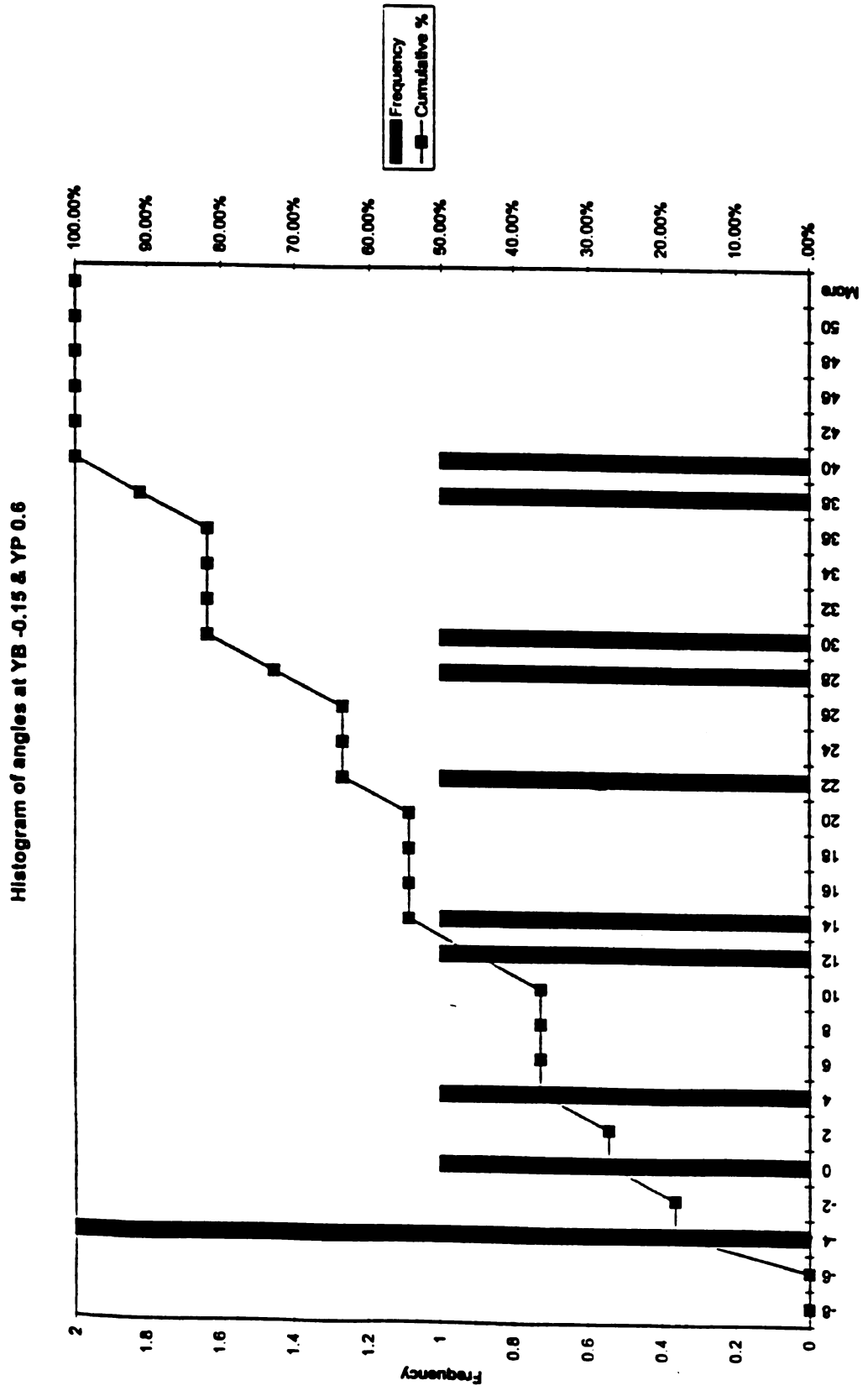

Figure 64. Histogram of flow angles at Yb/Wj=-0.15 and Yp/Wj= 0.6

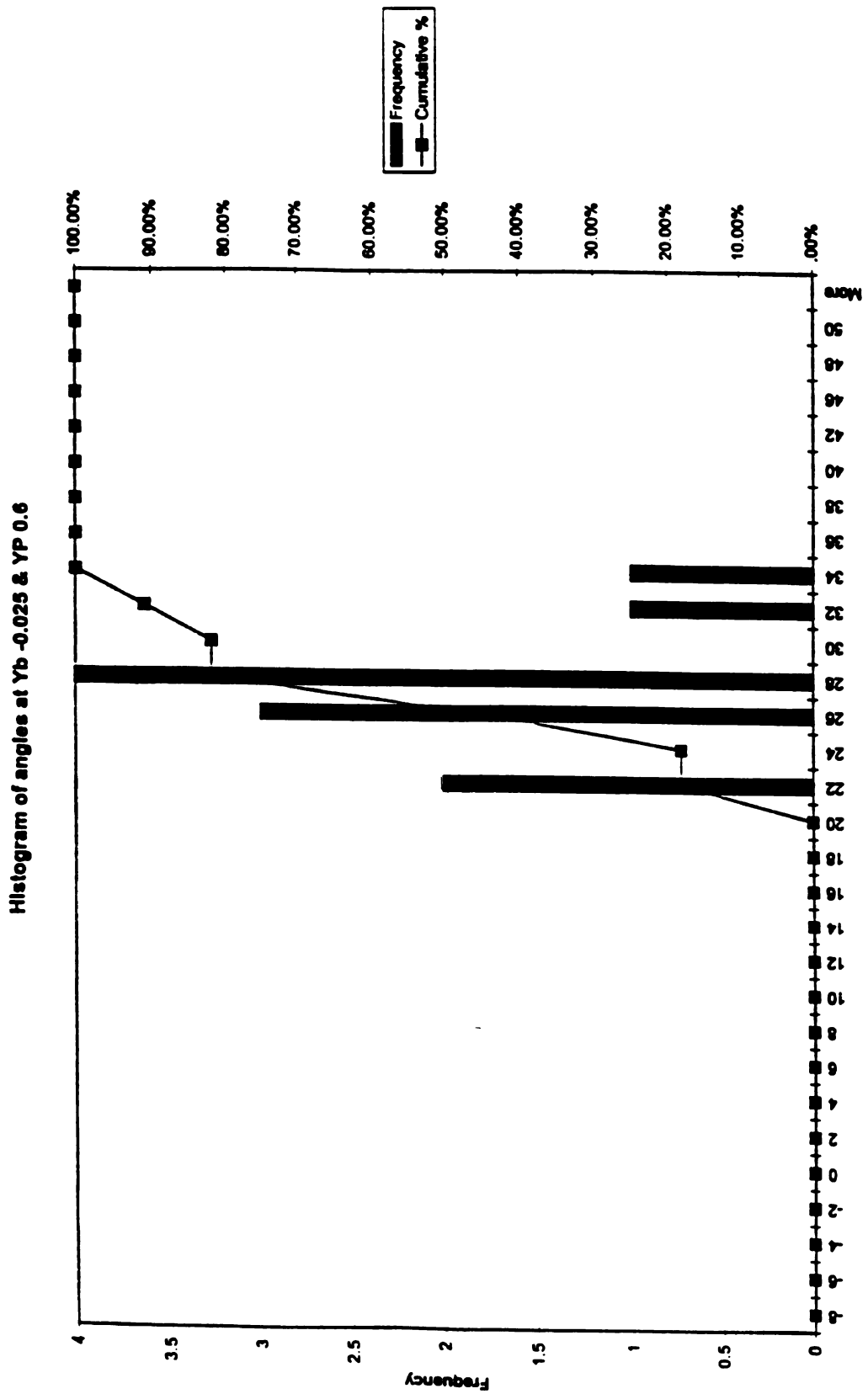

Figure 65. Histogram of flow angles at Yb/Wj=-0.025 and Yp/Wj= 0.6

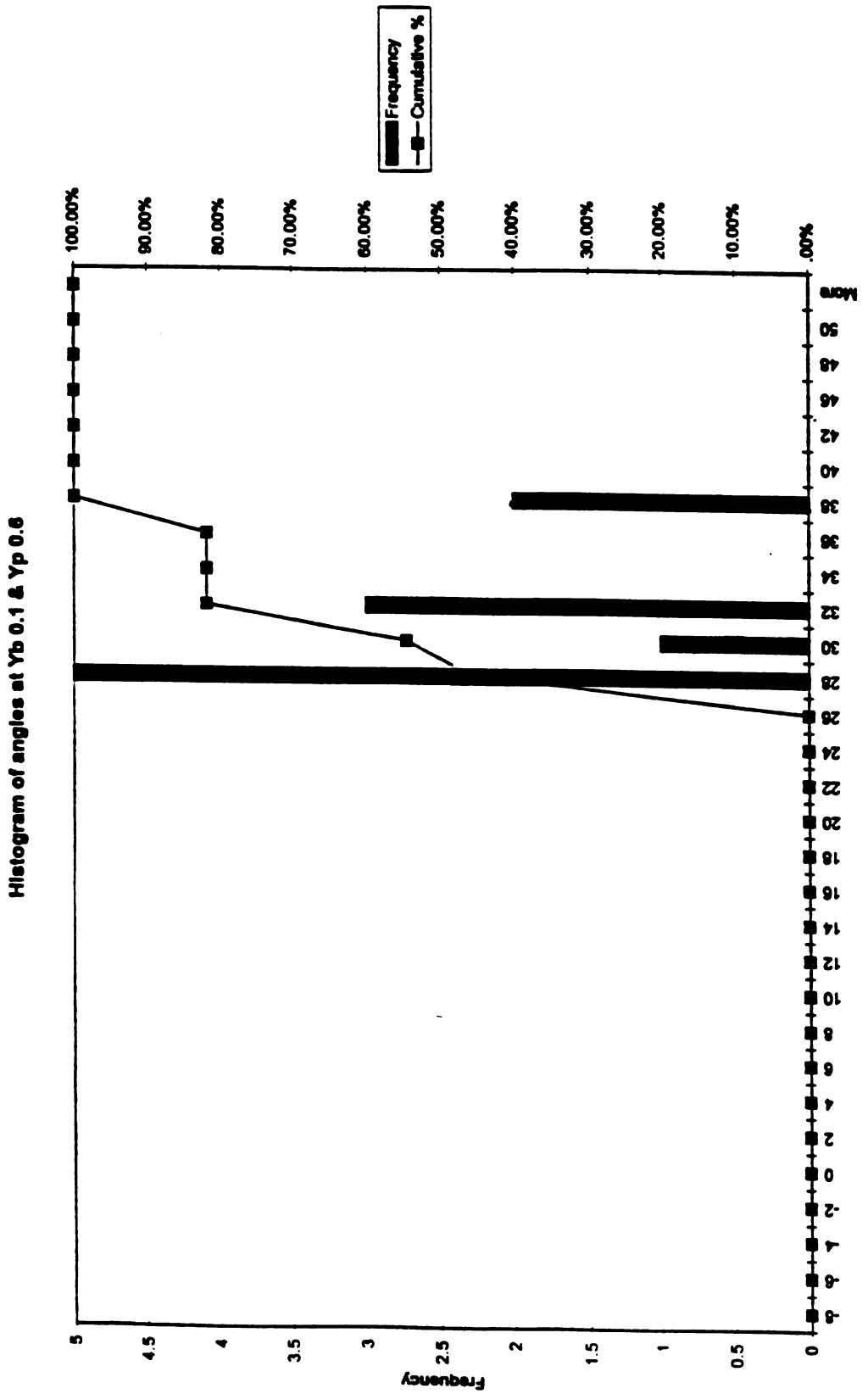

Figure 66. Histogram of flow angles at Yb/Wj=+0.1 and Yp/Wj= 0.6

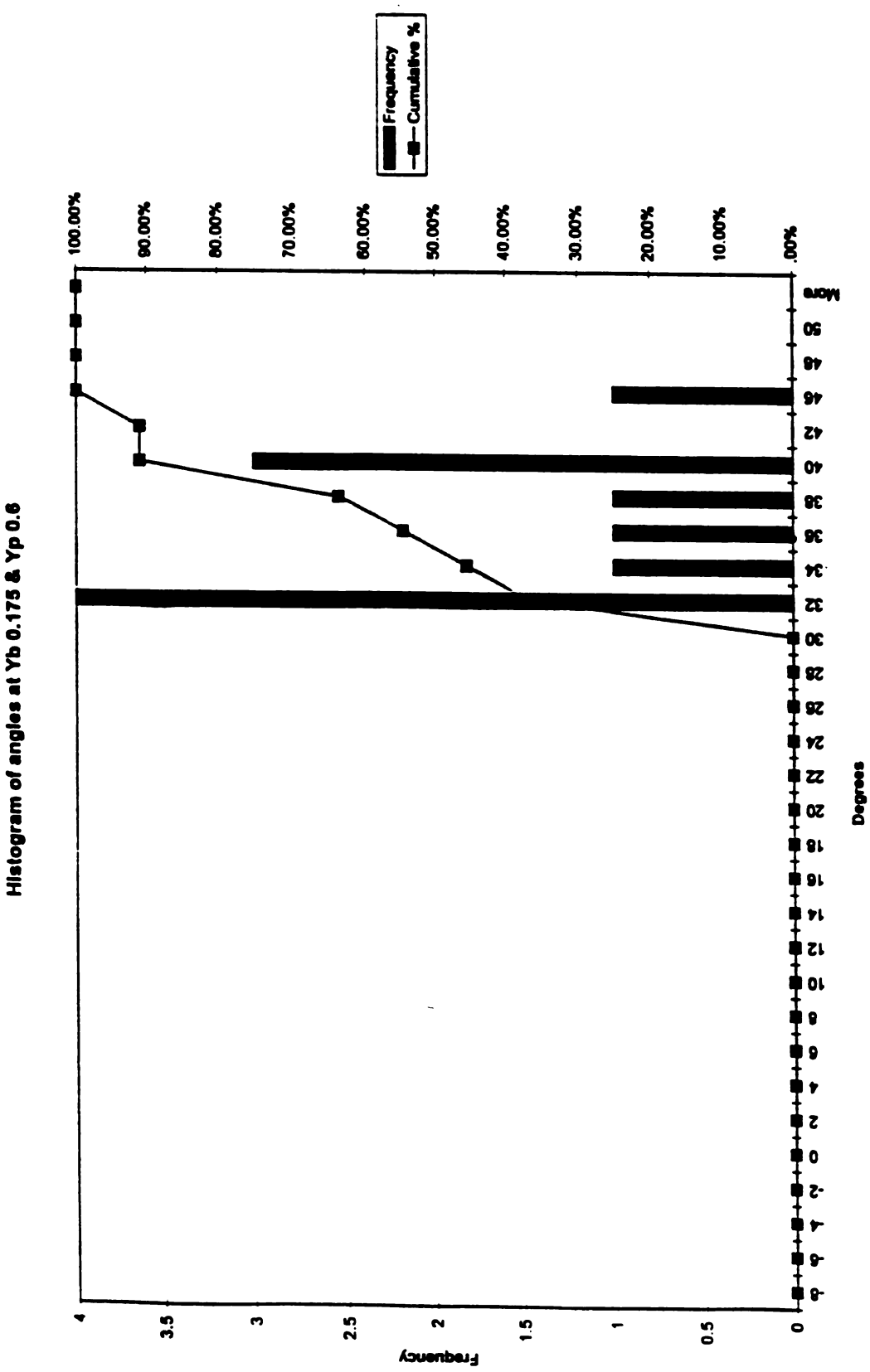

Figure 67. Histogram of flow angles at Yb/Wj=+0.175 and Yp/Wj= 0.6

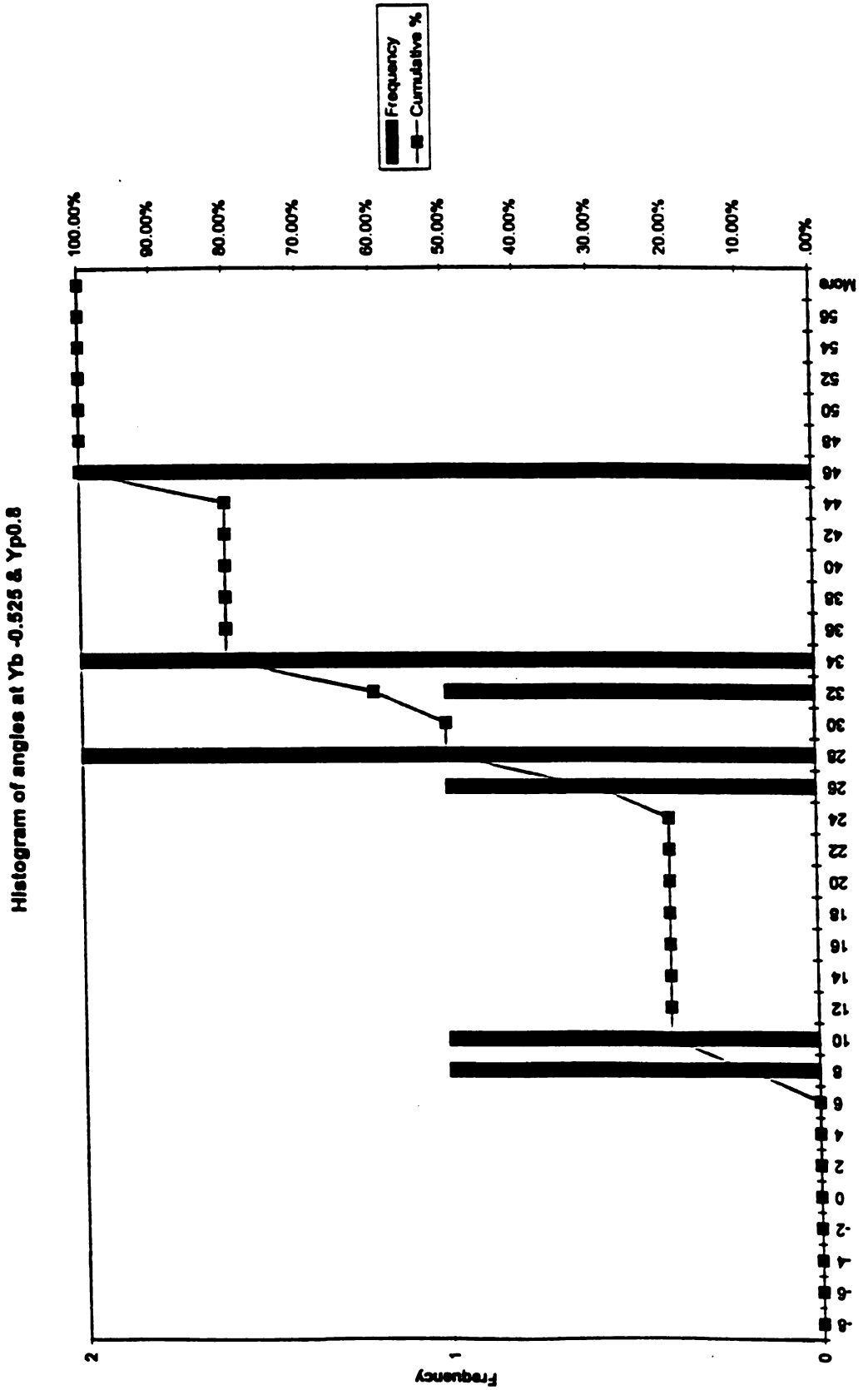

Figure 68. Histogram of flow angles at Yb/Wj=-0.525 and Yp/Wj= 0.8

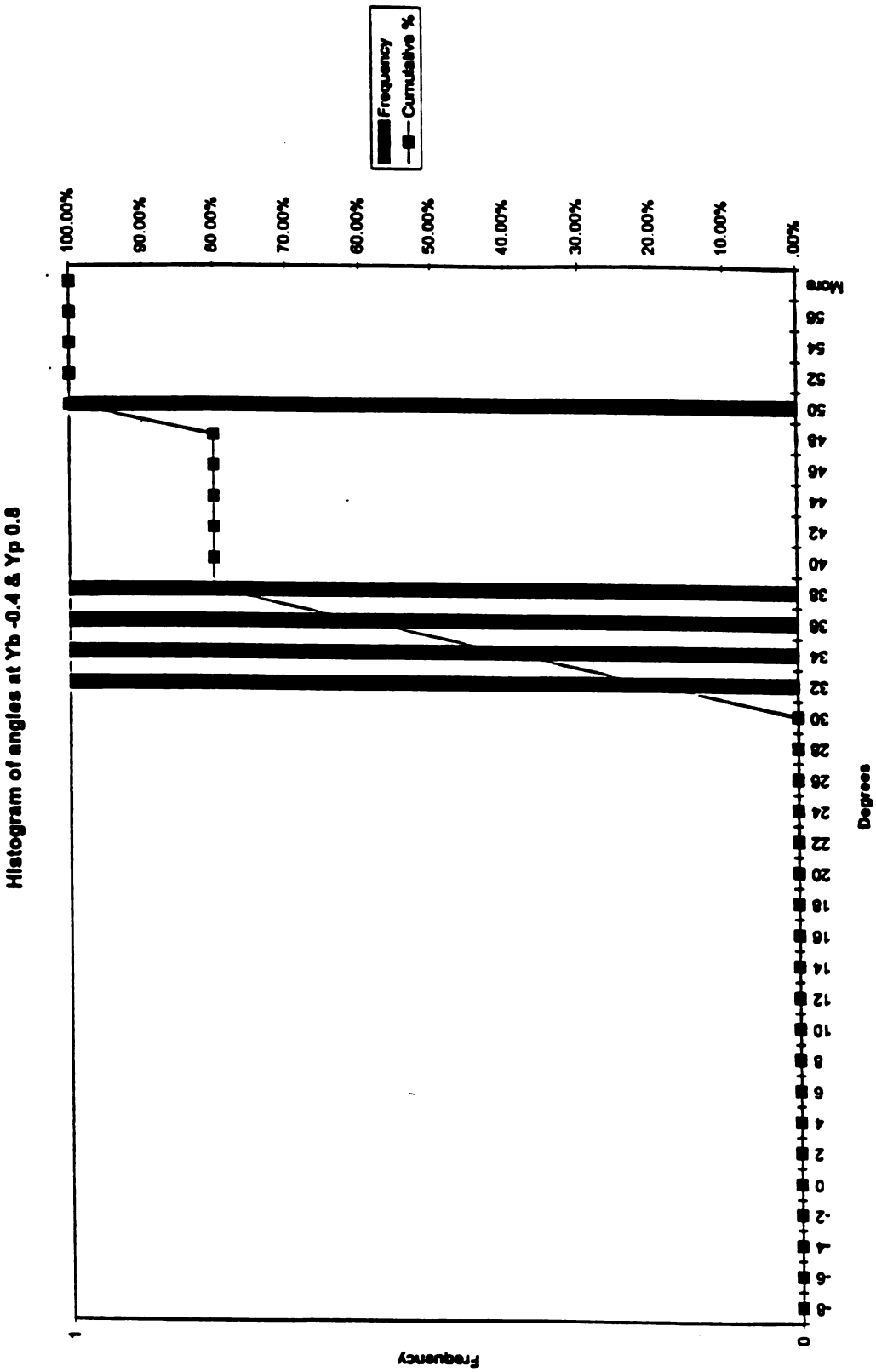

Figure 69. Histogram of flow angles at Yb/Wj=-0.4 and Yp/Wj=0.8

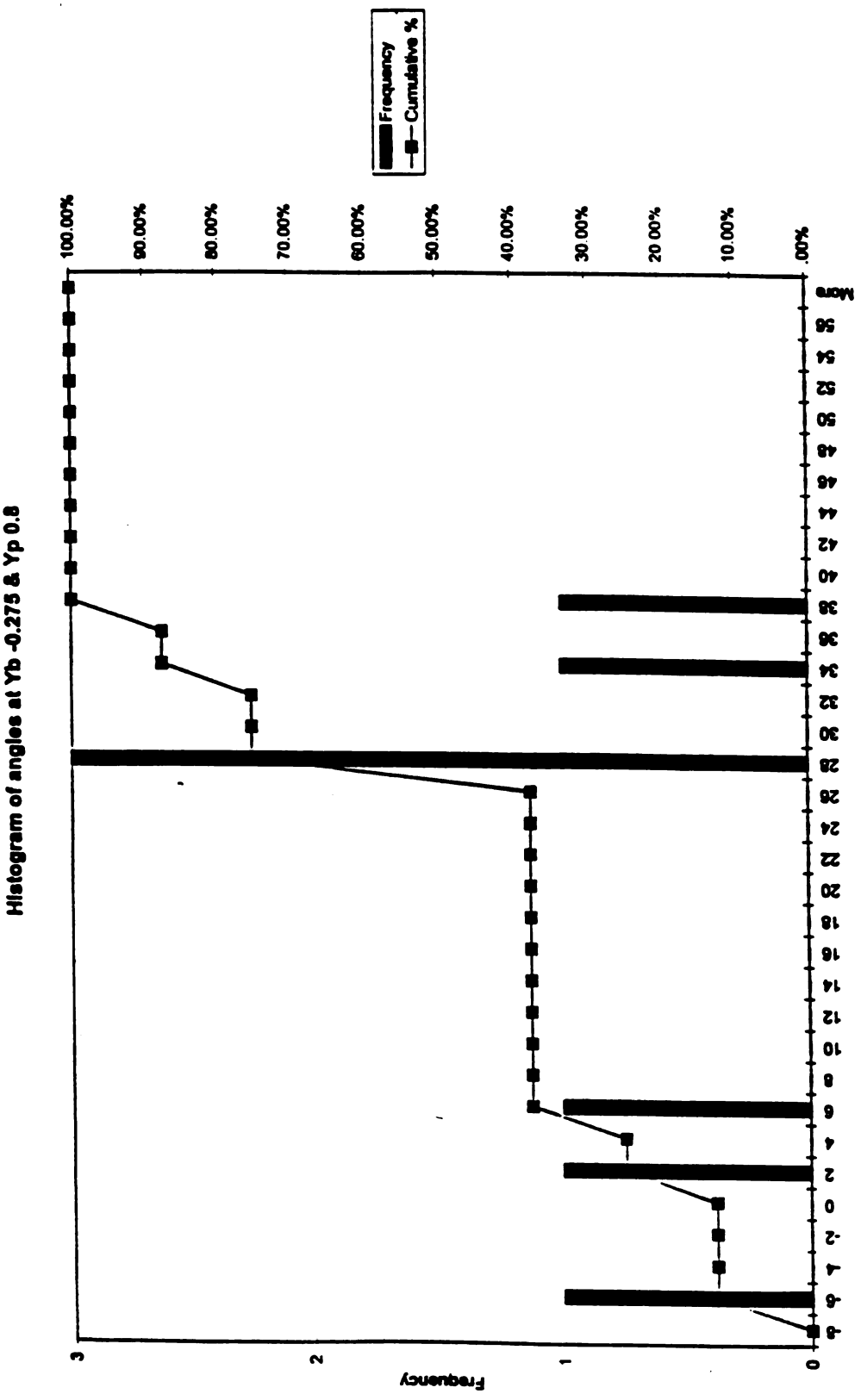

Figure 70. Histogram of flow angles at Yb/Wj=-0.275 and Yp/Wj= 0.8

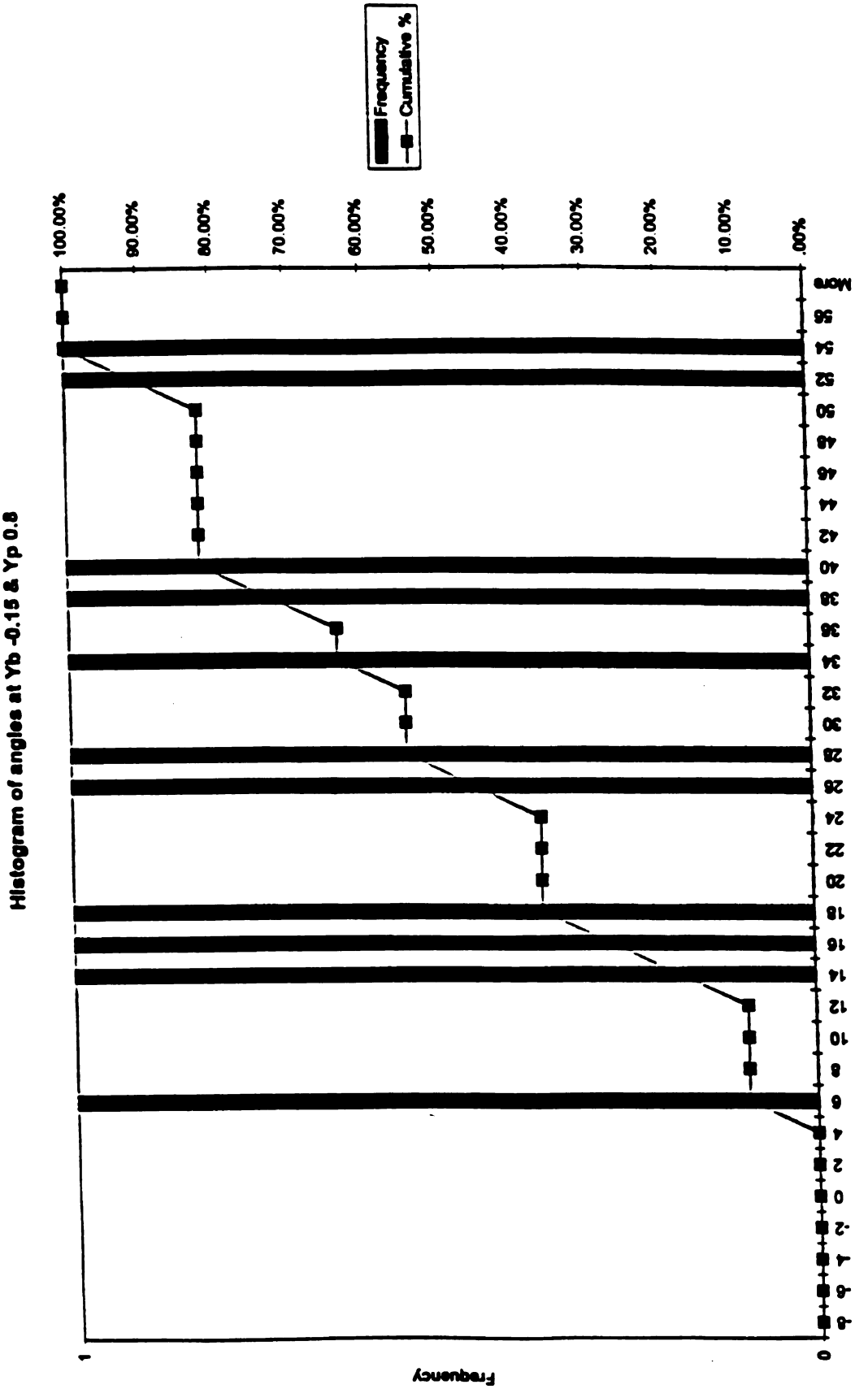

Figure 71. Histogram of flow angles at Yb/Wj=-0.15 and Yp/Wj= 0.8

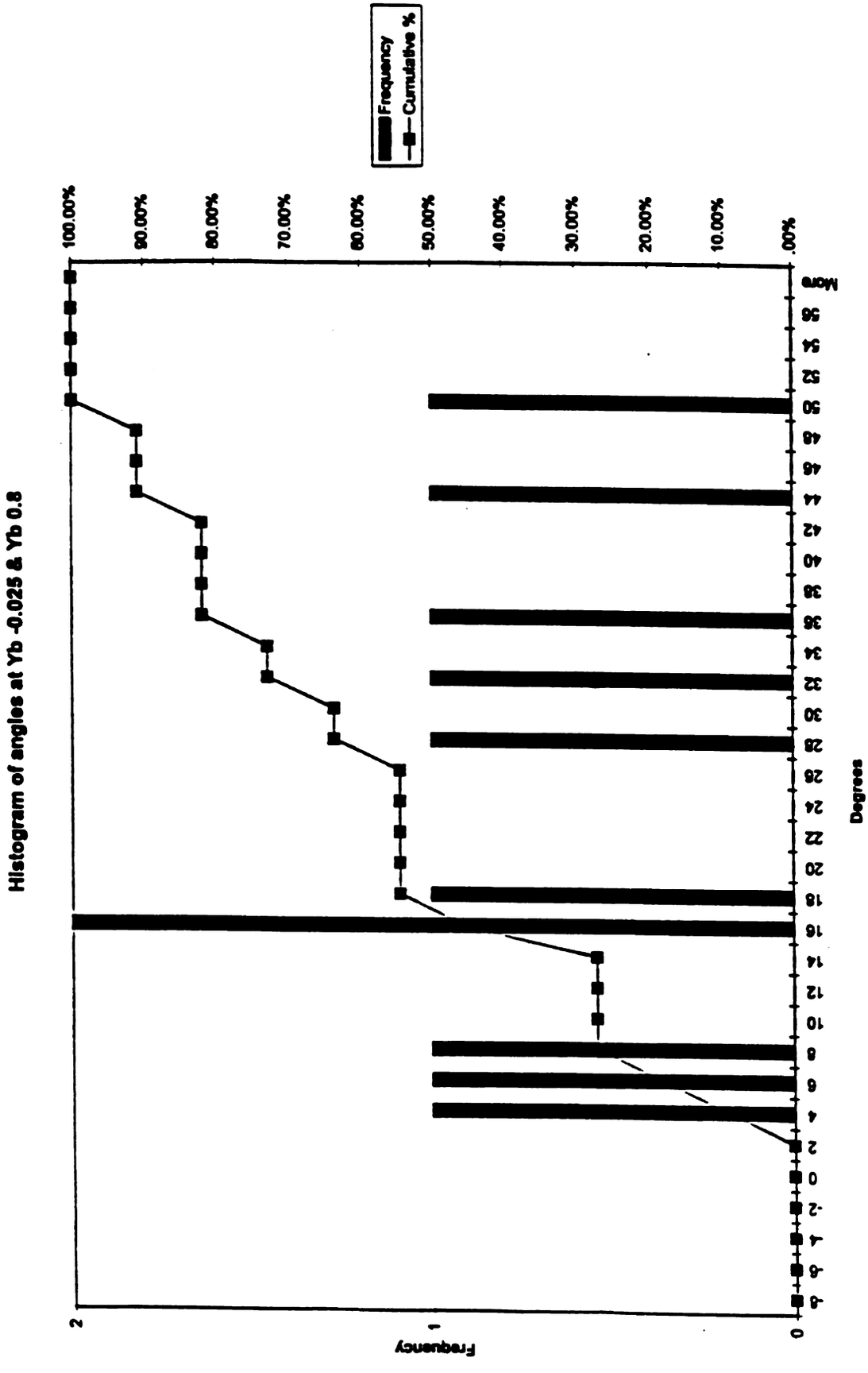

Figure 72. Histogram of flow angles at Yb/Wj=-0.025 and Yp/Wj= 0.8

Histogram of angles at Yb 0.1 & Yp 0.8

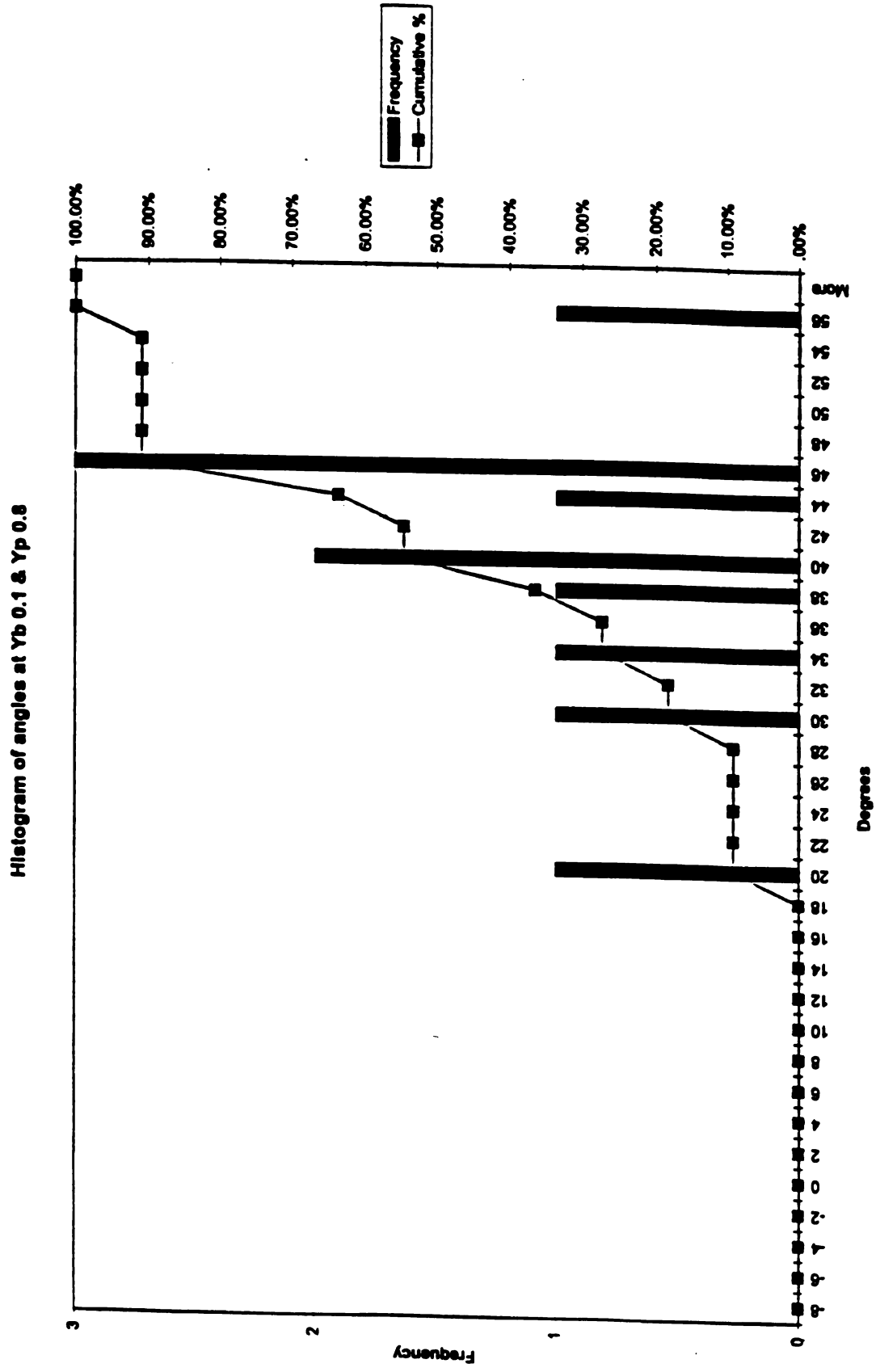

Figure 73. Histogram of flow angles at Yb/Wj=+0.1 and Yp/Wj= 0.8

Histogram of angles at Yb0.175 & Yp 0.8

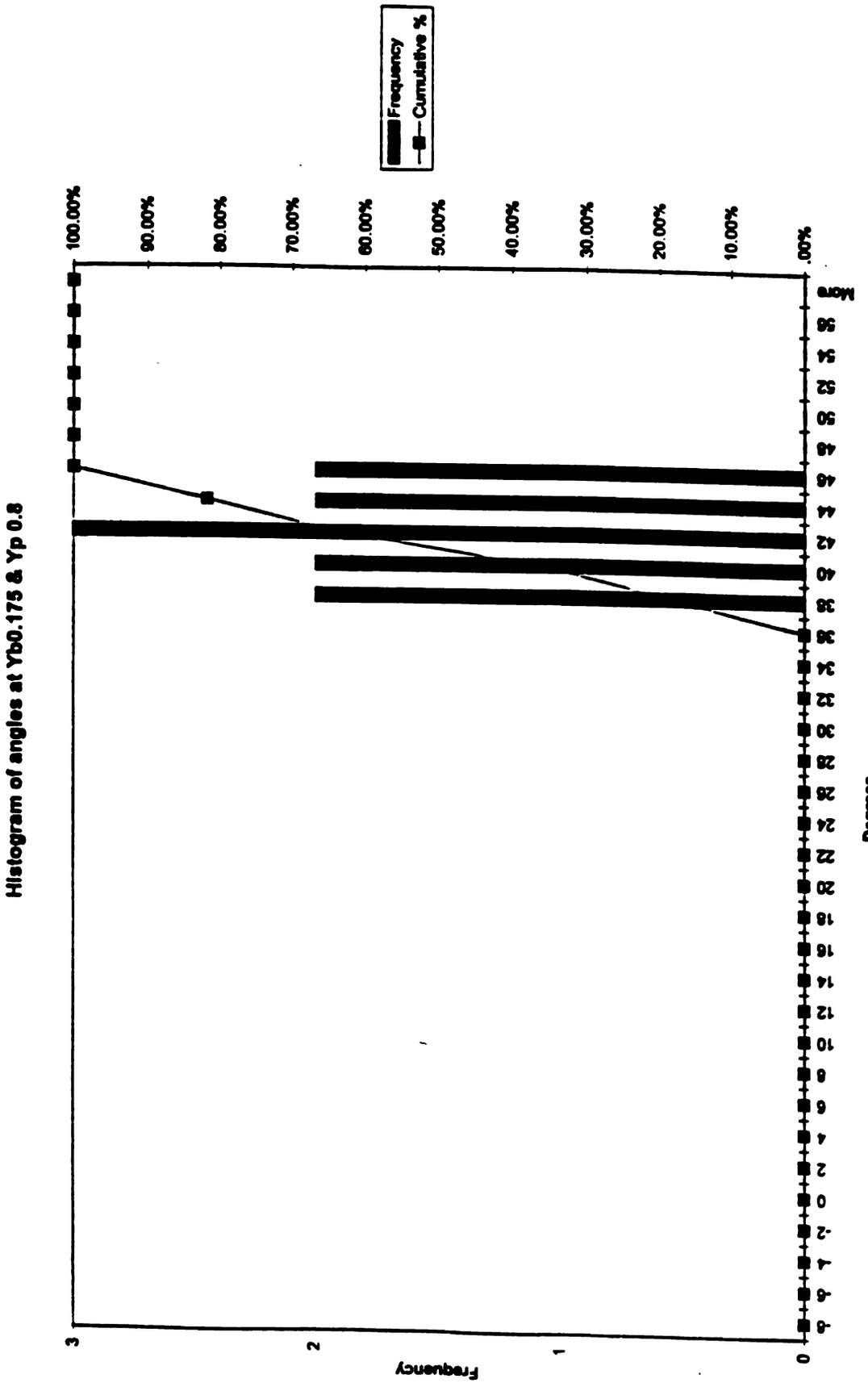

Figure 74. Histogram of flow angles at Yb/Wj=+0.175 and Yp/Wj= 0.8

Velocity profile <U>/Uo

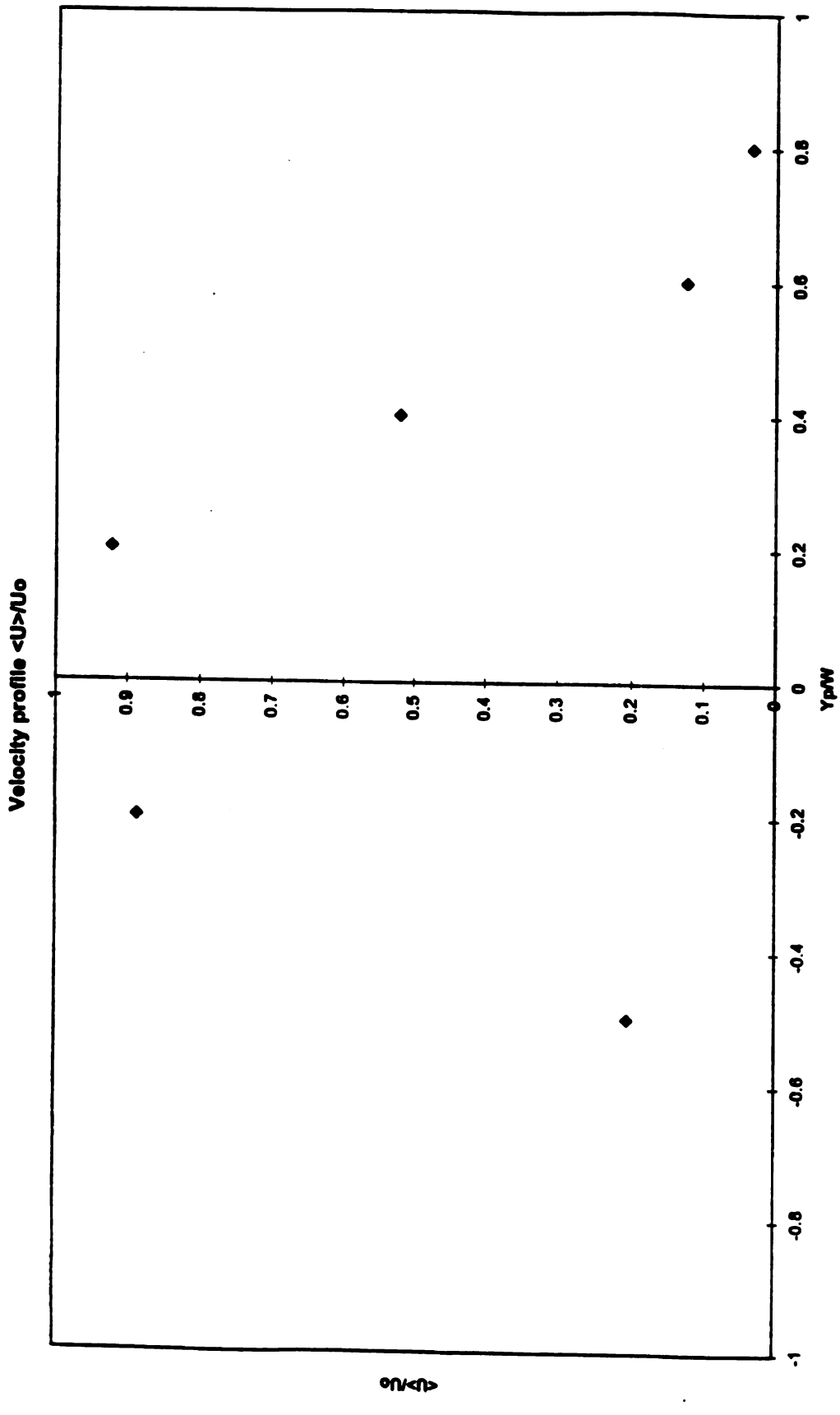

N.B Velocity profile at 75mm downstream of Sj with DB at infinty

Figure 75. Velocity distribution <U>/Uo at X/Wj=1.875 Yb/Wj= ∝

Velocity profile for Yb at -1.025

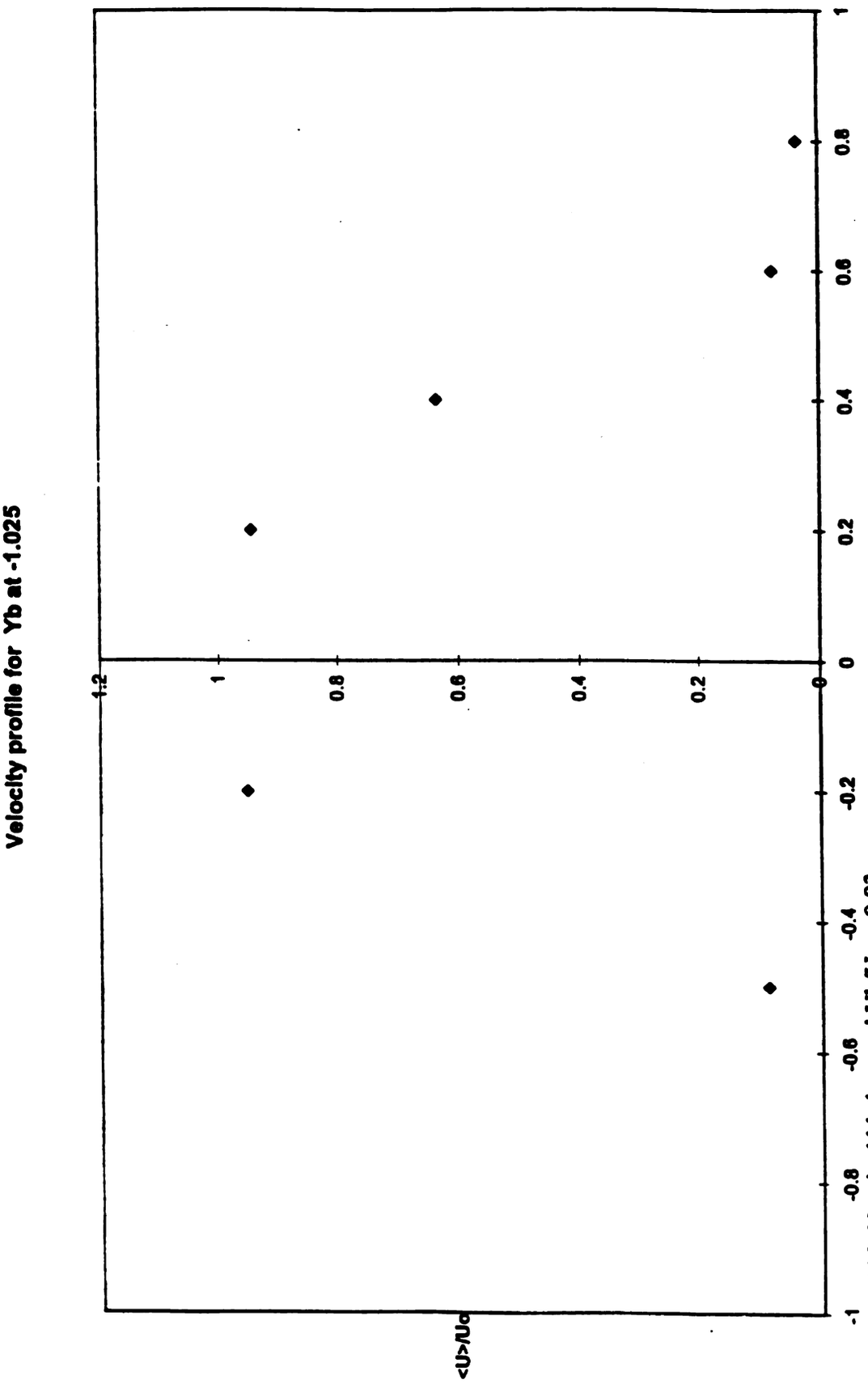

Figure 76. Velocity distribution <U>/Uo at X/Wj=1.875 Yb/Wj= - 1.025

Velocity profile for Yb at -0.9

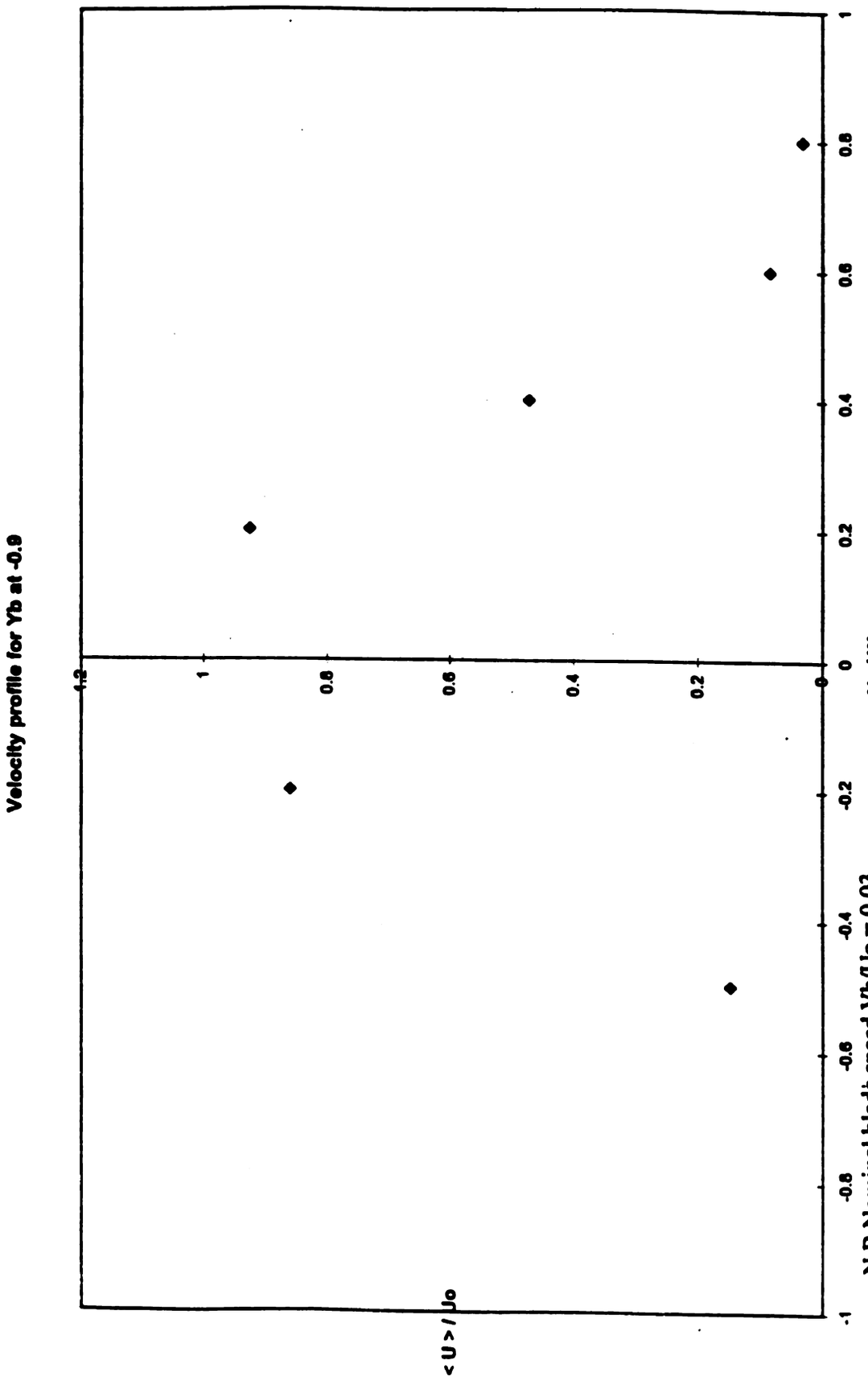

Figure 77. Velocity distribution <U>/Uo at X/Wj=1.875 Yb/Wj= - 0.9

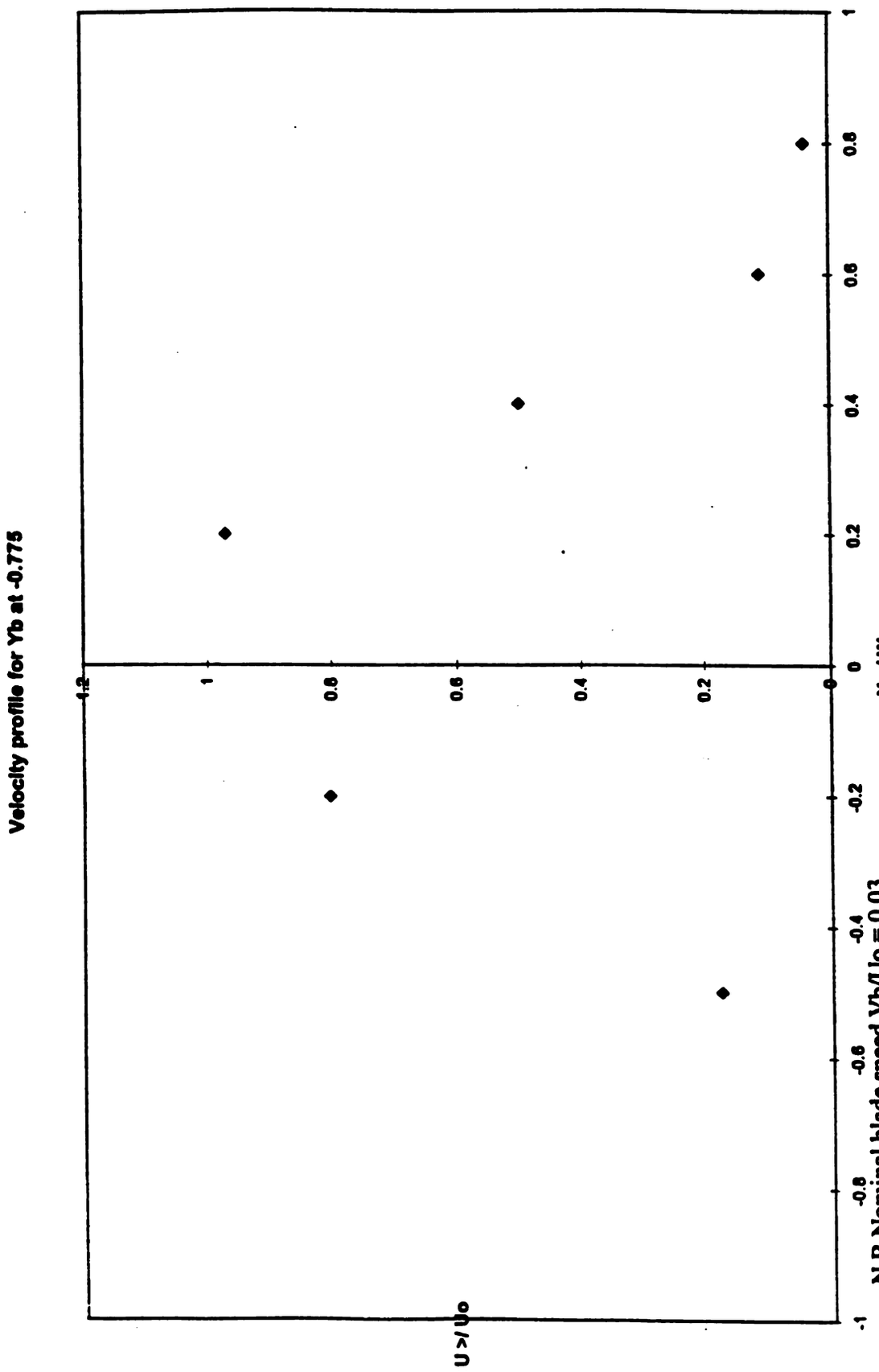

Figure 78. Velocity distribution <U>/Uo at X/Wj=1.875 Yb/Wj= - 0.775

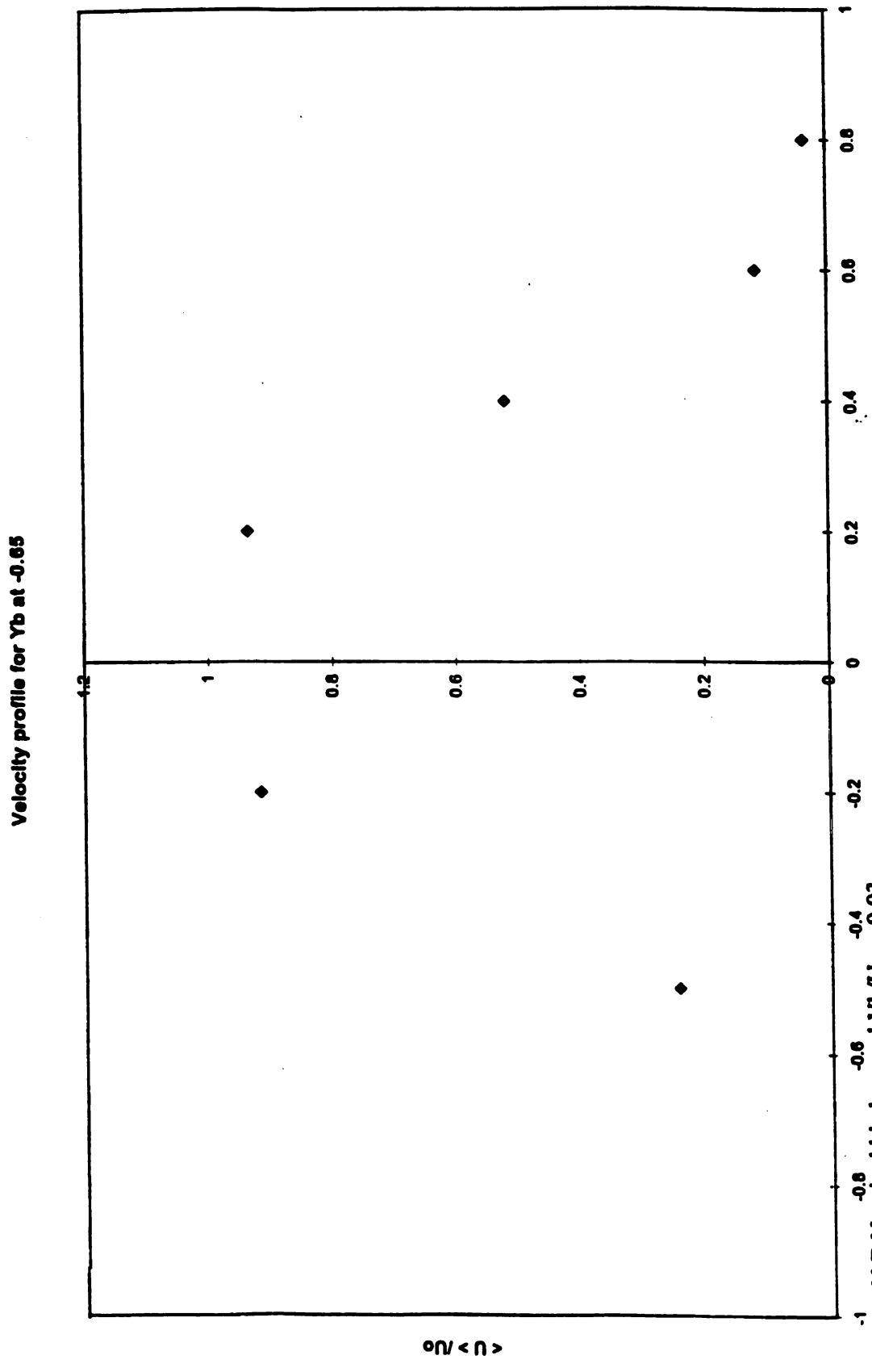

Figure 79. Velocity distribution <U>/Uo at X/Wj=1.875 Yb/Wj= - 0.65

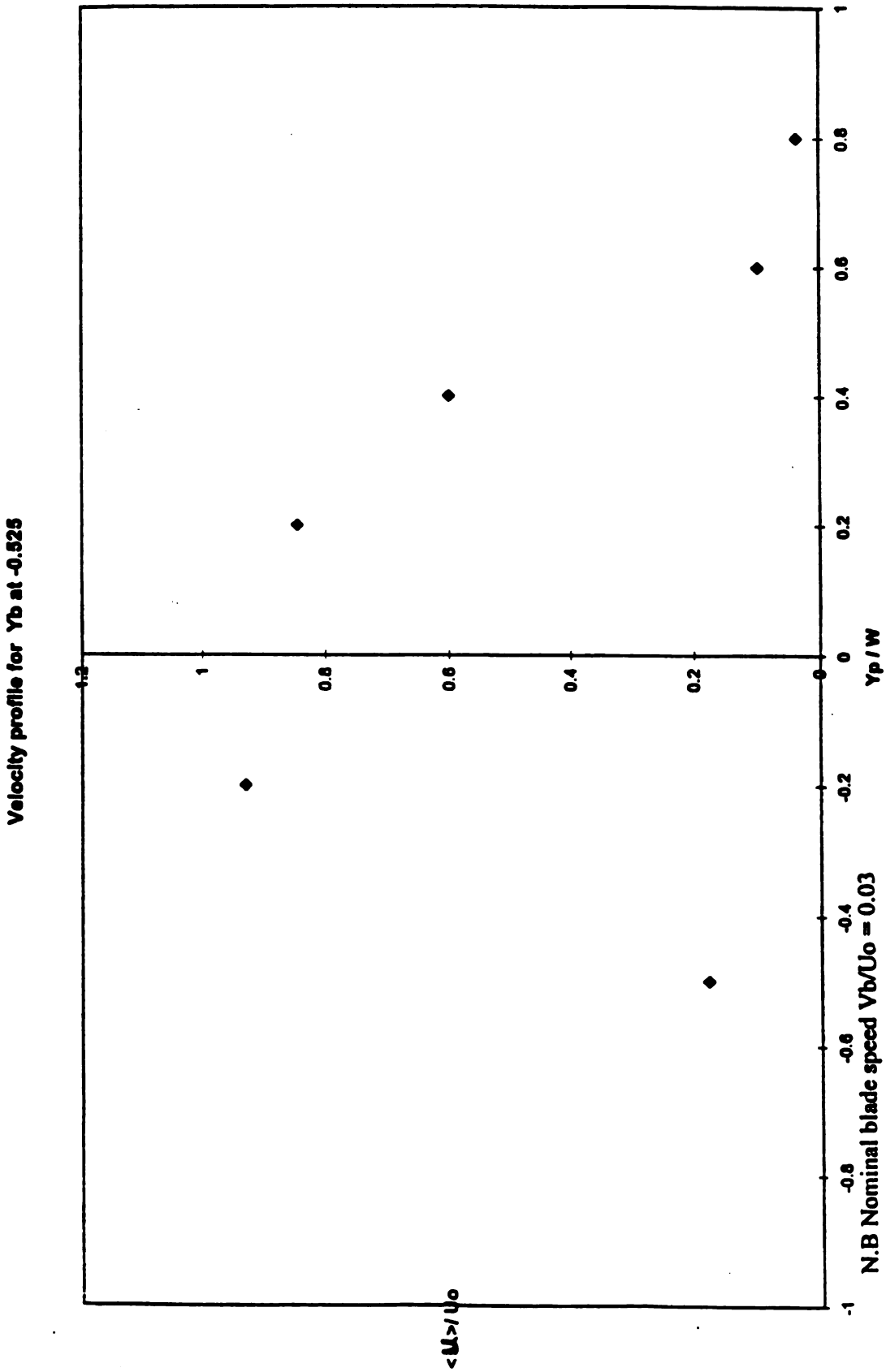

Figure 80. Velocity distribution <U>/Uo at X/Wj=1.875 Yb/Wj= - 0.525

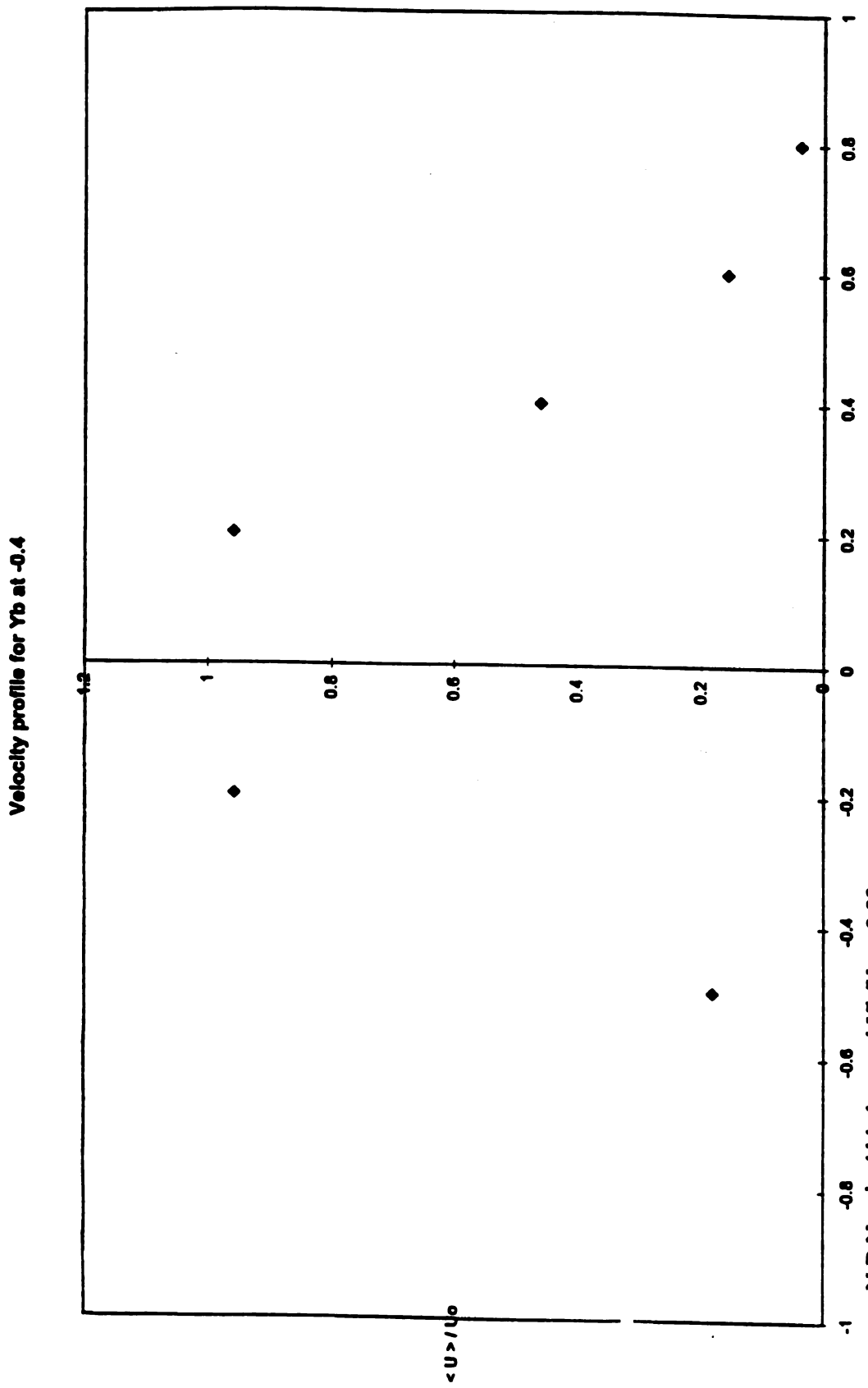

Figure 81. Velocity distribution <U>/Uo at X/Wj=1.875 Yb/Wj= - 0.4

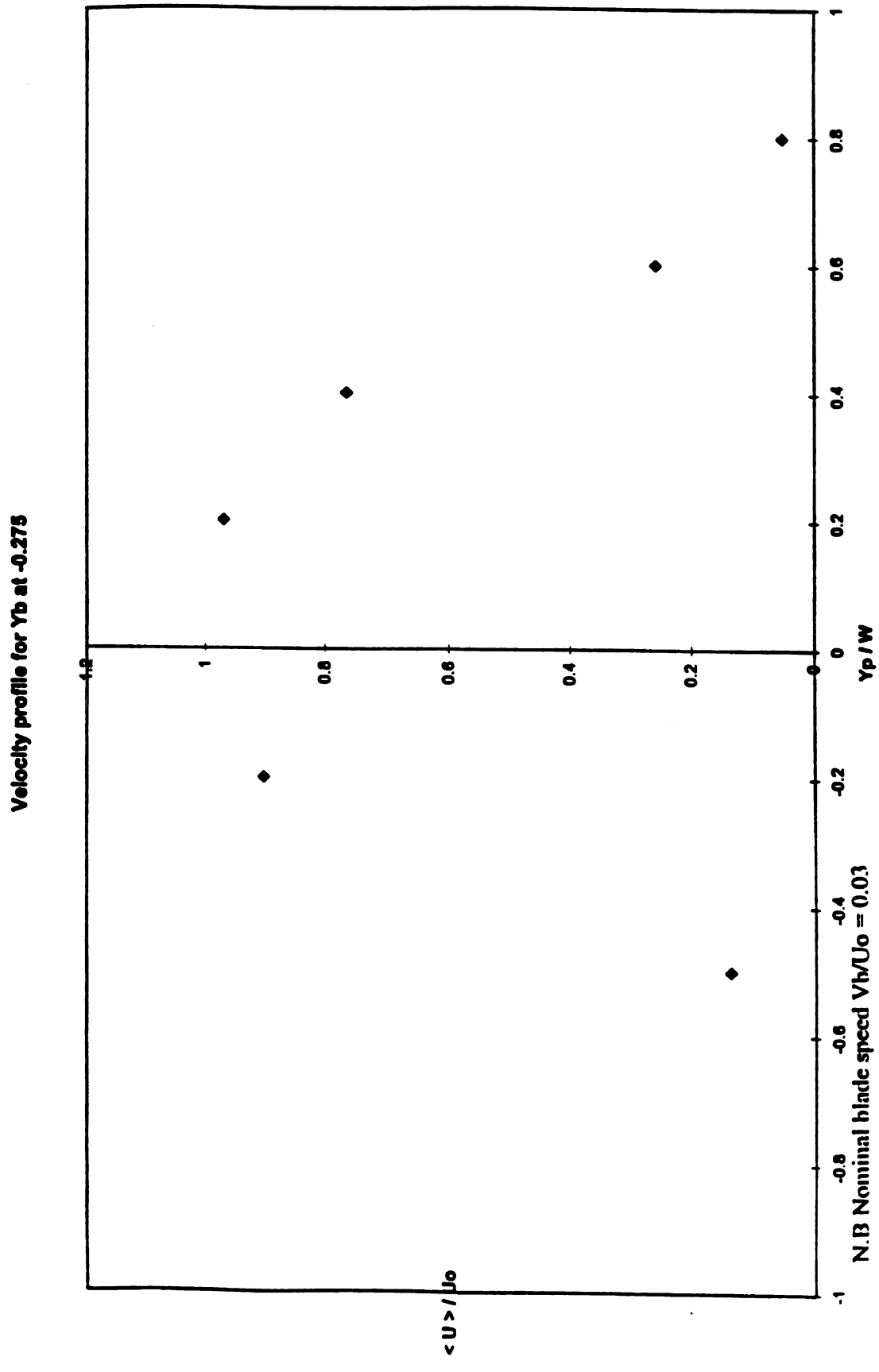

Figure 82. Velocity distribution <U>/Uo at X/Wj=1.875 Yb/Wj= - 0.275

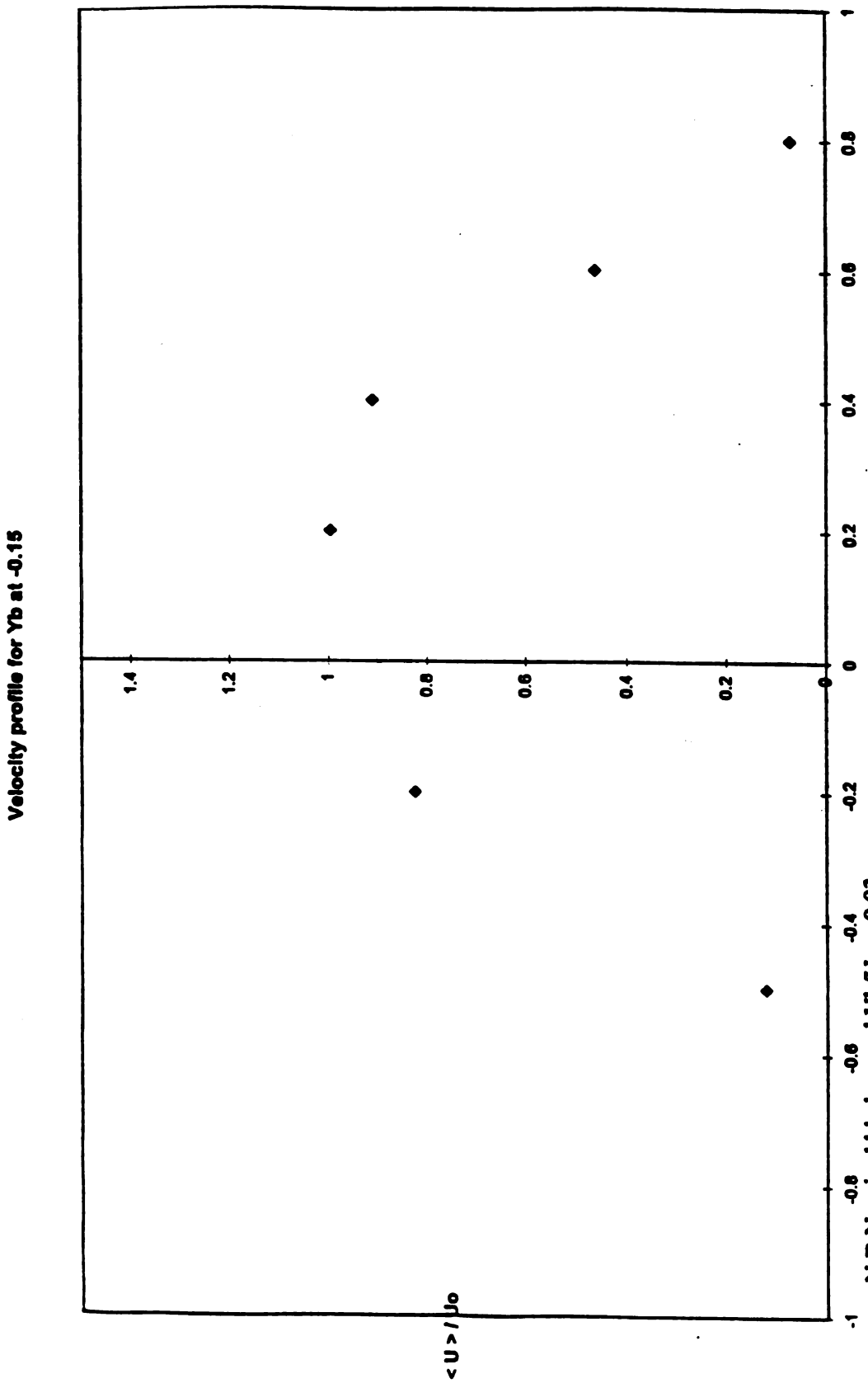

Figure 83. Velocity distribution <U>/Uo at X/Wj=1.875 Yb/Wj= - 0.15

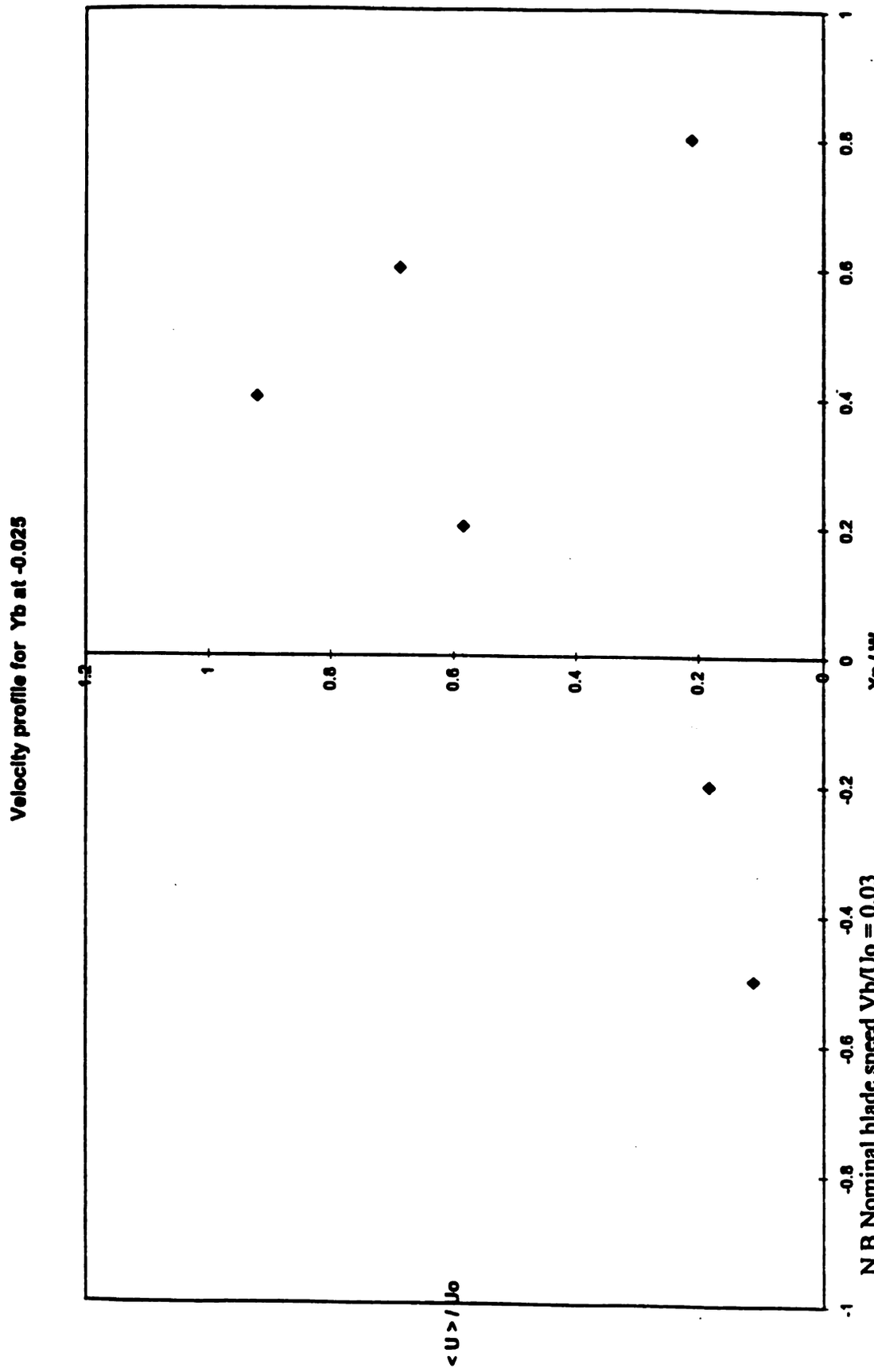

Figure 84. Velocity distribution <U>/Uo at X/Wj=1.875 Yb/Wj= - 0.025

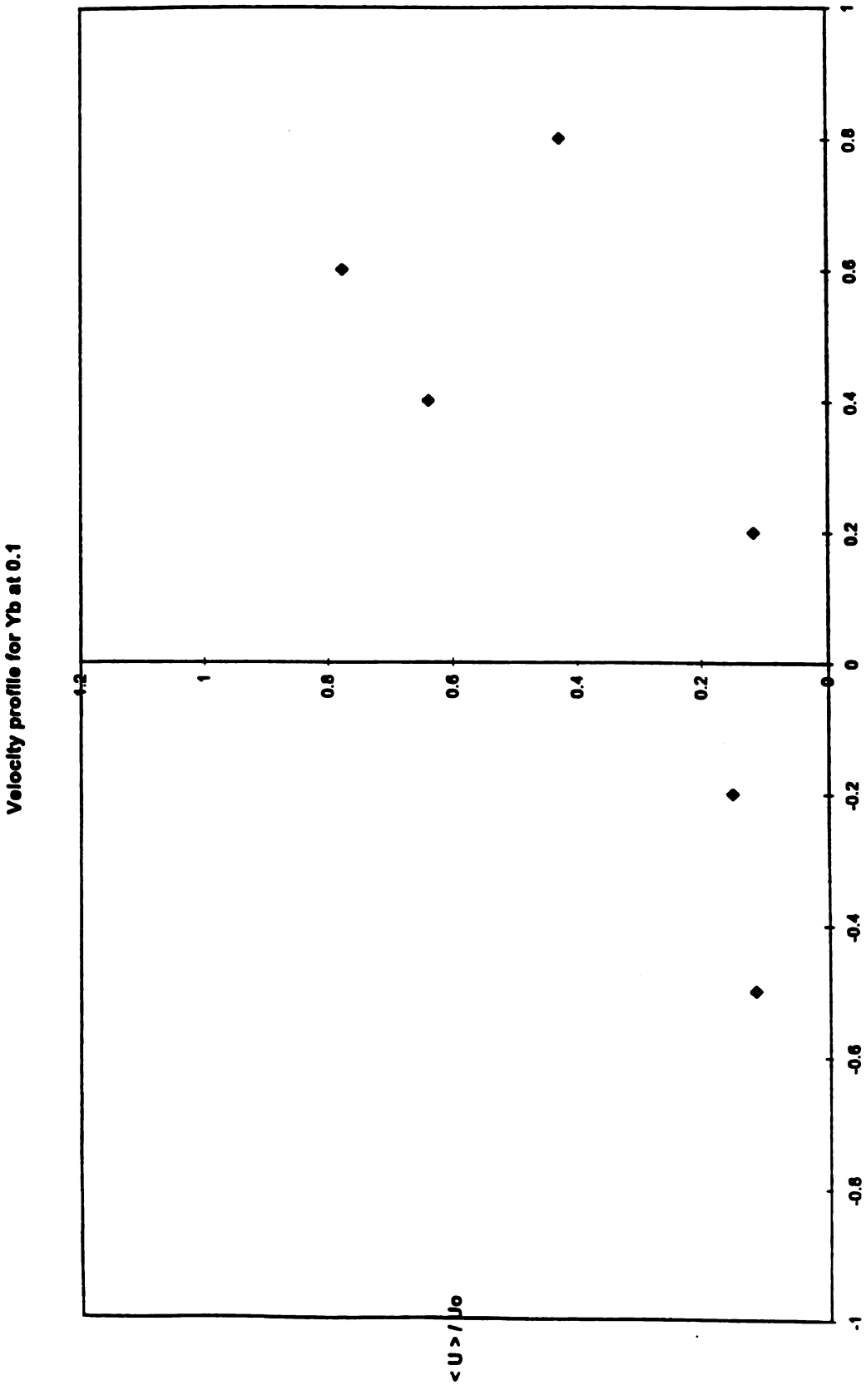

Figure 85. Velocity distribution <U>/Uo at X/Wj=1.875 Yb/Wj= 0.1

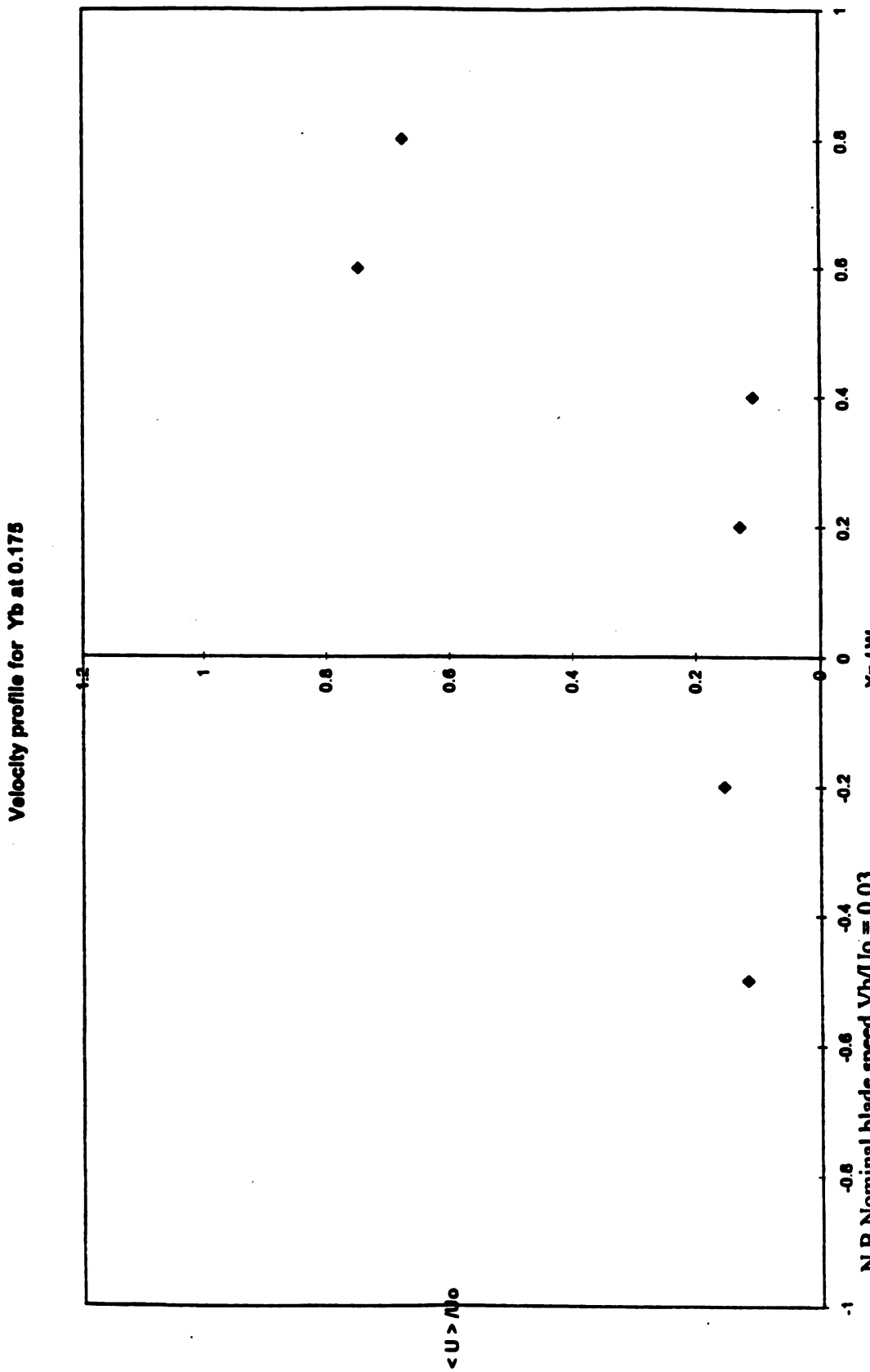

Figure 86. Velocity distribution <U>/Uo at X/Wj=1.875 Yb/Wj= C.175

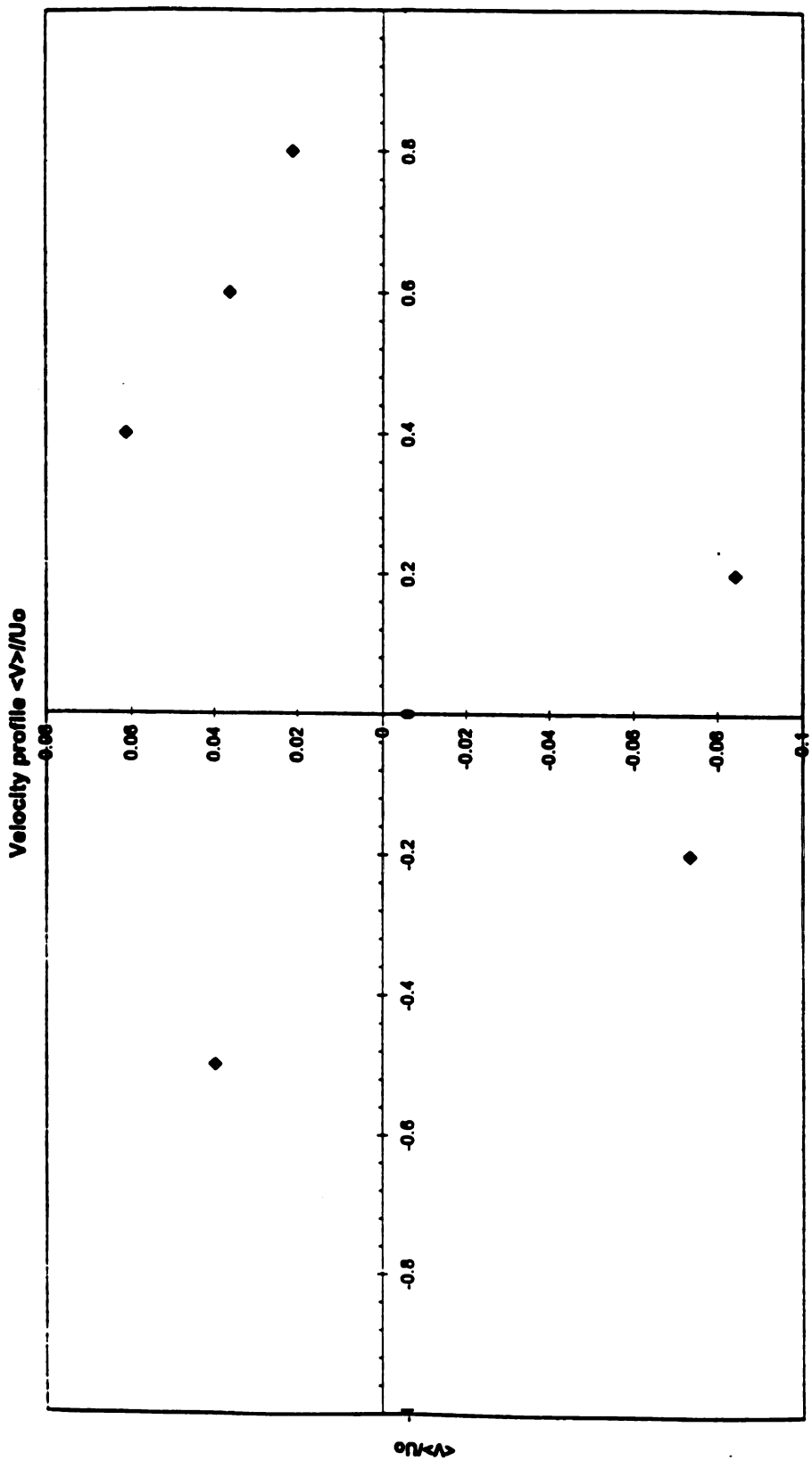

Figure 87. Velocity distribution <V>/Uo at X/Wj=1.875 Yb/Wj= ∝

N.B Velocity profile at 75mm downstream of Sj with DB at infinity

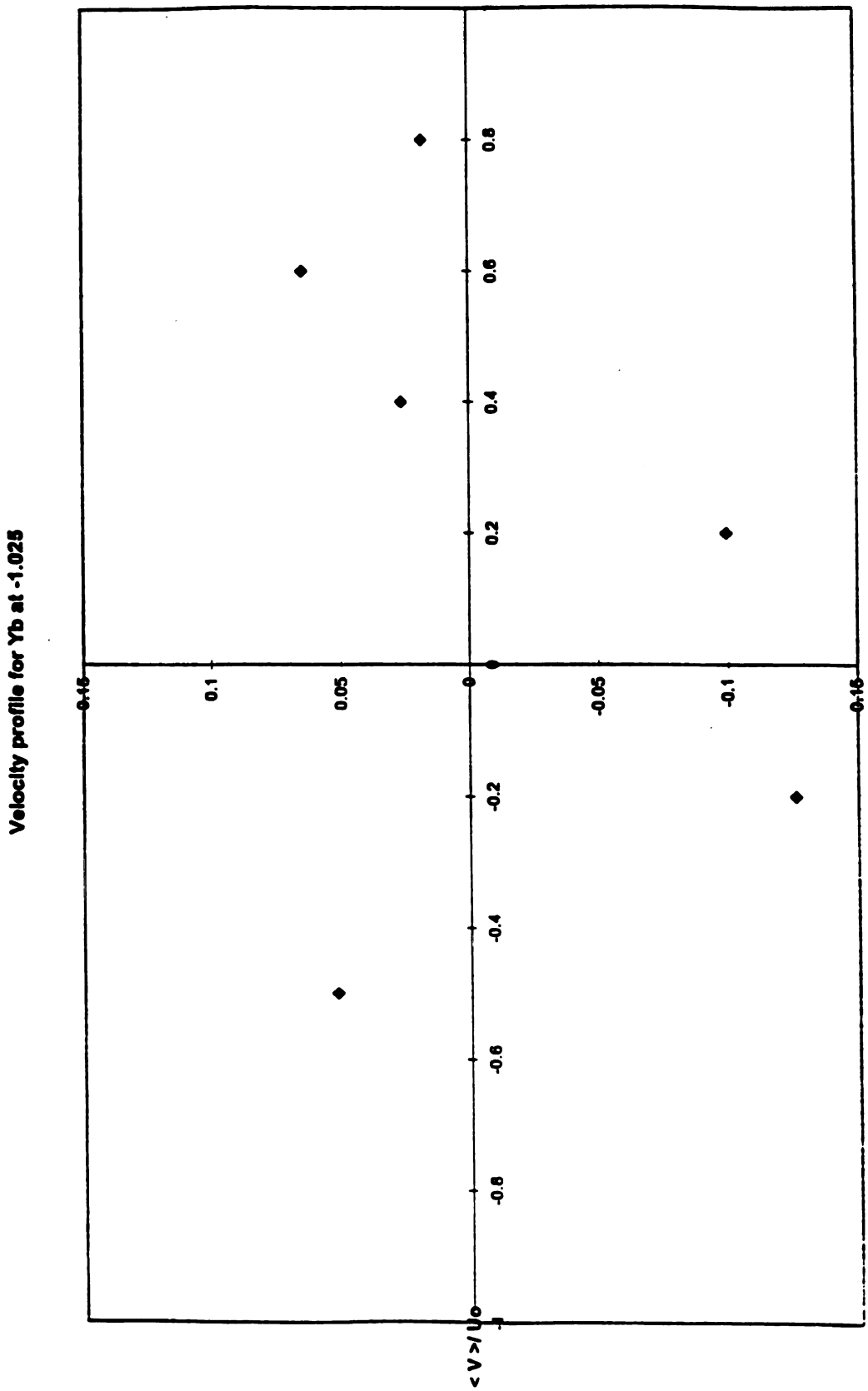

Figure 88. Velocity distribution <V>/Uo at X/Wj=1.875 Yb/Wj= - 1.025

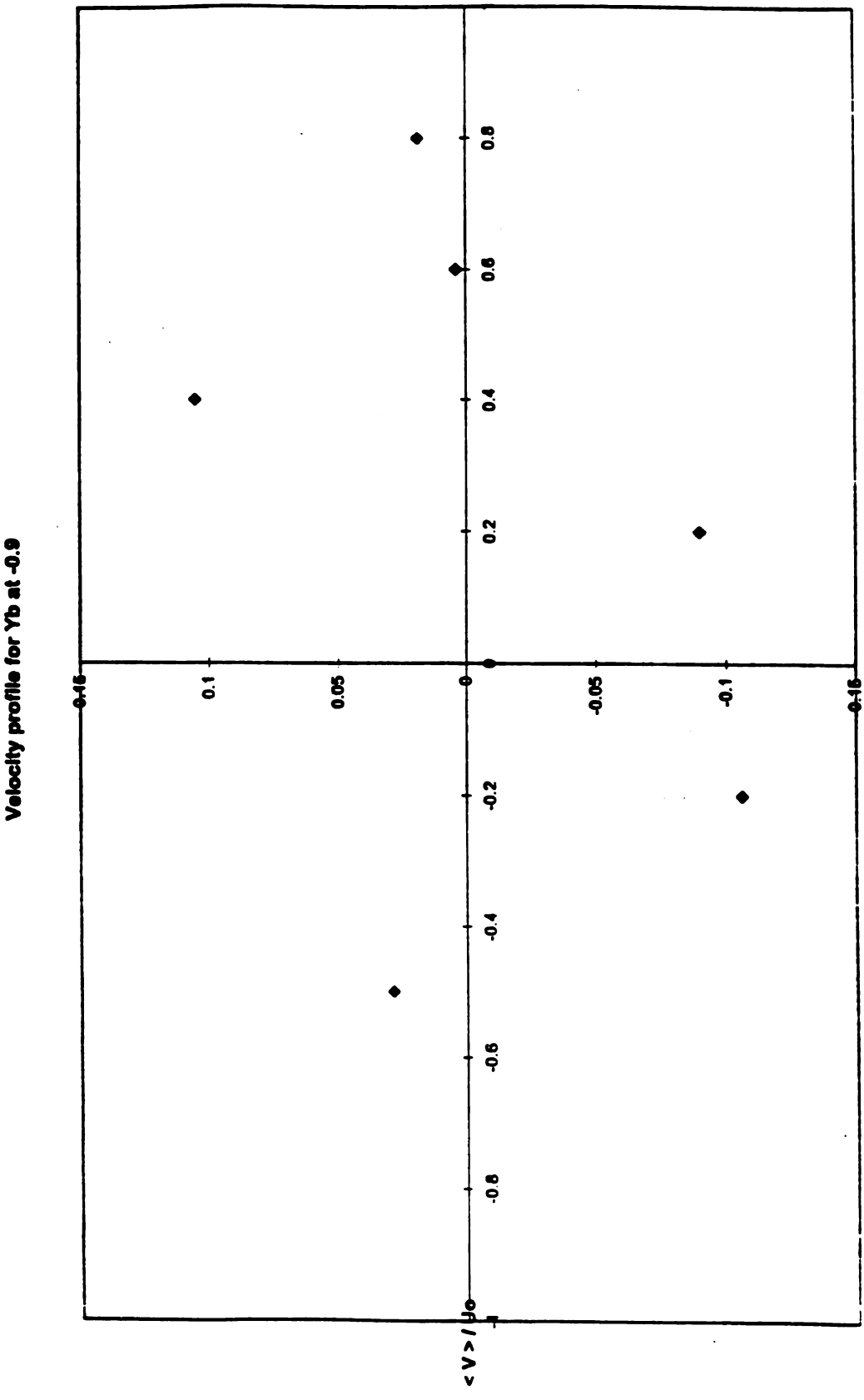

Figure 89. Velocity distribution <V>/Uo at X/Wj=1.875 Yb/Wj= - 0.9

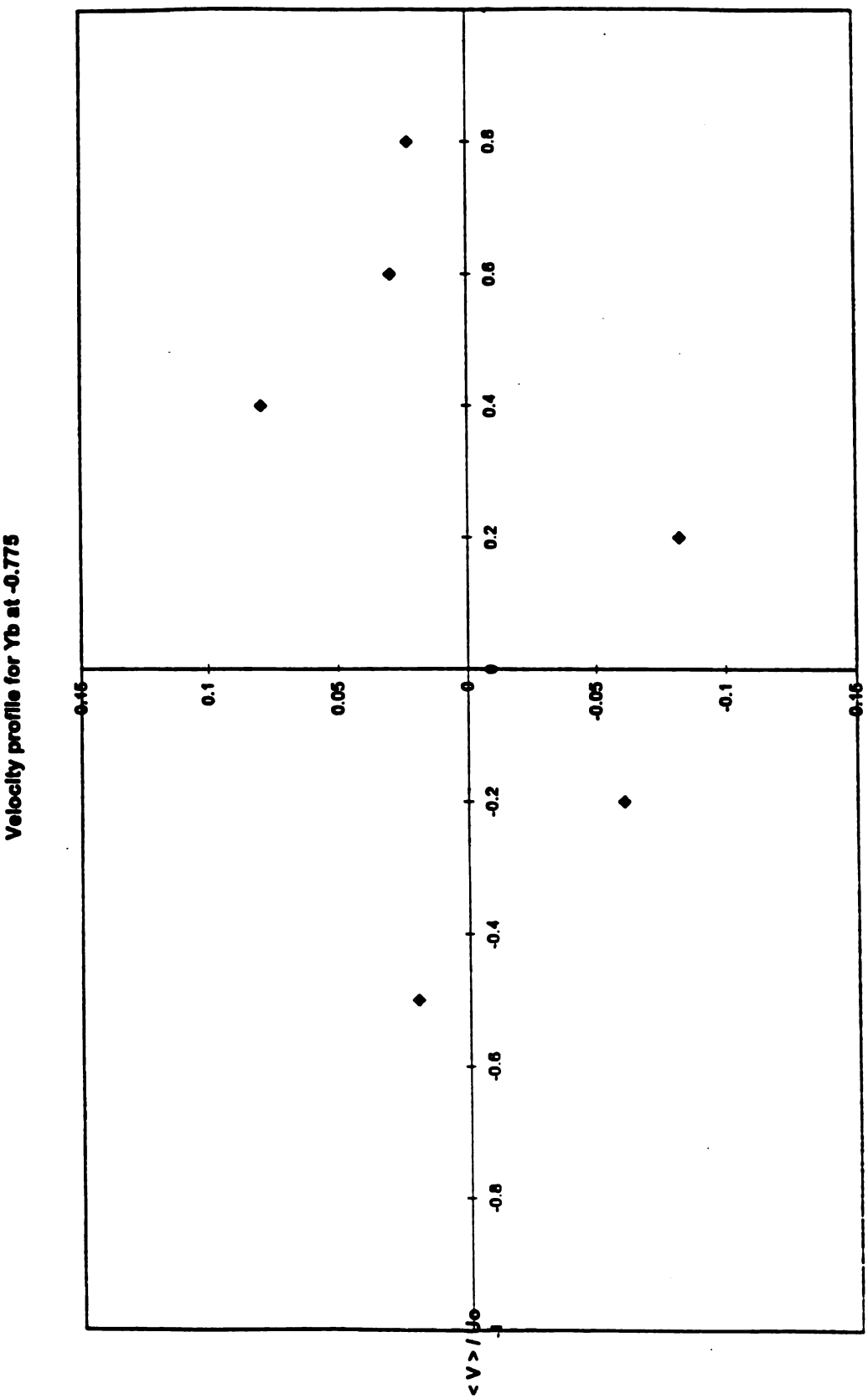

Figure 90. Velocity distribution <V>/Uo at X/Wj=1.875 Yb/Wj= - 0.775

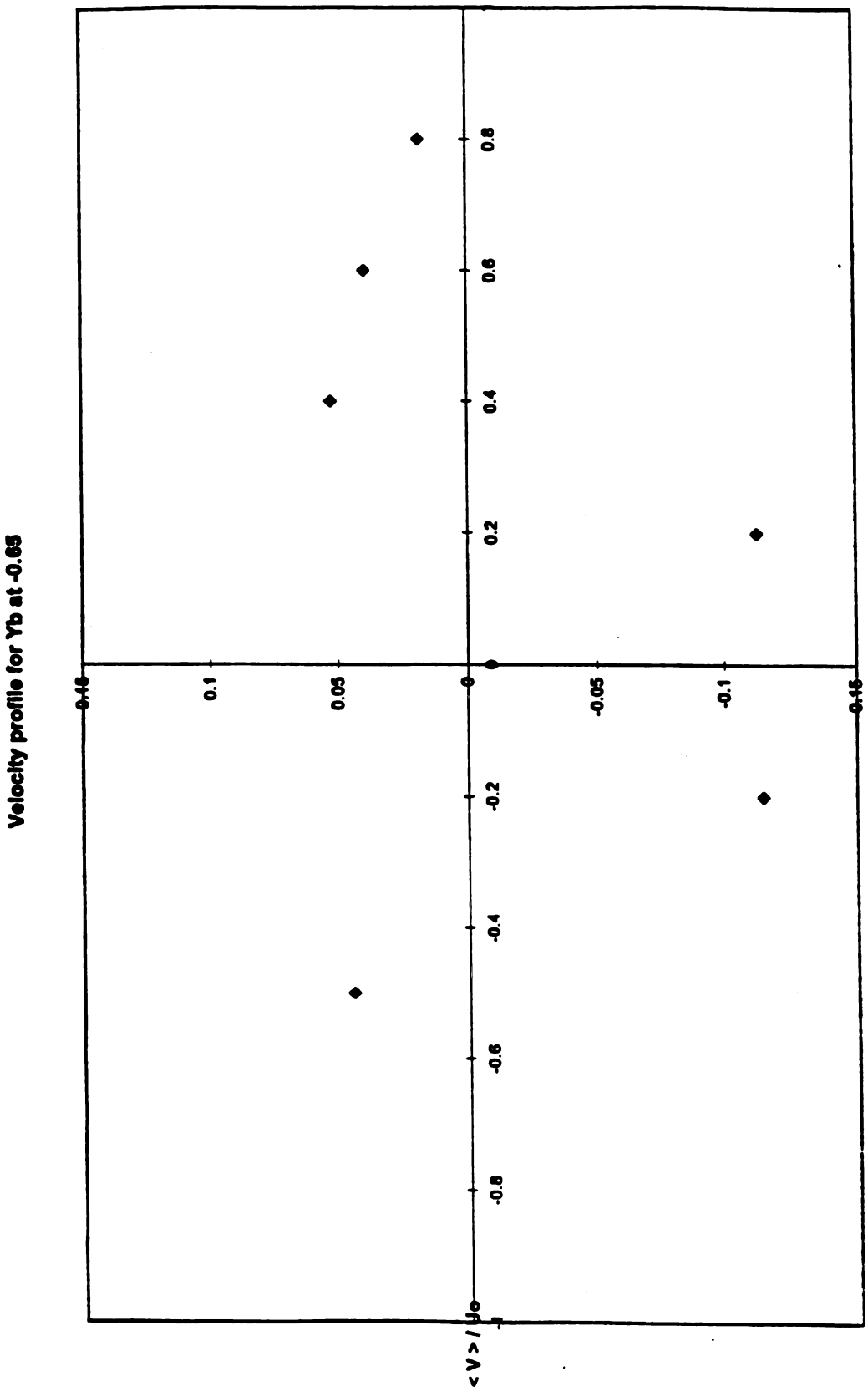

Figure 91. Velocity distribution <V>/Uo at X/Wj=1.875 Yb/Wj= - 0.65

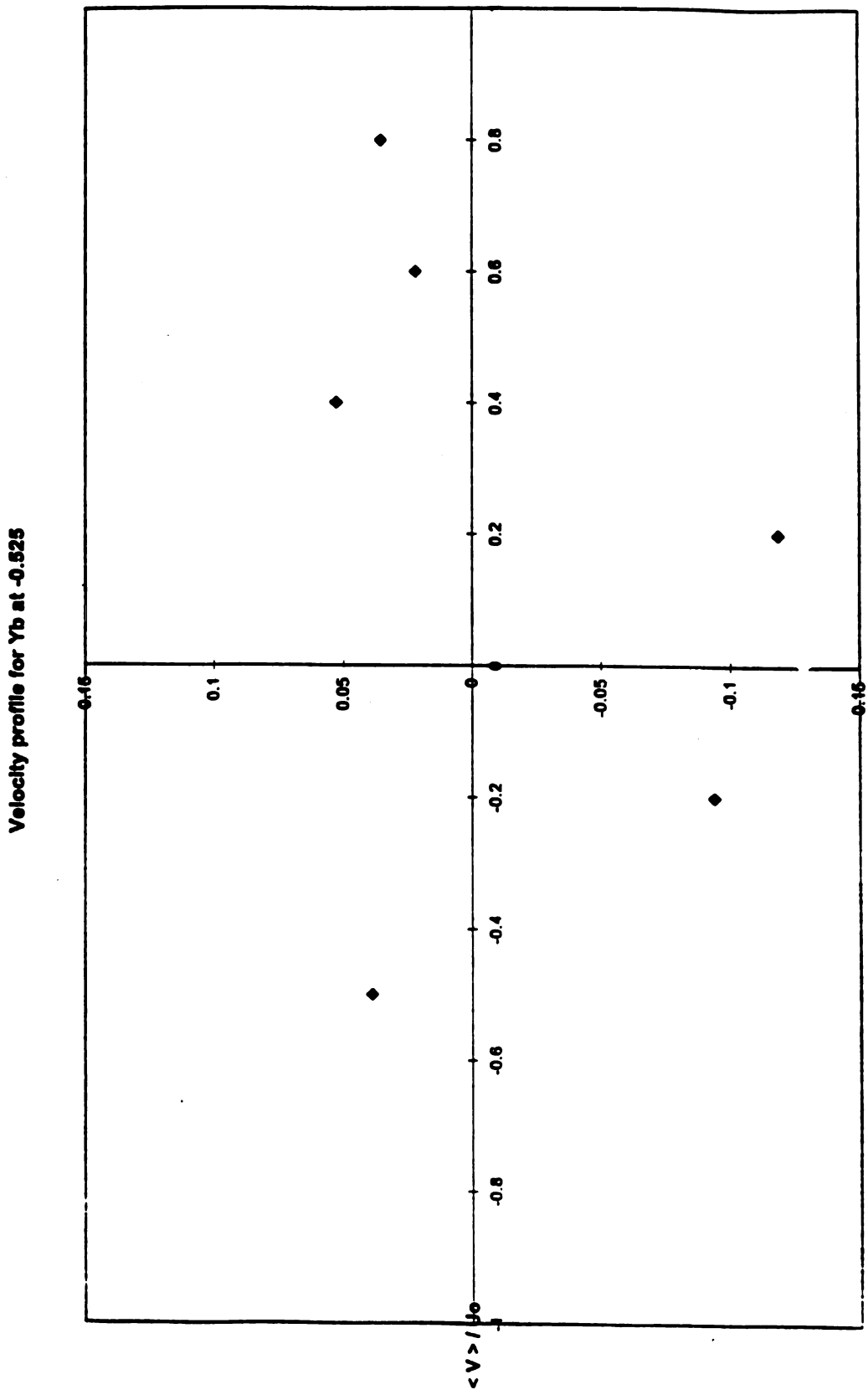

Figure 92. Velocity distribution <V>/Uo at X/Wj=1.875 Yb/Wj= - 0.525

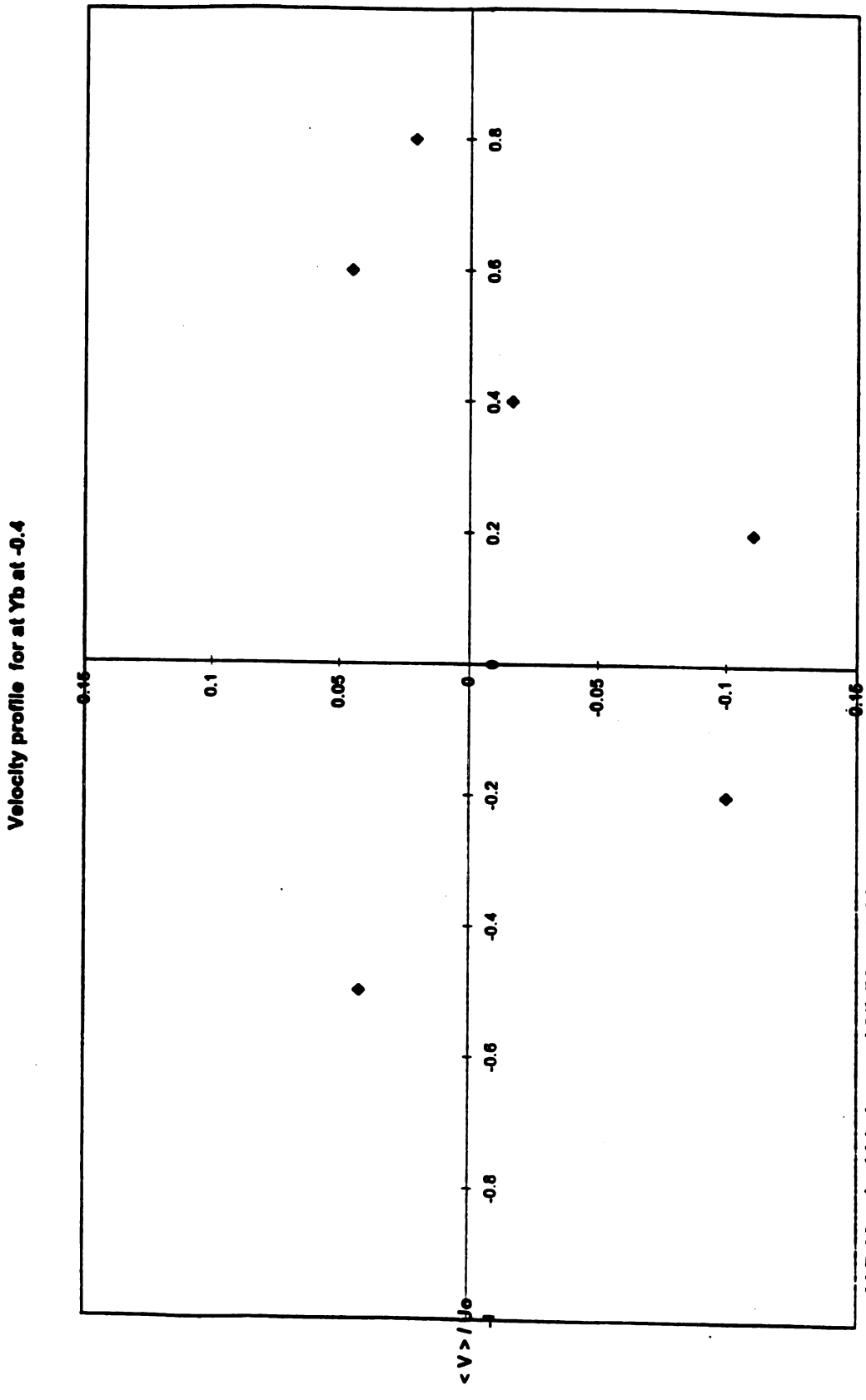

Figure 93. Velocity distribution <V>/Uo at X/Wj=1.875 Yb/Wj= - 0.4

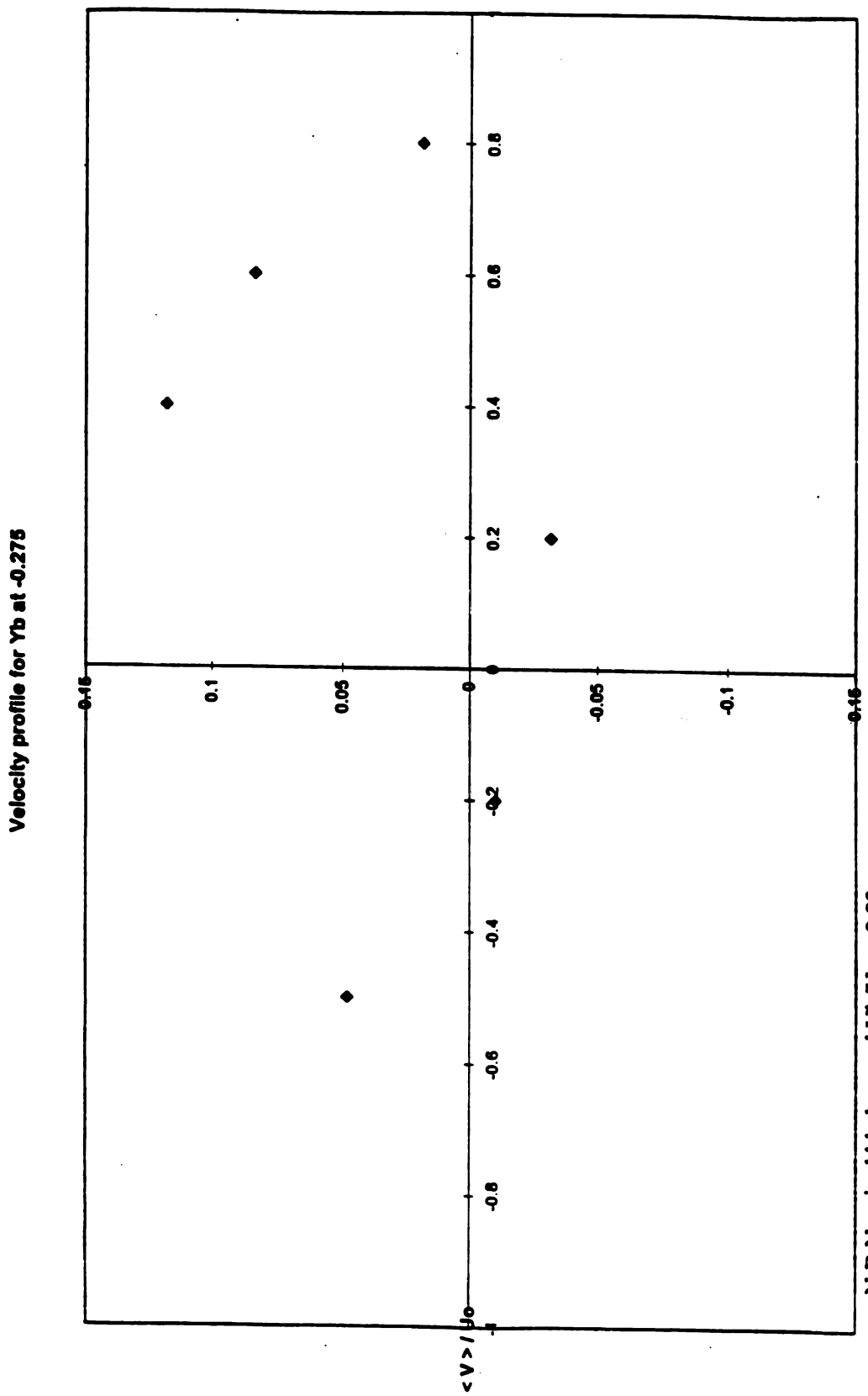

Figure 94. Velocity distribution <V>/Uo at X/Wj=1.875 Yb/Wj= - 0.275

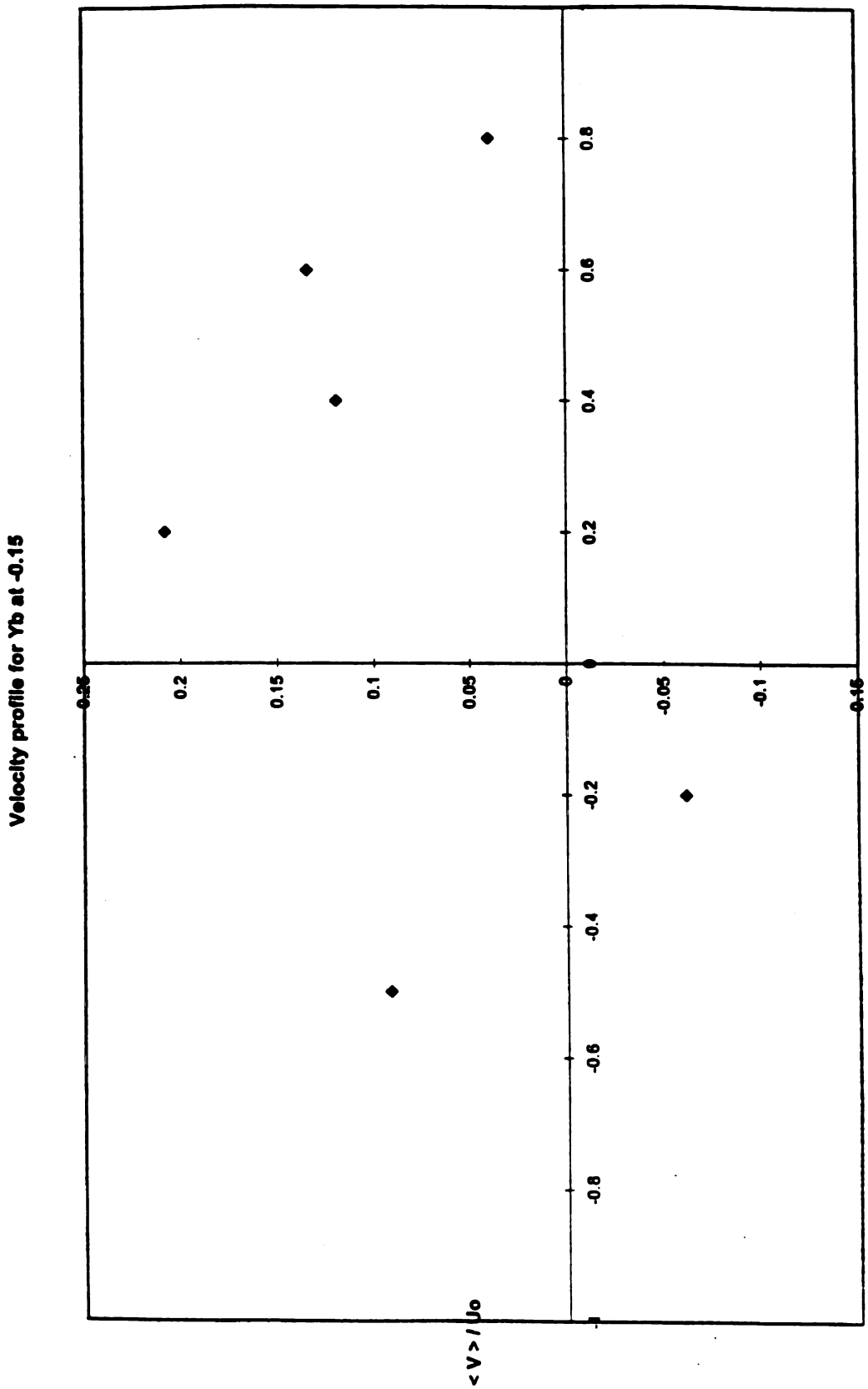

Figure 95. Velocity distribution <V>/Uo at X/Wj=1.875 Yb/Wj= - 0.15

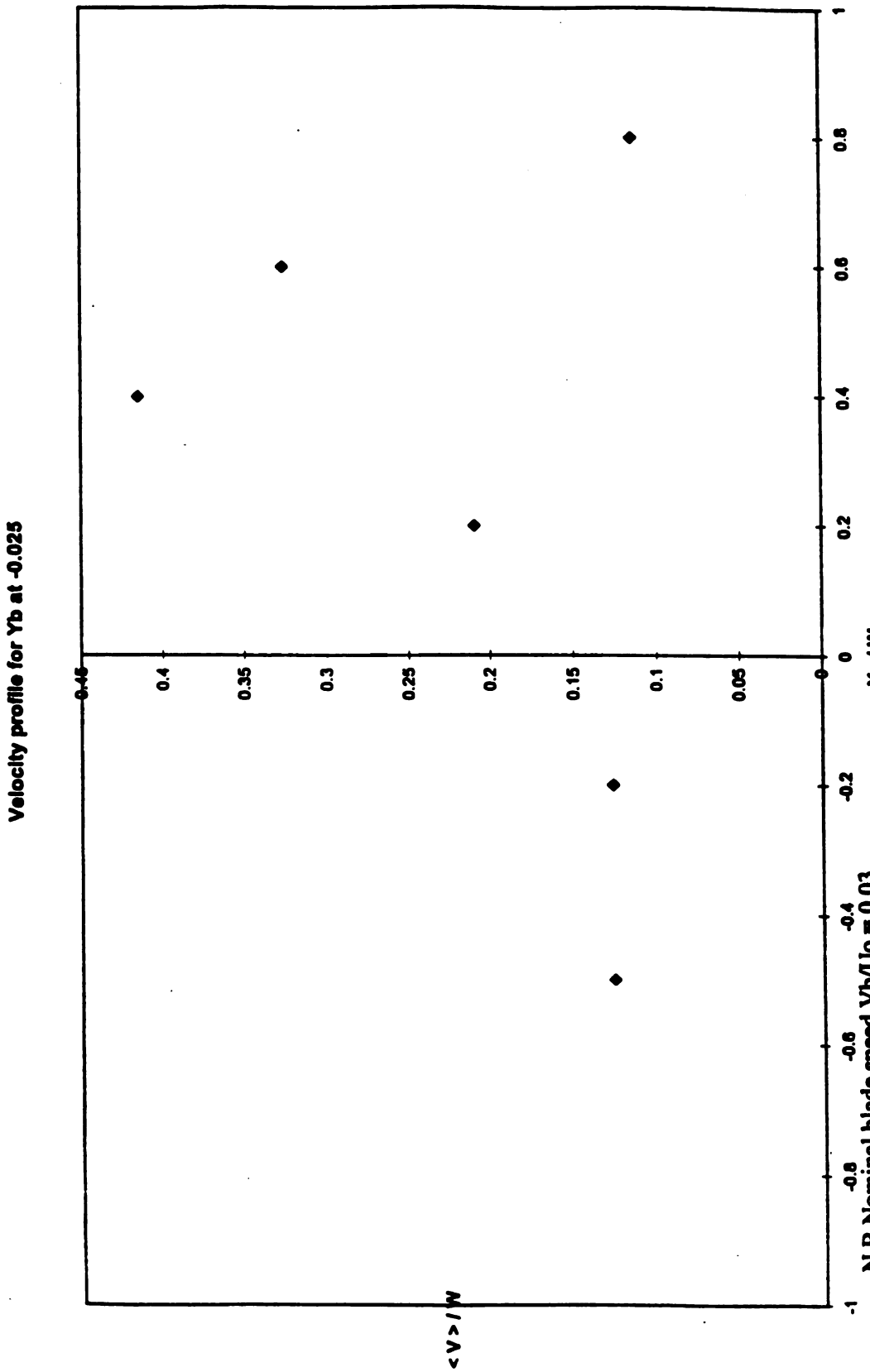

Figure 96. Velocity distribution <V>/Uo at X/Wj=1.875 Yb/Wj= - 0.025

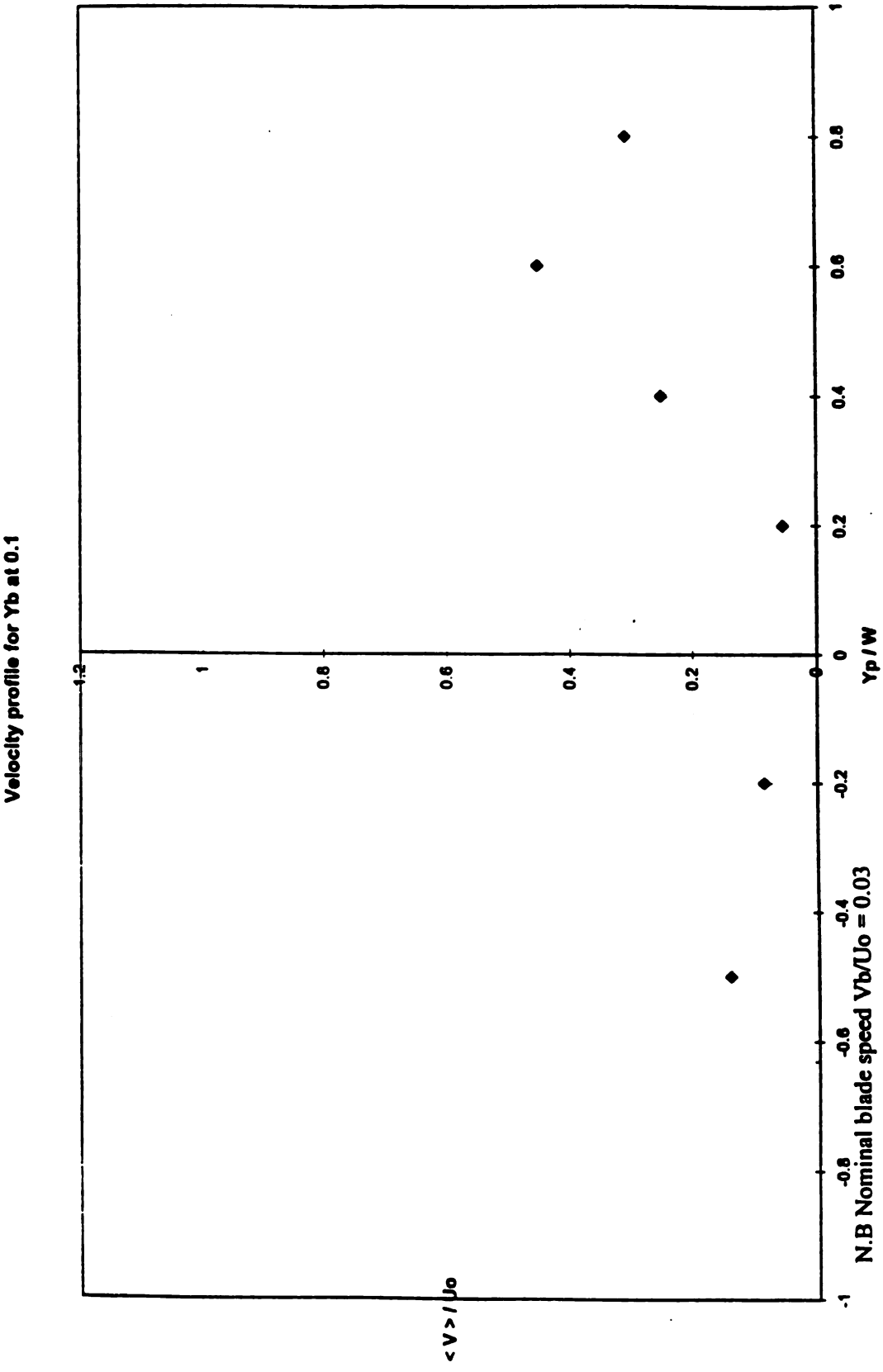

Figure 97. Velocity distribution <V>/Uo at X/Wj=1.875 Yb/Wj= 0.1

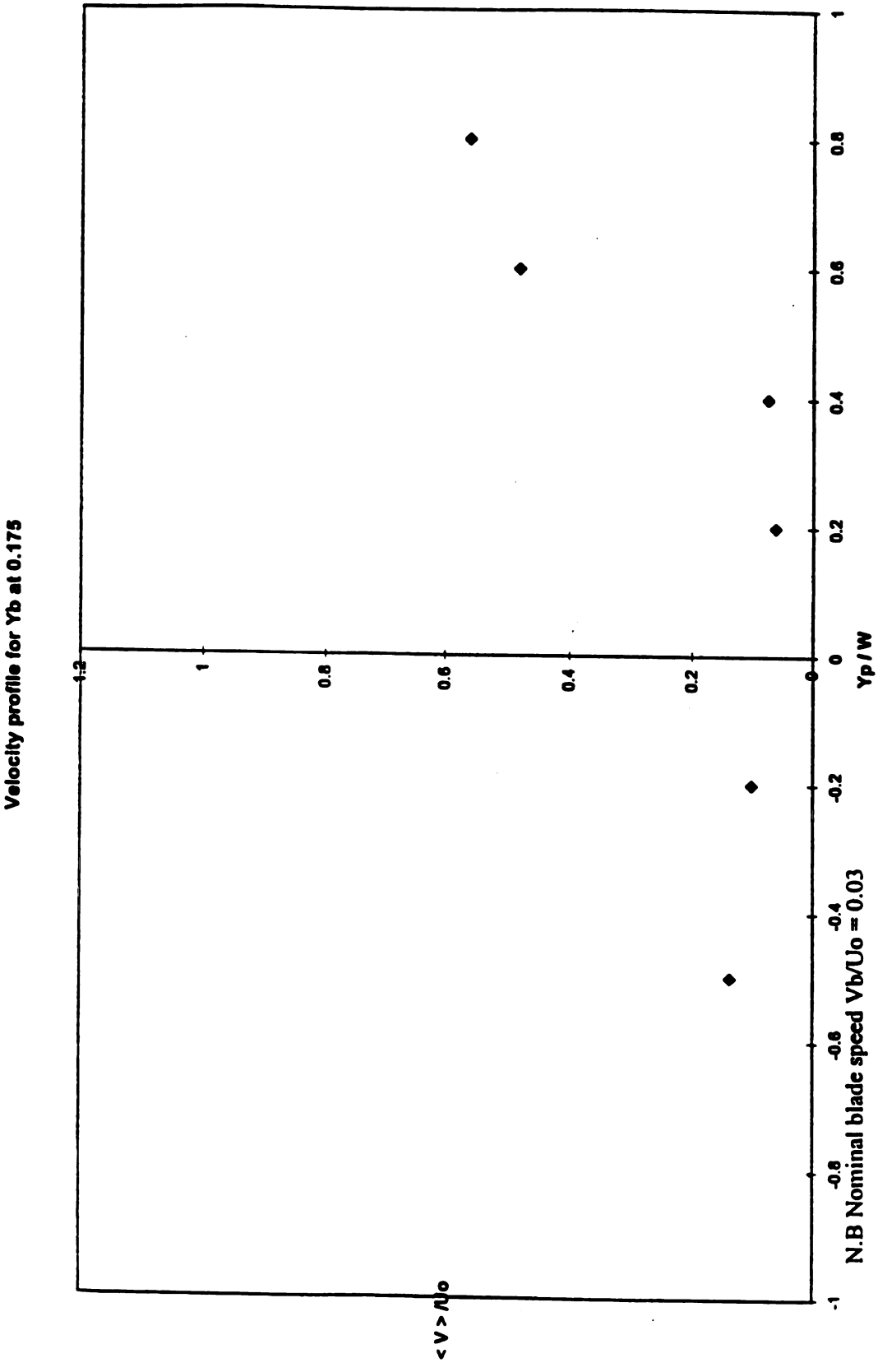

Figure 98. Velocity distribution <V>/Uo at X/Wj=1.875 Yb/Wj= 0.175

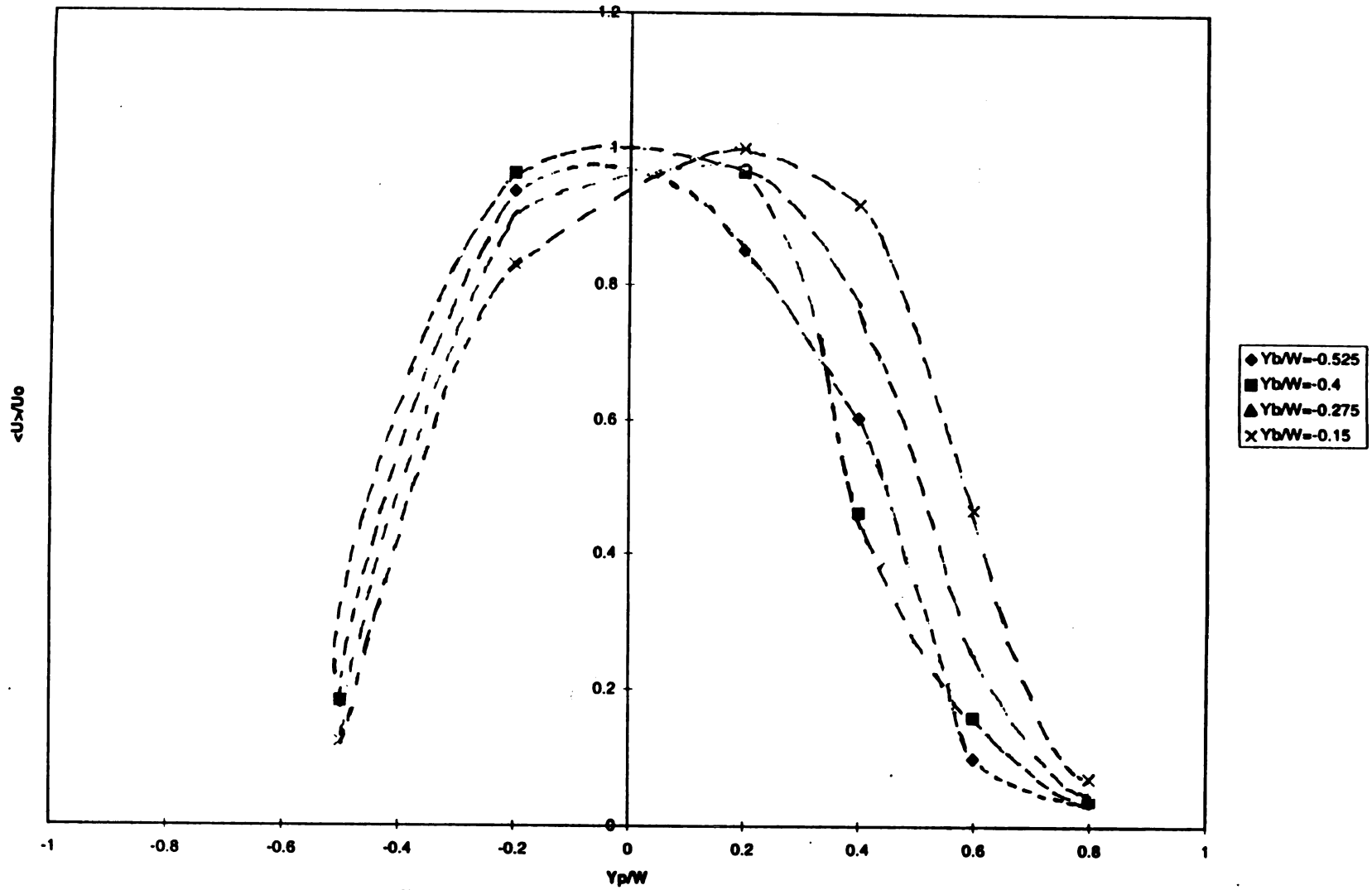

Figure 99. Velocity profiles(<U>/Uo)as a fuction of position of DB.

N.B Dashed lines are only for references.

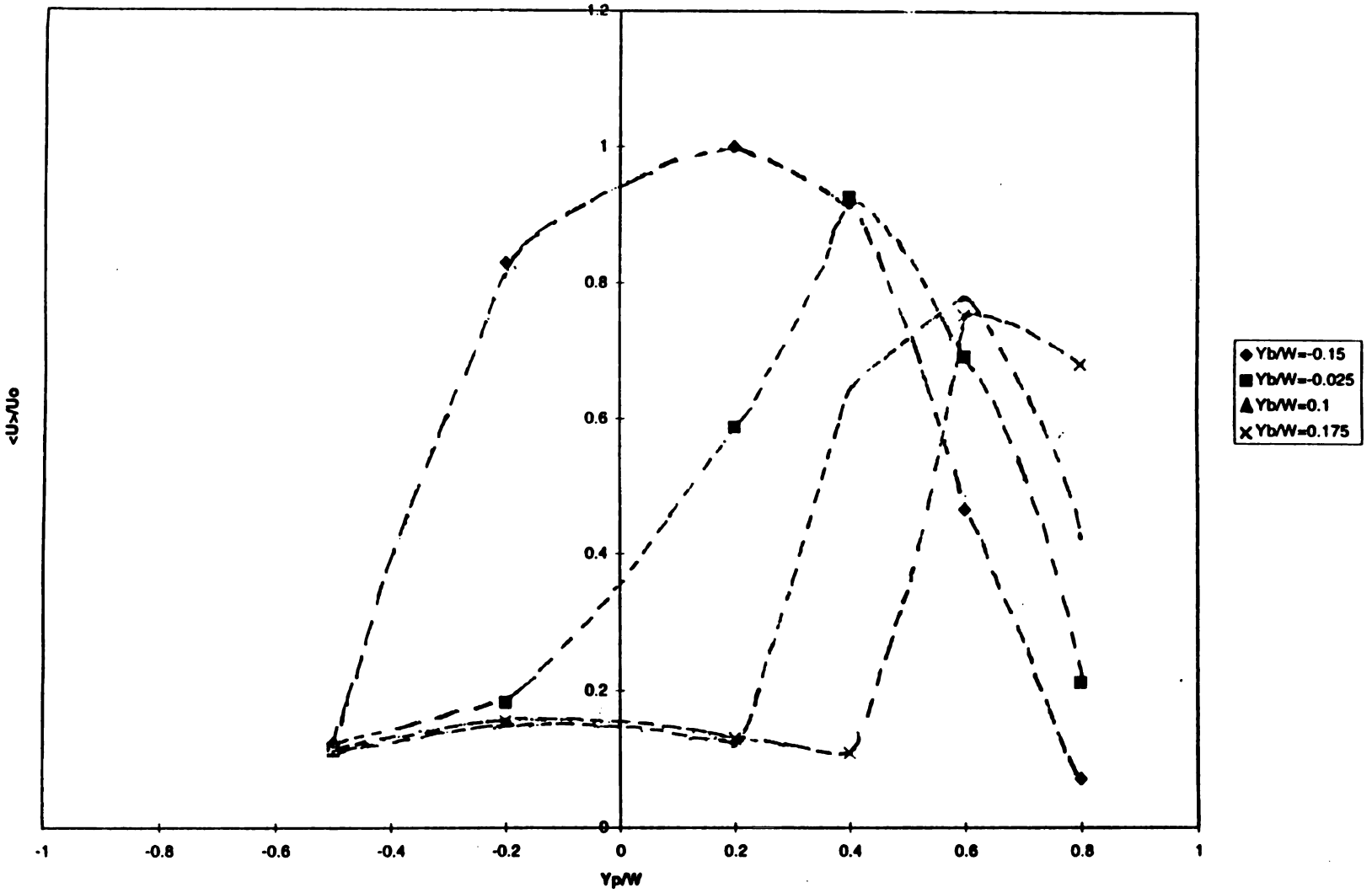

Figure 100. Velocity profiles (<U>/Uo) as a function of position of DB

N.B Dashed lines are only for references.

5. UNCERTAINTY CONSIDERATIONS

5.1 Pressure Measurements

For the calculation of the normal velocity in the wind tunnel, 1 Torr MKS Baratron was used; it has an associated uncertainty of 0.08% of the measured value (MKS Instruments (1994)). Furthermore, this level of uncertainty compares to 0.04 cm/sec in the measurement of the approach velocity. But since this experiment was conducted at a high speed of 35 m/sec, so the associated uncertainty with the normal speed of 35 m/sec seems to be negligible.

5.2 Uncertainty in the Position of the DB

For the measurement, the DB was aligned with one of the knife edges of the slit jet. The alignment was done with the help of the standard thread pendulum. Once the DB was properly aligned with the knife edges of the slit jet, it was then transverse back or forth to the desirable position. The uncertainty associated with the placing of the DB at the exact position less then be $\pm$ 0.3 mm as after the aligning the DB with the third pendulum; a scale was used to transverse it in and out of the center rod holder with the help of a vernier.

5.3 Traverses Uncertainty

The traverse used for positioning the hot wires and the tuft probe is run with the help of a stepper motor. The driving screw of the traverse does not exactly have the pitch of 1mm but 0.989 mm, so there is an error of 0.011mm for each mm of movement; which is a biased error and is calculated and added to the traverse when in use.

5.4 DB Assembly

The blade DB assembly is moved up or down with the help of the two left- and right-handed screws to position the DB at the vena contracta. The pitch of these screws is not exactly 1 mm for each turn, but 1.5 mm for each turn, therefore, every turn the DB moved 1.5 mm. So, again for positioning of DB ,the screws were turned and the assembly moved up and down ,and when DB was 35 mm above Sj, the locking nuts were tightened, and the distance measured with a Vernier, the error in adjustment would then be $\pm$ 0.01 mm (Max.) for all the adjustments of the DB at vena contracta.

5.5 Optical Encoders

As the optical encoder passed as the information about as the position of the DB, when it was triggered. The sampling rate was 2 K H Z, i.e., for every 0.0005 seconds, we were measuring the pulse of the OP. So to exactly know when the DB triggered the OP, in that

0.005 seconds gap was difficult to judge, so a middle value 0.0025 second was taken between the samples as the point of triggering the OP.

5.6 Hot Wire Anemometer

All the data taken by the hot wire was pre and post calibrated and was limited by 0.10 mm/sec for a speed of 35 m/sec. for the hot wire. The sampling frequency was 2 K H Z rate for 10 seconds. The time (sampling) was taken less as to observe the triggering of OP's but for hot wire the sampling rate was less to give us a good average. Then by changing the sampling rate of the would have made the correlation difficult. As we wanted a continuous sampling rate of both hot wire and that of the OP so they could be CO-related in the same time domain.

6. SUMMARY AND CONCLUSION

From the present results observed from the experiment, we see two basic things. One that the jet could be totally deflected out of the projected area of the Sj width when the insertion of the blade was +5 and second most important thing we observed was that the relation between the dynamic and the steady state was affected by the speed of D.blade; i.e., although we had a relatively smaller speed with respect to Uo, but even then there was a lag between the dynamic and the static response of the jet; In case of dynamic there was a lag involved, and the jet did not produce the same deflection angles as that which it did in the steady state.

So intuitively one can say that if DB speed was is much slower, then it would have the same response as that of the steady state ,but if the speed of DB blade tends to increase the lag factor plays an important part and the deflection obtained from the dynamic does not match with that of steady state. Although the respective measurements of the dynamic for different runs of the DB for a given speed, are independent of the speed of the blade as Vb./Uo factor is of 0.03, so if we are only considering it dynamic response of the DB, then the values obtained for the flow are independent of the blade speed.

7. RECOMMENDATIONS

There are certain important recommendations which are made for this experiment which would help in the foregoing study of the same; these recommendations are appended below:

1 The experiment should be conducted for variable speeds of the DB, so that the relation of dynamic and static could be formulated; and the speed of Vb./Uo = 1 could be very helpful for analyzing the jet flow behaviors. For this the mechanical device which was used here should be replaced with an air piston and linear rail mechanism as that would help to control the speed the DB to any desired level with controlling of the air pressure, and the linear rails would offer minimum friction to movement of the DB. (as it was not the case in this experiment.)

2 The calculations of relating the time series and that of DB were done manually, by using calculator, it would be much better to design a software that would help to correlate the two, and for a given instant of time tells the position of the blade along with the corresponding magnitude of the velocity obtained by the hot wires.

3. The apparatus used for these experiment was fixed upside down in the wind tunnel, which posed allot of problems for setting and adjusting the various parameters of DB assembly; it would be better that the assembly would be placed straight as that would help

the experimenter to easily adjust any parameter of the DB assembly to the desired setting without any hassle.

4 It would also be worthwhile that the experiment as stated earlier is carried out with variable jet speed and also with variable flow speed, as that would help to find out the relation between the dynamic and the static behavior of the flow field to the DB.

8. REFERENCES

1. Applied fluid Dynamics Hand Book by Robert D. Belvins
2. Turbulent jets by N. Rajaratnam
3. Fluid Mechanics By Victor L. Streeter and E Benjamin Wylie
4. Experimental Fluid Mechanics By P. Bradshaw
5. Mechanics Of Fluid By I H Shame
6. Syed K. Ali " Instability phenomena in two dimensional slit jet flow" Ph.D. dissertation MSU
7. Hand Book of fluid Dynamics and Fluid Mechanics Vol. 2. Experimental and Experimental Fluid Dynamics By Joseph A.Schetz
8. Hot wire and Hot Film Anemometer By Ron F. Blackwelder
9. Hot Wire Anemometry By Comet-Bellot
10. Foss,J,F , Wallance,J, Wark,C "vorticity measurement", Instrumentation for Fluid Dynamics, Joseph and Allen Fuhs ed. , Wiley and sons, Inc. , pp 1066-1067, 1995
11. MKS Instruments, Inc., Bulletin 120/150510-2/94,1994
12. Topics in Applied Physics Vol. 12. By P.Bradshaw.

APPENDIX A: DEFLECTOR BLADE ASSEMBLY

Introduction.

As stated earlier the experiment involves the study of a planner slit jet deflected impulsively by a deflector/impulse blade. The equipment needed for the generation of the flow field already existed in the laboratory, that is the flow system and the slit jet apparatus. But an intermediate device was designed that would fit over the slit jet assembly, and carry a DB with it. So the main flow field could be cut at different incremental depths. This device which is called the deflector blade carriage assembly (DBCA), has the following characteristics:

a. Deflector blade position adjustable in x-y-z co-ordinates.

b. Positive stop to the transient motion of the DB.

c. Primary drivers disengages when the DB is in position.

d. No pitching or yawing of the DB during its motion.

e. All parts detachable.

f. Can be operated from remote.

g. Cost-effectiveness.

To cater for all the above features, a detailed mechanical design was undertaken to fulfill the job and at the same time be cost-effective. A list of parts and their functions is appended below.

Component List

A detailed design was undertaken to achieve the target of making the DBAC, but being a mechanical device, it had some disadvantages to it, too. Those disadvantages will be stated later. All the major parts of the assembly were fabricated with the exceptions of a few which were locally purchased. This simple device had fifteen components, each component performing a unique function, a list of all these is as follows:

Description	Quantity
1. Deflector blade (knife edged)	01
2. DB extension	01
3. Center rod	01
4. Pullers (primary drivers)	02
5. Rails	06
6. End plates	02
7. Stop-center	01
8. Cushion-center rod	01

9. Stops-main springs	02
10. Right/left handed screws	02 each
11. Center rod holder	01
12. End plate clamps (angle iron)	02
13. I-beam in DB carriage	01
14. Remote release	01
15. Main springs	02

Description and Use of Components

With the use of the above items, it was possible for the DB to be released and be positioned at various locations in the exit plane of the flow field. The function of each is briefly described below and the characteristics of the assembly stated earlier would also be highlighted in the description.

Deflector blade

The deflector or the "impulsive blade" is used to deflect the flow of the main jet. It's made of curlicue and has a 45- degree knife edge. The length of the blade is 360 mm, having a knife edge of 300 mm, that is, 150 mm on either side of the center line, and a thickness of 11.5 mm a width of 50 mm. The L_{DB} was selected to be 300 mm because the Lj is also 300 mm, so the deflector blade could fully be utilized to cut the flow field. On one side of the DB there is a knife edge and on the other side there is a

female part for the connection of the blade extension, that is, the Allen screws pass through the blade extension and go into the female part of the main DB. figure A-1.

Deflector blade extension

An extension of 300 x 100 x 11.5 mm can be attached to the DB with the help of the Allen screws mentioned above. The material of the DB and of its extension is the same. The only difference is that the DB has a knife edge on one side, where as, the extension is a simple rectangular piece. But in the course of the experiment, it has provided (DB extension) a very vital role, and that was, that the sling of the remote release was attached by the Allen screws to the extension and it also prevented the swirling of air from the topside of the DB to rejoin the main flow stream which was deflected by the DB, but there was a disadvantage in having the extension – that it added extra weight.

Deflector blade carriage

The most important part of the whole assembly is the deflector blade carriage, as it performs the important task of carrying the DB from its initial to its final state Figure A-2. The deflector blade carriage has got a spring-loaded mechanism and an I-beam to hold the DB. The purpose of these items is quite unique. We shall first start from the spring-loaded mechanism. There are two 10 mm spring-loaded steel balls incorporated in the sides of the carriage Figure. A-2 . The strength of the springs is adjustable; the size of the balls used in the carriage is the same diameter as that of the indents on the center rod.

So, it is a precise fit when both are in position. What happens is, when the DB is in motion it has to be stopped in a specific location in space: so under the influence of the primary force provided by the pullers, the DB is set into an accelerating motion, as the DB approaches the pre-determined position in space, the spring loaded balls of the DB carriage pop into position and rigidly hold the DB at that particular point in space. This location is determined by positioning of the center rod .

Although a big disadvantage of having such a mechanism is that when the indent is not present on the center rod on which the DB is riding, the spring force pushes the 10 mm steel balls against the surface of the center rod which causes friction and reduction of speed of the DB. The stiffness "K" of the spring cannot be reduced much , as that would reduce the retarding force on the carriage when the carriage hits the indent on the center rod, and a positive stop could not be achieved. So a compromise has to be made between the speed of the blade and the friction posed by the springs in the DB carriage.

Center Rod

A circular steel rod of diameter 20 mm and length 510 mm is used to carry out the function of holding the carriage and preventing the yawing of the DB when in transient motion Figure A-3. The figure shows the way the center rod is constructed ; at one end of the center rod we have the indents to hold the DB carriage and a cap like stop is also attached to prevent the carriage from over shooting the indent (as we have reduced the spring force to reduce the friction) figure A-4. the desire to stop the blade at an exact position. For this number of adjustments were carried out in order to have enough spring

force to stop the DB at the desired position on the center rod and at same time to had minimum of friction.

In DB carriage a small brass ring is also fitted on the inside of the carriage to reduce the clearance between the center and itself; the clearance is about 1 thou. Brass material was preferred for this ring on the basis of its ability to have less friction with the steel center rod . Due to this the DB carriage does not shiver when its is riding on the center rod , otherwise the DB would cock on its way towards the Sj.

Stop on the center rod.

A circular disc type stop is placed at the end of the center rod Figure A-4. and it also has a circular foam packing attached to it . The main purpose of the stop is to prevent the over shoot of the DB as the springs in the carriage are not very stiff; so its possible that over shoot, may occur when the DB is speeding towards the its termination position and has gaining momentum . When the DB carriage is in position on the center rod the clearance between the stop and the carriage is less the a fraction of a mm. The circular piece of foam placed in between the center rod stop and the DB carriage fills up the clearance between the two. The reason for having this circular piece of foam is to prevent the slamming of the DB carriage against the stop, so the DB carriage is retarded gradually and does not bounce off the end stop.

Center rod holder

Another very important device connected to the center rod is the center rod holder Figure A-5 . It is a circular disc holding the center rod in it, with an internal diameter of 20 mm and an external diameter of 40 mm. The internal diameter is slightly ground so the center rod can easily be fitted into it. Two sets of screws are used at the bottom of the holder to tighten against the center rod, thereby holding it rigidly in position. This center rod holder is then fitted to the end plate. By loosening the screws which grip onto the center rod, one can easily move the center rod back and forth, thereby adjusting the position or the termination point of the DB while it is in motion.

Pullers

The main driving force is provided by the two pullers Figure A-6 , which are made of Teflon and are rectangular in shape with a gap in between to hold the DB. Both top and bottom of each puller have spring-loaded balls of 2.5 mm diameter. Having this spring-and-ball mechanism helps to hold the DB as they fit over the notch in the DB.

The stiffness of these springs is adjusted in such a manner that when the DB is pulled back against the main spring force, the pullers rigidly hold on to the DB, thus when the DB is released by the remote mechanism under the main spring force potential the DB is accelerated towards the main flow field. The spring force of all four spring-loaded (two in each puller) is less than that of the ones in the DB carriage. Because as soon as the balls of the DB carriage pop in place on the center rod, the motion of the DB is stopped, but the pullers are still under the influence of the main spring force and they continue their

motion by popping off the notch in the DB. Once the DB is in position and measurements undertaken by the x-array probe, the DB is ready for the next run.

Both the primary drivers (pullers) are positioned equidistant from the center line of the DB so there is a uniform pull on the DB Figure A-7 . Secondly, it would be worth mentioning that the pullers are made of Teflon, as to reduce their weight and to make them more robust against the number of runs that they have to go through; and being light also helps in reducing the utilization of the main spring force towards overcoming the inertia of the drivers and thus more force could be utilized in driving the DB.

I-Beam

An I-beam Figure A-8 is an intermediate connection between the DB and its carriage. The I-beam is mounted symmetrically on the DB and is then slid into the slot of the DB carriage. Also on the sides of the DB carriage there are four sets of Allen screws which tighten onto the I-beam when the I-beam is in position in the DB carriage. The I-beam does not only form the connection between the DB and the carriage but it also helps in the secondary adjustment of the DB. It acts like a vernier; the main adjustment of the final position of the DB in the exit plane of the Sj can be done by the movement of the center rod, the secondary adjustment/ final adjustment can be done by moving the I-beam and the DB carriage.

Rails

There are three types of rails used in the construction of the DB assembly. They are as follows:

1. Bottom and topside rails
2. Side rails

The function of the top and the bottom rails is to guide the motion of the pullers steadily during its linear travel. The bottom rail provides the main path for the motion of the pullers and guides it steadily from the start to the end in a straight line. There is a slight clearance between the walls of the bottom rail and the pullers, as this helps the pullers to self-adjust itself during its linear travel.

The top rail, which also helps in guiding the motion of the pullers, has a secondary function to it, that is,when the pullers pop off from the DB, it prevents the puller from jumping off the bottom rail. The third type of rail are the side rails. They have an important role to play in guiding the DB through its motion. There is a 1 mm clearance between the side walls of the side rails and that of the DB, top and bottom surface. The clearance is suggested to be minimal so that during the transient motion of the DB over the center rod, it does not roll.All the three different type of rails used in this assembly are made of Aluminum because of its inherent property of being light and robust (these rails were locally purchased).

Stops - Main Springs

The main spring used to provide the main driving force to the DB has pullers on one side and a stop on the other. These stops are circular pins which fit in the grooves drilled in the upper and the bottom rail Figure A-9 . These stops are adjustable at various positions on the rails, thereby increasing or decreasing the distance from the position the blade is released. So, indirectly, positioning of the stops determines the spring force.

End Plates

The whole DB assembly is held in position due to the end plates Figure A-10 . The end plates have two parts: the upper and the lower part. The lower part is used to form the rigid mounting for the assembly and is held in position onto the wooden platform carrying the slit jet with the help of angled iron and bolts. The upper half of the end plate houses the three rails on its sides and thus holds the DB assembly.

Both of the end plates are connected together with four long screws having a pitch of 1.5 mm. Two of the screws are right-handed and two of them are left-handed. Each set is placed in between the end plates.

Another safety device for the upper half of the end plate are the two locking nuts, which when tightened hold the end plate in position, and thus prevent it from coming down or moving up if accidentally the screws are tampered with.

Remote Release

The whole assembly is housed in the wind tunnel. We mount the DB assembly and the slit jet apparatus upside down on the suction plenum of the wind tunnel. The suction plenum acts as a vacuum chamber and sucks the air through the plenum of the slit jet and out of the reversible blower; so, it is a problem to operate the deflector blade manually in the suction plenum. So, a remote mechanism was needed to pull and release the blade. For this, a spindle in a bearing, Figure A-11 , was fitted on top of the wind tunnel. The bearing was supported by a circular disc through which the spindle passed and reached the center line of the DB assembly. Then, two equidistant cords were fitted on the rear side of the DB extension and connected by a single nylon cord to the spindle. Turning the spindle from the outside of the wind tunnel caused the nylon thread to be wound on the spindle, and thus the DB was pulled back against the spring force to a predetermined position. On release, the thread was unwound under the spring force and the DB was hauled in position, accelerating towards the main flow field out of Sj

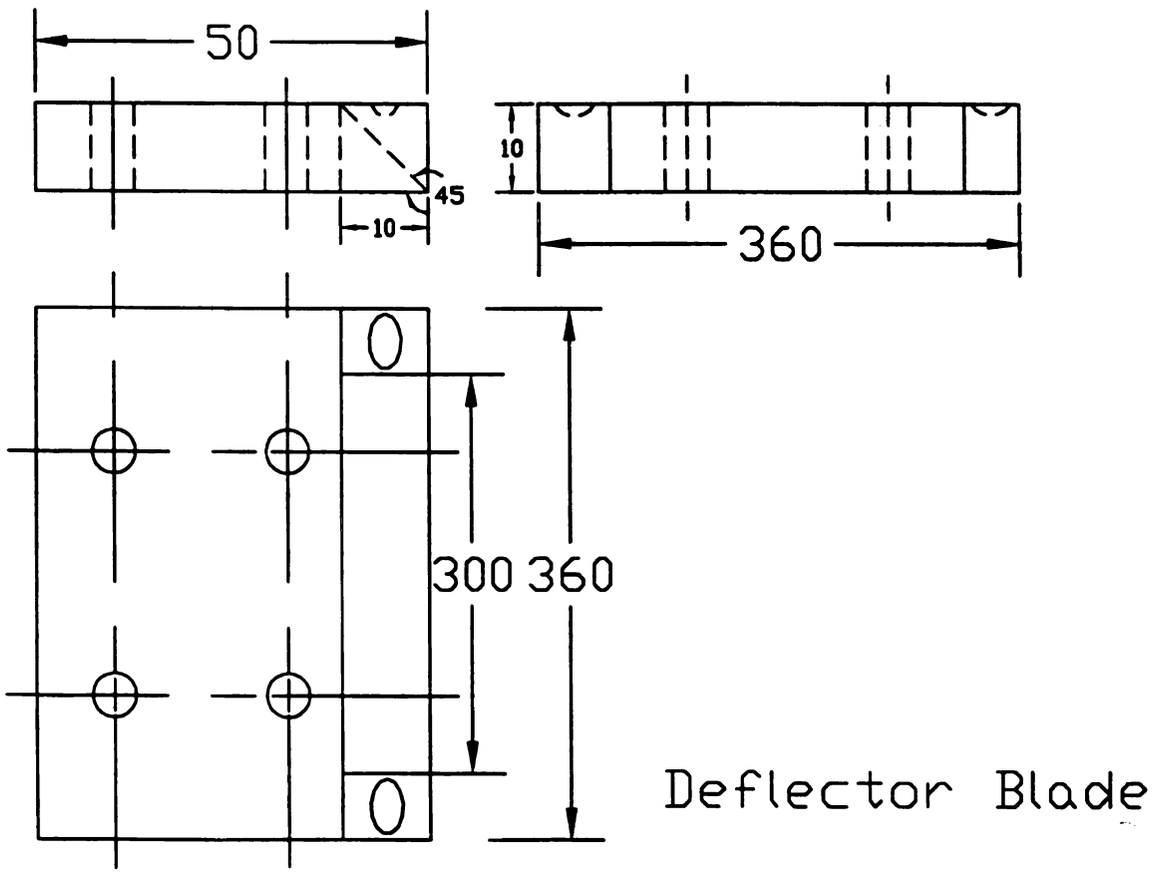

Fig A-1 Deflector blade design

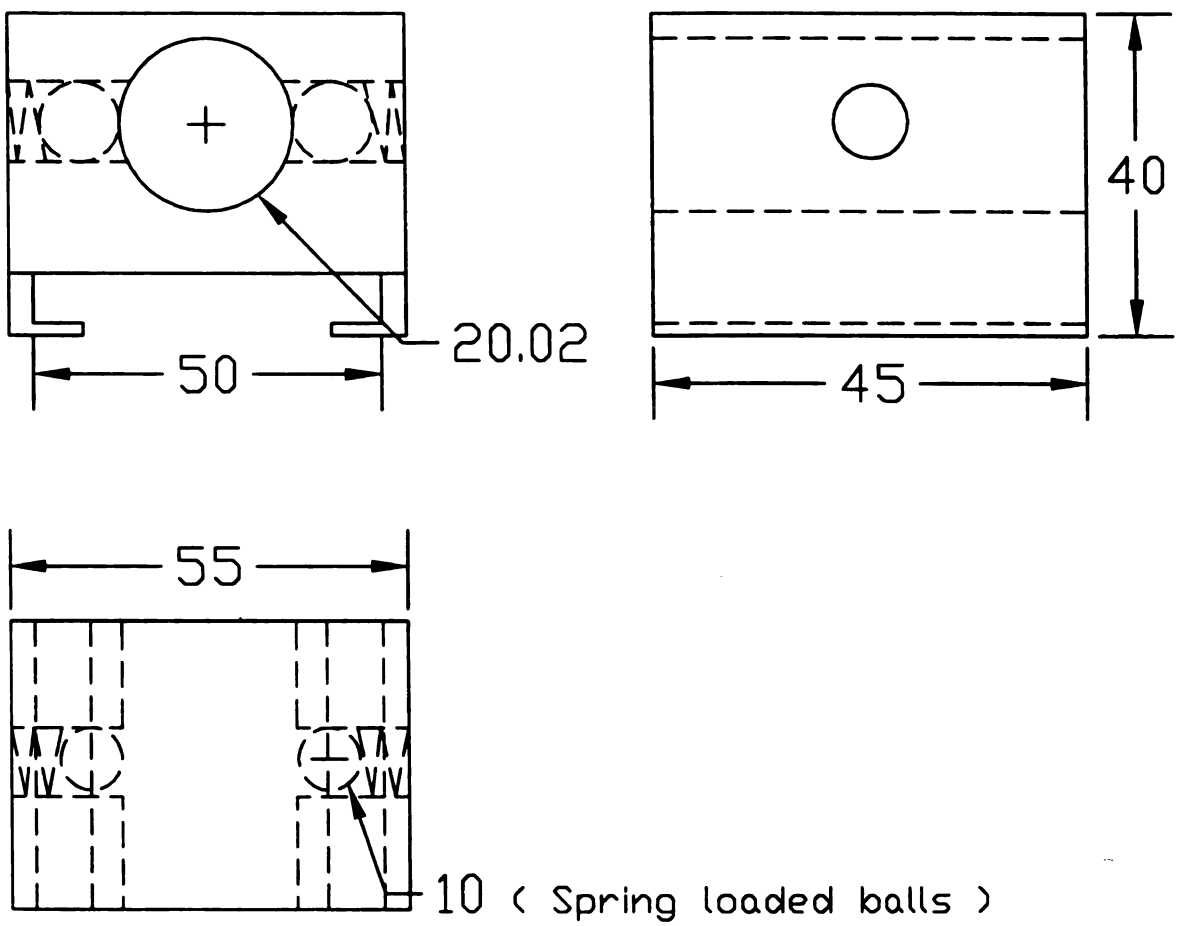

Fig A-2 Deflector blade carriage design.

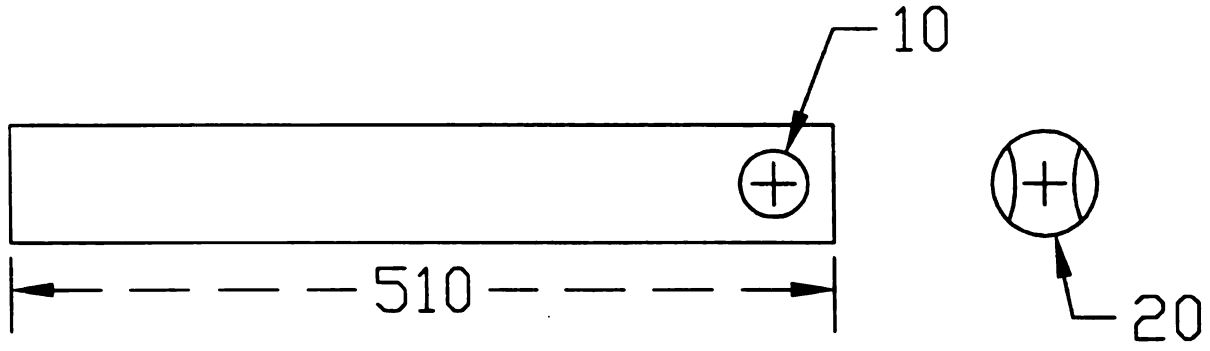

CENTER ROD FOR HOLDING
THE DB-CARRIAGE.

Fig A-3 Center rod for carrying the DB carriage

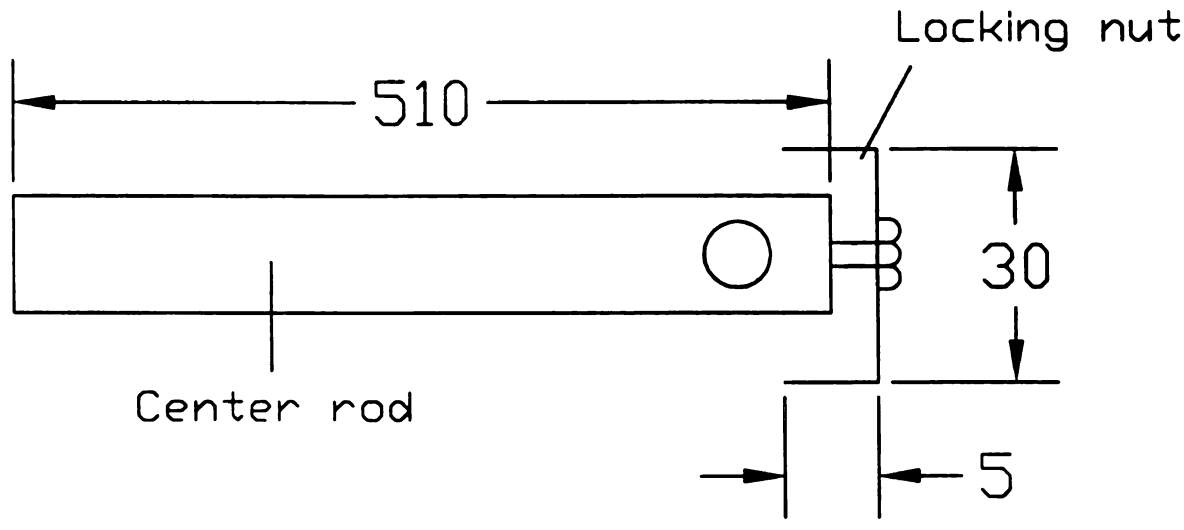

Fig A-4 Center rod with the locking nut.

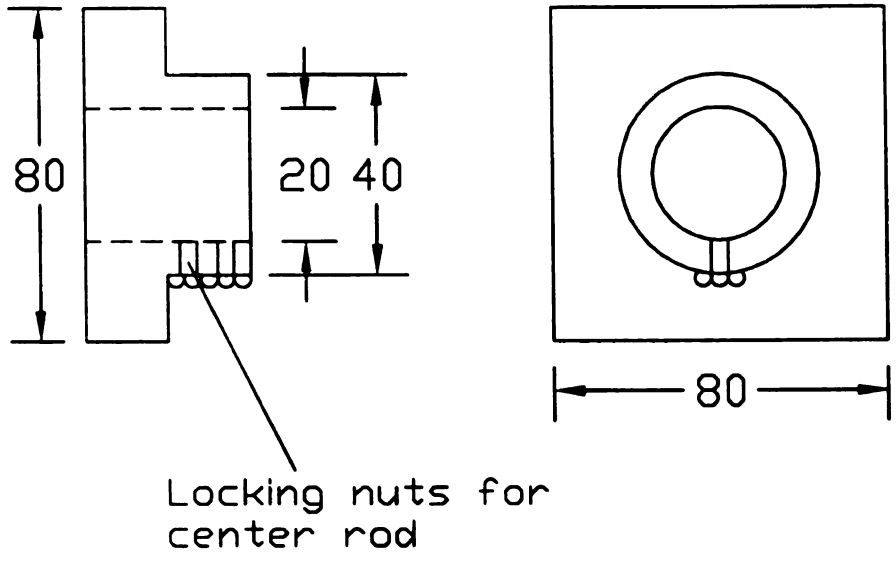

Fig A-5 Center rod holder.

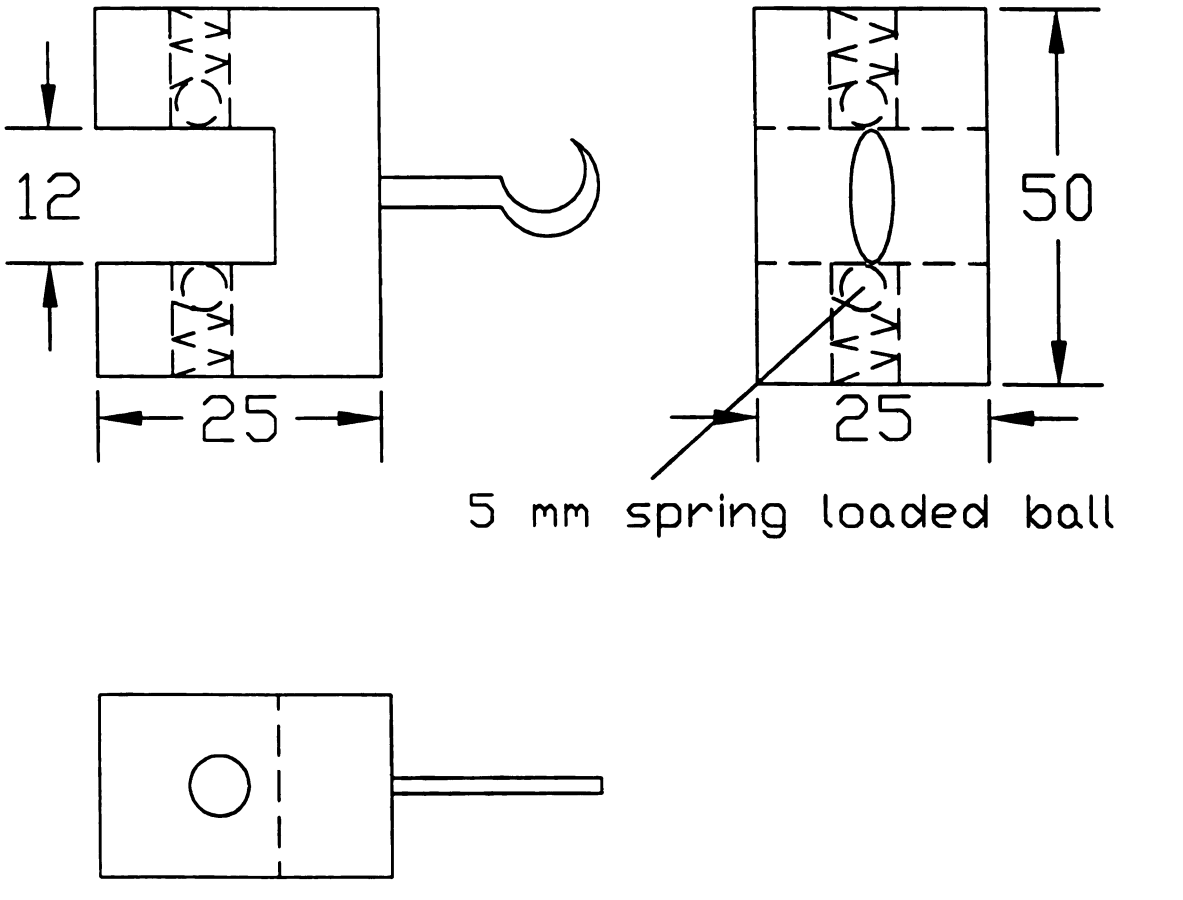

Fig A-6 Spring loaded pullers (Primary Drivers for the DB)

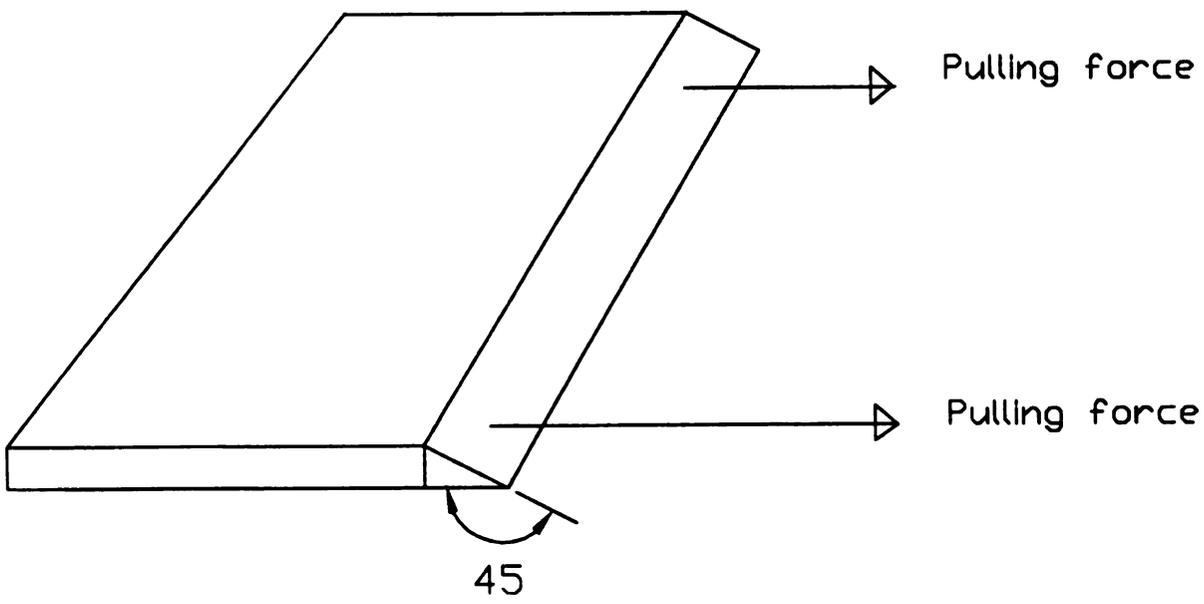

Fig A-7 Deflector Knife Edge.

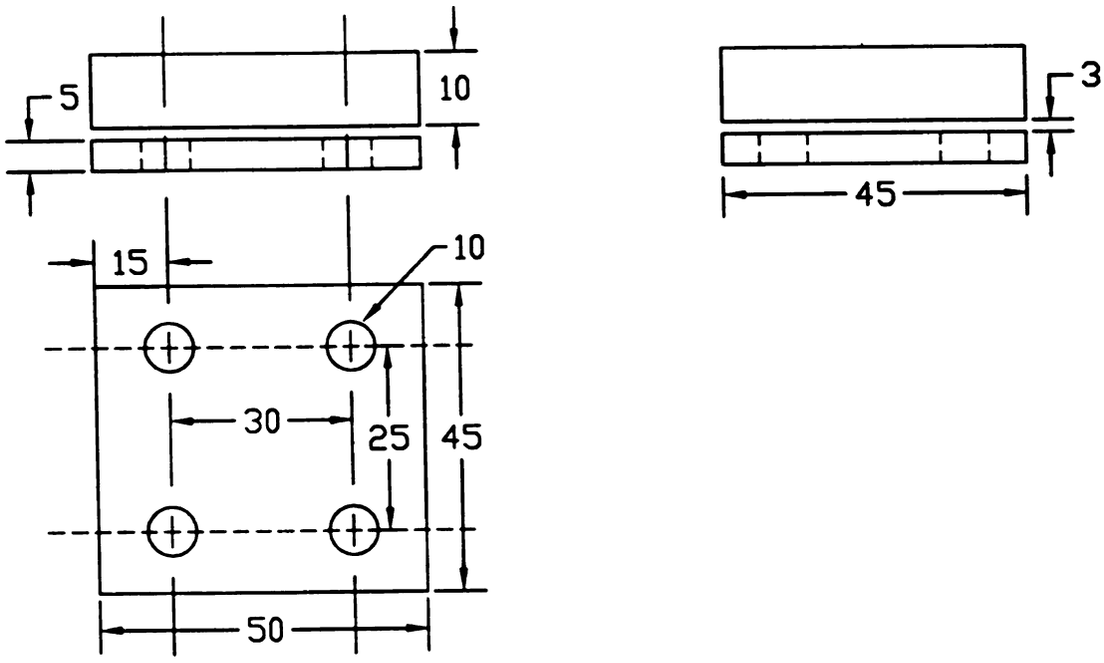

Fig A-8 I-Beam to connect DB with the DB carriage.

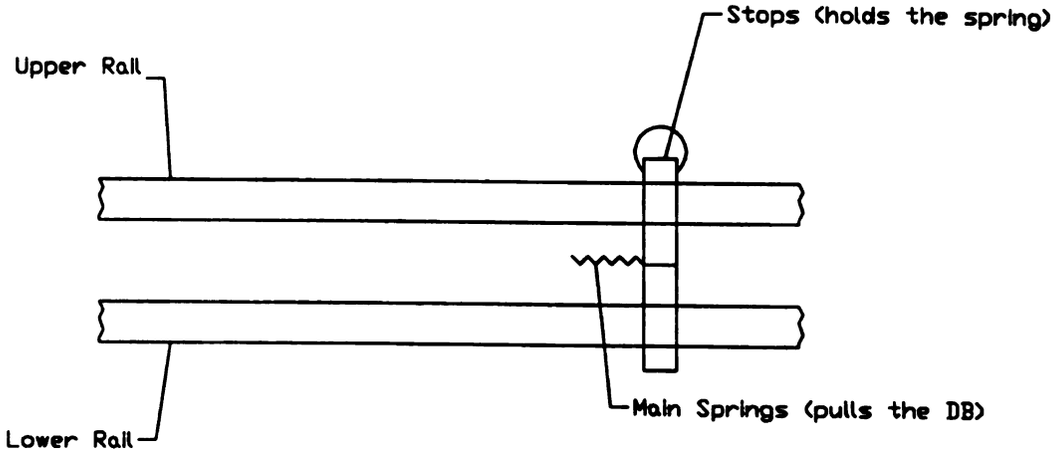

Fig A-9 Stops for the main springs.

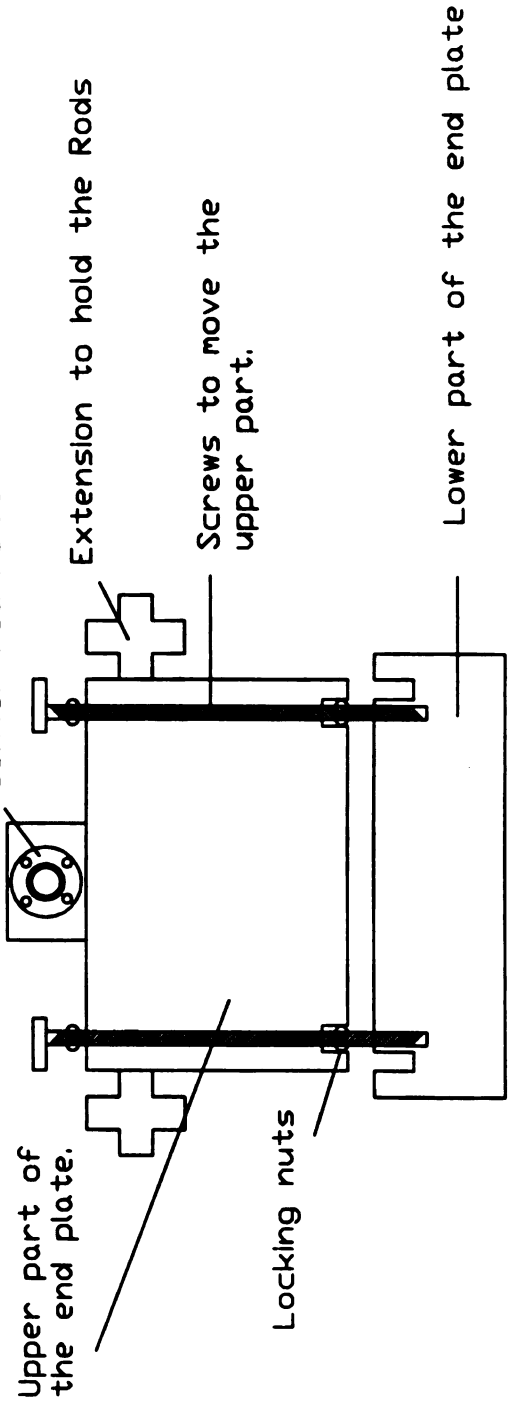

Fig A-10 End plates for holding the DB assembly.

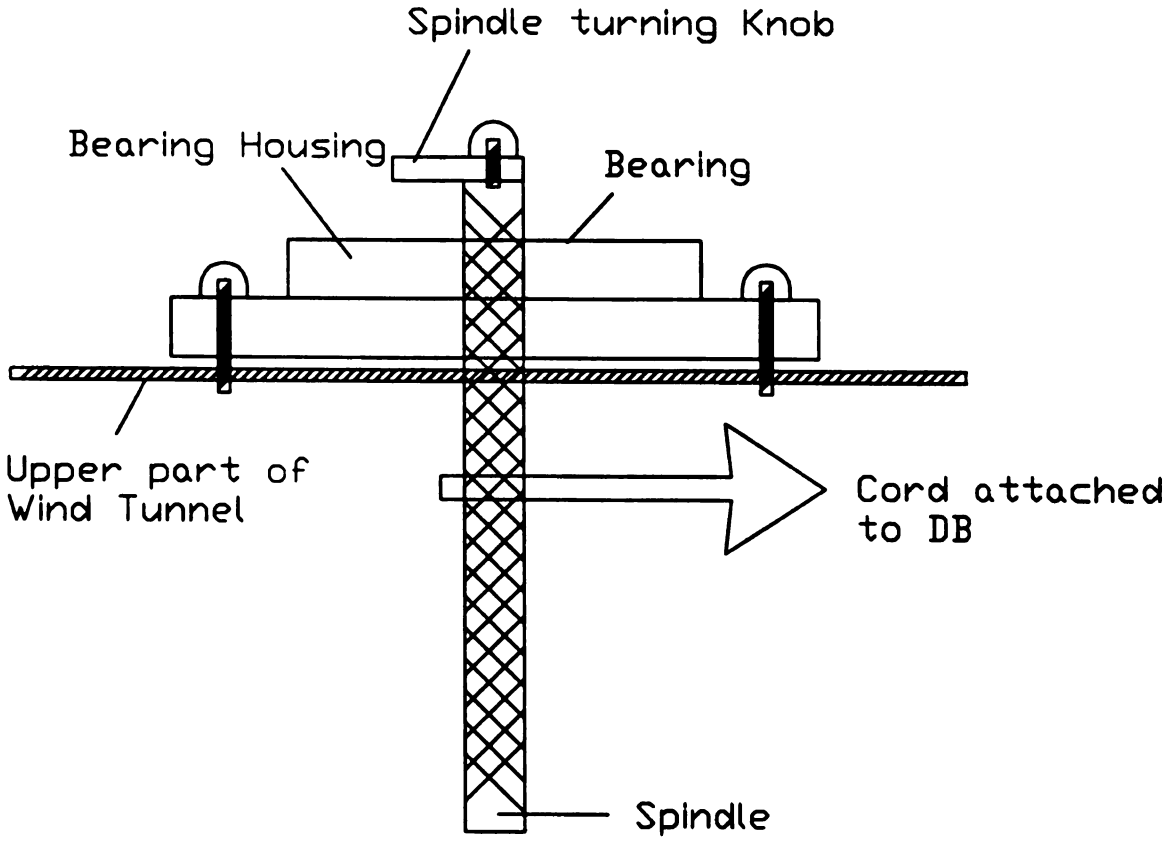

Fig A-11 Remote mechanism used for the release of the DB.

MICHIGAN STATE UNIVERSITY LIBRARIES
3 1293 02094 7093